

# Leptonic and semileptonic decays of charm and bottom hadrons

Jeffrey D. Richman\*

Department of Physics, University of California, Santa Barbara, California 93106

Patricia R. Burchat†

Department of Physics, Stanford University, Stanford, California 94305

The authors review the experimental measurements and theoretical descriptions of leptonic and semileptonic decays of particles containing a single heavy quark, either charm or bottom. Measurements of bottom semileptonic decays are used to determine the magnitudes of two fundamental parameters of the standard model, the Cabibbo-Kobayashi-Maskawa matrix elements  $V_{cb}$  and  $V_{ub}$ . These parameters are connected with the physics of quark flavor and mass, and they have important implications for the breakdown of  $CP$  symmetry. To extract precise values of  $|V_{cb}|$  and  $|V_{ub}|$  from measurements, however, requires a good understanding of the decay dynamics. Measurements of both charm and bottom decay distributions provide information on the interactions governing these processes. The underlying weak transition in each case is relatively simple, but the strong interactions that bind the quarks into hadrons introduce complications. The authors also discuss new theoretical approaches, especially heavy-quark effective theory and lattice QCD, which are providing insights and predictions now being tested by experiment. An international effort at many laboratories will rapidly advance knowledge of this area of physics during the next decade.

## CONTENTS

I. Introduction and Overview	893	1. Structure of hadronic currents	928
A. Semileptonic decays and the Cabibbo-Kobayashi-Maskawa matrix	895	2. Quark models	929
B. Decay dynamics and heavy-quark effective theory	896	3. Heavy-quark effective theory	931
C. Plan of the review	897	4. Predictions for the slope of the Isgur-Wise function	933
II. Theory of Leptonic and Semileptonic Decays	897	5. Decay distributions for $P \rightarrow P' \ell \nu$	933
A. Matrix elements for leptonic and semileptonic decays	897	6. Decay distributions for $P \rightarrow V \ell \nu$	934
B. The Cabibbo-Kobayashi-Maskawa matrix	898	B. Cabibbo-favored semileptonic decays of charm mesons	936
C. Dynamics of semileptonic decays	901	1. $D \rightarrow \bar{K} \ell^+ \nu$	936
III. General Remarks on Experimental Techniques	905	2. $D \rightarrow \bar{K}^* \ell^+ \nu$	938
A. Charm-hadron experiments	905	3. Ratio of $\Gamma(D \rightarrow \bar{K}^* \ell^+ \nu)$ to $\Gamma(D \rightarrow \bar{K} \ell^+ \nu)$	941
B. Bottom-hadron experiments	907	4. $D$ decays to other Cabibbo-favored states	942
C. Lepton identification	908	5. $D_s \rightarrow \phi \ell^+ \nu$	942
D. Assumed branching fractions	909	6. $D_s \rightarrow \eta \ell^+ \nu$ and $D_s \rightarrow \eta' \ell^+ \nu$	943
IV. Leptonic Decays	909	C. Cabibbo-suppressed semileptonic decays of charm mesons	944
A. Theory of leptonic decays	909	D. Summary of exclusive charm decays	946
B. Experimental results on leptonic decays	910	E. Exclusive $b \rightarrow c$ semileptonic decays of $B$ mesons and $ V_{cb} $	946
1. $D^+$ and $D_s$ leptonic decays	910	1. Overview and experimental techniques	946
2. $B^-$ leptonic decays	913	2. Branching fraction for $B \rightarrow D \ell^- \bar{\nu}$	949
V. Inclusive Semileptonic Decays	913	3. Branching fractions for $B \rightarrow D^* \ell^- \bar{\nu}$ and $B \rightarrow D^{**} \ell^- \bar{\nu}$	949
A. Introduction	913	4. The determination of $ V_{cb} $ with exclusive decays	953
B. Theoretical predictions for semileptonic decays	914	5. Measurement of the $B \rightarrow D^* \ell^- \bar{\nu}$ form factors	957
C. Inclusive charm semileptonic decays	917	F. Exclusive $b \rightarrow u$ semileptonic decays of bottom mesons and $ V_{ub} $	960
D. Inclusive bottom semileptonic decays and $ V_{cb} $	919	G. Semileptonic decays of charm and bottom baryons	964
1. Measurement of $\mathcal{B}_{SL}$ using the inclusive lepton spectrum	920	1. Decay distributions for $\Lambda_c \rightarrow \Lambda \ell^+ \nu$	964
2. Measurement of $\mathcal{B}_{SL}$ using charge and angular correlations in dilepton events	922	2. Charm-baryon decays	965
3. Measurement of $\mathcal{B}_{SL}$ for $B^0$ and $B^-$ with tagging	923	3. Bottom-baryon decays	967
4. Determination of $ V_{cb} $ from inclusive measurements	923	VII. Conclusions	967
E. Lepton end-point region in semileptonic $B$ decays and determination of $ V_{ub} $	925	A. CKM measurements	967
F. $B \rightarrow X \tau^- \bar{\nu}_\tau$ and other inclusive modes	927	B. Summary of leptonic and semileptonic charm decays	969
VI. Exclusive Semileptonic Decays	927	C. $B$ semileptonic branching fractions	970
A. Theory of exclusive semileptonic decays of mesons	928	D. Form factors for $B$ semileptonic decays	972
		Acknowledgments	972
		References	972

## I. INTRODUCTION AND OVERVIEW

In the extraordinarily diverse phenomenology of weak interactions, semileptonic and leptonic decays of hadrons have

\*Electronic address: richman@charm.physics.ucsb.edu

†Electronic address: pat@slac.stanford.edu

a special standing. In both types of decays, the final-state particles include a single charged lepton, the clearest experimental signature for a weak process mediated by the  $W$  boson. Because these decays are relatively simple from a theoretical perspective, they provide a means both to measure fundamental standard-model parameters and to perform detailed studies of decay dynamics.

Historically, the semileptonic process of nuclear  $\beta$  decay opened the era of weak-interaction physics and presented physicists with the mystery of the electron's undetected partner, the neutrino (Pais, 1986). The process underlying  $\beta$  decay is the  $W$ -boson-mediated weak transition  $d \rightarrow u W^-$ ,  $W^- \rightarrow e^- \bar{\nu}_e$ , where the decay of a  $d$  quark into a  $u$  quark transforms a neutron ( $udd$ ) into a proton ( $uud$ ).  $\beta$  decay was the only known weak process from the turn of the century until the late 1930s and 1940s, when muons, pions, and kaons were discovered in cosmic rays.

With the rapid improvement of accelerators, weak decays could be studied in detail. The process  $K \rightarrow \pi e^- \bar{\nu}_e$ , for example, showed that kaons could decay in a manner similar to the  $\beta$  decay of nucleons: the strange quark ( $s$ ) in the kaon undergoes the decay  $s \rightarrow u W^-$ ,  $W^- \rightarrow e^- \bar{\nu}_e$ . Leptonic decays—in which no hadrons appear in the final state—have also played a key role in understanding weak interactions. The striking  $10^{-4}$  suppression of the leptonic decay  $\pi^- \rightarrow e^- \bar{\nu}_e$  relative to  $\pi^- \rightarrow \mu^- \bar{\nu}_\mu$  was explained by weak-interaction theory, and precision measurements have confirmed that the underlying weak couplings of the electron and the muon are the same (Czapek *et al.*, 1993; Rolandi, 1993, Britton *et al.*, 1994).

In the 1970s, the discovery of two heavy quarks, charm ( $c$ ) (Aubert *et al.*, 1974; Augustin *et al.*, 1974) and bottom ( $b$ ) (Herb *et al.*, 1977), and a heavy lepton,  $\tau$  (Perl *et al.*, 1975), posed a profound mystery: the generation puzzle. The existence and properties of the new heavy quarks, together with indirect evidence for the top quark ( $t$ ) from  $B^0 \bar{B}^0$  mixing (Albrecht *et al.*, 1987), showed that there are two heavier versions of the basic pair of quarks ( $u, d$ ) found in ordinary stable matter. Recently, the  $t$  quark has been directly observed in  $p\bar{p}$  collisions (Abachi *et al.*, 1995; Abe *et al.*, 1995). Thus there are three quark generations,

$$\begin{pmatrix} u \\ d \end{pmatrix}, \quad \begin{pmatrix} c \\ s \end{pmatrix}, \quad \begin{pmatrix} t \\ b \end{pmatrix}, \quad (1)$$

where the upper member of each quark doublet has charge  $+2/3$  (measured in units of  $|e|$ , where  $-|e|$  is the electron charge), and the lower member has charge  $-1/3$ . The coupling of the quarks to  $W^+$  and  $W^-$  bosons results in weak-interaction transitions between any upper and any lower member of these doublets, when allowed by kinematic constraints such as energy conservation.

Because quarks are found only in bound states, the definition of quark masses is problematic (Gasser and Leutwyler, 1982). Roughly speaking, however,  $m_u \sim 0.004 \text{ GeV}/c^2$ ,  $m_d \sim 0.007 \text{ GeV}/c^2$ ,  $m_s \sim 0.3 \text{ GeV}/c^2$ ,  $m_c \sim 1.3 \text{ GeV}/c^2$ ,  $m_b \sim 4.8 \text{ GeV}/c^2$ , and  $m_t \sim 180 \text{ GeV}/c^2$ . Thus, on a scale set by the proton mass ( $m_p = 0.94 \text{ GeV}/c^2$ ), the  $u$ ,  $d$ , and  $s$

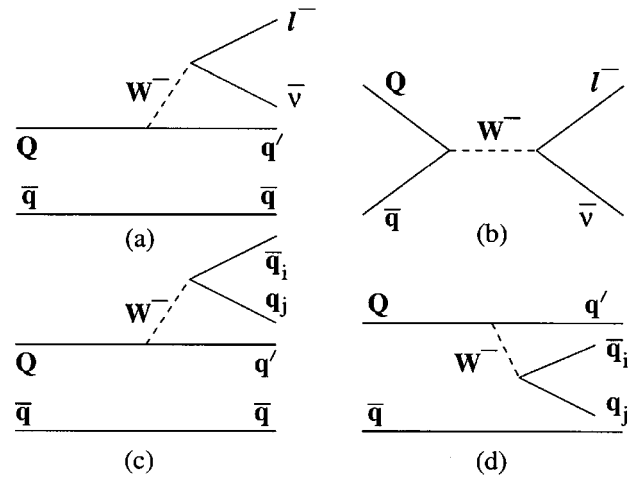


FIG. 1. Feynman diagrams for the  $W$ -mediated weak decay of a meson containing quarks  $Q\bar{q}$ : (a) semileptonic decay, (b) leptonic decay, (c) hadronic decay, and (d) hadronic decay. We have not shown the exchanges of gluons between the quarks, which significantly modify these processes.

quarks are light; the  $c$  and  $b$  quarks are heavy; and the  $t$  quark is enormously heavy, with a mass about twice that of the  $W$  boson ( $m_W = 80 \text{ GeV}/c^2$ ). At present, this progression of masses is not understood.

The discovery of the  $\tau$  lepton showed that the quark doublets are paralleled by three generations of leptons:

$$\begin{pmatrix} \nu_e \\ e^- \end{pmatrix}, \quad \begin{pmatrix} \nu_\mu \\ \mu^- \end{pmatrix}, \quad \begin{pmatrix} \nu_\tau \\ \tau^- \end{pmatrix}. \quad (2)$$

The masses of charged leptons also increase with generation ( $m_e = 0.0005 \text{ GeV}/c^2$ ,  $m_\mu = 0.106 \text{ GeV}/c^2$ ,  $m_\tau = 1.777 \text{ GeV}/c^2$ ), but at present there are only upper limits for the neutrino masses. In particular, it is known that  $m_{\nu_e}$  must be quite small, less than 5 to 7  $\text{eV}/c^2$  (Particle Data Group, 1994). If neutrino oscillations—transitions from one type of neutrino to another—are proven experimentally, then non-zero neutrino masses will have been established.

The existence of three generations of quarks and leptons is a striking phenomenon that is not understood. One of the goals of heavy-quark physics is to elucidate the relationships among the particles of different generations. The  $b$  quark is especially interesting in this respect. Because it is lighter than the  $t$  quark, the  $b$  can decay only into quarks of a different generation, and it has  $W$ -mediated decays to both first-generation ( $u$ ) and second-generation ( $c$ ) quarks. (Similarly, the  $s$  quark can decay only into a first-generation quark,  $u$ .) Even when large samples of  $t$ -quark decays are obtained, the mode  $t \rightarrow b W^+$  is expected to be dominant, and generation-changing decays of the  $t$  quark should be very rare.

Particles containing heavy quarks can decay semileptonically in a manner analogous to nuclear  $\beta$  decay. Figure 1(a) shows the underlying quark-level transition for the semileptonic decay of a meson containing a heavy quark, which we denote generically in this review by the symbol  $Q$ . The process is  $Q \rightarrow q' W^*$ ,  $W^* \rightarrow \ell^- \bar{\nu}$  [Fig. 1(a)], whereas for leptonic decays the transition is  $Q\bar{q} \rightarrow W^* \rightarrow \ell^- \bar{\nu}$  [Fig. 1(b)].

The symbol  $W^*$  indicates that the  $W$  boson is generally virtual, except in the case of decays of the  $t$  quark, whose mass is greater than that of the  $W$ . (Although we have labeled the lepton charge as negative, this is true only for decays of the  $b$  or  $\bar{c}$ ; for  $\bar{b}$  or  $c$  decays, the lepton charge is positive.) Examples of hadronic decays, in which the decay products of the  $W^*$  are also quarks, are shown in Fig. 1(c) and Fig. 1(d). The weak interactions underlying these processes are straightforward to describe theoretically, but complications arise because the quarks are bound inside hadrons by the strong force. These interactions, which are described by the theory of quantum chromodynamics (QCD) (Gross and Wilczek, 1973; Politzer, 1973), are very difficult to predict using perturbative methods because the strong coupling is large at the typical energies in these decays.

A key feature of leptonic and semileptonic decays is their relative simplicity, a consequence of the fact that here the effects of the strong interactions can be isolated. The decay amplitude for either type of decay can be written as the product of a well-understood leptonic current for the  $\ell^- \bar{\nu}$  system and a more complicated hadronic current for the quark transition. In leptonic decays, the hadronic current describes the annihilation of the quark and antiquark in the initial-state meson, whereas in semileptonic decays it describes the evolution from the initial- to final-state hadrons. Because strong interactions affect only one of the two currents, leptonic and semileptonic decays are much more tractable theoretically than hadronic decays, in which the decay products of the  $W^*$  are also hadrons. A further complication of hadronic decays is that the hadrons in the final state can interact strongly with each other. Leptonic and semileptonic decays therefore provide a means for studying the strong interactions in a relatively simple environment. Perhaps more important, the effects of strong interactions in these processes can be understood sufficiently well that the underlying weak couplings of quarks to the  $W$  boson can be determined, a point that we discuss in the following section.

In heavy-quark decays, semileptonic modes are generally much more accessible experimentally than leptonic modes, simply because semileptonic branching fractions are larger. (The reasons are explained in Sec. IV.A.) The very large charm data samples now available are just beginning to reveal leptonic decay signals for the  $D_s$  meson ( $c\bar{s}$ ), whereas no such decays have yet been seen for bottom hadrons. Thus there is much more information on semileptonic than leptonic decays, and the proportion of our review devoted to the two types of processes reflects this difference.

### A. Semileptonic decays and the Cabibbo-Kobayashi-Maskawa matrix

Because semileptonic decays are both relatively simple and experimentally accessible, they are the primary tool for addressing one of the fundamental questions of the generation puzzle: what are the couplings of the quarks to the  $W$  boson? These couplings appear to be deeply connected to the origin and values of quark masses. For comparison, the lepton transitions  $\ell^- \rightarrow W^* \nu_\ell$  (or  $W^* \rightarrow \ell^- \bar{\nu}$ ) are observed to have a single, universal weak-coupling strength  $g$ , which is the same for all three generations. Furthermore, transitions

from a charged lepton of one generation to a neutrino of another have not been observed. In contrast, quark transitions  $q \rightarrow W^* q'$  have strengths that depend on which quarks are involved. Although quark transitions within the same generation are highly favored, there are also transitions across generations. For the decay of a charge  $-1/3$  quark  $q$  to a charge  $+2/3$  quark  $q'$ , the coupling at the  $W$  vertex is proportional to  $gV_{q'q}$ , where  $V_{q'q}$  is, in general, a complex number. Thus the amplitudes for the processes  $b \rightarrow c \ell^- \bar{\nu}$  and  $b \rightarrow u \ell^- \bar{\nu}$  are proportional to  $V_{cb}$  and  $V_{ub}$ , respectively, and the amplitudes for  $c \rightarrow s \ell^+ \nu$  and  $c \rightarrow d \ell^+ \nu$  are proportional to  $V_{cs}^*$  and  $V_{cd}^*$ .

The  $3 \times 3$  matrix of these constants, known as the Cabibbo-Kobayashi-Maskawa (CKM) matrix (Kobayashi and Maskawa, 1973),

$$V = \begin{pmatrix} V_{ud} & V_{us} & V_{ub} \\ V_{cd} & V_{cs} & V_{cb} \\ V_{td} & V_{ts} & V_{tb} \end{pmatrix}, \quad (3)$$

is a generalization of the Cabibbo rotation known since the 1960s (Cabibbo, 1963). This rotation, characterized by  $\sin\theta_C \approx 0.22$ , was introduced to describe the semileptonic decays of strange hadrons, whose rates are suppressed by a factor of about  $\tan^2\theta_C \approx 0.05$  relative to that expected from the decays of nonstrange particles. In addition, the slight suppression of  $n \rightarrow p e^- \bar{\nu}_e$  relative to the rate expected from  $\mu^- \rightarrow e^- \nu_\mu \bar{\nu}_e$  was explained by the factor  $\cos^2\theta_C$ . Although the quark couplings to the  $W$  boson are nonuniversal, the departure from universality is constrained in the standard model by the unitarity of the CKM matrix. For example,  $|V_{ud}| = 0.9744 \pm 0.0010$  implies that either  $|V_{us}|$  or  $|V_{ub}|$  (or both) must be nonzero, with  $|V_{ud}|^2 + |V_{us}|^2 + |V_{ub}|^2 = 1$ .

The structure of the CKM matrix has major implications. With three generations of quarks, the matrix contains a phase that, if nonzero, leads to violation of  $CP$  symmetry. That is, there are amplitudes that are not invariant under the combined operation of particle-antiparticle conjugation ( $C$ ) and parity reversal of the coordinate system ( $P$ ). Besides its importance in understanding the structure of particle interactions,  $CP$  violation is necessary to explain the predominance of matter over antimatter in the universe. However, sources of  $CP$  violation beyond the standard model appear to be required to produce a large enough effect. The extremely interesting phenomenology of  $CP$  violation has been discussed by many authors; here we reference only some recent reviews (Jarlskog, 1989; Nelson, 1992; Nir, 1992; Winstein and Wolfenstein, 1993).

Experimentally,  $CP$  violation is so far seen only as a tiny effect—about a part in a thousand—in kaon decays. While these observations are consistent with predictions based on the standard model, there is no proof that the CKM matrix is the true source of  $CP$  violation in these decays, and alternative theories (beyond the standard model) could equally well explain the existing data. As we shall discuss in Sec. II.B., it is significant that  $|V_{ub}|$ , though small, is measured to be nonzero ( $|V_{ub}| \approx 0.003$ )—otherwise the standard model would predict no  $CP$  violation. Sizable  $CP$ -violating asymmetries are predicted by the standard model in  $B$  decays which, nevertheless, are rather difficult to observe. Currently,

major projects at nearly all of the world's high-energy physics laboratories, including SLAC (BaBar Collaboration, 1994), KEK (Belle Collaboration, 1994), CERN (CERN Reports, 1992, 1993), DESY (Lohse *et al.*, 1994), Cornell (CLEO Collaboration, 1994), and Fermilab (CDF Collaboration, 1994), have been initiated to search for  $CP$  violation in  $B$  decays. The intriguing problem of  $CP$  violation and the question of whether its origin lies truly within the CKM framework are central questions of particle physics.

Most of the known CKM elements have been measured using semileptonic decays (Particle Data Group, 1994). The value of  $|V_{ud}|$  ( $=0.9744 \pm 0.0010$ ) is determined from nuclear  $\beta$  decay, in particular from special transitions for which the uncertainties due to hadronic effects can be minimized. The value of  $|V_{us}|$  ( $=0.2205 \pm 0.0018$ ) is obtained from kaon semileptonic decays and, with somewhat larger theoretical errors, from hyperon semileptonic decays. Although uncertainties arising from the hadronic current might be expected to severely limit the precision of CKM determinations, one can exploit special strong-interaction symmetries that constrain the hadronic current and therefore permit high-precision measurements of  $|V_{ud}|$  and  $|V_{us}|$ . We shall see that symmetries of the strong interactions also play an important role in allowing a precise determination of  $|V_{cb}|$ .

The CKM elements associated with charm decays,  $V_{cs}$  and  $V_{cd}$ , can be determined independently of charm decay measurements. To do this, one assumes three-generation unitarity of the CKM matrix and uses the fact that the CKM elements for  $B$  decay are extremely small (see Sec. II.B.). (Alternatively,  $|V_{cd}|$  can be determined from the production of charm particles in neutrino or antineutrino scattering from nuclei.) An important consequence is that measurements of charm semileptonic decays can be used to test the absolute scale of theoretical predictions for decay amplitudes. The study of charm semileptonic decays is therefore focused more on understanding the dynamics of the hadronic current than on measuring CKM elements. This procedure cannot be used in  $B$  decay, however. The magnitudes of the CKM elements  $V_{ub}$  and  $V_{cb}$  must be determined from  $B$  semileptonic decays, and the scale of theoretical predictions for the decay rate cannot be tested but must be assumed in order to extract  $|V_{ub}|$  and  $|V_{cb}|$ .

## B. Decay dynamics and heavy-quark effective theory

The studies described in this review have two primary goals: first, to measure the magnitudes of the CKM elements  $V_{cb}$  and  $V_{ub}$ , and second, to understand the dynamics of leptonic and semileptonic decays, in particular the effect of strong interactions on the underlying weak process. These goals are related, because the determination of CKM elements relies on a good understanding of the decay process.

Our focus on particles containing heavy quarks is natural not only because they are being intensively studied by current experiments, but also because their decay dynamics are significantly different from those of particles containing only light quarks. In the last few years, a new theoretical approach known as heavy-quark effective theory (HQET) has emerged for analyzing so-called heavy-light mesons (mesons containing one heavy and one light quark), as well as baryons con-

taining a heavy quark and two light quarks. Many authors have contributed to the development of HQET, whose history is traced in the extensive review by Neubert (1994c). A number of the separate ideas underlying HQET emerged over a long period and can be found in the papers of, among others, Shuryak (1980), Nussinov and Wetzel (1987), and Voloshin and Shifman (1987, 1988). Two papers by Isgur and Wise (1989, 1990a) played a major role in synthesizing and extending this development, and they are among the most frequently cited papers in particle physics over the last few years. Their work led to a rapid expansion in the study of HQET; among the key papers are those of Eichten and Hill (1990a, 1990b), Falk *et al.* (1990), Georgi (1990), and Grinstein (1990). Several conference reviews are also available, such as those by Wise (1993, 1994) and Mannel (1993). The ideas of HQET are discussed and used in many places in this review, including Secs. II.C, V.B, VI.A.3, VI.E., and VI.E5. We present some of the basic ideas of HQET in the rest of this section.

A simple argument (Voloshin, 1994) indicates that within a hadron containing a heavy quark, the heavy quark moves nonrelativistically. The momentum of the heavy quark,  $\mathbf{p}_Q$ , must balance that of the light constituents of the hadron,  $\mathbf{p}_{\text{light}}$ :

$$|\mathbf{p}_Q| = |\mathbf{p}_{\text{light}}| \sim \Lambda_{\text{QCD}}, \quad (4)$$

where  $\Lambda_{\text{QCD}} \approx 0.2$  GeV is the scale governing the running of the strong-coupling constant  $\alpha_s$  with momentum transfer. For momentum transfers around  $\Lambda_{\text{QCD}}$  or below, the strong coupling is large; as the momentum transfer increases, the strong coupling decreases. In heavy-light hadrons, the typical momentum transfer to the light constituents is of order  $\Lambda_{\text{QCD}}$  and the size of the hadron is  $1/\Lambda_{\text{QCD}}$ . Thus

$$|\mathbf{v}_Q| = \frac{|\mathbf{p}_Q|}{m_Q} \sim \frac{\Lambda_{\text{QCD}}}{m_Q}, \quad (5)$$

so that in the limit  $m_Q \gg \Lambda_{\text{QCD}}$ , the heavy quark behaves essentially as a stationary source of a color field. Furthermore, the heavy quark's spin, which interacts with the system through a color magnetic moment proportional to  $1/m_Q$ , also decouples from the dynamics in this limit. Thus the actual value of the mass of the heavy quark becomes irrelevant. Imagine a hadron containing a heavy quark  $Q$  with velocity  $v$  and spin  $s$ . In the heavy-quark limit, the configuration of the light constituents in the hadron will not be affected by the replacement of  $Q(v, s)$  with another heavy quark  $Q'(v, s')$  of different mass and spin, as long as the velocities of  $Q$  and  $Q'$  are the same. Thus four-velocity rather than momentum is used to describe the dynamics of systems containing heavy quarks. These conclusions have important implications for both the spectroscopy and decays of heavy hadrons.

The heavy-quark symmetry limit provides a good description of a real physical system if the light constituents have sufficiently small momenta that they cannot probe distance scales of the order  $1/m_Q$ . In practice, the heavy-quark symmetry limit is the starting point for an expansion in the general framework of HQET. In HQET, the properties and decays of hadrons containing a heavy quark are analyzed in terms of a systematic expansion in the variable  $E/m_Q$ , where

$E$  can be due to a number of QCD effects such as the kinetic energy of the heavy quark or the chromomagnetic interaction energy. In the exact heavy-quark symmetry limit, both the masses of the initial- and final-state heavy quarks in a decay are taken to be infinite. In practice, for the symmetry to be useful, the higher-order terms in the HQET expansion must be small, at least in the regions of phase space of interest. The decays best suited to treatment using HQET involve  $b \rightarrow c \ell^- \bar{\nu}$  transitions, since both the initial- and final-state hadrons contain a heavy quark. Examples of such decays are  $B \rightarrow D \ell^- \bar{\nu}$ ,  $B \rightarrow D^* \ell^- \bar{\nu}$ , and  $\Lambda_b \rightarrow \Lambda_c \ell^- \bar{\nu}$ . Note that, compared with  $\Lambda_{\text{QCD}}$ , the strange quark cannot be regarded as heavy, since  $m_s \approx 0.3 \text{ GeV}/c^2$ . Thus HQET is not as successful in treating charm semileptonic decays  $c \rightarrow s \ell^+ \nu$  or  $c \rightarrow d \ell^+ \nu$ .

In contrast to calculations based on hadron models, the HQET expansion is derived directly from the fundamental theory of QCD. Although the terms in the expansion can be difficult to evaluate, the systematic and rigorous nature of HQET means that uncertainties are easier to identify and estimate than those for calculations based on hadron models.

Predictions for the dynamics of semileptonic decays are expressed in terms of form factors, which we shall discuss extensively. The amplitude for a semileptonic decay can be constructed from the available four-vectors in the decay, such as momenta and spin polarizations, and one or more form factors, which are Lorentz-invariant functions of  $q^2$ , the square of the mass of the virtual  $W$ . These functions describe how strong interactions modify the underlying weak decay, and nonperturbative techniques are needed to calculate them. (In leptonic decay,  $q^2$  is fixed, so the only quantity that requires nonperturbative calculation is the “decay constant.”) However, heavy-quark symmetry can significantly simplify the description of the decay by reducing the number of independent form factors. The form factors are related by heavy-quark symmetry to a minimal number of “universal” form factors, sometimes called Isgur-Wise functions. The program of testing heavy-quark symmetry and its corrections, which can be predicted using the HQET expansion, is a central goal in the study of heavy-quark semileptonic decays. It is important to recognize that heavy-quark symmetry does not predict the  $q^2$  dependence itself of the universal form factors. This dependence must be determined separately using nonperturbative techniques, such as lattice QCD calculations or QCD sum rules. These techniques are beginning to provide important quantitative information on the  $q^2$  dependence of the form factors and therefore play a role complementary to HQET.

### C. Plan of the review

Our review is organized in the following way. In Sec. II we introduce many of the theoretical topics, including decay matrix elements, the CKM matrix, and semileptonic decay dynamics from a simple, qualitative point of view. Detailed discussions of theoretical predictions are presented in the later sections on leptonic, inclusive semileptonic, and exclusive semileptonic decays. In Sec. III we briefly discuss the general features of the experiments that have obtained these measurements. Theoretical and experimental studies of lep-

tonic decays are discussed in Sec. IV, which is relatively brief due to the small number of available measurements. We review theoretical and experimental aspects of inclusive semileptonic decays in Sec. V and exclusive semileptonic decays in Sec. VI. In our conclusions, we discuss the implications of these measurements and indicate important areas of research for the future.

Three broad themes underlie our discussion. The first is that semileptonic decays offer a number of different ways to determine the values of  $|V_{cb}|$  and  $|V_{ub}|$ , and that the strengths and weaknesses of these methods derive not only from experimental issues, but also from their sensitivity to the detailed physics of the decay process. For example, inclusive and exclusive methods provide important alternative approaches that have different advantages and disadvantages. Second, the effort to understand the dynamics of semileptonic and leptonic decays is advancing rapidly. The model dependence of theoretical predictions is being reduced, and the development of HQET and nonperturbative methods, such as lattice QCD, is leading to significant gains in understanding. Finally, continued progress ultimately depends on experimental studies using very large data samples. Fortunately, the continued operation and upgrades of the Cornell Electron Storage Ring and the construction of  $B$ -meson factories at the Stanford Linear Accelerator Center and at the KEK laboratory in Japan, as well as  $B$  physics programs at CERN, DESY, and Fermilab, ensure that our knowledge of this physics will continue to expand.

In preparing this review we have used many articles, which we reference throughout the text. Several comprehensive review articles were particularly useful, and we recommend these for alternative treatments of many subjects (Grinstein, 1992; Stone, 1993; Ali, 1994; Morrison and Richman, 1994; Neubert, 1994c). There are also many shorter review articles that have appeared in conference proceedings, such as those by Bortoletto (1992), Artuso (1993), and Poling (1993). The literature on semileptonic decays is enormous, and although we have attempted to provide extensive references, we ask for the tolerance of our many colleagues whose papers are not listed.

## II. THEORY OF LEPTONIC AND SEMILEPTONIC DECAYS

In this section, we present an overview of the theory of leptonic and semileptonic decays, emphasizing general results that are useful for both charm and bottom hadrons. After a brief discussion of the form for the weak-decay matrix elements, we briefly review the phenomenology of the CKM matrix, focusing on the heavy-quark sector. In the final section we discuss the dynamics of semileptonic decays from a qualitative, physical point of view. Detailed discussions of theoretical predictions are presented later, in sections on leptonic decays (Sec. IV.A), inclusive semileptonic decays (Sec. V.B), and exclusive semileptonic decays (Sec. VI.A).

### A. Matrix elements for leptonic and semileptonic decays

The standard model successfully accounts for flavor-changing quark transitions in terms of a  $V-A$  charged weak-

current operator  $\mathcal{J}^\mu$  that couples to the  $W$  boson according to the interaction Lagrangian (Renton, 1990)

$$\mathcal{L}_{int} = -\frac{g}{\sqrt{2}}(\mathcal{J}^\mu W_\mu^+ + \mathcal{J}^{\mu\dagger} W_\mu^-), \quad (6)$$

where for quark transitions

$$\mathcal{J}^\mu = \sum_{i,j} V_{ij} J_{ij}^\mu = \sum_{i,j} \bar{u}_i \gamma^\mu \frac{1}{2}(1 - \gamma_5) V_{ij} d_j. \quad (7)$$

The indices  $i$  and  $j$  run over the three quark generations, so that the field operators  $u_i$  ( $i=1,2,3$ ) annihilate  $u$ ,  $c$ , and  $t$  (or create their antiparticles), and the  $d_j$  annihilate  $d$ ,  $s$ , and  $b$ . Thus the amplitudes for the processes  $d_j \rightarrow W^- u_i$  and  $\bar{u}_i \rightarrow W^- \bar{d}_j$  are proportional to  $V_{ij}$ , whereas the amplitudes for  $u_i \rightarrow W^+ d_j$  and  $\bar{d}_j \rightarrow W^+ \bar{u}_i$  are proportional to  $V_{ij}^*$ .

The coupling of leptons to the  $W$  is also governed by a  $V$ - $A$  charged current. The analog to the CKM matrix for leptons, however, is the unit matrix, because neutrinos are assumed to be exactly massless in the standard model. Leptonic and semileptonic decays result from the  $W$ -mediated interaction between a quark current and a leptonic current.

Generation-changing transitions between quarks are allowed because the CKM matrix  $V$  is nondiagonal. The CKM matrix can be regarded as a rotation from the quark mass eigenstates,  $d$ ,  $s$ , and  $b$ , to a set of new states,  $d'$ ,  $s'$ , and  $b'$ , with diagonal couplings to  $u$ ,  $c$ , and  $t$ . The standard notation is

$$\begin{pmatrix} d' \\ s' \\ b' \end{pmatrix} = \begin{pmatrix} V_{ud} & V_{us} & V_{ub} \\ V_{cd} & V_{cs} & V_{cb} \\ V_{td} & V_{ts} & V_{tb} \end{pmatrix} \begin{pmatrix} d \\ s \\ b \end{pmatrix}. \quad (8)$$

To obtain transition amplitudes, one must sandwich the quark and lepton current operators between physical states. For the leptons, this calculation yields directly an expression in terms of Dirac spinors. The hadronic current, however, cannot be so easily evaluated, since the quarks are embedded in hadrons, and nonperturbative, strong-interaction effects are important in describing the physical states.

For processes with energies much less than the  $W$  mass, one can obtain a useful phenomenological form of the decay amplitude by using an approximate form for the  $W$  propagator and the relation  $G_F/\sqrt{2} = g^2/(8M_W^2)$ . The amplitude for semileptonic decay  $M_{Q\bar{q}} \rightarrow X_{q'\bar{q}} \ell^- \bar{\nu}$  of a meson  $M$  into a meson  $X$  then takes the form (Hagiwara *et al.*, 1989; Gilman and Singleton, 1990)

$$\mathcal{M}(M_{Q\bar{q}} \rightarrow X_{q'\bar{q}} \ell^- \bar{\nu}) = -i \frac{G_F}{\sqrt{2}} V_{q'Q} L^\mu H_\mu, \quad (9)$$

where the leptonic current can be written in terms of Dirac spinors  $u_\ell$  and  $v_\nu$

$$L^\mu = \bar{u}_\ell \gamma^\mu (1 - \gamma_5) v_\nu. \quad (10)$$

The hadronic current  $H_\mu$  in Eq. (9) is related to the matrix element of the operator  $J_\mu$  given in Eq. (7),

$$H_\mu = \langle X | \bar{q}' \gamma_\mu (1 - \gamma_5) Q | M \rangle, \quad (11)$$

but it cannot be calculated in a simple manner. In Sec. VI.A.1 we shall write  $H_\mu$  in terms of form factors, which enable us to isolate the effects of strong interactions on the amplitude. To extract  $V_{q'Q}$  from a measurement of the semileptonic decay rate it is important to gain an understanding of the hadronic current. Some of the theoretical methods used for this purpose are discussed in Secs. VI.A.2 and VI.A.3.

The matrix element for leptonic decay of a pseudoscalar meson is extremely simple, since the only four-vector available to be contracted with the leptonic current  $L^\mu$  is (up to a constant factor)  $q_\mu$ , the four-momentum of the meson (Renton, 1990):

$$\mathcal{M}(M_{Q\bar{q}} \rightarrow \ell^- \bar{\nu}) = i \frac{G_F}{\sqrt{2}} V_{q'Q} f_M L^\mu q_\mu. \quad (12)$$

Because the two initial-state quarks must annihilate, the matrix element is sensitive to the so-called decay constant  $f_M$ , which measures the amplitude for the quarks to have zero separation. Predictions for this process are therefore dependent on knowledge of the initial hadronic bound state. The calculation of meson decay constants, one of the goals of lattice QCD, is discussed in Sec. IV.A.

## B. The Cabibbo-Kobayashi-Maskawa matrix

We now review the properties and phenomenology of the Cabibbo-Kobayashi-Maskawa (CKM) matrix (Cabibbo, 1963; Kobayashi and Maskawa, 1973), emphasizing the heavy-quark sector. The literature contains many discussions of the CKM matrix, including a summary of results by the Particle Data Group (1994), as well as numerous review articles (Rosner, 1992; Buras *et al.*, 1994). Our purpose here is to present the basic phenomenology of the CKM matrix so that the role of semileptonic decays in constraining its elements is apparent. Although we discuss the nature of these constraints below, the numerical results will be presented in the conclusions of this review.

Within the standard model, the values of CKM matrix elements, like fermion masses, are fundamental input parameters and cannot be predicted. In a comprehensive theory of quark flavor—beyond the standard model—these parameters would be explained in terms of other physics or, at the very least, related to a smaller set of constants (Dimopoulos *et al.*, 1992; Anderson *et al.*, 1994). Nevertheless, the standard model provides a key insight: the values of both fermion masses and CKM elements originate in the unknown couplings of the fermions to the Higgs field (Renton, 1990). The Yukawa terms in the Lagrangian that couple the Higgs field to the quarks are not initially diagonal in quark flavor, since this condition is not required for gauge invariance. To determine the quark masses, one must therefore diagonalize the matrices of Yukawa couplings. The CKM matrix is a product of unitary matrices that accomplish this task, and it is therefore unitary by construction.

By using the unitarity condition and removing unphysical quark phases, one can show (Kobayashi and Maskawa, 1973; Nachtman, 1990; Rosner, 1992) that the three-generation CKM matrix contains four independent, real parameters.

These parameters can be selected in many ways, but with three generations there must be exactly one phase factor  $e^{i\delta}$  that cannot be absorbed into the definitions of the quark fields. As a consequence, the CKM matrix must contain a

complex element. A standard parametrization for the CKM matrix used by the Particle Data Group (1994) is the set of angles  $\theta_{12}$ ,  $\theta_{23}$ ,  $\theta_{13}$ , and  $\delta_{13}$ , specifying the rotation

$$V = \begin{pmatrix} c_{12}c_{13} & s_{12}c_{13} & s_{13}e^{-i\delta_{13}} \\ -s_{12}c_{23} - c_{12}s_{23}s_{13}e^{i\delta_{13}} & c_{12}c_{23} - s_{12}s_{23}s_{13}e^{i\delta_{13}} & s_{23}c_{13} \\ s_{12}s_{23} - c_{12}c_{23}s_{13}e^{i\delta_{13}} & -c_{12}s_{23} - s_{12}c_{23}s_{13}e^{i\delta_{13}} & c_{23}c_{13} \end{pmatrix}, \tag{13}$$

where  $c_{12} = \cos\theta_{12}$ ,  $s_{12} = \sin\theta_{12}$ , etc. The phase  $\delta_{13}$  produces  $CP$  violation and would not appear if there were only two generations. [For the case of  $n$  generations, there are  $1/2 n(n-1)$  angles and  $1/2 (n-1)(n-2)$  observable phases (Jarlskog, 1989).] This formidable-looking matrix takes on a simpler form if we use the fact that  $|V_{ub}| \approx 0.003$  is very small, so that  $c_{13}$  is extremely close to unity. We can then neglect terms proportional to  $s_{13}$  relative to terms of order unity, which gives

$$V \approx \begin{pmatrix} c_{12} & s_{12} & s_{13}e^{-i\delta_{13}} \\ -s_{12}c_{23} & c_{12}c_{23} & s_{23} \\ s_{12}s_{23} - c_{12}c_{23}s_{13}e^{i\delta_{13}} & -c_{12}s_{23} & c_{23}c_{13} \end{pmatrix}. \tag{14}$$

Empirically, there is a hierarchy in the magnitudes of CKM elements, which we have already begun to exploit by using the smallness of  $|V_{ub}|$ . This hierarchy motivates a particular expansion of the CKM matrix, first given by Wolfenstein (1983), in the small parameter  $\lambda = \sin\theta_C \approx 0.22$ , where  $\theta_C$  is the Cabibbo angle:

$$V = \begin{pmatrix} V_{ud} & V_{us} & V_{ub} \\ V_{cd} & V_{cs} & V_{cb} \\ V_{td} & V_{ts} & V_{tb} \end{pmatrix} = \begin{pmatrix} 1 - \frac{1}{2}\lambda^2 & \lambda & A\lambda^3(\rho - i\eta) \\ -\lambda & 1 - \frac{1}{2}\lambda^2 & A\lambda^2 \\ A\lambda^3(1 - \rho - i\eta) & -A\lambda^2 & 1 \end{pmatrix} + \mathcal{O}(\lambda^4). \tag{15}$$

The known values of CKM elements can be used to motivate this form, in which only four independent parameters remain:  $A$ ,  $\lambda$ ,  $\rho$ , and  $\eta$ . The  $2 \times 2$  upper left portion of the CKM matrix—the matrix associated with Cabibbo rotations of the  $d$  and  $s$  quarks—is nearly unitary, in accord with experiment. (For example,  $\sqrt{|V_{ud}|^2 + |V_{us}|^2} = 0.999$ .) In the expansion given above, the magnitudes of the off-diagonal elements  $V_{us}$  and  $V_{cd}$  are equal to  $\lambda$ , and the diagonal elements, though nearly unity, have corrections that make the  $2 \times 2$  sector approximately unitary. Even though  $b \rightarrow c$  transitions involve only one generation change, the magnitude of  $V_{cb}$  is measured to be quite small—about 0.04—and is there-

fore of order  $\lambda^2$ . (As a consequence, the  $B$ -meson lifetime is long.) Thus it is natural to write  $V_{cb} = A\lambda^2$ , where  $A$  is a constant of order unity. Measurements also tell us that  $|V_{ub}/V_{cb}| \sim 0.08$ , or  $|V_{ub}| \sim 0.003$ . This suggests that we write  $V_{ub} = A\lambda^3(\rho - i\eta)$ , where we choose to incorporate the phase in this element [in accord with Eq. (14)].

From the unitarity of the third column, the magnitude of  $V_{tb}$  is equal to unity up to corrections of  $\mathcal{O}(\lambda^4)$ . The orthogonality of the second and third columns then gives  $V_{ts} \approx -V_{cb} = -A\lambda^2$ . Finally, orthogonality between the first and third columns specifies  $V_{td} = A\lambda^3(1 - \rho - i\eta)$ . This parametrization is very convenient for understanding how various measurements constrain the CKM matrix and is completely adequate for our purposes. For discussions in which higher accuracy is required, the expansion can be carried out further, as discussed by Buras *et al.* (1994).

By applying the orthogonality condition to the first and third columns, we can obtain a useful relation between the two smallest elements of the CKM matrix,  $V_{ub}$  and  $V_{td}$ :

$$V_{ud}V_{ub}^* + V_{cd}V_{cb}^* + V_{td}V_{tb}^* = 0, \tag{16}$$

in which each term in the sum is of order  $\lambda^3$ . In the parametrization given above,  $V_{cb}$ ,  $V_{cd}$ , and  $V_{tb}$  are real, and by using  $V_{ud} \approx V_{tb} \approx 1$  and  $V_{cd} < 0$  we obtain

$$\frac{V_{ub}^*}{|V_{cd}V_{cb}|} + \frac{V_{td}}{|V_{cd}V_{cb}|} = 1. \tag{17}$$

This relation, which has been emphasized by Bjorken and Chau and Keung (1984), can be represented by a triangle in the complex plane (Fig. 2). In terms of the Wolfenstein parameters given in Eq. (15), the coordinates of the vertices of the triangle are  $(0,0)$ ,  $(1,0)$ , and  $(\rho, \eta)$ . One can show that in order for  $CP$  violation to be permitted in the standard model, the area of this triangle must be nonzero. In particular,  $V_{ub}$  and  $V_{td}$  must be nonzero and complex relative to  $V_{cd}V_{cb}$ . More quantitatively, all  $CP$ -violating amplitudes in the standard model are proportional to the quantity (Jarlskog, 1989)

$$J_{CP} = |\text{Im}(V_{ij}V_{kl}V_{il}^*V_{kj}^*)|, \quad i \neq k, \quad j \neq l, \tag{18}$$

or, in the Wolfenstein parametrization,

$$J_{CP} \approx A^2 \eta \lambda^6. \tag{19}$$

Three of the four CKM parameters— $A$ ,  $\rho$ , and  $\eta$ —can be constrained by information obtained from  $B$  decays. By using Eq. (15), it is easy to see that measurements of  $|V_{cb}|$  and  $|V_{ub}|$  from semileptonic  $B$  decay can be used to calculate

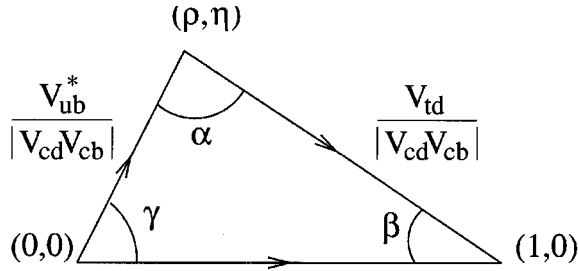


FIG. 2. The triangle expressing the unitarity condition applied to the first and third columns of the CKM matrix. The lengths of the two upper sides are proportional to the magnitudes of the least well known elements of the CKM matrix,  $V_{ub}$  and  $V_{td}$ .

$$|V_{cb}|/|V_{us}|^2 = A \quad \text{and} \quad |V_{ub}^*/V_{cd}V_{cb}| = \sqrt{\rho^2 + \eta^2}. \quad (20)$$

Since  $V_{us}$  and  $V_{cd}$  are well known, measurements of semi-leptonic  $B$  decays allow us to determine both  $A$  and the length of the upper left side of the CKM triangle.

The parameter  $\epsilon$  from  $CP$  violation in the  $K^0\bar{K}^0$  system can also be expressed in terms of  $A$ ,  $\rho$ , and  $\eta$  (Inami and Lim, 1981; Gilman and Wise, 1983; Buras *et al.*, 1984),

$$|\epsilon| = \frac{G_F^2 M_W^2}{6\sqrt{2}\pi^2} \frac{f_K^2 \mathcal{B}_K}{\Delta M_K / M_K} A^2 \lambda^6 \eta [-\eta_{cc} F(y_c) + \eta_{ct} F(y_c, y_t) + \eta_{tt} A^2 \lambda^4 (1-\rho) F(y_t)], \quad (21)$$

where  $y_i = m_i^2 / M_W^2$  ( $i = c, t$ ),  $f_K$  is the  $K$  decay constant, and  $\mathcal{B}_K$  is a phenomenological bag constant parametrizing non-perturbative QCD effects. The factors  $\eta_{cc}$ ,  $\eta_{ct}$ , and  $\eta_{tt}$  are relatively well-known QCD corrections that depend on the heavy-quark masses, and the functions  $F(y_i)$  and  $F(y_i, y_j)$  are defined by

$$F(y_i) = \frac{y_i}{4} \left[ 1 + \frac{9}{1-y_i} - \frac{6}{(1-y_i)^2} - \frac{6y_i^2 \ln y_i}{(1-y_i)^3} \right],$$

$$F(y_i, y_j) = \frac{y_i y_j}{4} \left[ \frac{(y_j^2 - 8y_j + 4) \ln y_j}{(y_j - 1)^2 (y_j - y_i)} - \frac{3}{2(1-y_i)(1-y_j)} + (y_i \leftrightarrow y_j) \right], \quad (22)$$

where the notation  $(y_i \leftrightarrow y_j)$  means that each of the preceding two terms is included with  $i$  and  $j$  interchanged. The largest uncertainty in using these relations has been in the value of  $\mathcal{B}_K$ ; typically, one assumed a range  $\mathcal{B}_K = 0.5$  to  $1$ . Recently, however, lattice QCD calculations (Gupta, 1995) have obtained the much more precise value  $\mathcal{B}_K = 0.75 \pm 0.05$ . Although the error does not include all possible uncertainties, such as that due to the quenched approximation, these are expected to be relatively small in this case. This result indicates that lattice QCD calculations will contribute substantially to our knowledge of  $\mathcal{B}_K$ .

Measurements of the  $B^0\bar{B}^0$  mixing rate allow one to determine  $|V_{td}|$  through the relation (Inami and Lim, 1981)

$$x_d = \frac{\Delta m_{B^0}}{\Gamma_B} = \tau_B \frac{G_F^2}{6\pi^2} M_B (f_B^2 \mathcal{B}_B) \eta_{\text{QCD}} |V_{td}^* V_{tb}|^2 m_W^2 F(y_t), \quad (23)$$

where  $\tau_B$  is the  $B^0$ -meson lifetime,  $f_B$  is the  $B$ -meson decay constant,  $\mathcal{B}_B$  is the  $B$ -meson bag constant ( $\approx 1$ ),  $\eta_{\text{QCD}}$  is a QCD correction factor, and the function  $F(y_i)$  is defined in Eq. (22). (LEP experiments have also performed direct measurements of  $\Delta m_{B^0}$ ; when these are used there is no dependence on  $\tau_B$ .) We can write Eq. (23) in the more convenient form

$$x_d = (3.9 \times 10^3) \left[ \frac{\tau_B}{1.5 \text{ ps}} \right] \left[ \frac{f_B \sqrt{\mathcal{B}_B}}{200 \text{ MeV}} \right]^2 \left[ \frac{\eta_{\text{QCD}}}{0.55} \right] A^2 \lambda^6 [(1-\rho)^2 + \eta^2] F(y_t). \quad (24)$$

Thus  $x_d$  can be used to determine  $\sqrt{(1-\rho)^2 + \eta^2}$ , which corresponds to the length of the upper right-hand side of the CKM triangle. Eventually, it should be possible to determine  $f_B$  from the  $B^- \rightarrow \tau^- \bar{\nu}_\tau$  decay rate, but many more data are required to observe a signal in this mode. For the present, one can take  $f_B$  from lattice QCD calculations, which give typical values ranging from 120 MeV to 230 MeV. It is also very desirable to measure  $x_s$  (the quantity in  $B_s$  mixing analogous to  $x_d$ ). The hadronic uncertainties in predicting the ratio  $x_d/x_s \propto |V_{td}|^2/|V_{ts}|^2$  are less than those for  $x_d$  alone. This measurement is difficult, however, since  $x_s$  is expected to be much larger than  $x_d$ .

The combined constraints on  $A$ ,  $\rho$ , and  $\eta$  arising from these measurements are discussed in the conclusions.

Finally, we note that, because  $|V_{ts}| \approx |V_{cb}|$ , measurements of  $V_{cb}$  are useful in predicting branching fractions for electromagnetic penguin decays  $b \rightarrow s \gamma$ . The  $b \rightarrow s$  transition occurs through a virtual intermediate state  $b \rightarrow Q W^{*-}$ , where the largest contributions come from  $Q = t$  or  $Q = c$ . The  $W^*$  is then absorbed by  $Q$ , producing an  $s$  quark, and the CKM element  $V_{ts}$  enters at this vertex when  $Q = t$ . The photon can be radiated from any of the charged particles in the process. The exclusive decay  $B \rightarrow K^* \gamma$  and the inclusive decay  $B \rightarrow X_s \gamma$  have both been observed by CLEO (Ammar *et al.*, 1993; Alam *et al.*, 1994). The branching fractions for these decays are consistent with the standard-model prediction using  $|V_{ts}| = |V_{cb}|$ , although the statistical uncertainties on the measurements are large. Details on the extraction of  $|V_{ts}|$  from  $B \rightarrow K^* \gamma$  and  $B \rightarrow X_s \gamma$  measurements can be found in Ali and Greub (1993).

Although we shall describe individual CKM measurements in detail later in this paper, it is useful to consider now the major sources of uncertainty that affect them. Generally, one extracts the magnitude of a CKM element in semileptonic  $B$  decays from a measured branching fraction using the formula

$$\mathcal{B}(B_{b\bar{q}} \rightarrow X_{q'\bar{q}} \ell^- \bar{\nu}) = \gamma_{\text{thy}} |V_{q'b}|^2 \tau_B, \quad (25)$$

where  $\gamma_{\text{thy}}$  is a constant obtained from models or theory and  $\tau_B$  is the lifetime of the initial  $B$  meson, or an appropriate average of lifetimes. Theoretical uncertainties are introduced primarily through  $\gamma_{\text{thy}}$ , but also in less obvious ways. The

branching fraction may have been obtained by fitting a measured distribution to theoretically motivated shapes. An example is the inclusive single-lepton spectrum in  $B$  decay, which is fit using theoretical models. Model uncertainties also enter in the conversion from a measured to a produced number of events: this calculation requires an efficiency factor that is usually obtained from Monte Carlo, which uses a model of the decay to simulate the event kinematics. Uncertainty in this model results in an uncertainty in detection efficiency. There is also a significant effect due to the uncertainty on the  $B$  lifetime. As the measured value of the  $B$  lifetime has moved systematically upward, the calculated value of  $|V_{cb}|$  has decreased.

### C. Dynamics of semileptonic decays

We now present a qualitative picture of the dynamics of the semileptonic decay  $M \rightarrow X \ell^- \bar{\nu}$ , where  $M$  is a pseudoscalar meson (a  $D$  or  $B$ ) containing a heavy quark. Much of our discussion concerns the case in which the hadronic system  $X$  is a single meson, usually a pseudoscalar or a vector particle.<sup>1</sup> Although we later discuss measurements of semileptonic decays of charm and bottom baryons, we shall not specifically address the dynamics of such decays here. We refer the reader to Sec. VI.G and references therein for theoretical discussions of these decays.

A powerful tool for describing the dynamics of semileptonic decay is the Dalitz plot, which maps the probability for different kinematic configurations over the allowed region of phase space. Figure 3 is based on a Monte Carlo simulation of a sample of  $B \rightarrow D^* \ell^- \bar{\nu}$  decays, which we have generated using HQET-based parameters given by Neubert (1994c). (These predicted values are similar to the measured values from CLEO; see Sec. VI.E.5) In this plot, each point represents a single  $B \rightarrow D^* \ell^- \bar{\nu}$  decay. Because we have selected Dalitz-plot variables (energies or squared masses), phase space is uniform over the plot, so that a constant matrix element would give a uniformly distributed set of points. In this section we analyze the physical significance of different Dalitz-plot regions and qualitatively explain the pattern shown in Fig. 3.

For Dalitz-plot variables, we have chosen  $E_\ell$ , the energy of the lepton measured in the rest frame of the initial meson  $M$  (whose mass is also labeled  $M$ ), and  $q^2$ , the variable mass-squared of the  $W^*$ :

$$q^2 = m_{W^*}^2 = (p_\ell + p_{\bar{\nu}})^2 = (P - p_X)^2 = M^2 + m_X^2 - 2ME_X, \quad (26)$$

where  $P$  is the four-momentum of  $M$  and  $E_X$  is the energy of  $X$  in the  $M$ -meson rest frame. For a given lepton energy  $E_\ell$ , the allowed range of  $q^2$  is given by

<sup>1</sup>Multibody, nonresonant final states have not been observed in  $D$  semileptonic decays, and the known resonant exclusive modes come close to saturating the inclusive semileptonic rate. In  $B$  decays, the two modes  $B \rightarrow D \ell^- \bar{\nu}$  and  $B \rightarrow D^* \ell^- \bar{\nu}$  account for about two-thirds of the semileptonic rate. Part of the remainder appears to be due to  $D^{**}$  production, but there is still room for nonresonant final states, and we shall see that in certain kinematic regions (low  $q^2$ ) they could play an important role.

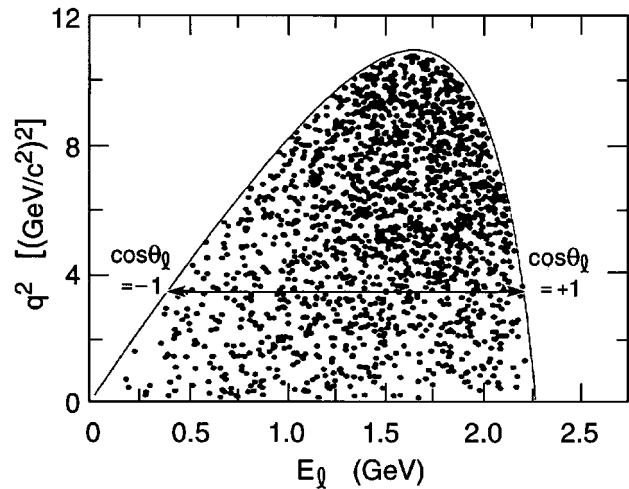


FIG. 3. A Monte Carlo simulation of the Dalitz plot for the process  $B \rightarrow D^* \ell^- \bar{\nu}$ , using HQET-based form factors from Neubert (1994c). The form factors are largest at high  $q^2$ , which increases the density of points towards the top of the plot. At a fixed value of  $q^2$ , the range in lepton energies from left to right corresponds to the variation of  $\cos\theta_\ell$ , where  $\theta_\ell$  is the polar angle of the lepton in the  $W^*$  rest frame, from  $-1$  to  $+1$  (see Fig. 5). The increase in density across the Dalitz plot from left to right can be traced to the  $\cos\theta_\ell$  distribution, which is asymmetric due to the  $V-A$  coupling. This coupling enhances the amplitude for the negative-helicity state of the  $W^*$  relative to the positive-helicity state. Special cases occur at  $q^2_{\max}$ , where the  $W^*$  (or the  $D^*$ ) is unpolarized, and at  $q^2=0$ , where it is in a pure helicity-zero state.

$$(m_\ell \approx 0) \Rightarrow q^2 \leq 2ME_\ell + \frac{2m_X^2 E_\ell}{2E_\ell - M}, \quad (27)$$

which defines the boundary of the physical region.

Because  $q^2$  is such an important quantity, we digress briefly to discuss how it is determined experimentally. Broadly speaking, there are two possible approaches. In an exclusive process (where  $X$  is a particular hadronic final state), one can measure  $q^2$  by identifying  $X$  or its decay products, measuring the energy of  $X$ , and transforming the energy to the rest frame of the decaying particle  $M$ . Equation (26) is then used to compute  $q^2$ . The determination of the  $M$  rest frame is not something to be taken for granted, because there is an unobserved particle, the neutrino. In fixed-target charm experiments,  $q^2$  is determined only up to a quadratic ambiguity, because the charm-meson direction, but not its energy, is determined by high-resolution tracking detectors. For  $B$  mesons produced in the process  $Y(4S) \rightarrow B\bar{B}$ , the  $B$  is produced nearly at rest in a symmetric-energy colliding-beam machine so, to a good approximation, the rest frame of the  $B$  coincides with that of the detector.

Much less common is a second approach to measuring  $q^2$  that can sometimes be used for inclusive measurements. In such measurements, the system  $X$  ranges over all allowed hadronic states but none are actually reconstructed. Thus  $q^2$  cannot be measured with the technique used for exclusive studies. With hermetic detectors, however, one can measure a missing-momentum vector for the event that can, to some approximation, be associated with the neutrino. Then  $q^2$  can be calculated from the lepton and neutrino momenta. This approach suffers from poorer resolution, both because par-

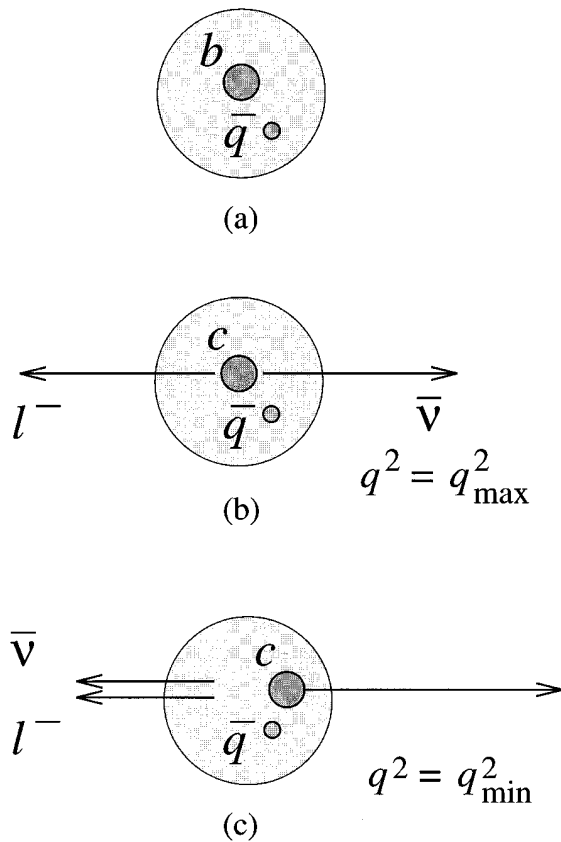


FIG. 4. Kinematic configurations for the semileptonic decay of a  $B$  meson: (a)  $B$  meson before decay; (b) decay configuration for  $q^2 = q^2_{\max}$ , where the form factors are largest for producing a  $D$  or  $D^*$  meson in the final state; and (c) configuration for  $q^2 = q^2_{\min}$ , where the form factors are smallest. There may well be significant production of nonresonant final states in the low- $q^2$  region, especially in  $b \rightarrow u \ell^- \bar{\nu}$  decays, where the recoil velocity is high.

ticles other than the neutrino, such as  $K_L$ 's, may not be observed, and because in colliding-beam detectors the component of the missing momentum along the beam direction is not always well measured. Nevertheless, even a crudely measured inclusive  $q^2$  distribution can be of interest, as in the case of  $b \rightarrow u \ell^- \bar{\nu}$  decays.

Our goal here is to understand qualitatively how the Dalitz-plot variables  $q^2$  and  $E_\ell$  are related to the underlying physics of the decay. Distributions of these variables are determined by two effects: the dynamics of the formation of the hadronic system  $X$  and the spin structure of the decay. We now analyze these effects, starting with the variable  $q^2$ .

Figure 4 compares the kinematics of decays at high and low values of  $q^2$ . The initial meson, which contains a  $b$  quark and a spectator quark  $\bar{q}$ , is shown in Fig. 4(a). At high  $q^2$  [Fig. 4(b)], the masses of the  $W^*$  and the daughter hadron take up most of the available energy, so the  $W^*$  is produced nearly at rest. The lepton and the neutrino are then produced nearly back-to-back, and the daughter quark receives little or no momentum kick.<sup>2</sup> The “zero-recoil” configuration, where

<sup>2</sup>This situation contrasts with that in a scattering process, where the minimum kick occurs at  $q^2 = 0$ . In a scattering process this is, however, still the highest value of  $q^2$ , which is either negative or zero.

$E_X = m_X$  and  $q^2_{\max} = (M - m_X)^2$ , is typically the most favorable for the formation of a low-mass meson. The motion of the daughter quark relative to the spectator quark and the gluons—the so-called light degrees of freedom—is then very similar to what it was before the decay. If both the initial and final quarks are heavy compared with  $\Lambda_{\text{QCD}}$ , as in a  $b \rightarrow c \ell^- \bar{\nu}$  decay, then the light degrees of freedom are almost completely undisturbed when  $q^2 \approx q^2_{\max}$ : a heavy, static source of color field at the center of the meson is replaced by a color source of a different flavor, but the color field is not changed. Relativistic effects, which depend on the mass of the heavy quark, become negligible. For example, the color magnetic moment of the heavy quark is proportional to  $1/m_Q$ . These observations are among the key ideas in HQET, which we discuss further in Sec. VI.A.3.

The region of phase space around the  $q^2_{\max}$  configuration is therefore quite special. The spectator quark and the daughter quark are produced in a state that has a large overlap with the wave function of an ordinary nonexcited meson. Thus the rates for decays like  $D \rightarrow \bar{K}^* \ell^+ \nu$  or  $B \rightarrow D^* \ell^- \bar{\nu}$  are largest at  $q^2_{\max}$  and decrease as  $q^2$  decreases, or as the hadronic recoil velocity increases. We can see this effect in Fig. 3: the density of points is highest at the top of the allowed region and becomes significantly smaller toward the bottom. We note, however, that the probability distribution of  $q^2$  does not peak at  $q^2_{\max}$  but somewhat below, because at  $q^2_{\max}$  the amount of phase space goes to zero.

At the minimum value of  $q^2$ ,  $q^2_{\min} = m_\ell^2$ , the lepton and neutrino momenta are parallel [Fig. 4(c)]. Except for the case  $\ell = \tau$ ,  $q^2_{\min} = 0$  is a very good approximation. In low- $q^2$  configurations, the daughter quark  $q'$  recoiling against the  $W^*$  receives a large kick and initially moves rapidly with respect to the spectator quark  $\bar{q}$ . For these particles to form a bound state, gluons must be exchanged in order to transfer momentum to the light degrees of freedom of the meson. As a consequence, the  $q^2 = 0$  configuration is typically the least favorable for the formation of a meson. (There are, however, important spin-related effects that we shall discuss later in this section.) Theoretical calculations are usually difficult at low  $q^2$ , because the hadronic system is highly disturbed, and it is at  $q^2 = 0$  that one might expect significant production of nonresonant final states to occur, in analogy to QCD jets.

For semileptonic decays in which both initial and final quarks are heavy, the form factors can be related to those for elastic scattering of a meson containing a heavy quark. Such a form factor gives the amplitude that a meson will remain intact if its heavy quark is suddenly given a kick with respect to the light degrees of freedom. As in the case of decay, gluons must be exchanged between the struck heavy quark and the light degrees of freedom if the meson is to remain intact. It is clear that the form factors describe nonperturbative QCD effects, and it should not be surprising that they are difficult to calculate.

The importance of the variation of the form factors with  $q^2$  in a particular decay depends partly on the kinematic range of  $q^2$ . For example, the  $q^2$  range is larger in  $b \rightarrow u \ell^- \bar{\nu}$  decays than in  $b \rightarrow c \ell^- \bar{\nu}$  decays, because the  $u$  quark is much lighter than the  $c$ . This point is discussed in Sec. VI.A.2 and Sec. VI.A.3.

The observed  $q^2$  distribution can be strongly affected by the spin of the particle  $X$ . Because the  $W^*$  behaves like a spin-1 particle,<sup>3</sup> the decay  $D \rightarrow KW^*$ , for example, must be a  $P$ -wave process, whereas  $D \rightarrow K^*W^*$  can occur in an  $S$ ,  $P$ , or  $D$  wave. As a consequence, the decay rate when  $X$  is a pseudoscalar meson contains a factor  $|\mathbf{p}_X|^3$ . [The complete result is given in Eq. (110) in Sec. VI.A.5]. As can be seen from Eq. (26),  $|\mathbf{p}_X|=0$  at  $q^2=q_{\max}^2$ , so the  $|\mathbf{p}_X|^3$  factor suppresses the rate at high  $q^2$ , where the large form-factor values would ordinarily lead to a large decay rate. (Alternatively, one can easily see that such a decay must be forbidden at  $q_{\max}^2$ , because the back-to-back lepton-neutrino system has one unit of angular momentum along its line of flight, and this angular momentum cannot be canceled by the daughter pseudoscalar meson.) If Fig. 3 were made for  $B \rightarrow D\ell^-\bar{\nu}$  rather than for  $B \rightarrow D^*\ell^-\bar{\nu}$ , the density of points in the upper region would be significantly reduced. This effect also tends to reduce the overall rate for pseudoscalar final states relative to vector final states, for which the decay can proceed in an  $S$  wave or  $D$  wave as well. The dramatic result of the  $P$ -wave suppression will be seen directly in Fig. 26 for  $D \rightarrow \bar{K}\ell^+\nu$ . Finally, we note that the  $q^2$  distribution will be different if the final-state meson has orbital excitation; under such circumstances the typical value of  $q^2$  can be pushed significantly lower.

Having discussed the physics that controls the  $q^2$  distribution, we turn now to the factors that influence the distribution of  $E_\ell$ . We can see directly from Fig. 3 that if phase space were populated uniformly, then the lepton-energy spectrum would be peaked toward the high end. However, the lepton-energy spectrum is strongly affected by three aspects of the dynamics: (1) the  $V$ - $A$  coupling, (2) the quantum numbers of the particle  $X$ , and (3) the distribution in  $q^2$ . We now consider each of these in turn.

A direct consequence of the  $V$ - $A$  coupling is that the charged lepton and the neutrino share the available energy differently for charm and bottom decays. The processes  $b \rightarrow c\ell^-\bar{\nu}$  and  $b \rightarrow u\ell^-\bar{\nu}$  produce  $c$  and  $u$  quarks that are predominantly helicity  $\lambda = -1/2$  in association with a charged lepton that is almost purely helicity  $\lambda = -1/2$ . The decays  $c \rightarrow s\ell^+\nu$  and  $c \rightarrow d\ell^+\nu$  also produce predominantly  $\lambda = -1/2$   $s$  and  $d$  quarks, but they are in association with a charged lepton that is almost purely  $\lambda = +1/2$ . As a result, the collinear configuration in which the charged lepton recoils against the daughter quark and the neutrino—the configuration leading to the highest lepton energy—is allowed for  $b$ -quark decays but forbidden by angular momentum conservation for  $c$ -quark decays. Thus, in the case of  $b$  (or  $\bar{b}$ ) decay, the lepton-energy spectrum peaks at a higher energy than the neutrino spectrum; the reverse is true for  $c$  decays.

<sup>3</sup>Even though the  $W^*$  is virtual, any  $J=0$  component in its wave function can be neglected when the charged lepton is sufficiently light—either an electron or a muon. In that case, the  $\ell^-\bar{\nu}$  system has  $J_z = -1$  along the  $\ell^-\bar{\nu}$  axis in the  $W^*$  rest frame, which excludes  $J=0$ . More formally, we shall see that certain form factors cannot significantly affect the decay unless the charged lepton is heavy, as for  $\ell = \tau$ .

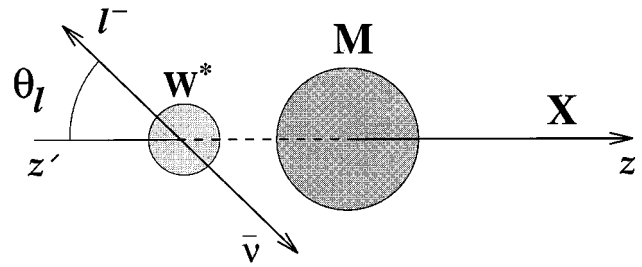


FIG. 5. The polar angle  $\theta_\ell$  is defined in the rest frame of the  $W^*$ , in which the charged lepton and the neutrino are back-to-back. The angle is measured with respect to the axis  $z'$  pointed opposite to the momentum vector of  $X$ , the daughter meson. Due to the Lorentz boost between the  $W^*$  and  $M$  rest frames, leptons with small values of  $\theta_\ell$  have higher energy in the  $M$  rest frame than leptons with large values of  $\theta_\ell$ , at fixed  $q^2$ .

The argument we have given ignores the quantum numbers of the meson  $X$ , but these are quite important in determining the lepton-energy spectrum in an exclusive decay. In particular, the  $V$ - $A$  effect described above is important when  $X$  is a spin-1 particle but is masked when  $X$  has spin 0. These effects are best understood by relating, via a Lorentz transformation, the distribution of  $E_\ell$  (in the rest frame of the parent meson  $M$ ) to the angular distribution of the charged lepton in the  $W^*$  rest frame. We define the angle  $\theta_\ell$  (Fig. 5) as the polar angle of the lepton in the  $W^*$  rest frame, with respect to the direction of the  $W^*$  momentum vector in the  $M$  rest frame. (In the  $M$  rest frame,  $\mathbf{p}_{W^*} = -\mathbf{p}_X$ .) Ignoring the charged-lepton mass, its energy in the  $W^*$  rest frame is simply  $E_\ell^{[W]} = 1/2\sqrt{q^2}$ . However, leptons going forward (along  $\mathbf{p}_{W^*}$ ) in the  $W^*$  rest frame are given a higher energy in the  $M$  rest frame, due to the boost, than those going backward. From the Lorentz transformation to the  $M$  rest frame,

$$E_\ell = \frac{1}{2}[(E_\ell^{\max} + E_\ell^{\min}) + (E_\ell^{\max} - E_\ell^{\min})\cos\theta_\ell], \quad (28)$$

where

$$E_\ell^{\max,\min} = \frac{1}{2M} \left[ \frac{1}{2}(M^2 + q^2 - m_X^2) \pm M|\mathbf{p}_X| \right] \quad (29)$$

and

$$|\mathbf{p}_X| = \sqrt{\frac{(M^2 - q^2 + m_X^2)^2}{4M^2} - m_X^2}. \quad (30)$$

As  $q^2$  increases, the lepton energy tends to increase as well, because

$$\frac{1}{2}(E_\ell^{\max} + E_\ell^{\min}) = \frac{(M^2 + q^2 - m_X^2)}{4M}. \quad (31)$$

The range of lepton energies observed in the  $M$  rest frame, however, decreases as  $q^2$  increases, because  $(E_\ell^{\max} - E_\ell^{\min}) = |\mathbf{p}_X| = |\mathbf{p}_{W^*}|$  decreases as the boost becomes smaller. At  $q^2 = q_{\max}^2$ , the  $W^*$  and the  $X$  system are each at rest in the  $M$  rest frame and the lepton energy is the same for all angles  $\theta_\ell$ . Both of these features—the increase in  $1/2(E_\ell^{\max} + E_\ell^{\min})$  with  $q^2$  and the diminishing range in lepton energies—are simply phase-space effects and can be seen directly from the shape of the Dalitz-plot boundary in Fig. 3.

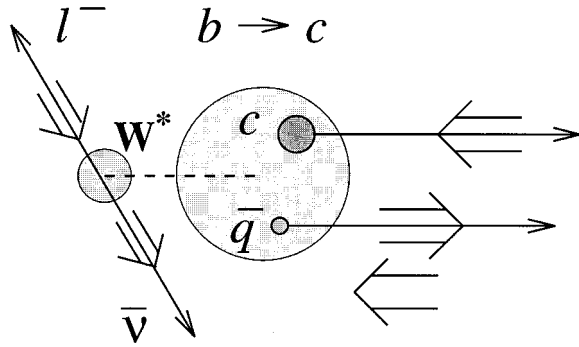


FIG. 6. In  $B$  semileptonic decay, the  $V-A$  coupling at the  $b \rightarrow c$  (or  $b \rightarrow u$ ) vertex produces a  $c$  quark that is predominantly helicity  $\lambda = -1/2$ . In the simple model shown here, the helicity of the meson  $X$  is then determined by whether the  $c$  quark combines with a spectator quark that has  $\lambda = +1/2$  or helicity  $\lambda = -1/2$ . If  $X$  is a spin-zero meson, only  $\lambda = 1/2$  spectator quarks can contribute. If  $X$  has spin 1, both helicities of the spectator quark contribute, leading to  $X$  helicities of  $\lambda = 0$  and  $\lambda = -1$ , but not  $\lambda = +1$ . It is easy to see that this  $V-A$  effect, combined with overall angular momentum conservation, results in a harder energy spectrum for the charged lepton than for the neutrino, as observed in the rest frame of  $M$ .

It is clear that to predict the observed lepton-energy spectrum, one must understand the physics underlying the distribution of  $\cos\theta_\ell$ . This distribution is connected to both the  $V-A$  couplings and to the quantum numbers of  $X$ . In  $b$ - or  $c$ -quark semileptonic decay, the daughter-quark helicity is predominantly  $\lambda = -1/2$ . If this quark combines with the spectator quark to form a pseudoscalar meson, as in  $B \rightarrow D \ell^- \bar{\nu}$ ,  $B \rightarrow \pi \ell^- \bar{\nu}$ , or  $D \rightarrow \bar{K}^* \ell^+ \nu$ , the helicity information is lost, since the helicity of the meson must be zero. Because the initial meson has spin zero, angular momentum conservation forces the  $W^*$  to have helicity zero as well, and  $dN/d\cos\theta_\ell \propto \sin^2\theta_\ell$ , independent of the value of  $q^2$ .

If, however, the daughter quark and the spectator form a spin-1 meson, as in  $D \rightarrow \bar{K}^* \ell^+ \nu$ ,  $B \rightarrow D^* \ell^- \bar{\nu}$ , or  $B \rightarrow \rho \ell^- \bar{\nu}$ , then the helicity information is not lost. It is manifested as a higher probability for the vector meson to have helicity  $\lambda = -1$  than  $\lambda = +1$ . Roughly speaking, a rapidly recoiling  $\lambda = -1/2$  daughter quark can combine with the spectator quark to form a  $\lambda = -1$  or  $\lambda = 0$  meson, as shown in Fig. 6. (This description is not appropriate when the daughter quark is nonrelativistic, or when the  $W^*$  is massless, as discussed below.) The probabilities for different vector-meson helicities also apply to the  $W^*$  because, to conserve overall angular momentum, the helicities of the  $W^*$  and the vector meson must be the same.

The predominance of  $\lambda_{W^*} = -1$  over  $\lambda_{W^*} = +1$  affects the lepton spectrum differently for  $b$ - and  $c$ -quark decays. In  $b$ -quark decay, the process  $W^{*-} \rightarrow \ell^- \bar{\nu}$  produces a  $\lambda = -1/2$  charged lepton; for  $\lambda_{W^*} = +1$  this lepton has a  $(1 \pm \cos\theta_\ell)^2$  angular distribution in the  $W^*$  rest frame. The Lorentz boost then typically produces a hard lepton spectrum for  $\lambda_{W^*} = -1$  and a soft lepton spectrum for  $\lambda_{W^*} = +1$ . Thus, for  $B$  decays to a spin-1 particle, the lepton spectrum is harder than the neutrino spectrum. For  $D$  decay, the process  $W^{*+} \rightarrow \ell^+ \nu$  produces a  $\lambda = +1/2$  charged lepton, so decays to a spin-1 meson lead to a softer energy spectrum for the lepton than for the neutrino. Similar arguments show that the

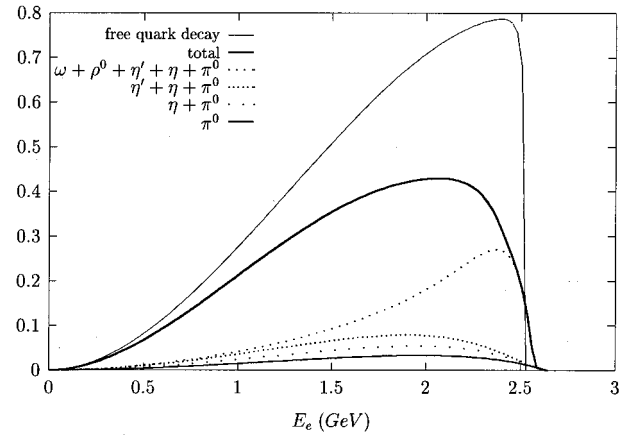


FIG. 7. The lepton-energy spectrum for  $b \rightarrow u \ell^- \bar{\nu}$  decays as calculated by Scora (1993). For reasons discussed in the text, the spectra for  $B \rightarrow \rho \ell^- \bar{\nu}$  and  $B^- \rightarrow \omega \ell^- \bar{\nu}$  are peaked at higher energies than that for  $B \rightarrow \pi \ell^- \bar{\nu}$ . The dark solid curve (total) gives the total rate for all exclusive modes that are expected to be important in the end-point region and includes radially excited and  $P$ -wave mesons up to a mass of about 2 GeV/ $c$ . Also shown for comparison is the lepton-energy spectrum from a simple free-quark decay calculation. The shape of the spectrum in the end-point region from such a calculation is not expected to be reliable. (More sophisticated calculations of the inclusive lepton-energy spectrum are discussed in Sec. V.B.) Used with permission of D. Scora.

shape of the spectrum is independent of whether the decay meson is a particle or an antiparticle.

Finally, the lepton-energy spectrum is affected by the  $q^2$  distribution. If  $q^2$  is forced to be high by the behavior of the form factors,  $E_\ell$  will also tend to be large [see Eq. (31)]. Conversely, in decays in which  $X$  is a spin-0 particle, the  $P$ -wave effect suppresses high- $q^2$  decays, softening the lepton-energy spectrum.

As a general rule, in  $B$  ( $D$ ) decays the process  $P \rightarrow V \ell \nu$  tends to have a harder (softer) lepton-energy spectrum than  $P \rightarrow P' \ell \nu$ , where  $P$  and  $P'$  represent pseudoscalars and  $V$  represents a vector meson. In  $B$  decays, the difference between the spectra is a consequence of both the  $V-A$  enhancement of high-energy leptons in  $P \rightarrow V \ell \nu$  and the  $P$ -wave effect in  $P \rightarrow P' \ell \nu$ , which tends to lower its average  $q^2$  and consequently the average lepton energy. An important consequence of these arguments is that, in  $b \rightarrow u \ell^- \bar{\nu}$  decays,  $B \rightarrow \rho \ell^- \bar{\nu}$  and  $B^- \rightarrow \omega \ell^- \bar{\nu}$  are expected to contribute more to the end-point region of the lepton-energy spectrum than  $B \rightarrow \pi \ell^- \bar{\nu}$ . Figures 7 and 8, from a theoretical calculation by Scora (1993), illustrate these features of the lepton-energy spectra, which are essentially model independent.

The simplified arguments we have made do not hold at  $q^2 = q_{\max}^2$  or at  $q^2 = 0$ . At  $q_{\max}^2$ , the daughter vector meson is at rest. Its helicity is therefore undefined, and both the vector meson and the  $W^*$  are unpolarized. As a result, the  $\cos\theta_\ell$  distribution becomes uniform at high  $q^2$ . At small values of  $q^2$ , the lepton and neutrino become parallel in the  $M$  rest frame, and their combined spin projection along their direction of motion is zero. The helicity  $\pm 1$  components are ab-

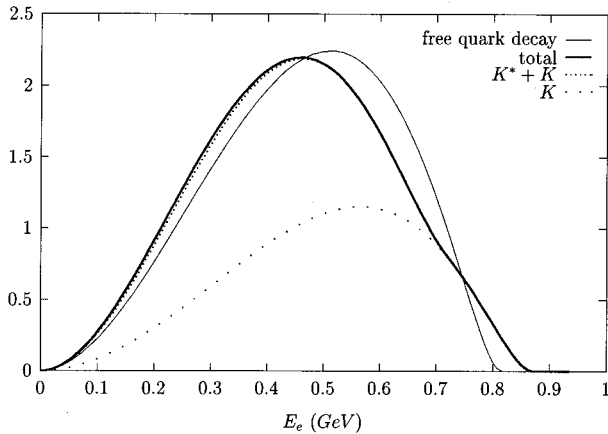


FIG. 8. The lepton-energy spectra for  $D \rightarrow \bar{K} \ell^+ \nu$  and  $D \rightarrow \bar{K}^* \ell^+ \nu$  decays as calculated by Scora (1993). In contrast to  $B$  decay, the mode with a vector meson has a softer lepton-energy spectrum than that with a pseudoscalar meson. Used with permission of D. Scora.

sent, and there is no lepton forward-backward asymmetry in the  $W^*$  frame. The helicity of the vector meson must also be zero in this configuration.

We now summarize our understanding of the Dalitz plot for  $B \rightarrow D^* \ell^- \bar{\nu}$  in Fig. 3. Near the top of the plot, where  $q^2$  is large, the  $D^*$  is moving very slowly and is nearly unpolarized:  $\lambda = -1, 0,$  and  $+1$  are present in approximately equal amounts. The distribution of  $\cos\theta_\ell$  is then uniform because the  $W^*$  is also unpolarized. The form factors are largest in this region, accounting for the high density of points. As  $q^2$  decreases, the  $\lambda = -1$  component of the  $D^*$  begins to dominate the  $\lambda = +1$  component, which explains the excess of points on the right side of the Dalitz plot compared with the left side. At the lowest value of  $q^2$ , the charged lepton and the neutrino are parallel in the lab frame, leading to maximum  $D^*$  recoil, and both the  $D^*$  and  $W^*$  are forced into a pure  $\lambda = 0$  state. There is no asymmetry in the  $\cos\theta_\ell$  distribution at  $q^2 = 0$ : its distribution at this edge of phase space is  $dN/d\cos\theta_\ell \propto \sin^2\theta_\ell$ . This effect can be seen in Fig. 3 in the depletion of points at high and low lepton energies for small values of  $q^2$ .

Although these simple arguments are useful for a qualitative discussion, a detailed calculation of the form factors is required to give the  $q^2$  dependence of each helicity amplitude. Conversely, it is by measuring the  $q^2$  and angular distributions that one can obtain information on the form factors. We shall discuss the form factors and helicity amplitudes in much more detail in Sec. VI.A (see, in particular, Fig. 25).

### III. GENERAL REMARKS ON EXPERIMENTAL TECHNIQUES

Hadrons containing charm or bottom quarks can be produced in a large variety of experimental environments:  $e^+e^-$  annihilation; collisions of hadrons, photons, or neutrinos with nuclear targets; and collisions of hadrons with

beams of other hadrons. In practice, most studies of charm semileptonic decays are performed in  $e^+e^-$  colliding-beam and fixed-target experiments. Data on bottom semileptonic decays come almost entirely from  $e^+e^-$  experiments operating at a resonance, either  $e^+e^- \rightarrow Y(4S) \rightarrow B\bar{B}$  or  $e^+e^- \rightarrow Z \rightarrow b\bar{b}$ . In this section, we discuss some of the features of experiments that have contributed to our knowledge of charm and bottom semileptonic decays. We divide our discussion into sections describing charm experiments, bottom experiments, lepton identification, and the branching fractions and lifetimes that are assumed throughout this paper. More details are given in the sections describing measurements of individual decay modes.

#### A. Charm-hadron experiments

Early studies of semileptonic charm decays came from  $e^+e^-$  colliding-beam experiments operating at or above the  $\psi(3770)$  resonance at the SPEAR storage ring at SLAC. The processes  $\psi(3770) \rightarrow D^0 \bar{D}^0$  and  $\psi(3770) \rightarrow D^+ D^-$  occur so close to threshold that  $D$  mesons are the only hadrons produced, without any accompanying pions. Using this technique, the Mark III experiment at SPEAR recorded about 50 000  $D\bar{D}$  pairs. Many subsequent experiments have studied charm decays using the continuum process  $e^+e^- \rightarrow c\bar{c}$ . The BES experiment in Beijing is analyzing  $D_s$  mesons produced at a center-of-mass energy of 4.0 GeV. The CLEO experiment at the CESR storage ring (Cornell) and ARGUS at the DORIS ring (Hamburg) have performed many studies of charm semileptonic decays by using continuum production at or near the  $Y(4S)$  resonance, where they are studying  $B$  mesons. For example, the CLEO collaboration has a sample of nearly four million  $e^+e^- \rightarrow c\bar{c}$  events. Table I lists the charm and bottom data samples for  $e^+e^-$  colliding-beam experiments. The term CLEO II refers to the CLEO detector after the installation of a CsI calorimeter and other improvements. Because this upgrade vastly improved the detector and because the largest data samples have been obtained after the upgrade, there are very few CLEO I results that are still competitive.

The major advantage offered by  $e^+e^-$  annihilation is that the fraction of hadronic events containing heavy quarks is relatively large. In the CLEO experiment, the  $e^+e^-$  collision energy is usually set to the  $Y(4S)$  mass, 10.58 GeV. The  $Y(4S)$  cross section is about 1.07 nb and is exceeded slightly by the continuum production of charm:  $\sigma(e^+e^- \rightarrow c\bar{c}) \approx 1.2$  nb. These are both reasonably large compared with the total continuum hadronic cross section,  $\sigma(e^+e^- \rightarrow q\bar{q}) \approx 3.3$  nb, where  $q\bar{q}$  represents the sum of  $u\bar{u}$ ,  $d\bar{d}$ ,  $s\bar{s}$ , and  $c\bar{c}$ . The continuum events at this energy have a very jetlike (collimated) topology, in contrast to the much more spherical distribution of tracks in  $B\bar{B}$  events.

Charm production in fixed-target experiments presents a situation that is complementary to that in  $e^+e^-$  collisions: the production cross sections are higher, but the fraction of hadronic events containing charm is much smaller. For example, charm production cross sections for protons incident on a nuclear target are (Appel, 1992) 20  $\mu\text{b}$  to 40  $\mu\text{b}$  for proton momenta in the range 400 GeV/c to 800 GeV/c, but these events represent only about  $10^{-3}$  of the total cross

TABLE I. Summary of charm and bottom samples produced in  $e^+e^-$  colliding-beam experiments. The numbers given for  $Z$  bosons refer to hadronic decays only.

Experiment	$\sqrt{s}$	$\int \mathcal{L} dt$	Produced charm
Mark III	3.77 GeV	9 pb <sup>-1</sup>	28 000 $D^0\bar{D}^0$ 20 000 $D^+D^-$
	4.14 GeV	6 pb <sup>-1</sup>	3 000 $D_s\bar{D}_s$
BES	4.03 GeV	9 pb <sup>-1</sup>	6 000 $D_s\bar{D}_s$
CLEO II	$\approx 10.5$ GeV	3.0 fb <sup>-1</sup>	$4 \times 10^6$ $c\bar{c}$
ARGUS	$\approx 10.5$ GeV	0.5 fb <sup>-1</sup>	$0.7 \times 10^6$ $c\bar{c}$
LEP	91 GeV	$1.6 \times 10^6$ $Z$ 's	220 000 $c\bar{c}$
SLD	91 GeV	per experiment $100 \times 10^3$ $Z$ 's	per experiment 14,000 $c\bar{c}$
Experiment	$\sqrt{s}$	$\int \mathcal{L} dt$	Produced bottom
CLEO II	10.58 GeV	2.0 fb <sup>-1</sup>	$2 \times 10^6$ $B\bar{B}$
ARGUS	10.58 GeV	0.2 fb <sup>-1</sup>	$2 \times 10^5$ $B\bar{B}$
LEP	91 GeV	$1.6 \times 10^6$ $Z$ 's	350 000 $b\bar{b}$
SLD	91 GeV	per experiment $100 \times 10^3$ $Z$ 's	per experiment 22 000 $b\bar{b}$

section. Photoproduction, in which a high-energy photon beam interacts with a nuclear target, has a lower charm cross section, but the ratio of charm-to-total cross sections is more favorable. The pioneering Fermilab experiment E691 measured a charm photoproduction cross section of about  $0.5 \mu\text{b}$ , or 0.5% of the  $100 \mu\text{b}$  total hadronic cross section. Table II lists the data samples and the number of fully reconstructed charm decays for fixed-target experiments at Fermilab and at CERN.

The challenge for fixed-target experiments is therefore to suppress a very large background from light-quark production. To achieve this goal, experiments exploit the relatively long charm-hadron lifetimes ( $10^{-13}$  s to  $10^{-12}$  s), which, together with the relativistic-boost factor, enable charm particles to travel measurable distances from the primary production point before they decay, producing a distinct, separated decay vertex. With precision particle-tracking detectors (vertex detectors), the presence of such secondary decay vertices can be detected, allowing charm decay events to be distinguished from the light-quark background. Studies of

$D^+$  semileptonic decays are easier than those of the  $D^0$ , because the  $D^+$  lifetime is about 2.5 times longer.

Most vertex detectors are based on silicon microstrip devices, which can be quickly read out and which have position resolutions for charged particles in the range  $5 \mu\text{m}$  to  $20 \mu\text{m}$ , about an order of magnitude better than conventional tracking devices based on wire chambers. The vertex detector is placed a short distance downstream from the target and is followed by a large spectrometer with components for momentum measurement and particle identification. The E691 experiment, shown in Fig. 9, was able to use a loose trigger and reconstructed a few hundred events in a typical semileptonic  $D$ -meson decay mode. Recently, the photoproduction experiment E687 and hadroproduction experiment E791 (both at Fermilab) have accumulated large samples of charm decays and have demonstrated charm signals in hadronic decay modes corresponding to about 10 and 20 times the E691 sample, respectively, with comparable signal-to-background ratios. In the WA75 experiment at CERN and E653 at Fermilab, fewer events were recorded, but a specialized muon

TABLE II. Fully reconstructed charm samples in fixed-target experiments.

Experiment	Year completed	Events recorded/ $10^6$	Fully reconstructed charm decays
Photoproduction:			
E691	1985	100	10 000
E687	1992	500	100 000
Hadroproduction:			
WA75		2	350
NA32 (ACCMOR)	1986	17	1 300
WA82	1989	10	3 000
E653	1988	10	1 000
E769	1988	500	4 000
E791	1992	20 000	200 000

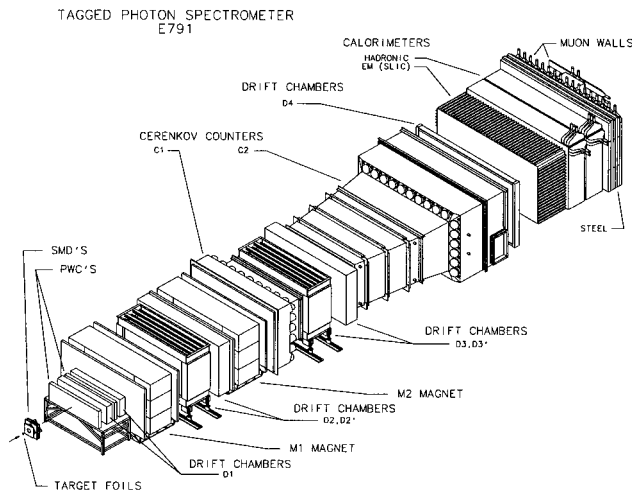


FIG. 9. The spectrometer used for the Fermilab charm photoproduction experiment E791 and the subsequent hadroproduction experiments E769 and E791. The silicon microstrip detectors (SMDs), located just downstream of the target foils, are crucial for extracting clean charm signals from the large light-quark background. In the hadroproduction experiments, the incoming charged-pion beam was tracked with silicon detectors upstream of the target foils as well.

trigger was used to enhance the number of leptonic and semileptonic decays, and an emulsion target provided very clean separation of charm decays from the light-quark background.

In semileptonic decays at fixed-target experiments, the neutrino momentum can be determined up to a quadratic ambiguity using the direction of flight of the hadron containing the heavy quark and the momenta of the other decay products. Usually, the solution that results in the lower  $D$  momentum in the laboratory frame has the least bias and the best resolution for the measurement of kinematic variables in the decay.

## B. Bottom-hadron experiments

Semileptonic decays of bottom hadrons have been studied almost exclusively by  $e^+e^-$  collider experiments operating at the  $Y(4S)$  or  $Z$  resonances. The largest  $B$ -meson sample—over two million  $B\bar{B}$  events—has been collected by the CLEO II detector (Kubota *et al.*, 1992) operating at the  $Y(4S)$ . Figure 10 shows the main features of the CLEO II detector. The ARGUS experiment (Albrecht *et al.*, 1989a) accumulated about 200 000  $Y(4S) \rightarrow B\bar{B}$  events before terminating operation. The CLEO experiment is ongoing, and the luminosity of the CESR ring should continue to increase well beyond its 1994 peak value of about  $2.5 \times 10^{32} \text{ cm}^{-2} \text{ s}^{-1}$ . Large  $b$ -hadron samples have also been obtained by the four LEP experiments (ALEPH, DELPHI, L3, and OPAL) running at the  $Z$  resonance. Each of these experiments has about 1.6 million hadronic  $Z$  decays, corresponding to about 350 000  $Z \rightarrow b\bar{b}$  events.

At the Tevatron, the  $p\bar{p}$  collider at Fermilab, the bottom-quark production cross section is high, 50–100  $\mu\text{b}$ , but it is only about 0.1% of the total cross section (Spalding, 1993).

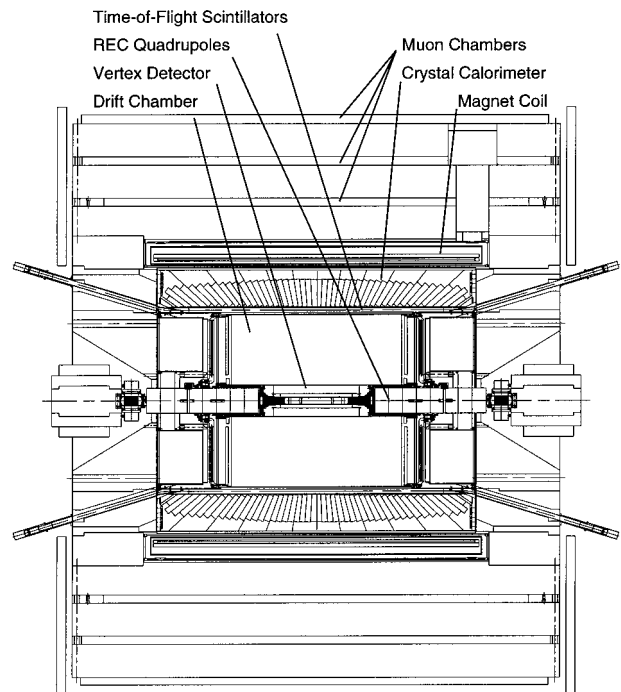


FIG. 10. A cross section of the CLEO II detector. The beamline is horizontal and contains the continuously circulating electron and positron bunches, which are focused at a collision point at the center of the detector. An important feature of CLEO II is the CsI-crystal calorimeter, which provides excellent photon detection efficiency and energy resolution (4% for 100 MeV photons). A double-sided silicon strip detector will be installed in 1995.

Bottom semileptonic decays have been observed, but so far they have been used only to measure the production cross section (Abe *et al.*, 1993). By using a high-resolution vertex detector, however, the CDF experiment has been able to make important contributions in other areas of  $B$  physics, such as studies of individual  $B$ -hadron lifetimes and certain hadronic modes, and  $p\bar{p}$  colliding-beam experiments may eventually contribute to our understanding of semileptonic decays as well. In fixed-target experiments, the bottom production cross section is typically only  $10^{-3}$  of that for charm, and these experiments have not yet made a significant impact on bottom physics.

The  $Y(4S)$  resonance has been the most productive source of information on  $B$ -meson semileptonic decays. The resonant cross section,  $\sigma_{Y(4S)} \approx 1.07 \text{ nb}$ , is reasonably large compared to that for continuum processes ( $\sigma_{\text{cont}} \approx 3.3 \text{ nb}$ ). The process  $Y(4S) \rightarrow B\bar{B}$  occurs very near threshold, and the decay of two  $B$  mesons, each nearly at rest, results in a spherical event topology. The presence of tracks from two overlapping  $B$  decays results in combinatoric backgrounds, but the known  $B$ -meson energy provides an important constraint, even in semileptonic decays. The spherical event topology is often used to suppress background from continuum events, which usually have a much more jetlike structure. Even with this suppression, continuum processes are the dominant background in many analyses. CLEO therefore takes about two-thirds of its data on the  $Y(4S)$  and one-third at a center-of-mass energy 60 MeV below the  $Y(4S)$  in or-

der to obtain pure continuum samples for background studies. By performing the same analysis on the pure continuum sample as on the sample obtained at the  $Y(4S)$  and correcting for the relative integrated luminosities and small energy difference, one can predict both the absolute scale and the shapes of continuum background distributions. Precise measurement of the continuum background is especially important for studies of  $b \rightarrow u \ell^- \bar{\nu}$  processes, because high-momentum leptons are produced in the continuum.

Most CLEO and ARGUS results are based on the assumption that  $B(Y(4S) \rightarrow B\bar{B}) = 100\%$ , with equal branching fractions for charged and neutral  $B$  mesons. The absence of non- $B\bar{B}$  decays of the  $Y(4S)$  is supported by studies of dilepton events, which indicate (Gronberg *et al.*, 1994) that  $B(Y(4S) \rightarrow \text{non-}B\bar{B}) < 5\%$  (95% C.L.). The very large decay width of the  $Y(4S)$  compared with the lower-mass  $Y$  resonances, which are below  $B\bar{B}$  threshold, also supports this assumption. The equality of the  $Y(4S)$  decay rates to charged and neutral  $B$  mesons is less clear; the  $B^0$  and  $B^-$  masses are equal to within about 0.4 MeV, but Coulomb corrections may result in slightly different charged and neutral branching fractions.

In  $Y(4S)$  decays the magnitude of the  $B$ -meson momentum vector is known ( $|\mathbf{p}_B| \approx 330 \text{ MeV}/c$ ), but its direction is not. In semileptonic decays, this means that one does not precisely know the correct Lorentz transformation to the  $B$ -meson rest frame. Fortunately, the  $B$  mesons have a low velocity ( $\beta \approx 0.06$ ), and for most purposes the lab frame is a good approximation to the  $B$  rest frame.

An interesting difference between the CLEO and ARGUS detectors is the strength of their magnetic fields: in CLEO II the superconducting solenoid provides a field of 1.5 T; in ARGUS the field is only 0.8 T. A higher field is an advantage for studying decays with high-momentum tracks, such as  $B \rightarrow \pi\pi$ . It can be a disadvantage, however, at the low-momentum end of the spectrum, where it results in a lower (and varying) track-detection efficiency. This situation occurs in the decay  $B \rightarrow D^* \ell^- \bar{\nu}$ ,  $D^* \rightarrow D\pi$ , where the maximum pion momentum is only about 225 MeV/ $c$ .

The LEP experiments at CERN use the process  $Z^0 \rightarrow b\bar{b}$ . The ratio of  $b\bar{b}$  to other hadronic decays is comparable to that at the  $Y(4S)$ :  $R_b = B(Z \rightarrow b\bar{b})/B(Z \rightarrow \text{hadrons}) \approx 22\%$ . The  $b$  hadrons are a mixture of  $B_u$ ,  $B_d$ ,  $B_s$ , and  $b$ -baryon states, which are thought to be produced with roughly the fractions 0.4, 0.4, 0.12, and 0.08. The high momentum imparted to the  $b$  quark and the hard  $b$  fragmentation result in events with jetlike topology and separated  $b$ -decay vertices. Here the  $b$ -hadron energy is not constrained to the beam energy, but the presence of displaced vertices and the ability to isolate  $B$  decay products within a single jet provide powerful tools for reducing combinatorial background.

At LEP, semileptonic decays have been extremely useful for tagging  $b$  hadrons, particularly for the study of  $b$  baryons using  $\Lambda$ -lepton correlations,  $B\bar{B}$  mixing, and forward-backward electroweak asymmetries. LEP experiments have also observed the semileptonic decays of both the  $B_s$  and the  $\Lambda_b$ . Studies of semileptonic decays for their own sake have concentrated primarily on the  $b$ -hadron semileptonic branch-

ing ratio and the measurement of the process  $B \rightarrow X\tau^- \bar{\nu}_\tau$ , but recently they have expanded to exclusive decays.

### C. Lepton identification

Lepton identification and the problem of hadrons faking lepton signatures are important issues in studies of semileptonic decays. Muons are identified by their ability to pass through several nuclear-interaction-lengths of material. This technique places a lower momentum cutoff on accepted muon candidates of around 1 to 2 GeV for current  $e^+e^-$  experiments and a somewhat higher value for fixed-target experiments. In CLEO and ARGUS, this cutoff is around 1.4 GeV/ $c$  and has a direct impact on many measurements. There are two major sources of hadrons misidentified as muons. Charged pions and kaons can decay in flight, producing real muons, especially if the hadron has low momentum. In fixed-target experiments, hadron decay in flight is a serious problem, due to the length of the spectrometers. Therefore muon candidates are required to have a momentum above a certain minimum, for example, 8 GeV/ $c$  in most E653 analyses and 10 GeV/ $c$  in E687. The second major source of background, punchthrough, is due to high-momentum hadrons that penetrate the material in front of the muon detectors, producing a fake muon candidate.

Electrons are identified primarily by the match between the deposited energy in an electromagnetic calorimeter and the momentum measured by a charged-particle tracking system. In CLEO, electrons with momenta as low as 0.6 GeV/ $c$  have been used in analyses. Backgrounds arise from  $\pi^0$  Dalitz decays and  $\gamma \rightarrow e^+e^-$  conversions in material. The second background is a particular problem in fixed-target experiments, where the amount of material upstream of the electromagnetic calorimeter can be in excess of 10% of a radiation length. In many analyses, the most serious backgrounds are not from fake leptons, but from leptons from sources other than the decay of interest. We shall consider many examples in the discussions of individual measurements.

The probability as a function of momentum for a hadron to fake a lepton signature is best determined using data. (Monte Carlo simulations are often unreliable for this purpose.) One method is to use tracks tagged as a particular hadron species by using clearly identified decays of  $K_s$ 's,  $D$ 's, or  $\Lambda$ 's and to determine the fraction of these tracks that are misidentified as leptons. A second technique sometimes used by CLEO and ARGUS is to count the number of tracks identified as leptons in  $Y(1S)$  events, where it is known that very few leptons are produced, apart from  $\pi^0$  Dalitz decays and photon conversions. These studies show that, for typical cuts, the probability of a hadron's faking an electron in CLEO is 0.05% to 0.2%; the probability of a hadron's faking a muon is about 1.4%. For some studies, the momentum dependence of these fake rates must be taken into account. A detailed discussion of lepton identification in the ALEPH experiment is given in Buskulic *et al.* (1994b).

TABLE III. Measured values of lifetimes and absolute branching fractions (Particle Data Group, 1994) used in this review to extract other branching fractions and decay rates from measured quantities. The uncertainties on the  $D^*$  branching fractions are not those from the Review of Particle Properties, which are incorrect, but from the CLEO II measurement (Butler *et al.*, 1992). The quantity  $\tau(X_b)$  represents an average  $b$ -hadron lifetime, obtained from inclusive LEP and CDF results.

Quantity	Value
$B(D^0 \rightarrow K^- \pi^+)$	$(4.01 \pm 0.14)\%$
$B(D^+ \rightarrow K^- \pi^+ \pi^+)$	$(9.1 \pm 0.6)\%$
$B(D^{*0} \rightarrow D^0 \pi^0)$	$(63.6 \pm 4.0)\%$
$B(D^{*0} \rightarrow D^0 \gamma)$	$(36.4 \pm 4.0)\%$
$B(D^{*+} \rightarrow D^0 \pi^+)$	$(68.1 \pm 1.6)\%$
$B(D^{*+} \rightarrow D^+ \pi^0)$	$(30.8 \pm 0.9)\%$
$\tau(D^0)$	$(0.415 \pm 0.004) \times 10^{-12}$ s
$\tau(D^+)$	$(1.057 \pm 0.015) \times 10^{-12}$ s
$\tau(\bar{B}^0)$	$(1.50 \pm 0.11) \times 10^{-12}$ s
$\tau(B^-)$	$(1.54 \pm 0.11) \times 10^{-12}$ s
$\tau(X_b)$	$(1.537 \pm 0.021) \times 10^{-12}$ s
$\Delta m_{B^0}$	$(0.51 \pm 0.06) \times 10^{12} \hbar \text{ s}^{-1}$

#### D. Assumed branching fractions

To compare measurements from different experiments, we have corrected some results using a consistent set of  $D$  and  $D^*$  branching fractions and charm- and bottom-hadron lifetimes. Such quantities are used, for example, in the normalization of semileptonic branching fractions and in the conversion of branching fractions to partial decay widths. The values used throughout this review, except where indicated, are those listed in the 1994 edition of the *Review of Particle Properties* by the Particle Data Group (1994) and are summarized in Table III. The measured values for  $B$  lifetimes have increased significantly over the past few years and may well continue to do so. For this reason, we shall indicate how to correct the measurements for such changes.

### IV. LEPTONIC DECAYS

#### A. Theory of leptonic decays

The simplest decays of charged mesons to describe theoretically are the purely leptonic processes shown in Fig. 1(b). The effects of the strong interaction can be parametrized in terms of just one factor, called the decay constant. In contrast to semileptonic decays, where  $q^2$  (and hence each form factor) varies from event to event, leptonic decays have a fixed value of  $q^2$ :  $q^2 = M^2$ , where  $M$  is the mass of the initial meson. The most general matrix element for the decay of a charged pseudoscalar meson  $M_{Q\bar{q}}$  to  $\ell^- \bar{\nu}$  was given in Eq. (12). The corresponding decay rate, ignoring radiative corrections, is

$$\Gamma(M_{Q\bar{q}} \rightarrow \ell^- \bar{\nu}) = \frac{G_F^2}{8\pi} |V_{qQ}|^2 f_M^2 M m_\ell^2 \left(1 - \frac{m_\ell^2}{M^2}\right)^2, \quad (32)$$

where  $f_M$  is the decay constant,  $V_{qQ}$  is the CKM matrix element, and  $m_\ell$  and  $M$  are the masses of the lepton and

charged meson  $M_{Q\bar{q}}$ , respectively. The decay constant  $f_M$  is a measure of the probability amplitude for the quarks to have zero separation, which is necessary for them to annihilate. In the heavy-quark limit,  $f_M$  is given by the nonrelativistic quark-model formula  $f_M^2 = 12 |\psi(0)|^2 / M$ , where  $\psi(0)$  is the wave function of the light quark  $\bar{q}$  and heavy quark  $Q$  at zero relative separation (Rosner, 1990).

An asymptotic scaling law, which can be derived in HQET (Neubert, 1994c), predicts that  $f_M^2 M$  approaches a constant as  $M$  becomes large. Since the total decay rate of a heavy meson scales as  $M^5$ , the leptonic branching fractions become small as  $M$  becomes large. Hence the leptonic branching fractions for the  $D$  and  $B$  meson are expected to be very small.

The factor  $m_\ell^2$  in Eq. (32) is a consequence of helicity suppression. For small  $m_\ell$ , both vector and axial-vector couplings at a vertex favor decays in which the resulting fermion and antifermion (here  $\ell^- \bar{\nu}$ ) have opposite helicities. Therefore the favored helicity configuration for the decay  $M_{Q\bar{q}} \rightarrow \ell^- \bar{\nu}$  violates conservation of angular momentum when  $M_{Q\bar{q}}$  is a spin-zero particle. This effect leads to a suppression of the decay rate when  $m_\ell$  is small compared with the mass of the parent meson.

Decay constants for pseudoscalar mesons containing a heavy quark have been predicted with lattice QCD, QCD sum rules, and quark potential models. Theoretical predictions are summarized in Table IV. Rosner (1990), Colangelo *et al.* (1991), Dominguez (1992), and Shigemitsu (1994) each summarize a subset of these predictions and give more details on the assumptions and methods used. Theoretical expectations for  $f_D$  are in the range 170 to 240 MeV;  $f_{D_s}$  is expected to be about 10% larger. The theoretical predictions for  $f_B$  range from 120 to 230 MeV. Some of the early predictions of  $f_B$  from QCD sum rules were significantly lower than the predictions of lattice QCD. Several new analyses based on QCD sum rules in the heavy-quark effective theory (Bagan *et al.*, 1992; Broadhurst and Grozin, 1992; Neubert, 1992) find that radiative corrections significantly increase the value of  $f_B$ .

Using a value of 200 MeV for the  $D^+$ ,  $D_s$ , and  $B$  decay constants, the central values of the CKM matrix elements from the Particle Data Group (1994) ( $|V_{cd}| = 0.21$ ,  $|V_{cs}| = 0.97$ , and  $|V_{ub}| = 0.003$ ), and the measured  $D^+$ ,  $D_s$ , and  $B$  lifetimes, we obtain the leptonic branching-fraction predictions shown in Table V. The leptonic decay rates for  $D_s$  are expected to be larger than those for  $D^+$  because  $|V_{cs}|^2$  is much larger than  $|V_{cd}|^2$ . In addition, the decay  $D_s \rightarrow \tau^+ \nu_\tau$  has less phase-space suppression than  $D^+ \rightarrow \tau^+ \nu_\tau$ . Leptonic  $B$  decays are strongly suppressed by the small value of  $|V_{ub}|^2$ . Therefore the leptonic heavy-quark decays that are easiest to detect experimentally are  $D_s \rightarrow \mu^+ \nu_\mu$  and  $D_s \rightarrow \tau^+ \nu_\tau$ .

If we know  $V_{qQ}$ , a measurement of the decay rate for a purely leptonic mode allows us to determine the decay constant  $f_M$ . The CKM matrix elements relevant for leptonic decays of the  $D^+$  and  $D_s$  are determined quite well from unitarity constraints, so a measurement of the leptonic decay rate for these particles provides a measurement of  $f_D$  and  $f_{D_s}$ .

TABLE IV. Predictions for the  $D^+$ ,  $D_s$ , and  $B$  decay constants.

Reference	$f_D$ (MeV)	$f_{D_s}$ (MeV)	$f_B$ (MeV)
Lattice calculations			
Abada <i>et al.</i> , 1992	$210 \pm 15$	$227 \pm 15$	$205 \pm 40$
Alexandrou <i>et al.</i> , 1994	$170 \pm 30$	$185 \pm 33$	$180 \pm 50$
Allton <i>et al.</i> , 1994a			$290 \pm 47$
Allton <i>et al.</i> , 1994b	$218 \pm 9$	$240 \pm 9$	
Baxter <i>et al.</i> , 1994	$185^{+42}_{-8}$	$212^{+46}_{-8}$	$160^{+53}_{-20}$
Bernard <i>et al.</i> , 1994	$208 \pm 38$	$230 \pm 36$	$187 \pm 38$
Bhattacharya and Gupta, 1994c	$241 \pm 19$	$266 \pm 15$	
Bitar <i>et al.</i> , 1994	$215 \pm 53$	$288 \pm 64$	
Duncan <i>et al.</i> , 1994			$188^{+41}_{-31}$
Hashimoto, 1994			$171^{+29}_{-50}$
QCD sum rules			
Aliev and Eletsksii, 1983	$176 \pm 25$		$135 \pm 15$
Dominguez and Paver, 1987	$224 \pm 21$	$277 \pm 17$	$178 \pm 25$
Narison, 1987	$173 \pm 16$	$217 \pm 20$	$187 \pm 24$
Shifman, 1987	$165 \pm 15$	$200 \pm 15$	$115 \pm 15$
Reinders, 1988			$170 \pm 20$
Bagan <i>et al.</i> , 1992			$195-245$
Dominguez and Paver, 1992			$125 \pm 7$
Neubert, 1992	$170 \pm 30$		$190 \pm 50$
Schilcher and Wu, 1992	$176 \pm 13$	$193 \pm 13$	$128 \pm 28$
Potential models			
Krasemann, 1980	150	210	125
Suzuki, 1985	117	129	75
Sinha, 1986	$287 \pm 40$	$356 \pm 50$	$229 \pm 32$
Cea, 1988	182	199	231
Capstick and Godfrey, 1990	$240 \pm 20$	$290 \pm 20$	$155 \pm 15$
Colangelo <i>et al.</i> , 1991	$180 \pm 27$	$200 \pm 30$	$230 \pm 35$

The decay constant also appears in numerous heavy-flavor transitions, such as those in mixing and  $CP$  violation. Of particular interest is the  $B$  decay constant  $f_B$ , which currently limits our ability to extract  $|V_{td}|$  from measurements of  $B^0\bar{B}^0$  mixing. [See Eq. (23) in Sec. II.] Given the current size of  $B$ -meson data samples and the expected branching

TABLE V. Predicted  $D^+$ ,  $D_s$ , and  $B$  leptonic decay rates and branching fractions assuming  $f_D=f_{D_s}=f_B=200$  MeV,  $|V_{cd}|=0.21$ ,  $|V_{cs}|=0.97$ , and  $|V_{ub}|=0.003$ .

Decay mode	Rate ( $s^{-1}$ )	Branching fraction
$D^+ \rightarrow e^+ \nu_e$	$7.1 \times 10^3$	$7.5 \times 10^{-9}$
$D^+ \rightarrow \mu^+ \nu_\mu$	$3.0 \times 10^8$	$3.2 \times 10^{-4}$
$D^+ \rightarrow \tau^+ \nu_\tau$	$6.8 \times 10^8$	$7.2 \times 10^{-4}$
$D_s \rightarrow e^+ \nu_e$	$1.6 \times 10^5$	$7.5 \times 10^{-8}$
$D_s \rightarrow \mu^+ \nu_\mu$	$6.8 \times 10^9$	$3.2 \times 10^{-3}$
$D_s \rightarrow \tau^+ \nu_\tau$	$6.1 \times 10^{10}$	$2.9 \times 10^{-2}$
$B^- \rightarrow e^- \bar{\nu}_e$	$4.1 \times 10^0$	$6.3 \times 10^{-12}$
$B^- \rightarrow \mu^- \bar{\nu}_\mu$	$1.7 \times 10^5$	$2.7 \times 10^{-7}$
$B^- \rightarrow \tau^- \bar{\nu}_\tau$	$3.9 \times 10^7$	$6.0 \times 10^{-5}$

fractions for  $B$  leptonic decays, it is unlikely that the  $B$  decay constant will be determined experimentally in the near future. Although there are large uncertainties in the theoretical predictions for  $f_B$ , an experimental determination of the  $D$  decay constant could be used as input to the models to reduce the theoretical uncertainty on the  $B$  decay constant. For example, HQET predicts that  $f_B/f_D \approx 0.69$  when terms of order  $1/m_Q$  are neglected (Neubert, 1994c). However, the  $1/m_Q$  corrections for heavy-meson decay constants are expected to be substantial and much more significant than those for weak decay form factors. (See Sec. 5.4 in Neubert, 1994c.)

## B. Experimental results on leptonic decays

### 1. $D^+$ and $D_s$ leptonic decays

Until recently, only limits existed for leptonic  $D^+$  and  $D_s$  decays. For  $D^+$  decays, the Mark III Collaboration (Adler *et al.*, 1988b) set an upper limit of  $B(D^+ \rightarrow \mu^+ \nu_\mu) < 7.2 \times 10^{-4}$  (90% C.L.), corresponding to

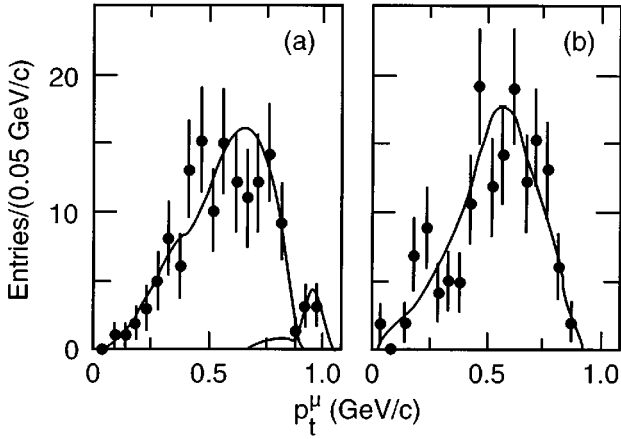


FIG. 11. Distribution of muon momentum perpendicular to the direction of flight of the  $D_{(s)}$  for the WA75 experiment for candidates consistent with (a) the decay of a charm particle to a single charged particle and (b) the decay to two charged particles. The solid lines represent the best fit to the data by means of a Monte Carlo simulation. Redrawn from Aoki *et al.* (1993).

an upper limit of 290 MeV on  $f_D$ . For  $D_s$  decays, the EMC Collaboration (Aubert *et al.*, 1983) set an upper limit of 3% on  $B(D_s \rightarrow \mu^+ \nu_\mu)$ .

Several experiments have now observed the muonic decay  $D_s \rightarrow \mu^+ \nu_\mu$ . The first indication of  $D_s \rightarrow \mu^+ \nu_\mu$  was presented in 1992 by the CERN WA75 Collaboration (Aoki *et al.*, 1993). In this fixed-target experiment, a  $\pi^-$  beam is incident on an emulsion target and a muon is required in the online trigger. The distribution of  $p_t^\mu$ , the momentum of the muon transverse to the line of flight of the decaying charmed hadron, is shown in Fig. 11(a) for candidates consistent with the decay of a charged particle to a single charged particle, and in Fig. 11(b) for candidates consistent with a neutral particle decaying to two charged particles. The line of flight is determined directly by scanning the emulsion. The kinematic upper limit on  $p_t^\mu$  is 0.98 GeV/c for  $D_s \rightarrow \mu^+ \nu_\mu$  and 0.93 GeV/c for  $D^+ \rightarrow \mu^+ \nu_\mu$ , whereas the  $p_t^\mu$  spectrum for semileptonic decays cuts off at 0.88 GeV/c. Figure 11(a) shows that, in the charged topology, six events (of 144 events total) are observed with  $p_t^\mu > 0.9$  GeV/c, but none is observed above this threshold in the neutral topology [Fig. 11(b)]. (Two-body leptonic decays can be observed in the charged topology but not the neutral topology.) The estimated contribution from  $D^+ \rightarrow \mu^+ \nu_\mu$  is  $0.6 \pm 0.2$  events. Using their signal for  $D^0 \rightarrow \mu^+ \nu_\mu X$  for normalization, WA75 determines a branching fraction for  $D_s \rightarrow \mu^+ \nu_\mu$  of  $(3.9_{-1.4}^{+1.8+0.8} \pm 1.4) \times 10^{-3}$  and a  $D_s$  decay constant of  $f_{D_s} = (225 \pm 45 \pm 20 \pm 41)$  MeV. In both results, the last error is the systematic error on the normalization, which depends on measurements of the  $D^0$  and  $D_s$  cross sections from NA32, the branching fraction for  $D_s \rightarrow K^+ K^- \pi^+$ , and the inclusive  $D^0$  branching fraction.<sup>4</sup>

The CLEO Collaboration (Acosta *et al.*, 1994) measures the  $D_s \rightarrow \mu^+ \nu_\mu$  decay rate relative to that for  $D_s \rightarrow \phi \pi^+$ , so

<sup>4</sup>We have updated the central value and the third error for current measurements of  $B(D_s \rightarrow K^+ K^- \pi^+)$  and  $B(D^0 \rightarrow X \ell^+ \nu)$ .

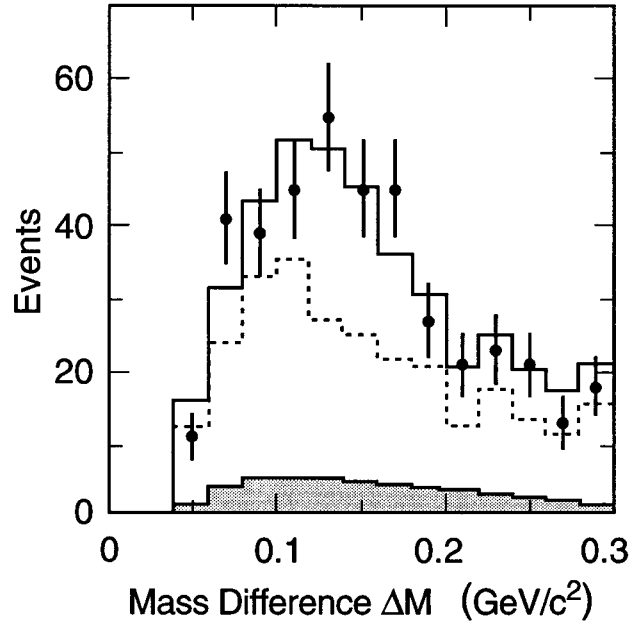


FIG. 12. Distribution of the mass difference  $\Delta M = m(\mu \nu_\mu \gamma) - m(\mu \nu_\mu)$  for candidates for the decay sequence  $D_s^* \rightarrow D_s \gamma$ ,  $D_s \rightarrow \mu^+ \nu_\mu$  in the CLEO II data. Points with error bars represent muon data. The dashed histogram corresponds to the background estimated with electrons, plus a small component represented by the shaded histogram due to differences in the electron and muon misidentification rates. The difference between the points and the dashed histogram is ascribed to  $D_s \rightarrow \mu^+ \nu_\mu$  candidates. The solid histogram corresponds to the best fit of signal and background components to the muon spectrum. Redrawn from Acosta *et al.* (1994).

the normalization is more straightforward than in the WA75 analysis. CLEO searches for  $\mu \gamma$  combinations from the decay chain  $D_s^* \rightarrow D_s \gamma$ ,  $D_s \rightarrow \mu^+ \nu_\mu$ . The neutrino momentum is estimated from the missing energy and momentum in the hemisphere of the muon and is used, along with the measured  $\mu$  and  $\gamma$  momenta, to determine the candidate  $D_s$  and  $D_s^*$  masses. The distribution for the mass difference  $\Delta M = m(\mu \nu_\mu \gamma) - m(\mu \nu_\mu)$  is shown in Fig. 12. Signal events should peak at  $m(D_s^*) - m(D_s) \approx 141$  MeV.

Most of the entries in Fig. 12 are due to other sources of  $\mu$ 's and  $\gamma$ 's. Since the branching fraction for  $D_s \rightarrow e^+ \nu_e$  is expected to be much less than that for  $D_s \rightarrow \mu^+ \nu_\mu$ , candidate events that satisfy the same selection criteria, but with an identified electron rather than a muon, are assumed to be dominated by backgrounds. Electron data (adjusted for differences in electron and muon misidentification rates) are represented by the dashed histogram in Fig. 12. The difference between the distributions for muons and electrons is fit to a combination of a Gaussian peak at 141 MeV ( $38 \pm 10$  events) and a broad distribution due to  $D_s \rightarrow \mu^+ \nu_\mu$  or  $D^+ \rightarrow \mu^+ \nu_\mu$  decays combined with random  $\gamma$ 's ( $52 \pm 14$  events). The branching fraction is measured relative to the  $\phi \pi^+$  decay mode:

$$B(D_s \rightarrow \mu^+ \nu_\mu) / B(D_s \rightarrow \phi \pi^+) = 0.245 \pm 0.052 \pm 0.074. \quad (33)$$

CLEO extracts a decay constant of

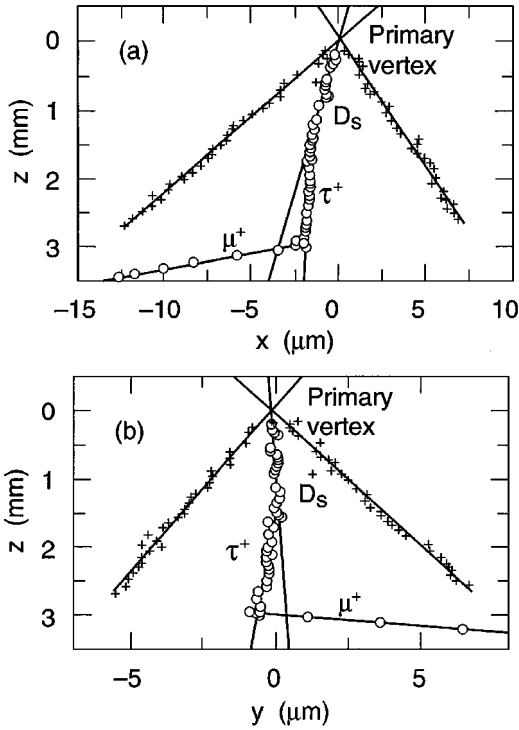


FIG. 13. Two views of a candidate  $D_s \rightarrow \tau^+ \nu_\tau$ ,  $\tau^+ \rightarrow \mu^+ \nu_\mu \bar{\nu}_\tau$  event in the E653 emulsion. Each point along the reconstructed tracks corresponds to a measurement in the emulsion. Note that the vertical and horizontal scales are not the same. The  $z$  axis corresponds to the beam direction. Redrawn with permission of E653 Collaboration.

$$f_{D_s} = (344 \pm 37 \pm 52) \sqrt{\frac{B(D_s \rightarrow \phi \pi^+)}{0.037}} \text{ MeV.} \quad (34)$$

The current world average for  $B(D_s \rightarrow \phi \pi^+)$  is  $0.037 \pm 0.005 \pm 0.004$  (see Sec. VI.B.5).

Additional evidence for purely leptonic  $D_s$  decays has been provided by the E653 Collaboration (1993). Like WA75, Fermilab E653 is a fixed-target experiment with an emulsion target and muon trigger. In a partial data sample (one-third of the total), 23 events are observed with high  $p_t^\mu$ . The E653 Collaboration exploits the power of emulsions in the observation of three candidates (in a partial data set) for  $D_s \rightarrow \tau^+ \nu_\tau$  decay in which  $\tau^+ \rightarrow \mu^+ \nu_\mu \bar{\nu}_\tau$ . In these events, both the  $D_s$  and the  $\tau^+$  decay in the emulsion. Figure 13 shows two views in the emulsion of one of these candidate  $D_s \rightarrow \tau^+ \nu_\tau$  decays. E653 will normalize the yield to the  $D_s \rightarrow \phi \mu \nu_\mu$  signal in the same data sample to extract branching fractions for  $D_s \rightarrow \mu^+ \nu_\mu$  and  $D_s \rightarrow \tau^+ \nu_\tau$  and to measure  $f_{D_s}$ .

The BES Collaboration has fully reconstructed three events in which one of the  $D_s$  mesons decays leptonically (Bai *et al.*, 1995a). By normalizing to the total number of events in which at least one  $D_s$  is fully reconstructed, they extract a value for the decay constant of

$$f_{D_s} = (430_{-130}^{+150} \pm 40) \text{ MeV} \quad (35)$$

where the first error is statistical and the second is the combined systematic uncertainty from tagging efficiency, back-

ground estimation, and the  $D_s$  lifetime. Unlike the measurements of  $f_{D_s}$  described above, the BES measurement is not normalized to other  $D_s$  decay modes and does not depend on knowing the  $D_s$  production rate.

Table VI lists the measurements of  $D^+$  and  $D_s$  decay constants, along with the  $\pi^+$  and  $K^+$  decay constants for comparison. Both the CLEO and BES values for  $f_{D_s}$  are about one standard deviation higher than the WA75 result. They are at the upper limit of the range of theoretical predictions, albeit with large uncertainties.

Although we now have the first observations of leptonic  $D_s$  decays, the statistical and systematic uncertainties are very large. As the statistical precision improves, the systematic uncertainty due to normalization will become significant in measurements of the type performed by WA75, E653, and CLEO. The technique used by BES does not depend on a normalization mode such as  $D_s \rightarrow \phi \pi^+$ . However, the statistical errors will remain very large for this type of measurement unless a charm factory is successfully built.

Less direct methods can also be used to extract the  $D_s$  decay constant, although a number of assumptions are required. Bortoletto and Stone (1990) have used published CLEO measurements of the branching fractions for  $B^0 \rightarrow D^{*-} D_s^+$ ,  $B^+ \rightarrow \bar{D}^0 D_s^+$ ,  $B^0 \rightarrow D^- D_s^+$ , and  $\bar{B}^0 \rightarrow D^{*+} \ell^- \bar{\nu}$ , and of the  $q^2$  distribution for  $\bar{B}^0 \rightarrow D^{*+} \ell^- \bar{\nu}$ , to extract  $f_{D_s}$ . Their method assumes factorization for the hadronic modes, which is expected to be a reasonable approximation since these decays cannot occur via so-called color-suppressed internal  $W$  emission diagrams. Under the factorization hypothesis, the hadronic decay rate for  $B^0 \rightarrow D^{*-} D_s^+$  can be related to the semileptonic decay rate  $\bar{B}^0 \rightarrow D^{*+} \ell^- \bar{\nu}$  at  $q^2 = m_{D_s}^2$ :

$$\Gamma(B^0 \rightarrow D^{*-} D_s^+) = \delta(\zeta, y) 6 \pi^2 f_{D_s}^2 |V_{cs}|^2 \times \left. \frac{d\Gamma(\bar{B}^0 \rightarrow D^{*+} \ell^- \bar{\nu})}{dq^2} \right|_{q^2 = m_{D_s}^2}, \quad (36)$$

where  $\zeta = m_D^2/m_B^2$ ,  $y = q^2/m_B^2$ , and  $\delta(\zeta, y)$  is a function that has been calculated by Rosner (1990). For  $q^2 = m_{D_s}^2$ ,  $\delta$  is 0.41. To increase the statistical precision of the result, HQET predictions are also used to relate the decay rates for  $B^+ \rightarrow \bar{D}^0 D_s^+$  and  $B^0 \rightarrow D^- D_s^+$  to that for  $B^0 \rightarrow D^{*-} D_s^+$ . The decay constant extracted from all three hadronic modes and the semileptonic mode  $\bar{B}^0 \rightarrow D^{*+} \ell^- \bar{\nu}$  is

$$f_{D_s} = (253 \pm 41) \sqrt{\frac{0.037}{B(D_s \rightarrow \phi \pi^+)}} \text{ MeV.} \quad (37)$$

The ARGUS Collaboration uses a similar method to extract a value for  $f_{D_s}$  from their measurements of inclusive and exclusive  $D_s^{(*)}$  production (Albrecht *et al.*, 1992b). Their result for the decay constant averaged over  $D_s$  and  $D_s^*$  mesons is

$$f_{D_s^{(*)}} = (228 \pm 24) \sqrt{\frac{0.037}{B(D_s \rightarrow \phi \pi^+)}} \text{ MeV.} \quad (38)$$

As more data are obtained, the validity of the assumptions of factorization and HQET can be checked on many modes, and the statistical uncertainty on the decay constant can be reduced.

TABLE VI. Summary of measurements of the decay constants for the  $D^+$  and  $D_s^-$ . For comparison, we also list the  $\pi^+$  and  $K^+$  decay constants. The CLEO result is quoted for  $B(D_s \rightarrow \phi \pi^+) = 3.7\%$ , the current world average. The 9% uncertainty on  $\sqrt{B(D_s \rightarrow \phi \pi^+)}$  is not included in the error on  $f_{D_s}$  quoted in the table. E653 also has evidence for  $D_s \rightarrow \mu^+ \nu_\mu$  but has not yet extracted  $f_{D_s}$ .

Decay constant	Experiment	Reference	Value (MeV)
$f_\pi$	PDG 94	Particle Data Group, 1994	$130.7 \pm 0.4$
$f_K$	PDG 94	Particle Data Group, 1994	$159.8 \pm 1.5$
$f_{D_s}$	WA75	Aoki <i>et al.</i> , 1993	$225 \pm 45 \pm 20 \pm 41$
$f_{D_s}$	CLEO II	Acosta <i>et al.</i> , 1994	$344 \pm 37 \pm 52$
$f_{D_s}$	BES	Bai <i>et al.</i> , 1995a	$430^{+150}_{-130} \pm 40$
$f_D$	Mark III	Adler <i>et al.</i> , 1988b	$< 290$ (90% C.L.)

## 2. $B^-$ leptonic decays

The decay  $B^- \rightarrow \tau^- \bar{\nu}_\tau$  is the most accessible of the leptonic  $B^-$  decays because the large  $\tau$  mass reduces the helicity suppression. However, all leptonic  $B^-$  decays are suppressed by the factor  $|V_{ub}|^2 \approx (0.003)^2$ , which puts the expected branching ratio more than an order of magnitude beyond the reach of current experiments. CLEO has searched for events consistent with the decay  $B^- \rightarrow \tau^- \bar{\nu}_\tau$ ,  $\tau^- \rightarrow \ell^- \bar{\nu}_\ell \nu_\tau$ . If such a decay occurs, then, apart from the lepton, all of the tracks and calorimeter energy in an  $Y(4S) \rightarrow B\bar{B}$  event must be produced in the decay chain of the other  $B$  meson. Furthermore, if this other decay chain is purely hadronic, then the total observed energy (excluding the lepton) should be consistent with the beam energy, and the total momentum can be used to compute a beam-energy-constrained mass that should be consistent with the  $B$ -meson mass. CLEO has performed a joint fit to the distribution of these two variables to obtain the preliminary upper limit  $B(B^- \rightarrow \tau^- \bar{\nu}_\tau) < 2.2 \times 10^{-3}$  (90% C.L.) (Alexander *et al.*, 1994a). An analysis by ALEPH (Buskulic *et al.*, 1995a) uses a similar approach, but also requires the lepton from the  $\tau$  decay to have a large impact parameter. ALEPH obtains the limit  $B(B^- \rightarrow \tau^- \bar{\nu}_\tau) < 1.8 \times 10^{-3}$ . While far above the rate expected in the standard model, these limits place restrictions on certain models with charged Higgs bosons, which can significantly enhance the leptonic decay rate.

## V. INCLUSIVE SEMILEPTONIC DECAYS

### A. Introduction

In the inclusive approach to semileptonic decays, one considers the sum over all possible final-state hadrons, ignoring the detailed breakdown among the individual decay modes that contribute to the semileptonic rate. Experimentally, it is necessary to observe only the lepton, eliminating the difficulty of reconstructing what are often very complex decay sequences of the daughter hadrons. Theoretical calculations of inclusive properties have certain advantages of simplicity as well, since calculations in which the heavy quark is assumed to decay as a free particle (with the light quark acting merely as a spectator) provide a good starting point for predictions. Recently, there has been great interest in refining calculations for  $b$ -hadron semileptonic decays using heavy-

quark expansions. It has been shown that spectator-model predictions correspond to the lowest-order term in such expansions.

Several inclusive quantities are of interest: semileptonic branching fractions and decay rates; lepton-energy spectra; and, in the case of  $B$ -meson decays, the rate in the end-point region of the spectrum, where  $B \rightarrow X_c \ell^- \bar{\nu}$  is suppressed relative to  $B \rightarrow X_u \ell^- \bar{\nu}$ . The semileptonic branching fraction is defined by

$$\mathcal{B}_{\text{SL}} = \frac{\sum_X \Gamma(M \rightarrow X \ell^- \bar{\nu})}{\Gamma(M \rightarrow \text{all})}, \tag{39}$$

where  $\ell$  is either an electron or a muon, but not both. (Because the  $\tau$ -lepton mass is large, the case  $\ell = \tau$  is treated separately.) Usually, the branching fraction measured by experiments is an average over more than one species of heavy hadron,  $M$ , because measurements of the lepton alone are not sufficient to distinguish between different types of hadrons carrying the same heavy quark. At the  $Y(4S)$ , for example,  $\mathcal{B}_{\text{SL}}$  is measured as an average over  $B^-$  and  $B^0$  mesons, although their semileptonic branching fractions have also been measured separately, but with poorer statistical precision.

Precise measurements of  $\mathcal{B}_{\text{SL}}$  are valuable partly because they allow us to determine what fraction of the semileptonic rate can be accounted for by known exclusive channels. The semileptonic branching fraction is difficult to predict, however, because the dominant contribution to the denominator in Eq. (39) is from hadronic decays, and calculations of hadronic rates suffer from uncertainties related to both perturbative and nonperturbative QCD effects. As we shall see, the measured value of  $\mathcal{B}_{\text{SL}}$  for the  $B$  meson is lower than that predicted by most calculations. The numerator in Eq. (39) may also be difficult to calculate using inclusive methods, if the semileptonic rate is distributed over only a small number of exclusive final states. In this case, the duality between quark final states and the physical hadronic final states may be only approximate.

Separate measurements of  $\mathcal{B}_{\text{SL}}$  for  $Q\bar{u}$  and  $Q\bar{d}$  mesons allow one to extract the ratio of the lifetimes of the charged and neutral mesons. For example, in  $D$ -meson decays,

$$\begin{aligned} \frac{\tau_+}{\tau_0} &= \frac{\Gamma(D^0 \rightarrow \text{all})}{\Gamma(D^+ \rightarrow \text{all})} = \frac{\Gamma(D^0 \rightarrow \text{all})}{\Gamma(D^0 \rightarrow X \ell^+ \nu)} \frac{\Gamma(D^+ \rightarrow X \ell^+ \nu)}{\Gamma(D^+ \rightarrow \text{all})} \\ &= \frac{\mathcal{B}_{\text{SL}}^+}{\mathcal{B}_{\text{SL}}^0}, \end{aligned} \tag{40}$$

where we have assumed that the charged and neutral  $D$  mesons have the same semileptonic partial widths. This assumption is expected to be very good, since the lepton cannot interact strongly with the final-state hadrons, and the two mesons differ only in the isospin of the light quark. (Comparison of  $\mathcal{B}_{\text{SL}}^+/\mathcal{B}_{\text{SL}}^0$  with  $\tau_+/\tau_0$  from direct lifetime measurements provides a test of this assumption.<sup>5</sup>) In contrast, the isospin of the light quark can, in principle, substantially affect the hadronic rate. In the spectator model, the light quark's flavor is assumed to be irrelevant, so the model predicts  $\tau_+/\tau_0 = 1$ . This prediction is consistent with measurements of  $B$  mesons, where the lifetimes are known to be the same within about 10%. In  $D$  decays, however, the lifetime ratio is about 2.5, showing that nonspectator effects are large. Measurements of hadronic decays indicate that this effect is primarily due to a suppression of the  $D^+$  hadronic rate as a result of interference between amplitudes related by interchanging the spectator  $\bar{d}$  quark and the  $\bar{d}$  quark from the  $W^*$  decay.

An important application of  $\mathcal{B}_{\text{SL}}$  is that it can be used to compute the total semileptonic decay width:  $\Gamma_{\text{SL}} = \mathcal{B}_{\text{SL}}/\tau_M$ , where  $\tau_M$  is the measured lifetime of the hadron  $M$ . In charm decays, one can test whether the semileptonic decay widths of different mesons are the same, as discussed above. In  $B$  decays, one can also compare the inclusive semileptonic decay width to theoretical calculations to determine  $|V_{cb}|$ . The measurement of  $|V_{cb}|$  using this method has attracted much interest, because  $\mathcal{B}_{\text{SL}}$  and  $\tau_B$  have been measured with very good precision, and some theorists believe that the theoretical uncertainties can also be made very small.

Recently, heavy-quark expansions have been used to predict the shape of the spectrum for  $B \rightarrow X_c \ell^- \bar{\nu}$ , although reliable predictions for the end-point region remain a source of

difficulty. The end-point region, a tiny part of phase space in which the lepton energies are very high, is of great importance in the determination of  $|V_{ub}|$ .

### B. Theoretical predictions for semileptonic decays

In the simplest possible estimate of  $\mathcal{B}_{\text{SL}}$ , the heavy quark is treated as a free particle, and  $\mathcal{B}_{\text{SL}}$  is given by the fraction of decays in which the virtual  $W$  produces an  $e^- \bar{\nu}_e$  pair. If one ignores the masses of the final-state fermions and gives equal weight to each final state (taking into account color), this fraction is  $\mathcal{B}_{\text{SL}} \approx 1/5$  for  $D$  mesons and  $\mathcal{B}_{\text{SL}} \approx 1/9$  for  $B$  mesons. The measured values of  $\mathcal{B}_{\text{SL}}$ , however, are very different for the  $D^+$  and  $D^0$ , showing that spectator-model calculations are inadequate for charm mesons. The result for  $B$ 's is very close to the measured value, but the agreement is accidental: there are large phase-space corrections due to particle masses, and accurate calculations of the semileptonic and hadronic widths and  $\mathcal{B}_{\text{SL}}$  must take into account strong-interaction effects as well. In this section, we review the status of the inclusive calculations, focusing mainly on the case of the  $B$  meson. Here, nonspectator effects are expected to be small, a prediction borne out by the similar values of the  $B^0$  and  $B^-$  lifetimes. With the development of heavy-quark expansions, inclusive calculations are evolving rapidly, and the reader should consult the literature for the latest results.

The partial width for the weak decay of a free quark  $Q$  to fermions of nonzero masses was obtained by Cortes *et al.* (1982). The rate for  $Q \rightarrow q f_1 \bar{f}_2$ ,  $W^* \rightarrow f_1 \bar{f}_2$ , where  $f_1$  and  $f_2$  are fermions and  $m_Q \ll m_W$ , is

$$\Gamma(Q \rightarrow q f_1 \bar{f}_2) = \Gamma_0 N_C |V_{qQ}|^2 |V_{f_2 f_1}|^2 I\left(\frac{m_q}{m_Q}, \frac{m_{f_1}}{m_Q}, \frac{m_{f_2}}{m_Q}\right), \tag{41}$$

where  $\Gamma_0 = G_F^2 m_Q^5 / 192 \pi^3$ . The color factor  $N_C$  is equal to 3 for hadronic decay and 1 for semileptonic decay;  $V_{f_2 f_1}$  is the CKM element for  $W^* \rightarrow f_1 \bar{f}_2$  for decay to quarks but is equal to 1 for semileptonic decay; and  $I(x, y, z)$  is given by

$$I(x, y, z) = 12 \int_{(x+y)^2}^{(1-z)^2} \frac{ds}{s} (s - x^2 - y^2)(1 + z^2 - s) \{ [s - (x - y)^2] [s - (x + y)^2] [(1 + z)^2 - s] [(1 - z)^2 - s] \}^{1/2}. \tag{42}$$

When all the final-state particles are massless,  $I = I(0, 0, 0) = 1$ ; for any other values of the quark masses,  $I(x, y, z) < 1$ . The result for the case in which only one final-state particle has nonzero mass is familiar from muon decay:

$$I(x, 0, 0) = I(0, x, 0) = I(0, 0, x) = 1 - 8x^2 + 8x^6 - x^8 - 24x^4 \ln x. \tag{43}$$

The  $b$ -hadron semileptonic branching fraction is given by

$$\mathcal{B}_{\text{SL}} \approx \frac{\Gamma(b \rightarrow c e^- \bar{\nu})}{2\Gamma(b \rightarrow c e^- \bar{\nu}) + \Gamma(b \rightarrow c \tau^- \bar{\nu}) + \Gamma(b \rightarrow c \bar{u} d + c \bar{u} s) + \Gamma(b \rightarrow c \bar{c} s + c \bar{c} d)} \approx \frac{1}{2 + R_\tau + R_c + R_{cc}}, \tag{44}$$

<sup>5</sup>The Cabibbo-suppressed semileptonic rates of the  $D^0$  and  $D^+$  could differ very slightly, resulting in a small difference in their inclusive rates. The  $D^0 \rightarrow \pi^- \ell^+ \nu$  rate, for example, might exceed the sum of the rates for  $D^+$  semileptonic decays to  $\pi^0$ ,  $\eta$ , and  $\eta'$ , simply due to phase space.

where we have ignored  $b \rightarrow u$  decays, the contribution of rare processes such as penguin decays, and the small phase-space difference between  $e$  and  $\mu$  semileptonic decays. The terms in the denominator of the second expression are

$$R_\tau = \frac{\Gamma(b \rightarrow c\tau^-\bar{\nu})}{\Gamma(b \rightarrow ce^-\bar{\nu})}, \quad R_c = \frac{\Gamma(b \rightarrow c\bar{u}d + c\bar{u}s)}{\Gamma(b \rightarrow ce^-\bar{\nu})},$$

$$R_{cc} = \frac{\Gamma(b \rightarrow c\bar{c}s + c\bar{c}d)}{\Gamma(b \rightarrow ce^-\bar{\nu})}. \quad (45)$$

We can use Eqs. (41) and (42) to estimate these ratios. For example, with  $m_b = 4.8 \text{ GeV}/c^2$ ,  $m_c = 1.5 \text{ GeV}/c^2$ ,  $m_s = 0.3 \text{ GeV}/c^2$ , and  $m_u = m_d = 0$ , we obtain  $R_\tau \approx 0.20$ ,  $R_c/3 \approx 1$ , and  $R_{cc}/3 \approx 0.31$ , which lead to  $\mathcal{B}_{\text{SL}} = 16\%$ . The measured value is around 10% to 11%, so with these masses the free-quark spectator model, ignoring QCD corrections, substantially overestimates the  $B$  semileptonic branching fraction.

Two key issues must be resolved before  $\mathcal{B}_{\text{SL}}$  can be reliably computed: determining the appropriate values for the quark masses and calculating the QCD corrections to the hadronic rate. We summarize the main results on perturbative QCD corrections, which were first obtained by Altarelli *et al.* (1982) and Altarelli and Petrarca (1991). [A useful synopsis of this work has been presented by Bigi, Blok, Shifman, and Vainshtein (1994), who also extend it using a heavy-quark expansion, as discussed below.] The exchange of hard gluons between quarks in the decay modifies the color structure of the process and enhances the nonleptonic rate by the factor (Altarelli and Maiani, 1974; Gaillard and Lee, 1974; Altarelli *et al.*, 1981a, 1981b; Buras and Weisz, 1990)

$$\eta = \frac{c_-^2 + 2c_+^2}{3}, \quad (46)$$

where the Wilson coefficients  $c_+$  and  $c_-$  are given by

$$c_\pm = \left[ \frac{\alpha_s(\mu)}{\alpha_s(M_W)} \right]^{d_\pm}, \quad (47)$$

with  $d_+ = -6/23$  and  $d_- = 12/23$ . The renormalization scale  $\mu$  is a nonphysical artifact of the calculation, which includes only the effect of virtual gluons in the momentum range  $\mu$  to  $M_W$ . Softer gluons, with momentum below this cutoff, are in principle dealt with by an additional factor  $J$ , so that the nonleptonic rate is proportional to  $\eta J$ . For example,

$$\Gamma(b \rightarrow c\bar{u}d) = 3\Gamma_0 I\left(\frac{m_c}{m_b}, 0, 0\right) \eta J, \quad (48)$$

where we have used  $|V_{ud}|^2 \approx 1$  and where  $\Gamma_0$  is defined after Eq. (41). For  $\mu = m_b$ , the values are  $\eta \approx 1.1$  and  $J \approx 1.15$ , giving a net enhancement factor for  $b \rightarrow c\bar{u}d$  of about 1.27. In practice, due to the approximate nature of the calculation, the factor  $\eta J$  still has some dependence on the scale  $\mu$ .

Altarelli and Petrarca (1991) estimate uncertainties associated with the possible variation in  $\mu$  and  $\alpha_s$  and present two values of  $\mathcal{B}_{\text{SL}}$  depending on whether light or heavy values of the quark masses are used:

$$\mathcal{B}_{\text{SL}} = [12.2 \pm 0.45(\text{scale}) \pm 0.8(\alpha_s)]\% \quad (\text{light masses}) \quad (49)$$

and

$$\mathcal{B}_{\text{SL}} = [14.4 \pm 0.45(\text{scale}) \pm 0.8(\alpha_s)]\% \quad (\text{heavy masses}), \quad (50)$$

where the scale uncertainty is evaluated by allowing  $\mu$  to vary between  $m_b/2$  and  $m_b$ . The light (heavy) masses, in  $\text{GeV}/c^2$ , are  $m_b = 4.6$  (5.0),  $m_c = 1.2$  (1.7),  $m_s = 0.15$  (0.3), and  $m_u = m_d = 0$  (0.16).

Although the result for light quark masses is consistent with the measured value of  $\mathcal{B}_{\text{SL}}$  within errors, there is not yet consensus as to whether the assumptions required to push the theoretical prediction down to the measured value are realistic, or whether the estimates of the uncertainties are reasonable. In addition, there are uncertainties on the size of possible additional corrections due to both perturbative and nonperturbative QCD effects.

Recently, there has been great interest in applying heavy-quark expansions to inclusive processes. The uncertainties in such calculations are easier to isolate and to express quantitatively than those in phenomenological models. Chay, Georgi, and Grinstein (1990) first applied HQET and the operator product expansion to the problem of semileptonic  $B$  decay. Their analysis demonstrated that the lowest-order term in a  $1/m_b$  expansion corresponds to the result from a free-quark decay model, assuming that  $m_b$  is suitably defined. Furthermore, they showed that there are no nonperturbative QCD corrections of order  $\Lambda_{\text{QCD}}/m_b$ . Thus one can write

$$\Gamma(B \rightarrow X) = \Gamma(b \rightarrow x) + \mathcal{O}(1/m_b^2). \quad (51)$$

Bigi *et al.* (Bigi and Uraltsev, 1992; Bigi *et al.*, 1992; Bigi, Blok, Shifman, and Vainshtein, 1994); have argued that the  $\mathcal{O}(1/m_b^2)$  corrections are likely to be small, with a natural scale set by  $1 \text{ GeV}^2/m_b^2$ , and that a significant enhancement of the nonleptonic rate would therefore have to come from perturbative corrections. Although these are not completely known, Bigi *et al.* estimate that the natural range of predictions for  $\mathcal{B}_{\text{SL}}$  satisfies the bound

$$\mathcal{B}_{\text{SL}} \geq 12.5\%. \quad (52)$$

As discussed in the following section, the measured values from CLEO and ARGUS are in the range 10% to 11%, while those from LEP are slightly higher, around 11.5%.

An analysis of the perturbative QCD corrections has recently been performed by Bagan *et al.* (1995). The calculation is based on a study of the charm-quark mass dependence of the radiative corrections, as discussed in an earlier paper by the same authors (Bagan *et al.*, 1994). The rate in the  $b \rightarrow c\bar{c}s$  channel is increased, leading to

$$\mathcal{B}_{\text{SL}} = (11.8 \pm 0.8 \pm 0.5 \pm 0.2 \pm 0.2_{-1.3}^{+0.9})\%, \quad (53)$$

where the first error is from the uncertainty on  $m_b = (4.8 \pm 0.2) \text{ GeV}/c^2$ , the second from the uncertainty on  $\alpha_s(m_Z) = 0.117 \pm 0.007$ , the third from the uncertainty on  $\lambda_1 = (-0.5 \pm 0.1) \text{ GeV}^2$ , which parametrizes the kinetic energy of the  $b$  quark inside the hadron, the fourth from the uncertainty on  $\Gamma(b \rightarrow c\bar{c}s)$ , and the last from the variation in the renormalization scale. The scale error is large, indicating that higher-order perturbative QCD corrections are important. An alternative renormalization scheme gives

$\mathcal{B}_{\text{SL}}=11.0\%$  with similar errors. This analysis shows that the perturbative QCD corrections are quite important and that they tend to push the value  $\mathcal{B}_{\text{SL}}$  down towards the measurements. The  $b \rightarrow c\bar{c}s$  rate is increased by 35% in this calculation by taking into account the effect of the  $c$ -quark mass in the QCD radiative corrections.

There has been much speculation on the difference between the measured and calculated values of  $\mathcal{B}_{\text{SL}}$ . Some theorists have argued that the QCD calculations are simply not precise enough to indicate a real problem; others have suggested specific mechanisms to increase the hadronic rate. Enhancement of the  $b \rightarrow c\bar{c}s$  channel, discussed above, has also been suggested by Falk, Wise, and Dunietz (1994). CLEO has measured the average number of charm quarks per  $B$  decay,  $n_c = [B \rightarrow cX + 2(B \rightarrow c\bar{c}X)]/[B \rightarrow X]$ , obtaining  $n_c = 1.07 \pm 0.08$  (Muheim, 1994). In the Bagan *et al.* calculation,  $n_c = 1.28 \pm 0.08$ . Thus the measurement does not give one great confidence that the problem is solved, but neither does it indicate a strong contradiction. The problem of  $\mathcal{B}_{\text{SL}}$  is perhaps best rephrased as the joint problem of understanding  $\mathcal{B}_{\text{SL}}$  and  $n_c$ .

It is also possible that  $\mathcal{B}_{\text{SL}}$  is being reduced by unexpected hadronic decays that have no final-state charm particles. For example, large contributions from  $b \rightarrow s + \text{gluon}$ , arising from physics at the TeV scale, have been suggested (Kagan, 1994) as a possible enhancement to the hadronic rate; the mechanism invoked might also explain the  $\Delta I = 1/2$  rule in kaon decays. The difficulty in explaining the observed value of  $\mathcal{B}_{\text{SL}}$  remains an unresolved problem, but steady progress is being made towards better calculations and measurements.

We turn now to predictions of the total semileptonic rate and the shape of the lepton-energy spectrum. These quantities have less uncertainty than  $\mathcal{B}_{\text{SL}}$ , since knowledge of the hadronic rate is not required. The ACCMM model (Altarelli, Cabibbo, Corbò, Maiani, and Martinelli, 1982) was one of the first to incorporate bound-state effects in the initial heavy meson, which can significantly affect the spectrum. This phenomenological model is used extensively by experimentalists in fitting single-lepton momentum spectra, and it has become a benchmark for theoretical calculations as well. In the ACCMM model, the momentum of the heavy quark (or that of the spectator quark) within the decaying meson is described by a distribution  $\phi(p)$ , which is assumed to be Gaussian:

$$\phi(p) = \frac{4}{\sqrt{\pi} p_F^3} e^{-p^2/p_F^2}. \quad (54)$$

The Fermi-momentum parameter  $p_F$  determines the width of  $\phi(p)$ , and the normalization is such that the integral of  $\phi(p)p^2$  over all momenta is equal to 1. The spectator quark is assumed to have a definite mass  $m_{\text{sp}}$ , but the  $b$  quark is a virtual particle of variable mass  $m_b$ , constrained by energy and momentum conservation to be

$$m_b^2 = m_B^2 + m_{\text{sp}}^2 - 2M_B \sqrt{m_{\text{sp}}^2 + p^2}. \quad (55)$$

This somewhat peculiar result means that in this model the free parameters are  $p_F$ ,  $m_{\text{sp}}$ , and the mass of the daughter

quark,  $m_q = m_c$  or  $m_q = m_u$ . To compute the lepton-energy spectrum, the decay distribution in the  $b$ -quark rest frame is boosted to the  $B$  frame. The lepton-energy spectrum for  $b \rightarrow q\ell^-\bar{\nu}$  in the  $b$ -quark rest frame is given by

$$\frac{d\Gamma(m_b, x)}{dx} = \frac{G_F^2 m_b^5}{96\pi^3} \frac{x^2(x_m - x)^2}{(1-x)^3} [(1-x)(3-2x) + (1-x_m)(3-x)] \left[ 1 - \frac{2\alpha_s}{3\pi} G(x, \epsilon) \right], \quad (56)$$

where  $x = 2E/m_b$ ,  $x_m = 1 - (m_q/m_b)^2$ , and  $\epsilon = m_q/m_b$ . The function  $G(x, \epsilon)$  is discussed by Altarelli *et al.* (1982), Jezabek and Kuhn (1989), and Czarnecki and Jezabek (1994) and incorporates the effect of gluon radiation on the lepton-energy spectrum. We shall refer to this model extensively in the discussion of fits to the lepton-energy spectrum in  $b$ -hadron decay. The ACCMM model also predicts the spectrum for charm semileptonic decay

$$\frac{d\Gamma(m_c, x)}{dx} = \frac{G_F^2 m_c^5}{16\pi^3} \frac{x^2(x_m - x)^2}{(1-x)} \left[ 1 - \frac{2\alpha_s}{3\pi} G(x, \epsilon) \right], \quad (57)$$

which is used in the parametrization of the secondary lepton spectrum in the same fits. A controversial issue is whether the ACCMM model provides a reliable description of the  $b \rightarrow u\ell^-\bar{\nu}$  lepton-energy spectrum in the end-point region. This question has significant impact on the determination of  $|V_{ub}|$  (see Sec. V.E). Another early approach to inclusive semileptonic  $B$  decays was that of Bareiss and Paschos (1989), who considered both the lepton-energy spectrum and the decay rate in the parton model.

Recently, much attention has been devoted to applying the heavy-quark expansion to the lepton-energy spectrum (Bigi *et al.*, 1993; Falk *et al.*, 1994; Manohar and Wise, 1994; Neubert, 1994a), in particular to the end-point region. Although the spectrum can be calculated over much of the momentum range, the end-point region remains problematic. Manohar and Wise (1994) conclude that the predictions of the heavy-quark expansion near the end point are valid only if they are smeared over a region of size 500 MeV, which is larger than the difference in the end points for  $b \rightarrow c\ell^-\bar{\nu}$  and  $b \rightarrow u\ell^-\bar{\nu}$ .

The ACCMM model has now been analyzed in the context of HQET (Baillie, 1994; Csaki and Randall, 1994). The model is found to be inconsistent in certain respects with HQET results, but for a suitably defined  $b$ -quark mass, the differences between the predicted spectra are in general quite small. The exception is the end-point region, where neither approach is on solid footing.

Accurate prediction of the semileptonic rate is of great importance for the determination of  $|V_{cb}|$ . Using heavy-quark expansions, Shifman, Uraltsev, and Vainshtein (1995), Luke and Savage (1994), and Ball, Beneke, and Braun (1995) have obtained predictions for the rate and have analyzed the uncertainties in the calculations. Shifman *et al.* obtain the result

$$\Gamma(B \rightarrow X_c \ell^- \bar{\nu}) = \frac{G_F^2 m_b^5}{192 \pi^3} |V_{cb}|^2 \left\{ \left[ z_0(x) - \frac{2\alpha_s}{3\pi} \left( \pi^2 - \frac{25}{4} \right) z_0^{(1)}(x) \right] \left( 1 - \frac{\mu_\pi^2 - \mu_G^2}{2m_b^2} \right) - z_1(x) \frac{\mu_G^2}{m_b^2} + \mathcal{O}(\alpha_s^2, \alpha_s/m_b^2, 1/m_b^3) \right\}, \quad (58)$$

where  $x = m_c/m_b$  and

$$z_0(x) = 1 - 8x^2 + 8x^6 - x^8 - 24x^4 \ln x, \\ z_1(x) = (1 - x^2)^4, \quad (59)$$

and  $z_0^{(1)}(x)$  has been tabulated by Cabibbo and Maiani (1978). This function, which incorporates the one-gluon perturbative QCD corrections, has the values  $z_0^{(1)}(0) = 1$  and  $z_0^{(1)}(1) \approx 0.41$ . These QCD effects are calculated analogously to the QED radiative corrections to muon decay. Non-perturbative QCD effects are contained in the parameters  $\mu_\pi$  and  $\mu_G$ , which are matrix elements of the bottom-quark kinetic energy and chromomagnetic-moment operators, respectively. The value of  $\mu_G$  can be related to the  $B^* - B$  mass difference:

$$\mu_G^2 = \frac{3}{4} (M_{B^*}^2 - M_B^2) \approx 0.35 \text{ GeV}^2, \quad (60)$$

but  $\mu_\pi$  is much more difficult to determine. Using QCD sum rules, Shifman *et al.* obtain  $0.35 \leq \mu_\pi^2 < 0.8 \text{ GeV}^2$  with a preferred value of  $\mu_\pi^2 = 0.54 \text{ GeV}^2$ . These authors consider this range to be an overestimate of the uncertainty; even so, it results in only about a 3% uncertainty in  $|V_{cb}|$ . The factor  $m_b^5$  that appears in the semileptonic decay rate (but not in the branching fraction) has long been a source of difficulty. These authors argue that one can take  $m_b = (4.8 \pm 0.1) \text{ GeV}/c^2$  from a QCD sum-rule analysis of the  $Y$  system. Moreover, the actual direct dependence on  $m_b$  is not  $m_b^5$ : the product of  $m_b^5 z_0(m_c^2/m_b^2)$  that appears in the decay-rate formula results in less sensitivity to  $m_b$ , assuming that  $m_b - m_c$  is constrained. With HQET, this mass difference can be related to bottom- and charm-meson masses and  $\mu_\pi$ :

$$m_b - m_c = \frac{M_B + 3M_{B^*}}{4} - \frac{M_D + 3M_{D^*}}{4} \\ + \mu_\pi^2 \left( \frac{1}{2m_c} - \frac{1}{2m_b} \right) + \mathcal{O}(1/m_c^3, 1/m_b^3), \quad (61)$$

leading to  $m_c = (1.3 \pm 0.1) \text{ GeV}/c^2$  for  $m_b = (4.8 \pm 0.1) \text{ GeV}/c^2$ . These values yield the following relation between  $|V_{cb}|$  and the  $B \rightarrow X_c \ell^- \bar{\nu}$  branching fraction:

$$|V_{cb}| = 0.0415 \left( \frac{1.49 \text{ ps}}{\tau_B} \right)^{1/2} \left[ \frac{B(B \rightarrow X_c \ell^- \bar{\nu})}{0.106} \right]^{1/2}. \quad (62)$$

The conclusion of Shifman, Uraltsev, and Vainshtein is that the uncertainty in  $|V_{cb}|$  obtained with this procedure is less than 5%, and they regard this estimate as very conservative.

The analysis presented by Luke and Savage (1994) is similar in approach, although their conclusions regarding the uncertainty are quite different. The quoted uncertainty in  $|V_{cb}|$  is about  $\pm 20\%$ , although this range is meant to correspond to a larger range than  $\pm 1\sigma$ . Another detailed HQET-based analysis of the semileptonic rate has been performed

by Ball, Beneke, and Braun (1995). They use a pole mass of  $m_b = (5.05 \pm 0.06) \text{ GeV}/c^2$  and a mass difference of  $m_b - m_c = (3.43 \pm 0.04) \text{ GeV}/c^2$ , giving

$$|V_{cb}| = (0.041 \pm 0.002) \left( \frac{1.5 \text{ ps}}{\tau_B} \right)^{1/2} \left[ \frac{B(B \rightarrow X_c \ell^- \bar{\nu})}{0.109} \right]^{1/2}. \quad (63)$$

(The second error quoted in their paper corresponds to the experimental uncertainty on  $\mathcal{B}_{\text{SL}}$  and is removed here.) In Sec. V.D.4 we present the decay-rate predictions of all these calculations and the values of  $|V_{cb}|$  obtained using the measured value of  $\mathcal{B}_{\text{SL}}$  (see Table XI below).

There is not yet a consensus on the size of the errors on  $|V_{cb}|$  that arise from theoretical uncertainty. Rapid progress is being made, and it is likely that many of these issues will be clarified in the relatively near future.

### C. Inclusive charm semileptonic decays

Historically, measurements of the inclusive semileptonic branching fractions for  $D$  mesons were of interest because of the large difference in the  $D^0$  and  $D^+$  lifetimes. Early measurements of the ratio of  $D^0$  and  $D^+$  inclusive semileptonic branching fractions by Mark II (Schindler *et al.*, 1981) and DELCO (Bacino *et al.*, 1980) at SPEAR indicated that the  $D^+$  lifetime is significantly larger than the  $D^0$  lifetime. Direct measurements of the lifetimes confirmed these results.

Most inclusive studies of semileptonic charm decays have been carried out with  $e^+e^-$  colliders rather than fixed-target experiments. In  $e^+e^-$  experiments, single leptons from charm decay can be isolated from background processes by reconstructing the other charm hadron in the event or by associating the lepton with a slow pion from  $D^*$  decay. In the fixed-target environment, the efficiency for even partially reconstructing both charm hadrons in an event is very low. The background from noncharm events is generally so high that the combination of a lepton and a slow pion is not a sufficiently distinctive signature to isolate inclusive semileptonic charm decays.

Until recently, the most precise values of the inclusive semileptonic branching fractions were those measured by the Mark III collaboration at SPEAR (Baltrusaitis *et al.*, 1985). CLEO now has a measurement of the inclusive branching fraction for the neutral  $D$  meson that is more precise (Kubota *et al.*, 1995). In addition, E653 has measured the ratio of rates  $\Gamma(D^0 \rightarrow K^- \mu^+ \nu_\mu) / \Gamma(D^0 \rightarrow X \mu^+ \nu_\mu)$  (Kodama *et al.*, 1994), from which they extract the inclusive branching fraction using the precisely known rate for  $D^0 \rightarrow K^- \ell^+ \nu$ .

The Mark III measurement used about 50 000  $D\bar{D}$  events produced just above threshold at the  $\psi(3770)$ . Events were selected in which one of the  $D$  decays was fully reconstructed in a hadronic mode, yielding approximately 1700  $D^+D^-$  and 3400  $D^0\bar{D}^0$  events. The numbers of identified

electrons observed recoiling against the reconstructed  $D^0$  or  $D^+$  decays were used to extract the branching fractions,

$$B(D^+ \rightarrow X e^+ \nu_e) = (17.0 \pm 1.9 \pm 0.7)\%,$$

$$B(D^0 \rightarrow X e^+ \nu_e) = (7.5 \pm 1.1 \pm 0.4)\%, \quad (64)$$

and the ratio of branching fractions

$$\frac{B(D^+ \rightarrow X e^+ \nu_e)}{B(D^0 \rightarrow X e^+ \nu_e)} = 2.3_{-0.4}^{+0.5} \pm 0.1. \quad (65)$$

The Mark III measurements are consistent with the ratio of measured lifetimes (Particle Data Group, 1994)

$$\frac{\tau(D^+)}{\tau(D^0)} = 2.55 \pm 0.05. \quad (66)$$

For the measurement of  $B(D^0 \rightarrow X e^+ \nu_e)$ , CLEO uses  $D^0$  mesons from  $D^{*+} \rightarrow D^0 \pi^+$  where the  $D^{*+}$  decay is identified through the slow pion. This method was pioneered by HRS (Abachi *et al.*, 1988) and was used in CLEO's measurement of the absolute branching fraction for  $D^0 \rightarrow K^- \pi^+$  (Akerib *et al.*, 1993). The method depends on two characteristics of  $D^{*+}$  production and decay. When a  $D^*$  is created in  $e^+e^-$  annihilation above  $c\bar{c}$  threshold, its momentum is nearly parallel to the thrust axis of the event. Second, because the  $Q$  value of the decay  $D^{*+} \rightarrow D^0 \pi^+$  is small, the angle between the  $\pi^+$  and the  $D^{*+}$  (in the laboratory frame) is also small. Therefore the number of  $D^{*+} \rightarrow D^0 \pi^+$  decays can be determined from the excess of slow pions with a small lab angle  $\alpha$  with respect to the thrust axis of the event. The branching fraction for  $D^0 \rightarrow X e^+ \nu_e$  is determined from the fraction of events containing a slow pion with small  $\alpha$  that also have an electron with the same charge as the pion, in the vicinity of the pion.

In the CLEO analysis, only charged pions with momentum greater than 225 MeV/ $c$  and less than 425 MeV/ $c$  are used. The lower momentum cut eliminates events with  $D^{*+}$ 's from  $B$  decays, in which the thrust axis is not a good measure of the  $D^*$  direction. The distribution of  $\alpha$  is shown in Fig. 14 or all charged tracks with momenta between 225 and 425 MeV/ $c$  (top set of solid data points), and for those with an electron of the same charge as the pion, with momentum above 0.7 GeV/ $c$ , within a  $37^\circ$  cone around the pion (bottom set of solid data points). Background estimates are also shown in Fig. 14. For the normalizing events, charged particles with the same charge as the tagged  $\pi^+$ , but in the opposite hemisphere, are used to determine the background shape (histogram in top part of Fig. 14). For the background under the leptonic signal, events in which the reconstructed electron has charge opposite that of the slow pion are used (open data points at bottom of Fig. 14). There is clearly an excess of slow pions at low  $\sin^2\alpha$ . The peak near  $\sin^2\alpha=1$  ( $\alpha \approx 90^\circ$ ) is due to particles that are fairly uniformly distributed in  $\cos\alpha$ . In the analysis, the signal sizes and efficiencies are determined separately for eight 25 MeV/ $c$ -wide momentum ranges for the slow pion. The result from this analysis is

$$B(D^0 \rightarrow X e^+ \nu_e) = (6.64 \pm 0.18 \pm 0.29)\% \quad (\text{CLEO II}), \quad (67)$$

consistent with the Mark III measurement, but with a significantly smaller statistical uncertainty. (This CLEO result has been updated since the preprint version of this article.)

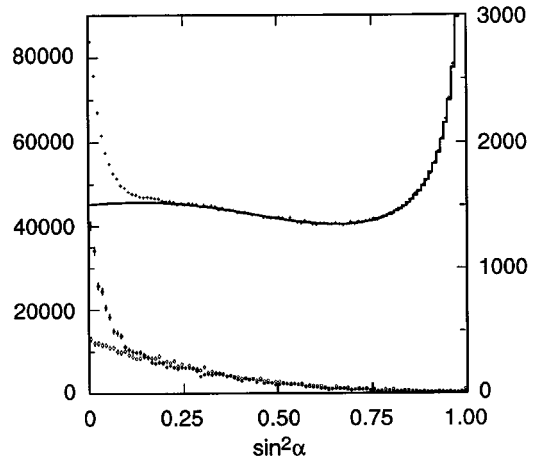


FIG. 14. CLEO measurement of the  $D^0$  inclusive semileptonic branching fraction. The soft pion from the decay  $D^{*+} \rightarrow D^0 \pi^+$  is used to tag a  $D^0$  sample; within this sample, one counts the number of events with leptons. The upper set of data points and the associated background curve give the distribution of  $\sin^2\alpha$ , where  $\alpha$  is the angle between the thrust axis of the event and pions with momenta in the range 225–425 MeV/ $c$ . The excess events with low values of  $\sin^2\alpha$  are due to  $D^{*+} \rightarrow D^0 \pi^+$  decays, since the soft pion is usually produced with a small angle relative to the  $D^{*+}$  direction. (The left axis applies to this set of data.) The two lower sets of data points correspond to the subset of events in which an electron is found within a  $37^\circ$  cone centered on the slow pion. (The right axis applies to these data points.) The open circles give the background level within the lepton sample. This background is determined with wrong-sign candidates, as described in the text.

For the E653 measurement, the decay chain  $D^{*+} \rightarrow D^0 \pi^+$  with the subsequent decay of the  $D^0$  to a muon and at least one oppositely charged hadron was used to identify 232 semimuonic  $D^0$  decay candidates. The ratio  $\Gamma(D^0 \rightarrow K^- \mu^+ \nu_\mu) / \Gamma(D^0 \rightarrow X \mu^+ \nu_\mu)$  was then extracted from the joint distribution of these events in two  $D$  decay variables calculated from the measured momenta of the charged particles and the  $D$  flight direction (as determined by the positions of the primary and decay vertices). The two variables are the minimum mass of the parent particle that allows momentum to be conserved for the candidate  $D$  decay, and the momentum component of the charged hadron transverse to the  $D$  flight direction. The measured ratio of

$$\frac{\Gamma(D^0 \rightarrow K^- \mu^+ \nu_\mu)}{\Gamma(D^0 \rightarrow X \mu^+ \nu_\mu)} = 0.472 \pm 0.051 \pm 0.040 \quad (68)$$

has a total fractional error of about 14%. The fractional error on  $B(D^0 \rightarrow K^- \ell^+ \nu)$  is only about 5%. The world average for  $B(D^0 \rightarrow K^- \ell^+ \nu)$  from Eq. (126) is used to extract an inclusive branching-fraction measurement of

$$B(D^0 \rightarrow X \ell^+ \nu) = (7.86 \pm 1.15)\% \quad (\text{E653}). \quad (69)$$

In summary, the weighted world averages of all measurements of inclusive branching fractions (Particle Data Group, 1994), including the E653 and CLEO results, are

$$B(D^+ \rightarrow X \ell^+ \nu) = (17.2 \pm 1.9)\%$$

and

$$B(D^0 \rightarrow X \ell^+ \nu) = (6.85 \pm 0.31)\%. \quad (70)$$

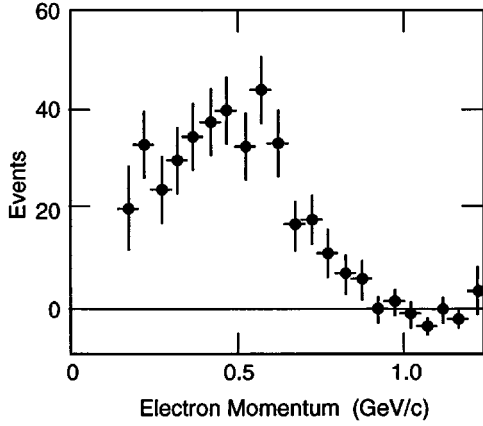


FIG. 15. Background-subtracted, efficiency-corrected electron momentum spectrum for a mixture of  $D^0$  and  $D^+$  decays reconstructed by DELCO. Redrawn from Bacino *et al.* (1979).

Using the values of the  $D^+$  and  $D^0$  lifetimes listed in Table III, we calculate the inclusive semileptonic decay rates to be

$$\Gamma(D^+ \rightarrow X\ell^+\nu) = (16.3 \pm 1.8) \times 10^{10} \text{ s}^{-1}$$

and

$$\Gamma(D^0 \rightarrow X\ell^+\nu) = (16.5 \pm 0.8) \times 10^{10} \text{ s}^{-1} \quad (71)$$

with an average of

$$\Gamma(D \rightarrow X\ell^+\nu) = (16.5 \pm 0.7) \times 10^{10} \text{ s}^{-1}. \quad (72)$$

The fact that the  $D^0$  and  $D^+$  semileptonic widths are measured to be equal means that the source of the lifetime difference between the  $D^0$  and  $D^+$  mesons lies in the hadronic width. The inclusive semileptonic branching fraction for the  $D^+$  is close to the value of 1/5 one would expect from the simple spectator model, while that for the  $D^0$  is significantly smaller. However, it is believed that the difference in hadronic widths is caused by the suppression of the  $D^+$  hadronic decay rate due to destructive interference between amplitudes for internal and external  $W$  emission. The branching fraction of around 7% for the  $D^0$  is closer to what one would predict from the expected enhancement in hadronic decays due to hard-gluon exchange discussed in Sec. V.B. We compare the sum of exclusive semileptonic  $D$  decay rates to the inclusive rate in Sec. VI.D.

Although the preliminary CLEO measurement of the inclusive semileptonic branching fraction for  $D^0$  is the most precise to date, it has not yielded a measurement of the inclusive electron momentum spectrum. The best published inclusive lepton momentum spectrum for semileptonic charm decays was measured by DELCO in 1979, with an approximately equal combination of  $D^0$  and  $D^+$  decays produced just above threshold at the  $\psi(3770)$  resonance (Bacino *et al.*, 1979). This is an ideal environment for measuring the inclusive spectrum because there is no smearing of the momentum spectrum due to a Lorentz boost, as there is for  $c\bar{c}$  production significantly above threshold. A Čerenkov counter was used to identify electrons with high efficiency down to momenta of a few hundred MeV/c, yielding about 600 candidate events. The efficiency-corrected, background-subtracted spectrum is shown in Fig. 15. Knowledge of this spectrum is important for several studies of semileptonic  $B$

decays, since leptons from charm decays are often a significant background. However, the form factors and relative branching fractions for the dominant semileptonic  $D$  decay modes,  $D \rightarrow \bar{K}\ell^+\nu$  and  $D \rightarrow \bar{K}^*\ell^+\nu$ , have now been measured sufficiently well (see Sec. VI) that one can obtain the expected lepton-energy spectrum by summing the spectra for the individual exclusive modes.

#### D. Inclusive bottom semileptonic decays and $|V_{cb}|$

The inclusive semileptonic branching fraction for  $b$  hadrons has been measured both at the  $Y(4S)$ , where the  $b$  hadrons are a mixture of  $B_u$  and  $B_d$  mesons, and at the  $Z$ , where  $B_s$  mesons and  $b$  baryons are produced as well. The largest data samples are obtained by measuring only the lepton, without using any tagging procedure to determine the species of decaying  $b$  hadron. Thus, at the  $Y(4S)$ , the quantity measured with the highest statistical precision is

$$\mathcal{B}_{\text{SL}} = f_0 \mathcal{B}_{\text{SL}}^0 + f_- \mathcal{B}_{\text{SL}}^-, \quad (73)$$

where  $f_0$  and  $f_-$  are the fractions of neutral and charged  $B$  mesons, and

$$\mathcal{B}_{\text{SL}}^0 \equiv B(\bar{B}^0 \rightarrow X^+ \ell^- \bar{\nu})$$

and

$$\mathcal{B}_{\text{SL}}^- \equiv B(B^- \rightarrow X^0 \ell^- \bar{\nu}). \quad (74)$$

Here  $\ell^-$  represents either  $e^-$  or  $\mu^-$  but not their sum. At the  $Y(4S)$ ,  $f_0 \approx f_- \approx 1/2$ , but these fractions have not been precisely measured. Experiments at the  $Z$  measure

$$\mathcal{B}_{\text{SL}} \equiv f_0 \mathcal{B}_{\text{SL}}^0 + f_- \mathcal{B}_{\text{SL}}^- + f_s \mathcal{B}_{\text{SL}}^s + f_{\text{bar}} \langle \mathcal{B}_{\text{SL}}^{\text{bar}} \rangle, \quad (75)$$

where  $f_s$  and  $f_{\text{bar}}$  give the fraction of  $b\bar{s}$  and  $b$ -baryon states, respectively;  $\mathcal{B}_{\text{SL}}^s$  is the semileptonic branching fraction of the  $B_s$ ; and  $\langle \mathcal{B}_{\text{SL}}^{\text{bar}} \rangle$  is the average (weighted by production fractions) of the  $b$ -baryon semileptonic branching fractions. The production fractions of different  $b$  hadrons at the  $Z$  are not well known; expected values are  $f_0 = f_- = 0.4$ ,  $f_s = 0.12$ , and  $f_{\text{bar}} = 0.08$ .

Below we describe three types of measurements:

(i) Measurement of the inclusive single-lepton momentum spectrum. This technique determines  $\mathcal{B}_{\text{SL}}$  with the smallest statistical error, but with significant model dependence from the fitting procedure, which is used to separate the contributions from primary and secondary leptons. However, this measurement gives the most precise determination of the shape of the  $B \rightarrow X\ell^-\bar{\nu}$  momentum spectrum in the upper part of the momentum range.

(ii) Measurement of  $\mathcal{B}_{\text{SL}}$  using charge and angular correlations in dilepton events at the  $Y(4S)$ . This technique determines  $\mathcal{B}_{\text{SL}}$  with the least model dependence, because models are needed only for a relatively small extrapolation from the minimum momentum for identified leptons down to zero momentum.

(iii) Separate measurement of  $\mathcal{B}_{\text{SL}}^0$  and  $\mathcal{B}_{\text{SL}}^-$ . By reconstructing one  $B$  meson in an  $Y(4S)$  event, it is possible to tag the charge of the other. Using this technique, CLEO has separately measured  $\mathcal{B}_{\text{SL}}^0$  and  $\mathcal{B}_{\text{SL}}^-$ , but the statistical errors are much larger than those for the average.

We then discuss the determination of  $|V_{cb}|$  from measurements of the  $B$ -meson semileptonic branching fraction.

### 1. Measurement of $\mathcal{B}_{SL}$ using the inclusive lepton spectrum

The challenge for inclusive measurements is to determine what part of the observed lepton-momentum spectrum is due to leptons from  $b$ -hadron decay (primary leptons) and what part is due to leptons from charm decay (secondary leptons) or other sources (misidentified hadrons, photon conversions,  $J/\psi$  decays, etc.). The standard technique is to fit the observed lepton-momentum spectrum to a sum of the shapes expected for primary and secondary decays, after subtracting backgrounds from other sources. Thus a large part of the effort (and uncertainty) in the analysis is in the determination of these shapes.

Experiments at the  $Y(4S)$  (ARGUS and CLEO) use theoretical models, either inclusive or exclusive, to describe the primary-lepton spectrum. The ACCMM model (Altarelli *et al.*, 1982) discussed in Sec. V.B is the standard inclusive model used for this purpose. It has free parameters (determined from the fit) corresponding to the  $c$ -quark mass, the Fermi momentum of the  $b$  quark, and the spectator-quark mass. Alternatively, one can use exclusive models to predict the shape of the primary-lepton spectrum by summing the predicted distributions for exclusive modes. Because the ISGW model (Isgur, Scora, Grinstein, and Wise, 1989) makes predictions for nearly all modes expected to contribute significantly to the spectrum, this exclusive model is most commonly used in the fits. In this model, the dominant contributions to the primary spectrum are from  $B \rightarrow D\ell^-\bar{\nu}$  and  $B \rightarrow D^*\ell^-\bar{\nu}$ , with some from  $B \rightarrow D^{**}\ell^-\bar{\nu}$ . Here,  $D^{**}$  refers to a mixture of  $p$ -wave and radially excited charm mesons. The contribution from these higher-mass states is important primarily in the lower part of the momentum spectrum.

It is important to recognize that, when using a theoretical model to extract  $\mathcal{B}_{SL}$ , one is sensitive only to the shapes predicted by the model; however, the calculation of  $|V_{cb}|$  from the value of  $\mathcal{B}_{SL}$  involves not the shapes but the normalization. This latter step can be performed with the same or different models.

The shape used to describe the secondary-lepton spectrum in these fits, although somewhat more complicated to obtain, is based on data. The inclusive charm decay lepton spectrum, measured by DELCO (Bacino *et al.*, 1979) using  $\psi''(3770) \rightarrow D\bar{D}$  decays at SPEAR (see Sec. V.C), is fit to the ACCMM model. The lepton spectrum in the  $D$  rest frame is then boosted according to the momentum spectrum of  $D$  mesons measured at the  $Y(4S)$ . Future measurements should be able to use a charm decay lepton spectrum obtained by summing the spectra for the known exclusive charm semileptonic modes, which account for most of the inclusive rate.

Figure 16 shows the electron and muon data from CLEO II (Bartelt *et al.*, 1993b), which has the largest event sample. The muon spectrum cuts off below 1.3 GeV/ $c$  due to the iron absorber in front of the muon detectors, but the electron spectrum is measured down to 0.6 GeV/ $c$ . Backgrounds from continuum processes,  $\psi \rightarrow \ell^+\ell^-$ , photon conversions,  $\pi^0$  Dalitz decays, and  $B \rightarrow X\tau^-\bar{\nu}_\tau$  decays have been sub-

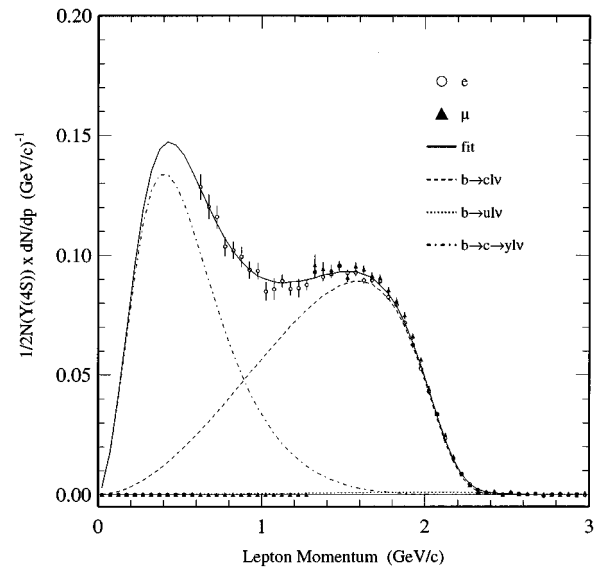


FIG. 16. The inclusive lepton spectrum from CLEO II, with a fit based on the ACCMM inclusive model. The fit is used to extract the component of the spectrum due to  $B \rightarrow X\ell^-\bar{\nu}$  decays (primary leptons), which is shown as a dashed curve. Secondary leptons from  $b \rightarrow c \rightarrow y\ell^+\nu$  decays are shown as a dot-dashed curve; their spectrum is much softer. Finally, there is a very small contribution from primary leptons from  $B \rightarrow X_u\ell^-\bar{\nu}$  decays (dotted curve). This method has very little sensitivity to  $B \rightarrow X_u\ell^-\bar{\nu}$  processes, which are best studied in a specialized analysis of the end-point region.

tracted. The electron spectrum has been radiatively corrected according to the prescription of Atwood and Marciano (1990), so the electron and muon data can be directly compared. The agreement between the electron and muon spectra is extremely good.

The data shown in Fig. 16 are fit with the ACCMM model. This model is able to describe the spectrum well, giving  $\chi^2/N_{df}=0.9$ . The primary ( $B \rightarrow X_c\ell^-\bar{\nu}$ ) component of the spectrum accounts for most of the large hump above 1.0 GeV/ $c$ ; its contribution is determined essentially by the falling edge of the distribution above 1.5 GeV/ $c$ . The contribution of secondary leptons rises rapidly towards low momenta and dominates below 0.8 GeV/ $c$ . A third component, from  $B \rightarrow X_u\ell^-\bar{\nu}$  decays, is also included in the fit. It is barely visible at the bottom of the plot, and it is clear that the fit has very poor sensitivity to  $B \rightarrow X_u\ell^-\bar{\nu}$  decays. It is important to note that  $|V_{ub}|$  is not determined from this fit. Rather, a special analysis of the end-point region is required, in which strong cuts must be used to suppress continuum background (see Sec. V.E). Otherwise, the fluctuations in the large continuum subtraction performed for the analysis of the full spectrum would overwhelm the tiny  $B \rightarrow X_u\ell^-\bar{\nu}$  signal.

The ISGW model describes the  $B \rightarrow X_c\ell^-\bar{\nu}$  rate in terms of contributions from  $B \rightarrow D\ell^-\bar{\nu}$  (27%),  $B \rightarrow D^*\ell^-\bar{\nu}$  (60%), and  $B \rightarrow D^{**}\ell^-\bar{\nu}$  (13%), where  $D^{**}$  represents several  $p$ -wave and radially excited charm mesons whose separate rates are predicted by the model. Unlike the ACCMM model, the ISGW model has no free parameters, and it does not describe as well the shape of the CLEO II spectrum, giving  $\chi^2/N_{df}=1.5$ . The ISGW fit was also poor in the CLEO I data (Henderson *et al.*, 1992).

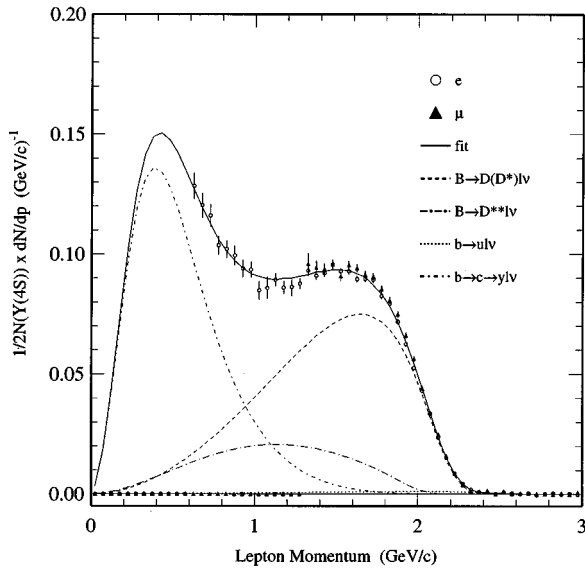


FIG. 17. The inclusive lepton spectrum from CLEO II, with a fit based on the ISGW\*\* model. In this modified version of the ISGW model, the  $D^*/D$  ratio is fixed at 2.3, but the  $D^{**}$  fraction is allowed to float. This degree of freedom improves the fit significantly, and the  $D^{**}$  fraction increases with respect to the value predicted in the ISGW model.

The difficulty in the ISGW fit can be traced to an excess of observed low-momentum leptons relative to the number predicted. A modified version of the ISGW model, ISGW\*\*, has therefore been created. In ISGW\*\*, the  $D^{**}$  fraction is allowed to vary, but the  $D^*$ -to- $D$  ratio is fixed at the value (2.3) predicted by ISGW. The fit to the CLEO data using ISGW\*\* gives  $\chi^2/N_{df}=0.9$ , significantly better than that us-

ing ISGW. The  $D^{**}$  fraction of the  $B \rightarrow X_c \ell^- \bar{\nu}$  rate has risen from 11% in the ISGW model to  $(21.2 \pm 1.6 \pm 8.0)\%$ . The systematic error is obtained by varying the  $D^*/D$  fraction and the mixture of  $D^{**}$  states. However, we caution against taking this  $D^{**}$  fraction too literally, since it is obtained in the framework of a particular model that does not include all possible contributions to the leptonic rate, such as  $B \rightarrow D \pi \ell^- \bar{\nu}$ , where the  $D \pi$  system is nonresonant. Figure 17 shows the fit to the CLEO II data with the ISGW\*\* model; the large  $D^{**}$  contribution is explicitly shown.

Similar analyses have been carried out by other experiments operating at the  $Y(4S)$ , including ARGUS, CUSB, and the Crystal Ball. The results are listed in Table VII. All of the measurements lie below 12.5%, the minimum discussed by Bigi *et al.* The difference between the CLEO II results obtained with the ACCMM and ISGW\*\* models is greater than the errors on the separate values, showing that model dependence is a problem at the 5% level. (The systematic errors on the individual CLEO II measurements are dominated by uncertainties on lepton identification and tracking efficiencies.) While the dilepton measurement discussed in the following section is able to reduce model dependence in the determination of  $\mathcal{B}_{SL}$ , the shape of the lepton spectrum in the upper part of the momentum range is determined best in the single-lepton analysis.

LEP experiments (ALEPH, DELPHI, L3, and OPAL) measure  $\mathcal{B}_{SL}$  by fitting the spectra of  $p$  and  $p_T$  (the lepton momentum transverse to the jet axis) in single-lepton and dilepton events. At the  $Z$ , the number of single-lepton events is used to determine the branching fraction for  $Z \rightarrow b \bar{b}$ , whereas the ratio of dilepton to single-lepton events can be used to determine  $\mathcal{B}_{SL}$ . The shape of the primary  $B \rightarrow X \ell^- \bar{\nu}$  spectrum is usually taken from CLEO or

TABLE VII. Single-lepton measurements of the inclusive semileptonic branching fraction (%),  $\mathcal{B}_{SL} = B(B \rightarrow X \ell^- \bar{\nu})$ , averaged over the  $B$  mesons produced at the  $Y(4S)$  ( $B_u$  and  $B_d$ ). Results are given separately for each of the models used to extract  $\mathcal{B}_{SL}$ . In the ARGUS measurement, the first error combines both statistical and systematic uncertainties; the second error in their ACCMM value is due to the extra free parameters present in the ACCMM model. The fit of the CLEO data using the unmodified ISGW model is poor, so the results from that fit are less reliable. The table also gives the CLEO inclusive branching fraction to charm final states ( $X_c$ ) only, which is extracted from the same fit. This value is appropriate for computing  $|V_{cb}|$ , although it is not very different from  $\mathcal{B}_{SL}$ . Sources of error in these measurements are discussed in the text.

Experiment	ACCMM	ISGW	ISGW**
ARGUS (Albrecht <i>et al.</i> , 1990b)	$10.2 \pm 0.5 \pm 0.2$	$9.8 \pm 0.5$	
CRYSTAL BALL (Wachs <i>et al.</i> , 1989)	$12.0 \pm 0.5 \pm 0.7$	$11.9 \pm 0.4 \pm 0.7$	
CUSB II (Yanagisawa <i>et al.</i> , 1991)	$10.0 \pm 0.4 \pm 0.3$	$10.0 \pm 0.4 \pm 0.3$	
CLEO I (Henderson <i>et al.</i> , 1992)	$10.5 \pm 0.2 \pm 0.4$	$9.9 \pm 0.1 \pm 0.4$	$11.2 \pm 0.3 \pm 0.4$
CLEO II (prelim.) (Bartelt <i>et al.</i> , 1993b)	$10.65 \pm 0.05 \pm 0.33$	$10.42 \pm 0.05 \pm 0.33$	$10.98 \pm 0.10 \pm 0.33$
Average	$10.51 \pm 0.21$	$10.22 \pm 0.20$	$11.05 \pm 0.28$
CLEO II (prelim.) $B \rightarrow X_c \ell^- \bar{\nu}$ (Bartelt <i>et al.</i> , 1993b)	$10.48 \pm 0.07 \pm 0.33$	$10.41 \pm 0.07 \pm 0.33$	$10.87 \pm 0.10 \pm 0.33$

TABLE VIII. Measurements from LEP experiments of the inclusive  $b$ -hadron semileptonic branching fraction,  $B(X_b \rightarrow X \ell^- \bar{\nu})$ , where  $X_b$  is a hadron containing a  $b$  quark. At the  $Z$ , the population of  $b$  hadrons includes not only  $B_u$  and  $B_d$  mesons, but also a smaller fraction of  $B_s$  mesons and  $b$  baryons. The first error is statistical, the second systematic, and the third also systematic from the decay model.

Experiment	Reference	$B(X_b \rightarrow X \ell^- \bar{\nu})\%$
ALEPH	Buskulic <i>et al.</i> , 1994a	$11.39 \pm 0.33 \pm 0.33 \pm 0.26$
DELPHI	DELPHI Collaboration, 1995	$11.06 \pm 0.39 \pm 0.12 \pm 0.19$
L3 (prelim.)	Venus, 1993	$11.73 \pm 0.48 \pm 0.28 \pm 0.31$
OPAL	Akers <i>et al.</i> , 1993	$10.5 \pm 0.6 \pm 0.4 \pm 0.3$
LEP average		$11.2 \pm 0.4$

ARGUS, so that model-related uncertainties in these experiments are propagated into the LEP results. (This uncertainty is part of the third error in the LEP results given in Table VIII.) The results from LEP experiments are consistent with those at the  $Y(4S)$ , although they are systematically higher.

## 2. Measurement of $\mathcal{B}_{SL}$ using charge and angular correlations in dilepton events

The ARGUS Collaboration (Albrecht *et al.*, 1993b) has introduced a second method, using dilepton events, that allows one to separate the contributions of primary and secondary leptons without relying on model-dependent shapes. This technique, which has now been used by both ARGUS and CLEO (Gronberg *et al.*, 1994; Barish *et al.*, 1995b), substantially reduces the need for models in the determination of  $\mathcal{B}_{SL}$ .

The first step is to require that one lepton (the “tagging lepton”) have high momentum, so that it must nearly always be primary. For example, with  $p_{\ell} > 1.4$  GeV/ $c$ , only about 2.8% of these leptons are secondary. The lepton spectrum extracted is that for the other lepton in the event, for which no such cut is applied.

Assuming that the tagging lepton is always primary (a small correction for secondary tags must be made), there are three possibilities for the other lepton. These possibilities and the corresponding lepton charge correlations are, assuming no  $B^0 \bar{B}^0$  mixing,

(i) the other lepton is primary and from the decay of the other  $B$  meson, resulting in opposite-sign leptons ( $\ell^+ \ell^-$ );

(ii) the other lepton is secondary and from the decay chain of the other  $B$  meson, resulting in same-sign leptons ( $\ell^+ \ell^+$  or  $\ell^- \ell^-$ ); or

(iii) the other lepton is secondary and from the decay chain of the same  $B$  meson in the event, resulting in opposite-sign leptons ( $\ell^+ \ell^-$ ).

Thus, if one can eliminate events corresponding to the third scenario, then a lepton with charge opposite to that of the tag must be primary, whereas a lepton with the same charge as the tag must be secondary. This discussion ignores mixing, but the  $B^0 \bar{B}^0$  mixing rate is well measured, and it is not difficult to correct for this effect.

If the two leptons are from the decay chain of the same  $B$  meson (the last case listed above), there is a strong angular

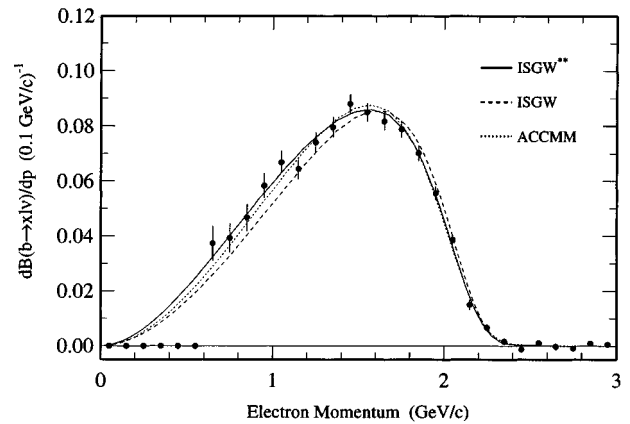


FIG. 18. The primary-lepton spectrum from the CLEO II dilepton analysis. In this analysis, a high-momentum lepton is used to tag a second lepton as either primary or secondary. (In the single-lepton analysis, this distinction is made using model-dependent fits.) The curves correspond to fits using the ISGW\*\* model (solid curve), ISGW model (dashed curve), the ACCMM model (dotted curve). As in the single-lepton analysis, the ISGW\*\* and ACCMM models both describe the data well, but the ISGW model does not. These fits are used to extrapolate the spectrum to momenta below the acceptance of the experiment.

correlation, resulting from momentum conservation, such that they tend to be in opposite hemispheres. In contrast, leptons from different  $B$  mesons have uncorrelated angular distributions. [The two  $B$  mesons are produced nearly at rest at the  $Y(4S)$ ; see Sec. III.B.] By requiring both leptons to be in the same hemisphere, one effectively removes events in which the two leptons come from the decay chain of a single  $B$  meson. (In the CLEO analysis, the lepton opening-angle cut is momentum dependent.)

Because a lepton whose charge is opposite to that of the tagging lepton must be primary, while one with the same charge as the tagging lepton must be secondary (up to the mixing correction), one can measure the number of primary

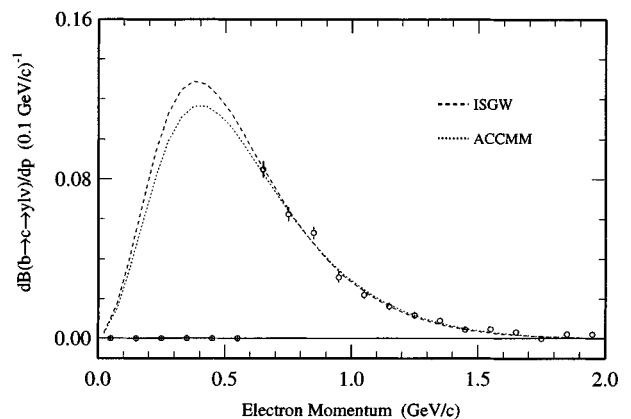


FIG. 19. The secondary-lepton spectrum from the CLEO II dilepton analysis. The curves correspond to fits using the ISGW model (dashed curve) and the ACCMM model (dotted curve).

TABLE IX. Measurements of the inclusive semileptonic branching fraction (%), at the  $Y(4S)$ , using dilepton events. These measurements have less model dependence than those using the single-lepton spectrum, because charge correlations rather than model-dependent shapes have been used to separate the primary and secondary lepton spectra.

Experiment	$B(B \rightarrow X\ell\nu)$ (%), $p_e > 0.6$ GeV/c	$B(B \rightarrow X\ell\nu)$ (%)
ARGUS (Albrecht <i>et al.</i> , 1993b)	$9.1 \pm 0.5 \pm 0.4$	$9.6 \pm 0.5 \pm 0.4$
CLEO II (Barish <i>et al.</i> , 1995b)	$9.85 \pm 0.16 \pm 0.40$	$10.49 \pm 0.17 \pm 0.43$
Average		$10.19 \pm 0.37$

and secondary leptons in each momentum bin. Figures 18 and 19 show the primary- and secondary-electron momentum spectra obtained from the CLEO analysis. There is a lower cutoff in the electron identification efficiency, however, and a small extrapolation, based on models, is required to obtain the total semileptonic rate. In the CLEO II measurement, the minimum momentum in the measurement is 0.6 GeV/c, and the extrapolation to zero momentum amounts to only  $(6.1 \pm 0.5)\%$  of the semileptonic rate. The central value is based on the average of the ACCMM and ISGW predictions, and the error is based on the difference between these two models.

Table IX lists the values of  $\mathcal{B}_{SL}$  obtained from the ARGUS and CLEO II dilepton analyses. These results are in agreement with the value of  $\mathcal{B}_{SL}$  obtained from the single-lepton analyses. The reduced sensitivity to models has been achieved at the expense of some statistical power, but in the CLEO II result the statistical error is still smaller than the systematic error. This method also very much reduces the sensitivity to any possible non- $B\bar{B}$  decays of the  $Y(4S)$ , which are assumed to be negligible in the single-lepton method.

### 3. Measurement of $\mathcal{B}_{SL}$ for $B^0$ and $B^-$ with tagging

The semileptonic branching fraction has been measured separately for charged and neutral  $B$  mesons by CLEO and for neutral  $B$ 's by ARGUS. One  $B$  meson from the  $Y(4S)$  decay is fully or partially reconstructed so that its charge can be determined. The semileptonic branching fraction is then obtained from the fraction of such events in which the other  $B$  meson produces a lepton. To obtain as large a tagged sample as possible, CLEO has used a large number of decay modes. Hadronic decays are reconstructed in eight modes:  $D\pi^-$ ,  $D^*\pi^-$ ,  $D\rho^-$ ,  $D^*\rho^-$ ,  $Da_1^-$ ,  $D^*a_1^-$ ,  $\psi K$ , and  $\psi K^*$ . These decays yield  $834 \pm 42 B^-$  and  $515 \pm 31 \bar{B}^0$  tags. A large sample of additional  $\bar{B}^0$  tags is obtained using the semileptonic decay  $\bar{B}^0 \rightarrow D^{*+} \ell^- \bar{\nu}$ . To obtain high effi-

ciency, the  $D^{*+}$  is identified using only the characteristic soft pion from  $D^{*+} \rightarrow D^0 \pi^+$ , without reconstructing the  $D^0$  decay. (For a discussion of this partial reconstruction technique, see Sec. VI.E.) This mode yields  $7119 \pm 139 \bar{B}^0$  tags. An additional  $822 \pm 53 \bar{B}^0$  tags are obtained from a partial reconstruction of  $\bar{B}^0 \rightarrow D^{*+} \pi^-$ . The fraction of events in each charge sample with a lepton in the momentum range 1.4 GeV/c to 2.4 GeV/c is used, together with an extrapolation to low momenta based on the ISGW\*\* model, to determine the charged and neutral semileptonic branching fractions. Table X summarizes the measurements from CLEO and ARGUS. These values are consistent with measurements based only on the inclusive lepton spectrum. The CLEO II values yield a ratio

$$\frac{B(B^- \rightarrow X\ell^- \bar{\nu})}{B(\bar{B}^0 \rightarrow X\ell^- \bar{\nu})} = 0.93 \pm 0.18 \pm 0.12, \quad (76)$$

consistent with the world average lifetime ratio but with rather large errors.

### 4. Determination of $|V_{cb}|$ from inclusive measurements

To calculate  $|V_{cb}|$  from  $\mathcal{B}_{SL}$ , we first convert the branching fraction to a decay rate using the appropriate  $B$  lifetime and then normalize to a theoretical calculation, which predicts the constant  $\gamma_c$ :

$$|V_{cb}| = \sqrt{\frac{\mathcal{B}_{SL}}{\gamma_c \tau_B}}. \quad (77)$$

Table XI gives values of  $|V_{cb}|$  based on measurements of  $\mathcal{B}_{SL}$ . The uncertainties on  $|V_{cb}|$  arise from several sources, which are listed in Table XII: the experimental error on  $\mathcal{B}_{SL}$ , the model dependence in the measurement of  $\mathcal{B}_{SL}$ , the uncertainty on the  $B$  lifetime, and the theoretical uncertainty on  $\gamma_c$ . Apart from the uncertainty on the lifetime, the experimental uncertainty on  $|V_{cb}|$  from the single-lepton analysis, including the model dependence of the branching frac-

TABLE X. Measurements of the inclusive semileptonic branching fractions of charged and neutral  $B$  mesons.

Experiment	$B(\bar{B}^0 \rightarrow X\ell^- \bar{\nu})$ (%)	$B(B^- \rightarrow X\ell^- \bar{\nu})$ (%)
CLEO (Henderson <i>et al.</i> , 1992)	$9.9 \pm 3.0 \pm 0.9$	
ARGUS (Albrecht <i>et al.</i> , 1994a)	$9.3 \pm 1.1 \pm 1.15$	
CLEO II (Athanas <i>et al.</i> , 1994)	$10.9 \pm 0.7 \pm 1.1$	$10.1 \pm 1.8 \pm 1.4$
Average	$10.22 \pm 0.96$	$10.1 \pm 2.3$

TABLE XI. Measurements of  $|V_{cb}|$  from the inclusive semileptonic rate, using the ACCMM inclusive model, the ISGW\*\* exclusive model, and three HQET-based calculations. The third column gives values of  $|V_{cb}|$  calculated from the CLEO II measurement of  $B \rightarrow X_c \ell^- \bar{\nu}$  using the inclusive lepton spectrum. In this case, the ACCMM and ISGW\*\* values of  $|V_{cb}|$  were calculated using not only the values of  $\gamma_c$  from these models, but also the branching fractions extracted from fits using the predicted lepton-energy spectra [ $B(B \rightarrow X_c \ell^- \bar{\nu}) = (10.48 \pm 0.34)\%$  for ACCMM and  $(10.87 \pm 0.34)\%$  for ISGW\*\*]. In contrast, the CLEO II values of  $|V_{cb}|$  based on the Shifman *et al.* (1995), Luke and Savage (1994), and Ball *et al.* (1995) values of  $\gamma_c$  were calculated using the branching ratio extracted by fitting the single-lepton spectrum with the ACCMM model. The fourth column gives the values of  $|V_{cb}|$  calculated using the average of the CLEO II and ARGUS values for  $B \rightarrow X \ell^- \bar{\nu}$  [ $(10.19 \pm 0.37)\%$ ] measured using the dilepton method, which has less model dependence than the fits of the single-lepton spectrum. Finally, the fifth column uses the average value  $B(X_b \rightarrow X \ell^- \bar{\nu}) = (11.2 \pm 0.4)\%$  from the LEP experiments. The first error on  $|V_{cb}|$  is experimental, the second theoretical. To correct these  $|V_{cb}|$  values for a different value of  $\tau_B$ , multiply by  $\sqrt{1.54 \text{ ps}/\tau_B}$ .

Model	$\gamma_c$ (ps) <sup>-1</sup>	CLEO II (1 $\ell$ ) $ V_{cb} /10^{-2}$	CLEO II/ARGUS avg. (2 $\ell$ ) $ V_{cb} /10^{-2}$	LEP avg. $ V_{cb} /10^{-2}$
ACCMM	40 ± 8	4.1 ± 0.1 ± 0.4	4.1 ± 0.1 ± 0.4	4.3 ± 0.1 ± 0.4
ISGW**	42 ± 8	4.1 ± 0.1 ± 0.4		
Shifman <i>et al.</i> , 1995	41.3 ± 4	4.1 ± 0.1 ± 0.2	4.0 ± 0.1 ± 0.2	4.2 ± 0.1 ± 0.2
Luke and Savage, 1994	25 to 51	3.7 to 5.2	3.6 to 5.1	3.8 to 5.4
Ball <i>et al.</i> , 1995	43.2 ± 4.2	4.0 ± 0.1 ± 0.2	3.9 ± 0.1 ± 0.2	4.1 ± 0.1 ± 0.2

tion (but not  $\gamma_c$ ), is about 2.5%. The corresponding uncertainty in the dilepton analysis is 2.2%. The error associated with the lifetime is the source of some difficulty. If one used only the uncertainties on the individually measured charged and neutral  $B$  lifetimes (about 0.1 ps), the resulting error on  $|V_{cb}|$  would be about 3%. Our view, however, is that one should not completely ignore the inclusive  $B$  lifetime measurements, which have much smaller errors but which include some contamination from  $b$  baryons. Since this contamination is thought to be relatively small, we take the uncertainty on the  $B^0$  and  $B^-$  lifetimes to be  $\pm 0.07$  ps, which contributes a 2.3% uncertainty on  $|V_{cb}|$ . The combined uncertainty in  $|V_{cb}|$  from all errors except that on  $\gamma_c$  is about 0.001.

It is difficult to assign errors to predictions of  $\gamma_c$  based on quark-model calculations. Traditionally, a nominal theoret-

ical error of 20% in the rate is assumed, leading to a 10% theoretical error on  $|V_{cb}|$ . We assign this error when quoting results using the ACCMM or ISGW\*\* models. As discussed in Sec. V.B, HQET is being used to obtain a value of  $|V_{cb}|$  from the inclusive spectrum with a more precisely defined error. Shifman, Uraltsev, and Vainshtein (Shifman *et al.*, 1995) argue that the theoretical uncertainty on  $|V_{cb}|$  using their results is 5% or less. Luke and Savage (1994), however, quote a somewhat larger uncertainty, which they express as an allowed range. There is not yet a consensus on the size of these theoretical errors, but rapid progress is being made on this question.

As our final value of  $|V_{cb}|$  from the inclusive semileptonic branching fraction, we take the average over different models of the values of  $|V_{cb}|$  from the CLEO II single-lepton analysis. (We do not use the Luke and Savage result, where

TABLE XII. Sources of error on  $|V_{cb}|$  using the inclusive semileptonic rate. The experimental error is based on the CLEO II error on  $\mathcal{B}_{\text{SL}}$ , apart from model-related effects. The model-dependent error on the branching fraction is based on the difference between the CLEO II ACCMM and ISGW\*\* values for  $B \rightarrow X_c \ell^- \bar{\nu}$ . There is a correlation in the errors introduced when a given model is used to extract both  $\mathcal{B}_{\text{SL}}$  and  $|V_{cb}|$ , but we ignore this effect here. The model-dependent error on  $\mathcal{B}_{\text{SL}}$  is negligible in the dilepton analysis, but the experimental error is slightly larger. Errors on the lifetime in the range 0.02 ps to 0.1 ps correspond to an uncertainty of 0.6% to 3.2% on  $|V_{cb}|$ . As discussed in the text we take a 0.07 ps uncertainty in the lifetime. The error on  $\gamma_c$  for the quark-model calculations is set somewhat arbitrarily at 20% (or 10% in the amplitude), whereas the errors on HQET-based calculations are based on real estimates of the uncertainties in the calculation. We take a bottom-line theoretical uncertainty of  $\pm 0.003$  on  $|V_{cb}|$ .

Source	$(\delta\Gamma/\Gamma)\%$	$(\delta V_{cb} / V_{cb} )\%$	$(\delta V_{cb} )/10^{-3}$
Error on $B(B \rightarrow X_c \ell^- \bar{\nu})$ (1 $\ell$ analysis)	3.2	1.6	0.6
Model dependence of $B(B \rightarrow X_c \ell^- \bar{\nu})$ (1 $\ell$ analysis)	3.8	1.9	0.8
Error on $B(B \rightarrow X_c \ell^- \bar{\nu})$ (2 $\ell$ analysis)	4.4	2.2	0.9
Error on lifetime ( $\tau_B$ )	4.5	2.3	0.9
Error on $\gamma_c$	10 to 20	5 to 10	2 to 4
Total error (either 1 $\ell$ or 2 $\ell$ )			$\pm 1$ (expt) $\pm 3$ (thy)

only a range is given.) For our final theoretical uncertainty, we use a value that is smaller than the traditional  $\pm 0.004$  associated with the quark-model predictions but larger than the  $\pm 0.002$  uncertainty claimed by some of the HQET-based calculations. Thus

$$|V_{cb}| = 0.041 \pm 0.001(\text{expt}) \pm 0.003(\text{theory}). \quad (78)$$

This value of  $|V_{cb}|$  agrees well with the value obtained from the  $B \rightarrow D^* \ell^- \bar{\nu}$  measurement [see Eq. (160)].

### E. Lepton end-point region in semileptonic $B$ decays and determination of $|V_{ub}|$

The determination of  $|V_{ub}|$  is one of the most important and challenging measurements in  $B$  physics. The curve in Fig. 16 representing the  $b \rightarrow u \ell^- \bar{\nu}$  rate shows clearly how little these processes perturb the total spectrum below the end-point region. In fact, over all lepton energies, simple free-quark models predict that (Rosner, 1992)

$$\frac{\Gamma(b \rightarrow u \ell^- \bar{\nu})}{\Gamma(b \rightarrow c \ell^- \bar{\nu})} = (1.85 \text{ to } 2.44) \left| \frac{V_{ub}}{V_{cb}} \right|^2 \approx (1.2 \text{ to } 1.6)\%, \quad (79)$$

where we have used the typical value  $|V_{ub}/V_{cb}| \approx 0.08$ . The key to measuring  $|V_{ub}|$  is to take advantage of the large lepton momenta made accessible by the small mass of the daughter  $u$  quark. By working in the region at and beyond the lepton-momentum-spectrum end point for  $B \rightarrow X_c \ell^- \bar{\nu}$  processes, one gains enormously in sensitivity to  $B \rightarrow X_u \ell^- \bar{\nu}$  decays.

Although the advantages of working in this end-point region ( $2.3 < p_\ell < 2.6$  GeV/ $c$ ) are decisive, there are also disadvantages. The major difficulty is the need to convert the measured rate for this tiny portion of phase space into a value of  $|V_{ub}|$ . This calculation can be performed using either inclusive or exclusive models, but both have substantial uncertainties. Inclusive models are expected to be fairly reliable if one considers a large enough part of phase space, but their ability to predict the  $B \rightarrow X_u \ell^- \bar{\nu}$  spectrum in the end-point region can be questioned. The ACCMM (inclusive) model predicts a significantly larger rate in this region than the ISGW (exclusive) model, in which a small number of modes ( $B \rightarrow \rho \ell^- \bar{\nu}$ ,  $B^- \rightarrow \omega \ell^- \bar{\nu}$ , and  $B \rightarrow \pi \ell^- \bar{\nu}$ ) produce about 70% of the leptons with  $p > 2.3$  GeV/ $c$ . Figure 7, discussed in Sec. II.C, shows that  $B \rightarrow \rho \ell^- \bar{\nu}$  and  $B^- \rightarrow \omega \ell^- \bar{\nu}$ , with their hard lepton-momentum spectra, are expected to be particularly important. Thus, in this region of phase space, there may not be enough hadronic final states for an inclusive model to work well. However, it is possible that, in addition to resonant hadronic final states, there are also nonresonant modes, such as  $B \rightarrow \pi \pi \ell^- \bar{\nu}$ . In particular, such modes might be important at low  $q^2$ , where the daughter  $u$  quark recoils very rapidly with respect to the spectator quark, and the form factors for resonant hadronic final states are suppressed. If these nonresonant modes do contribute substantially, then the predictions of inclusive models might be more reliable. This question is controversial and has not yet been resolved.

An alternative is to use exclusive models to extract  $|V_{ub}|$  by summing the rates for all modes expected to contribute in

the end-point region. However, in addition to the question of possible nonresonant contributions to the observed rate, large uncertainties exist in the calculations of the rates for resonant modes. Thus the factors  $\gamma_{\text{thy}}$  in Eq. (25) are difficult to calculate, much more so than the corresponding factors for  $B \rightarrow X_c \ell^- \bar{\nu}$ . Due to the small value of the  $u$ -quark mass, the  $q_{\text{max}}^2$  region cannot be used to provide a relatively solid normalization point for the form factors, as it does in  $b \rightarrow c \ell^- \bar{\nu}$  decays. In addition, the range of recoil velocities available to the light final-state mesons produced in  $B \rightarrow X_u \ell^- \bar{\nu}$  decays is much larger than that for charm-meson final states (see Table XVII below). The larger range produces a much larger variation in the form factors and hence greater uncertainty. Consequently measurements of  $|V_{ub}|$  are currently quite model dependent, and there is substantial variation among values obtained using different models. In the future, lattice QCD calculations of the  $B \rightarrow \pi \ell^- \bar{\nu}$  or  $B^- \rightarrow \omega \ell^- \bar{\nu}$  decay rate at high  $q^2$  may provide an alternative method. Useful information on the form factors may also be obtained from measurements of  $b \rightarrow s \gamma$  decays, providing constraints on the theory.

We turn now to the measurement of the rate in the end-point region. Although the measurement is properly described as “inclusive,” the analysis is rather different from that of the inclusive lepton spectrum described in Sec. V.D.1. The reason is that continuum processes produce high-momentum leptons, which constitute an enormous background unless suppressed by kinematic cuts. The signal efficiency of these cuts is much more sensitive to the shapes of kinematic distributions (especially to that of  $q^2$ ) than the very loose cuts used in the analysis of the inclusive lepton spectrum. This sensitivity introduces another source of model dependence into the results, beyond the overall scale  $\gamma_{\text{thy}}$ .

The primary characteristic used to remove continuum events is event topology: continuum events are usually much more jetlike than  $Y(4S) \rightarrow B\bar{B}$  events, which are quite spherical. In the CLEO II measurement (Bartelt *et al.*, 1993a), which has the highest statistics, the event shape is described quantitatively using the variable  $R_2 = H_2/H_0$ , where the  $H_i$  are Fox-Wolfram moments (Fox and Wolfram, 1978). The  $R_2$  variable ranges from 0 (completely spherical) to 1 (completely jetlike); for the end-point analysis CLEO requires  $R_2 < 0.2$ . The other important variable in suppressing continuum events is the magnitude  $p_{\text{miss}}$  of the missing-momentum vector. A large value of  $p_{\text{miss}}$  is indicative of a  $b \rightarrow u \ell^- \bar{\nu}$  process; the analysis requires  $p_{\text{miss}} > 1$  GeV/ $c$ , which is 90% efficient for the signal but suppresses continuum events by a factor of 2.3. Finally, the lepton momentum and missing-momentum vectors are required to be in opposite hemispheres. Together, these cuts suppress the continuum by a factor of 70 while retaining 38% of signal events (as determined with Monte Carlo).

Even with these cuts, a significant background from continuum events remains. Fortunately, this background can be directly measured by running just below the  $Y(4S)$  resonance and performing the same analysis. This procedure leads to a background level that must be scaled by the luminosity ratio between on- and off-resonance running and corrected slightly for the energy difference. Additional back-

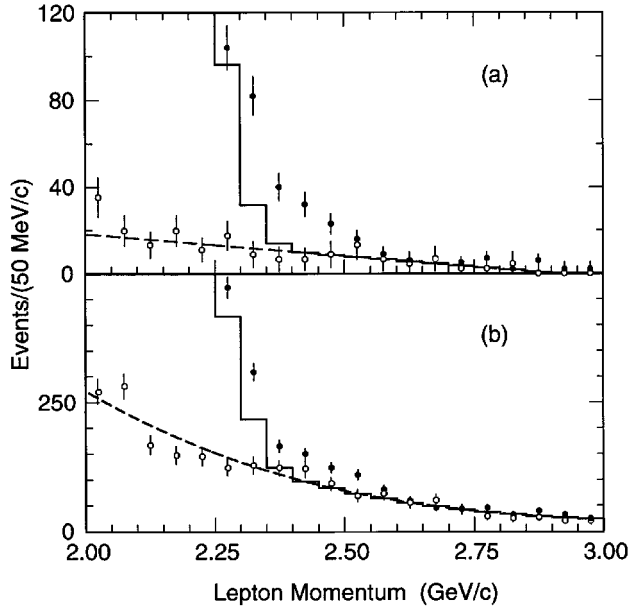


FIG. 20. Inclusive end-point spectrum from CLEO II. The upper plot is from the analysis with tight cuts; the lower plot is from the analysis with looser cuts. Efficiencies in the latter analysis have less sensitivity to models, but the background is larger. In both plots, the solid points with error bars are the data taken at the  $\Upsilon(4S)$ , whereas the open points with error bars represent the continuum background, which is determined using data taken below the  $\Upsilon(4S)$  resonance. The histogram shows the total background prediction, which includes both continuum and  $B \rightarrow X_c \ell^- \bar{\nu}$ . The excess of observed events over this total background prediction constitutes evidence for  $B \rightarrow X_u \ell^- \bar{\nu}$  decays.

grounds to the analysis arise from hadrons that fake a lepton signature in the detector and from leptons from  $J/\psi$ 's. These backgrounds are minor but not entirely negligible and must be accurately determined.

Figure 20 shows the CLEO lepton-momentum spectrum (including both electrons and muons) in the end-point region. The upper plot was made using the cuts described above; the lower one uses only a relatively loose  $R_2$  cut ( $<0.3$ ). As a result, the lower plot has a larger background, but the efficiency correction involves less model dependence. In these plots the solid points are the data after analysis cuts are applied, and the open points represent the continuum background as measured from below-resonance running. The continuum-background level is obtained from a fit to these points. The background from  $b \rightarrow c \ell^- \bar{\nu}$  processes is shown as a solid histogram (added onto the continuum background). This background is very small in the upper momentum bin ( $2.4 < p_\ell < 2.6$  GeV/c) but is substantial in the lower bin and must be accurately determined. It is obtained by fitting the data below the end point to theoretical models for  $b \rightarrow c \ell^- \bar{\nu}$  and extrapolating them into the end-point region; the uncertainty in the extrapolation is relatively small ( $<10\%$  of the  $b \rightarrow c \ell^- \bar{\nu}$  background) and is included in the error on the yields. In the upper plot, for which the stricter cuts were used, the  $b \rightarrow u \ell^- \bar{\nu}$  yields in the two bins are  $43.0 \pm 10.2 \pm 6.7$  events ( $2.4 < p_\ell < 2.6$  GeV/c) and  $64.3 \pm 11.4 \pm 4.4$  events ( $2.3 < p_\ell < 2.4$  GeV/c), with a total of  $107 \pm 15 \pm 11$  events. These yields constitute the most sig-

TABLE XIII. Measurements of the partial branching fraction  $\Delta B_{ub}$  from CLEO (Bartelt *et al.*, 1993a) using the inclusive rate in the lepton-spectrum end-point region. The lepton-momentum interval for this partial branching fraction is  $2.3 < p < 2.6$  GeV/c.

Model	$\Delta B_{ub}/10^{-4}$
ACCMM	$1.21 \pm 0.17 \pm 0.15$
KS	$1.15 \pm 0.16 \pm 0.15$
WSB	$1.22 \pm 0.17 \pm 0.16$
ISGW	$1.54 \pm 0.22 \pm 0.20$

nificant evidence that  $|V_{ub}|$  is nonzero. The corresponding yields with the looser, less model-dependent cuts are  $128.4 \pm 26.3 \pm 15.3$  events and  $98.1 \pm 23.6 \pm 14.9$  events.

These signals, together with efficiencies obtained from Monte Carlos of theoretical models, are used to obtain a partial branching fraction  $\Delta B_{ub} = B(B \rightarrow X_u \ell^- \bar{\nu}; 2.3 < p_\ell < 2.6 \text{ GeV/c})$ . Values of  $\Delta B_{ub}$  for the CLEO II measurement and four models are given in Table XIII. The use of the KS and WSB models for this purpose can be questioned, since they predict only two modes,  $B \rightarrow \rho \ell^- \bar{\nu}$  and  $B \rightarrow \pi \ell^- \bar{\nu}$ . The 25% difference in the results for ISGW and ACCMM, however, is indicative of the uncertainty associated with different shapes for the kinematic distributions.

The magnitude of  $V_{ub}/V_{cb}$  is then calculated using

$$\left| \frac{V_{ub}}{V_{cb}} \right|^2 = \frac{\Delta B_{ub}/f(p)}{B_{cb}} \frac{\gamma_c}{\gamma_u}, \quad (80)$$

where  $\Delta B_{ub}$  is the branching fraction to a given momentum interval;  $f(p)$  is the fraction of the spectrum in this momentum interval, as predicted by a particular model;  $B_{cb}$  is the measured  $B \rightarrow X_c \ell^- \bar{\nu}$  branching fraction; and  $\gamma_c$  and  $\gamma_u$  are defined in Eq. (25). For an exclusive model, both  $f(p)$  and  $\gamma_u$  refer only to the sum of exclusive modes predicted by the model. The ISGW model, for example, may predict enough modes to adequately describe the end-point region, but not the large region below it. Thus, although one can calculate  $V_{ub}$ , the quantity  $\Delta B_{ub}/f(p)$  cannot be interpreted as  $B(B \rightarrow X_u \ell^- \bar{\nu})$  for this type of model, but rather as the total branching fraction to the predicted set of modes only. For this reason, we expect  $\gamma_u$  for an exclusive model to be less than that for an inclusive model; for comparisons between models, the quantity  $f(p)\gamma_u$  or  $d(p) = f(p)\gamma_u/\gamma_c$  is more useful. The efficiency of the analysis cuts is model dependent and is sensitive to the  $q^2$  distribution of the  $B \rightarrow X_u \ell^- \bar{\nu}$  events in the end-point region. The variation in the efficiencies between the ACCMM and ISGW models is about 25%, corresponding to a 12.5% effect on  $|V_{ub}|$ . While this uncertainty is fairly large, it is still much smaller than that in the overall rates predicted by the models.

Table XIV summarizes the measurements of  $|V_{ub}/V_{cb}|$  from CLEO and ARGUS. The new CLEO values of  $|V_{ub}/V_{cb}|$ , which are based on about five times as many data as the original CLEO and ARGUS measurements, are about  $2\sigma$  lower than the older values.

Improving the reliability of theoretical predictions for the inclusive  $B \rightarrow X_u \ell^- \bar{\nu}$  rate in the end-point region is extremely desirable. Several authors (Bigi, Shifman, Uraltsev, and Vainshtein, 1994; Korchemsky and Sterman, 1994; Neu-

TABLE XIV. Measurements of  $|V_{ub}/V_{cb}|$  using the inclusive rate in the end-point region. The ARGUS and CLEO I results are each based on about 200 000  $B\bar{B}$  events, and the CLEO II results are based on about 955 000  $B\bar{B}$  events.

Model	ARGUS (Albrecht <i>et al.</i> , 1991a)	CLEO I (Fulton <i>et al.</i> , 1990)	CLEO II (Bartelt <i>et al.</i> , 1993a)
ACMM	$0.11 \pm 0.01$	$0.09 \pm 0.01$	$0.076 \pm 0.008$
ISGW	$0.20 \pm 0.02$	$0.15 \pm 0.02$	$0.101 \pm 0.010$

bert, 1994d) have pointed out that measurements of  $B \rightarrow X_s \gamma$  decays provide information that can help to reduce the hadronic uncertainties in  $B \rightarrow X_u \ell \bar{\nu}$ . In particular, the photon energy spectrum in  $B \rightarrow X_s \gamma$  is sensitive to the motion of the  $b$  quark within the  $B$  meson. The inclusive  $B \rightarrow X_s \gamma$  decay has recently been observed (Alam *et al.*, 1994), and with larger data samples and more theoretical work this approach may prove to be very useful.

#### F. $B \rightarrow X \tau^- \bar{\nu}_\tau$ and other inclusive modes

Table XV lists results for  $B \rightarrow X \tau^- \bar{\nu}_\tau$  and for certain semi-inclusive  $B$  decays. Because two neutrinos are produced in  $B \rightarrow X \tau^- \bar{\nu}_\tau$  and the lepton-energy spectrum from the  $\tau$  decay is relatively soft, experiments at the  $Y(4S)$  have not been able to observe this process. LEP experiments, however, have found a way to circumvent these problems by exploiting the jet-like topology and the large boost given to the  $b$  quark in  $Z \rightarrow b\bar{b}$  events. The jet topology allows the tracks in each hemisphere of the event—as defined by a plane perpendicular to the thrust axis—to be associated with the decay or fragmentation of a single  $b$  quark. The presence of two neutrinos in the  $B \rightarrow X \tau^- \bar{\nu}_\tau$  decay results in configurations with a relatively large missing energy in the  $b$ -hadron rest frame. The boost of the  $b$  hadron to the lab frame can result in a very large missing energy (10–30 GeV) for the event hemisphere containing the decay. By looking for events with both a large missing energy ( $E_{\text{miss}} > 16$  GeV) and a tagged  $b$  hadron (using vertex detector information), ALEPH (Buskulic *et al.*, 1993, 1995a) has been able to observe a signal, as shown in Fig. 21. A similar analysis has been carried out by L3 (Adeva *et al.*, 1994), whose result is also given in Table XV.

Within the large errors, the measured value for  $B(B \rightarrow X \tau^- \bar{\nu}_\tau)$  is consistent with standard-model predictions. For example, a calculation (Falk, Ligeti, Neubert, and Nir, 1994) based on the operator product expansion and HQET predicts  $B(B \rightarrow X \tau^- \bar{\nu}_\tau) = (2.30 \pm 0.25)\%$ . This calculation uses as input the measured inclusive semileptonic

branching fraction, taken to be  $B \rightarrow X \ell^- \bar{\nu} = (10.7 \pm 0.5)\%$ , and the largest contribution to the uncertainty in the prediction for  $B \rightarrow X \tau^- \bar{\nu}_\tau$  arises from the error on  $B \rightarrow X \ell^- \bar{\nu}$ . An earlier calculation (Heiliger and Sehgal, 1989) gave the somewhat higher prediction  $B(B \rightarrow X \tau^- \bar{\nu}_\tau) = (2.83 \pm 0.31)\%$ .

In certain supersymmetric (SUSY) models with charged Higgs bosons, the rate for  $B \rightarrow X \tau^- \bar{\nu}_\tau$  can be substantially enhanced by decays in which the  $H^-$  replaces the  $W^-$ . Thus part of the parameter space of such models can be excluded by the measured branching fraction. Predictions of SUSY models for this mode have been discussed in the literature (Grzadkowski and Hou, 1992; Grossman and Ligeti, 1994), and the resulting constraints are discussed in the ALEPH paper (Buskulic *et al.*, 1995a).

## VI. EXCLUSIVE SEMILEPTONIC DECAYS

With the enormous data samples now available for the study of charm and bottom hadrons, knowledge of their exclusive semileptonic decays is improving rapidly. In the following sections, we present theoretical and experimental results on exclusive semileptonic decays. Section VI.A continues the discussion begun in Sec. II.C, where we introduced some of the basic theoretical ideas. Here we discuss form factors, HQET, decay rates, and kinematic distributions in much more detail.

Our presentation of exclusive decays of charm and bottom mesons is organized according to whether the decays are favored or suppressed by CKM matrix elements. In the sections on charm decays, we discuss measurements of branching fractions and form factors; in the sections on bottom decays we discuss the determination of  $|V_{cb}|$  and  $|V_{ub}|$  as well. As in the case of inclusive decays, extraction of these CKM matrix elements involves a close interplay between experiment and theory. The theoretical ideas that underlie our understanding of semileptonic decay dynamics can to some extent be tested by measurements of form factors.

TABLE XV. Measurements of branching fractions for  $B \rightarrow X \tau^- \bar{\nu}_\tau$  and other semi-inclusive modes.  $B$  semileptonic decays to final states with baryons have not been observed. The ARGUS result for  $B \rightarrow D_s^- X \ell^+ \nu$  has been rescaled using the Particle Data Group value for  $D_s^+ \rightarrow \phi \pi^+$ .

Mode	Experiment	Reference	$B(\%)$
$B \rightarrow X \tau^- \bar{\nu}_\tau$	ALEPH	Buskulic <i>et al.</i> , 1995a	$2.75 \pm 0.30 \pm 0.37$
$B \rightarrow X \tau^- \bar{\nu}_\tau$	L3	Adeva <i>et al.</i> , 1994	$2.4 \pm 0.7 \pm 0.8$
$B \rightarrow D_s^- X \ell^+ \nu$	ARGUS	Albrecht <i>et al.</i> , 1993d	$< 0.9$ (90% C.L.)
$B \rightarrow \bar{p} X \ell^+ \nu$	ARGUS	Albrecht <i>et al.</i> , 1990b	$< 0.16$ (90% C.L.)

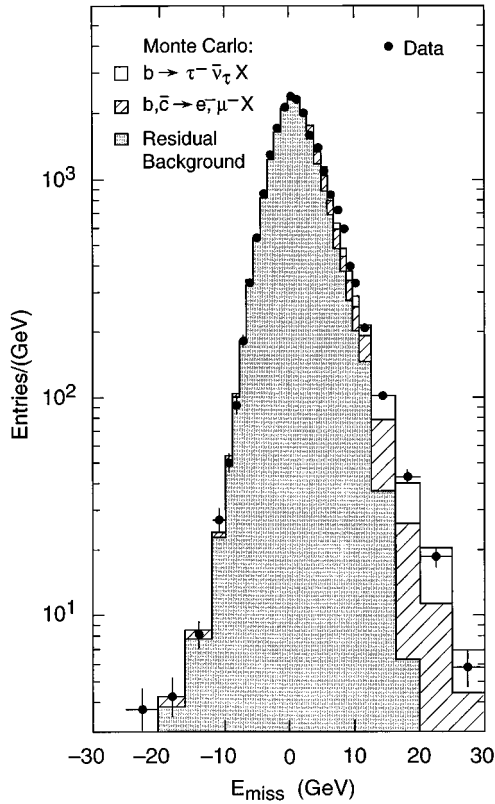


FIG. 21. Evidence for a  $B \rightarrow X \tau^- \bar{\nu}_\tau$  signal from ALEPH. The presence of two neutrinos in the decay can result in a large observed missing energy, especially in  $Z \rightarrow b\bar{b}$  events, where the velocity of the  $b$  hadron is large. Thus a substantial part of the tail at large values of  $E_{\text{miss}}$  is attributed to  $B \rightarrow X \tau^- \bar{\nu}_\tau$  decays.

In the last section on exclusive decays, we discuss semileptonic decays of the baryons  $\Lambda_c$ ,  $\Xi_c$ ,  $\Omega_c$ , and  $\Lambda_b$ . The information here is more limited, since the production cross sections for baryons are generally much smaller than those for mesons. In addition, the individual baryon production cross sections are not yet known, so that normalization of the branching ratios is difficult. Nevertheless, important progress is being made in this area, and from a theoretical standpoint baryon semileptonic decays are quite interesting.

#### A. Theory of exclusive semileptonic decays of mesons

In this section we describe some of the theoretical approaches used to predict exclusive semileptonic decays of hadrons containing heavy quarks. We begin with the standard parametrizations of the hadronic currents in terms of form factors. Turning to the form factors themselves, we next discuss quark-model calculations and some of their predictions. These calculations consist of two parts: first, the determination of the values of the form factors at a particular value of  $q^2$ , and second, the extrapolation over the full  $q^2$  range. When both the parent and daughter quarks are heavy, as in a  $b \rightarrow c \ell^- \bar{\nu}$  decay, both aspects are easiest to treat, because the form factors can be determined reasonably well in the zero-recoil configuration and the range of the extrapolation to other values of  $q^2$  is small. We shall compare the available range of  $q^2$  and recoil velocities in various charm and bottom semileptonic decays, since this provides a guide to how reli-

able the form-factor extrapolations are likely to be. We then examine the predictions of heavy-quark symmetry, which relates the form factors to each other and to the Isgur-Wise function. Because four-velocity rather than four-momentum provides the simplest description when both the initial and the final-state quarks are very heavy, we introduce a new set of form factors for decays in which the departures from heavy-quark symmetry are reasonably small. We also consider the size of the corrections to heavy-quark symmetry predictions for  $B \rightarrow D^* \ell^- \bar{\nu}$ . These corrections, though model dependent, have been estimated within the framework of HQET. To determine the behavior of the Isgur-Wise function itself, one must use nonperturbative methods, and we next summarize predictions for the slope of the Isgur-Wise function for  $B \rightarrow D^* \ell^- \bar{\nu}$  and  $B \rightarrow D \ell^- \bar{\nu}$  from lattice QCD and QCD sum rules. The reliability of lattice QCD calculations is improving, and they may eventually provide accurate predictions that are tied in a rigorous way to the fundamental theory of QCD. Finally, we give standard results for differential decay distributions in both the conventional notation and in the form best suited to testing HQET.

The channels  $P \rightarrow P' \ell \nu$  and  $P \rightarrow V \ell \nu$ , where  $P$  and  $P'$  are pseudoscalars and  $V$  is a vector meson, play an extremely important role because they dominate the semileptonic rate and are generally the easiest modes to study experimentally. Our theoretical discussion therefore focuses on decays with these quantum numbers. We let  $p$  denote the four-momentum of  $P$  and  $p'$  denote the four-momentum of either  $P'$  or  $V$ , depending on the context. The masses of the mesons  $P$ ,  $P'$ , and  $V$  are labeled, respectively,  $M$ ,  $m_{p'}$ , and  $m_V$ . When the quantum numbers of the final-state meson are irrelevant, we denote its mass by  $m_X$ .

#### 1. Structure of hadronic currents

The hadronic current in semileptonic decay must be constructed from the available four-vectors, which are momenta and spin-polarization vectors. The Lorentz-vector or axial-vector quantities thus formed have Lorentz-invariant coefficients (form factors) that are functions of  $q^2$ .

In the case of a  $P(Q\bar{q}) \rightarrow P'(q'\bar{q}) \ell \nu$  decay, there are only two independent four-vectors, which we can take to be  $p+p'$  and  $q=p-p'$ . For these quantum numbers, the hadronic current  $H^\mu$  [see Eq. (9)] has no axial-vector contribution and can be written (Wirbel *et al.*, 1985; Neubert, 1994c)

$$\langle P'(p') | V^\mu | P(p) \rangle = F_1(q^2) \left[ (p+p')^\mu - \frac{M^2 - m_{p'}^2}{q^2} q^\mu \right] + F_0(q^2) \frac{M^2 - m_{p'}^2}{q^2} q^\mu, \quad (81)$$

where  $V^\mu = \bar{q}' \gamma^\mu Q$  and  $F_0(0) = F_1(0)$ , so there is no singular behavior at  $q^2 = 0$ . The form factors  $F_0(q^2)$  and  $F_1(q^2)$  can be associated with the exchange of particles with quantum numbers  $J^P = 0^+$  and  $J^P = 1^-$ , respectively (Wirbel *et al.*, 1985). Another common way to write the current is

$$\langle P'(p') | V^\mu | P(p) \rangle = f_+(q^2) (p+p')^\mu + f_-(q^2) (p-p')^\mu, \quad (82)$$

where  $f_+(q^2) = F_1(q^2)$  and

$$F_0(q^2) = f_+(q^2) + \frac{q^2}{M^2 - m_{P'}^2} f_-(q^2). \quad (83)$$

In practice, these expressions for the currents simplify, because the terms proportional to  $q^\mu$  are nearly always negligible, both here and for the case  $P \rightarrow V \ell \nu$ . The reason is that, in the limit  $m_\ell \rightarrow 0$ ,  $q^\mu L_\mu = 0$ , where  $L_\mu$  is the lepton current. Thus  $P \rightarrow P' \ell \nu$  is, to a very good approximation, described by only one form factor  $F_1(q^2)$  when  $\ell = e$  or  $\mu$ :

$$\langle P'(p') | V^\mu | P(p) \rangle = F_1(q^2) (p + p')^\mu. \quad (84)$$

For the process  $P(Q\bar{q}) \rightarrow V(q') \ell \nu$ , each term in the current must be linear in the polarization vector  $\varepsilon$  of the vector meson. This requirement leads to the general form (Wirbel *et al.*, 1985; Neubert, 1994c)

$$\begin{aligned} \langle V(p', \varepsilon) | V^\mu - A^\mu | P(p) \rangle &= \frac{2i \varepsilon^{\mu\nu\alpha\beta}}{M + m_V} \varepsilon_\nu^* p'_\alpha p_\beta V(q^2) - (M + m_V) \varepsilon^{*\mu} A_1(q^2) \\ &+ \frac{\varepsilon^* \cdot q}{M + m_V} (p + p')^\mu A_2(q^2) + 2m_V \frac{\varepsilon^* \cdot q}{q^2} q^\mu A_3(q^2) \\ &- 2m_V \frac{\varepsilon^* \cdot q}{q^2} q^\mu A_0(q^2), \end{aligned} \quad (85)$$

where  $V^\mu = \bar{q}' \gamma^\mu Q$ ,  $A^\mu = \bar{q}' \gamma^\mu \gamma_5 Q$ , and

$$A_3(q^2) = \frac{M + m_V}{2m_V} A_1(q^2) - \frac{M - m_V}{2m_V} A_2(q^2), \quad (86)$$

with  $A_0(0) = A_3(0)$ . Again, terms proportional to  $q^\mu$  only play an important role for the case  $\ell = \tau$ . Thus  $P \rightarrow V \ell \nu$  is essentially described by three form factors:  $A_1(q^2)$ ,  $V(q^2)$ , and  $A_2(q^2)$ :

$$\begin{aligned} \langle V(p', \varepsilon) | V^\mu - A^\mu | P(p) \rangle &= \frac{2i \varepsilon^{\mu\nu\alpha\beta}}{M + m_V} \varepsilon_\nu^* p'_\alpha p_\beta V(q^2) - (M + m_V) \varepsilon^{*\mu} A_1(q^2) \\ &+ \frac{\varepsilon^* \cdot q}{M + m_V} (p + p')^\mu A_2(q^2). \end{aligned} \quad (87)$$

The form factors  $A_1(q^2)$  and  $A_2(q^2)$  can be associated with the exchange of a particle with quantum numbers  $J^P = 1^+$ , whereas  $V(q^2)$  is associated with  $J^P = 1^-$ . We shall see later [Eqs. (116) and (115)] that  $A_1$  contributes to all three helicity components of the final-state vector meson (or the  $W^*$ ),  $A_2$  contributes only to the helicity-zero component, and  $V(q^2)$  contributes only to the helicity  $\pm 1$  components.

We now consider the information that can be obtained on the form factors from quark models, HQET, and nonperturbative methods and then return to the problem of computing decay distributions.

## 2. Quark models

Numerous quark-model calculations have been performed to determine form factors for exclusive decays, from which complete predictions for kinematic distributions and decay rates follow. As we discussed in Sec. II.C, form factors de-

scribe the effect of strong interactions on the decay. The higher the recoil velocity of the daughter quark (or the lower the value of  $q^2$ ), the smaller the value of the form factor, since more momentum must be transferred to the light constituents of the original hadron to form the new system. Some of the models most frequently discussed are those of Isgur, Scora, Grinstein, and Wise (ISGW; Isgur *et al.*, 1989; Isgur and Wise, 1990b), Körner and Schuler (KS; Körner and Schuler, 1988, 1989, 1990; Körner, Schilcher, Wirbel, and Wu, 1990), and Wirbel, Stech, and Bauer (WSB; Wirbel *et al.*, 1985; Bauer and Wirbel, 1989). Scora (1993) has improved the ISGW model, taking into account various relativistic effects and constraints from heavy-quark symmetry, and a new version of the model, called ISGW2 (Scora and Isgur, 1994) is currently being completed. Although these papers describe the models most commonly used in comparisons with data, there is a vast literature on this subject, and we shall be able to reference only part of it in the following sections. We note here that useful discussions of model predictions can be found in the papers of Hagiwara, Martin, and Wade (1989); Gilman and Singleton (1990); Kramer and Palmer (1990); Ramirez, Donoghue, and Burdman (1990); Burdman and Donoghue (1992); and Yaouanc (1994).

Quark-model calculations estimate meson wave functions and use them to compute the matrix elements that appear in the hadronic currents. These integrals are performed by analyzing the decay at a particular value of  $q^2$ , either  $q^2 = 0$  or  $q^2 = q_{\max}^2$ . One perspective (in the spirit of HQET, as discussed in the following section) is that the hadronic system is least disturbed at high  $q^2$ , so  $q_{\max}^2$  is where the integrals are most naturally evaluated. Historically, however, the convention in charm decays has been to specify the form factors at  $q^2 = 0$ .

In quark-model calculations, the variation of the form factors with  $q^2$  is determined as a separate step in the calculation. In fact, this variation is usually assumed to have a very simple form. Because the physics being described is nonperturbative, none of these phenomenological forms should be taken too seriously. One approach, used in the KS and WSB models, is called “nearest pole dominance,” which has its origin in vector-dominance ideas. Here, the  $q^2$  dependence of a form factor  $f_i$  is assumed to have the form

$$f_i(q^2) = \frac{f_i(0)}{\left(1 - \frac{q^2}{m_{\text{pole}}^2}\right)^n}, \quad (88)$$

where  $n$  is an integer, usually one for mesons. The pole mass  $m_{\text{pole}}$  is the mass of the lowest-lying  $Q\bar{q}'$  meson with the quantum numbers appropriate to a given part of the hadronic current. Thus, for a  $D \rightarrow \bar{K}^* \ell^+ \nu$  decay, the quark transition is  $c \rightarrow s$ , so the pole mass for the vector form factor is equal to  $m_{D_s^*}$ .

The ISGW calculation is based on a nonrelativistic constituent-quark potential model, with an assumed Coulomb-plus-linear form for  $V(r)$ . Such a calculation is expected to work best near zero recoil, so the form factors are calculated at  $q_{\max}^2$ . The more problematic extrapolation to larger recoils (lower  $q^2$ ) is performed by assuming an exponential governed by a parameter representing the “tran-

TABLE XVI. Quark-model predictions for form-factor values for the decay  $B \rightarrow D^* \ell^- \bar{\nu}$ . The values are given at  $q^2 = q_{\max}^2$  or  $q^2 = 0$ , depending on the model. For the WSB and KS models, which use pole forms to parametrize the  $q^2$  dependence of the form factors, the values of the exponent  $n$  and the pole masses in Eq. (88) are also given. The  $q^2$  dependence of the form factors in the ISGW model is exponential, as discussed in the text.

Form factor	ISGW ( $q_{\max}^2$ )	WSB ( $q^2=0$ )	KS ( $q^2=0$ )
$F_1$	1.13	0.69 ( $n=1$ )	0.7 ( $n=1$ )
$V$	1.19	0.71 ( $n=1$ )	0.7 ( $n=1$ )
$A_2$	1.06	0.69 ( $n=1$ )	0.7 ( $n=2$ )
$A_1$	0.94	0.65 ( $n=1$ )	0.7 ( $n=2$ )
$M_V$ (GeV/ $c^2$ )		6.34	6.34
$M_A$ (GeV/ $c^2$ )		6.73	6.34

sition charge radius” and an *ad hoc* relativistic correction factor. The ISGW form factors for  $B \rightarrow D^* \ell^- \bar{\nu}$ , for example, all have the same  $q^2$  dependence,

$$f_i(q^2) = f_i(q_{\max}^2) \exp[-(0.03 \text{ GeV}^{-2} c^4)(q_{\max}^2 - q^2)]. \quad (89)$$

Note that the slope at  $q_{\max}^2$ ,  $0.03 \text{ GeV}^{-2} c^4$ , is similar to the typical slope for the predictions based on a pole model,  $1/m_{\text{pole}}^2 \approx 1/(m_b + m_c)^2$ .

As an example, we consider in more detail the model predictions for  $B \rightarrow D \ell^- \bar{\nu}$  and  $B \rightarrow D^* \ell^- \bar{\nu}$  decays. Table XVI lists the constants predicted in three models. Since the functional forms used are not identical, it is useful to compare them visually, as in Fig. 22. It is clear that although the predictions are roughly in the same range, there are significant differences in both shape and normalization of the form factors. Instead of giving the  $q^2$  dependence of  $A_1$ , these

plots show  $A_1(q^2)/[1 - q^2/(m_B + m_{D^*})^2]$ . The reason for this choice is that in the heavy-quark symmetry limit all of the curves shown would have the same shape [see Eq. (100) and Fig. 23]. This is clearly not the case for the models discussed here, which preceded the development of HQET. In the following section, we shall see the same form factors obtained from an HQET-based calculation.

It is not obvious that either type of expression for the  $q^2$  dependence is generally valid, since the physics underlying the  $q^2$  dependence is inherently nonperturbative and difficult to predict. The assumptions embodied in the models should therefore be regarded only as reasonable approximations in certain situations, in particular, when the available range of  $q^2$  is not too large. The influence of a pole should be strongest when  $m_{\text{pole}}^2$  is not very much larger than  $q_{\max}^2$ . In  $D \rightarrow \bar{K} \ell^+ \nu$ , the only semileptonic charm decay for which the  $q^2$  dependence of the form factor has been studied, the data are well described by the form given in Eq. (88) with  $n=1$  and  $m_{\text{pole}} = (2.00 \pm 0.12 \pm 0.18) \text{ GeV}/c^2$  (see Sec. VI.B.1), which is consistent with the mass of the  $D_s^*$ . Bur-

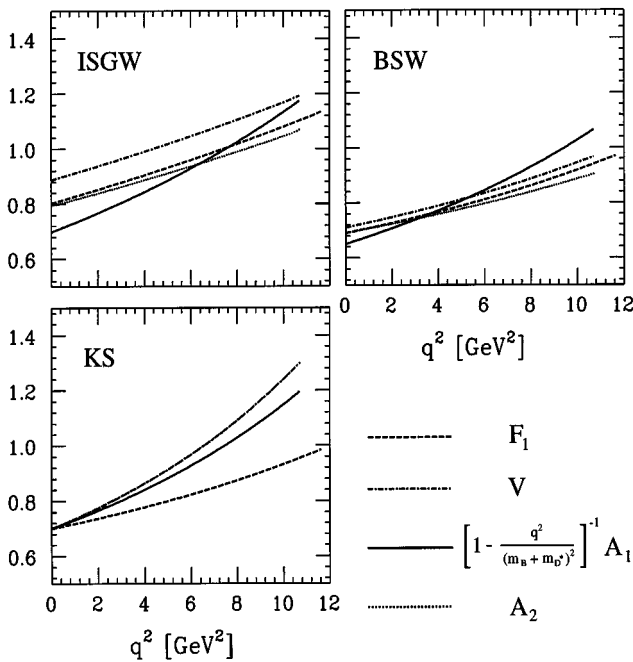


FIG. 22. The predicted  $q^2$  dependence of the form factors for  $B \rightarrow D \ell^- \bar{\nu}$  and  $B \rightarrow D^* \ell^- \bar{\nu}$ , according to three quark-model calculations described in the text. From Neubert (1994c), used with permission from M. Neubert.

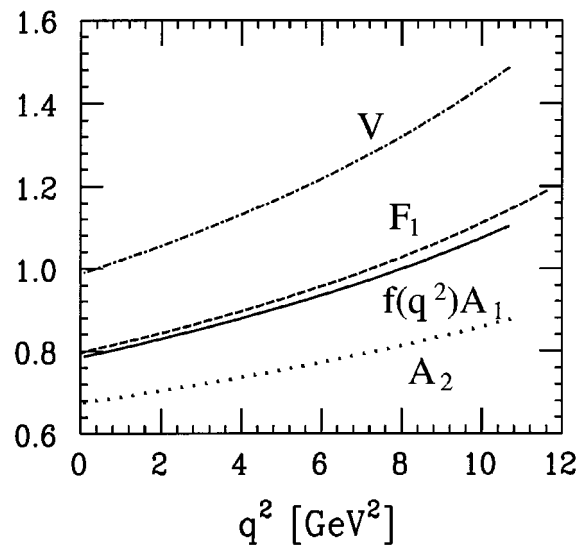


FIG. 23. The  $q^2$  dependence of form factors in  $B \rightarrow D \ell^- \bar{\nu}$  and  $B \rightarrow D^* \ell^- \bar{\nu}$  according to an HQET-based calculation by Neubert. The curves represent  $V$  (dot-dashed),  $F_1$  (dashed),  $f(q^2)A_1$  (where  $f(q^2) = [1 - q^2/(m_B + m_{D^*})^2]^{-1}$ ) (solid), and  $A_2$  (dotted). From Neubert (1994c), used with permission from M. Neubert.

TABLE XVII. Ranges of  $q^2$  and  $w$  for semileptonic decays of charm and bottom mesons. The variable  $w$  is the relativistic factor  $\gamma_X$  for the daughter meson  $X$ , as measured in the rest frame of the parent meson. Note that  $w_{\max}$  is the  $\gamma$  factor at maximum recoil velocity, which occurs at the minimum value of  $q^2$ ,  $q_{\min}^2 \approx 0$ .

Decay	$q_{\max}^2 \approx \Delta q^2$ (GeV <sup>2</sup> /c <sup>4</sup> )	$\Delta \gamma = \gamma_{\max} - 1$
$D \rightarrow \pi \ell^+ \nu$	2.97	5.70
$D \rightarrow \bar{K} \ell^+ \nu$	1.87	1.01
$D \rightarrow \rho \ell^+ \nu$	1.20	0.42
$D \rightarrow \bar{K}^* \ell^+ \nu$	0.94	0.28
$B \rightarrow \pi \ell^- \bar{\nu}$	26.4	17.9
$B \rightarrow \rho \ell^- \bar{\nu}$	20.3	2.51
$B \rightarrow D \ell^- \bar{\nu}$	11.7	0.59
$B \rightarrow D^* \ell^- \bar{\nu}$	10.7	0.50

dman and Donoghue (1992) provide a useful discussion of the different assumptions regarding the  $q^2$  dependence of form factors, and they advocate the use of more complicated form factors in certain decays in which the range of recoil velocities is large, as in  $B \rightarrow \pi \ell^- \bar{\nu}$ .

The available range of  $q^2$  in a decay is a key quantity, since it gives an indication of whether there will be a large variation in the form factors. In general, the larger the variation, the less likely it is that predictions will be reliable over the full range. Table XVII gives the  $q^2$  range for several processes of interest. For the  $b \rightarrow u \ell^- \bar{\nu}$  decays  $B \rightarrow \rho \ell^- \bar{\nu}$  and  $B \rightarrow \pi \ell^- \bar{\nu}$ , the range is large, since the initial meson is heavy and the final mesons are very light. Model predictions for these modes are not considered very reliable. It is interesting to compare  $q_{\max}^2$  with the relevant pole mass in some of these decays. For  $D \rightarrow \bar{K} \ell^+ \nu$ ,  $q_{\max}^2 = 1.87$  GeV<sup>2</sup>/c<sup>4</sup>, while the mass squared of the lowest-lying  $c\bar{s}$  vector meson is about 4 GeV<sup>2</sup>/c<sup>4</sup>. In  $B \rightarrow \pi \ell^- \bar{\nu}$  decay, one expects the  $B^*$  pole to strongly affect the region near  $q_{\max}^2$ , since the pole is just beyond the upper boundary of the Dalitz plot. However, the  $q^2$  dependence at low  $q^2$ , far from the pole, is probably not governed by the pole. Although comparison of  $q^2$  ranges can be useful, we shall see in the following section that it is preferable to study the velocity range of the recoil system.

More information on the form-factor predictions of these and other models for charm and bottom decays, as well as comparisons with data, are given in the following sections (see, for example, Tables XXVII, XXVIII, XLIII, and XLIV).

### 3. Heavy-quark effective theory

The form factors used in HQET are somewhat different from those described in the previous section because, in the limit of very heavy quark masses, the four-velocities of the hadrons, rather than their four-momenta, are the appropriate quantities to use. According to HQET, the configuration of the light constituents of a heavy-light hadron is not affected by the replacement of a heavy quark  $Q(v_Q, s)$  with another heavy quark  $Q'(v_Q, s')$ , where the heavy quarks have the same four-velocity  $v_Q$  but different flavors  $Q$  and  $Q'$  and different spins  $s$  and  $s'$ . Even though the initial and final

state heavy quarks have different masses, if they are sufficiently heavy, only their velocities are important in characterizing the hadronic systems. Furthermore, in the heavy-quark limit, the velocity of a heavy-light meson is the same as that of the heavy quark inside it.

Thus instead of describing the form-factor variation of the semileptonic decay  $M \rightarrow X \ell^- \bar{\nu}$  in terms of the square of the four-momentum transfer  $q^2$ , HQET calculations use the square of the four-velocity transfer,  $(v - v')^2 = 2(1 - v \cdot v')$ , where  $v$  and  $v'$  are the four-velocities of the initial and final hadrons. In fact, since the typical mass scale for the light constituents within the hadron is  $\Lambda_{\text{QCD}}$ , the square of the four-momentum transferred to these constituents during the decay must be  $\sim \Lambda_{\text{QCD}}^2 (v - v')^2$ , independent of the heavy-quark mass.

In the rest frame of the initial hadron,  $v \cdot v'$  has a simple physical interpretation:

$$v \cdot v' = \gamma_X = \frac{1}{\sqrt{1 - \beta_X^2}}, \tag{90}$$

where  $\beta_X$  is the velocity of the final-state hadron. The quantity  $v \cdot v'$ , which is often called  $w$  or  $y$  in the literature, is dimensionless and ranges from  $\gamma_X = 1$  at minimum recoil to the maximum value  $(M^2 + m_X^2)/(2Mm_X)$ . It is linearly related to  $q^2$  by

$$w \equiv v \cdot v' = \frac{M^2 + m_X^2 - q^2}{2Mm_X} \tag{91}$$

or

$$v \cdot v' - 1 = \frac{q_{\max}^2 - q^2}{2Mm_X}. \tag{92}$$

In general, heavy-quark symmetry relations are useful if the recoiling light constituents can only probe distances that are large compared with  $1/m_Q$ . Since the momentum transfer to the light constituents has the typical scale  $\Lambda_{\text{QCD}}(v \cdot v' - 1)$ , this condition is equivalent to the statement  $(v \cdot v' - 1) \ll m_Q/\Lambda_{\text{QCD}}$ . If this condition is violated in a certain region of phase space, then the quark under consideration cannot be regarded as heavy, and the form factors will be much harder to predict there.

Although one might be tempted to compare form factors for different processes at the same value of  $q^2$ , the comparison should be made at the same  $w$ . For example, at maximum recoil,  $q^2 = 0$ , but the recoil velocities at  $q^2 = 0$  can be completely different in different processes. Table XVII gives the range  $\delta w = \delta \gamma_X = |\delta q^2 / 2Mm_X|$  for many of the semileptonic decays of interest. The largest value occurs for  $B \rightarrow \pi \ell^- \bar{\nu}$ ,  $\delta w = 17.9$ , so that the recoiling pion can become highly relativistic. In contrast, for  $B \rightarrow D^* \ell^- \bar{\nu}$ , the range is much smaller,  $\delta w = 0.5$ . This small range results in a relatively mild variation of the form factors, which is helpful in the extraction of  $|V_{cb}|$  from  $B \rightarrow D^* \ell^- \bar{\nu}$  (see Sec. VI.E.4).

The hadronic current for  $P \rightarrow P' \ell \nu$  is expressed (Isgur and Wise, 1989, 1990a; Neubert and Rieckert, 1992; Falk and Neubert, 1993a; Neubert, 1994c); in terms of HQET form factors  $h_+(v \cdot v')$  and  $h_-(v \cdot v')$ :

$$\langle P'(v')|V^\mu|P(v)\rangle = \sqrt{Mm_{P'}}[h_+(v \cdot v')(v+v')^\mu + h_-(v \cdot v')(v-v')^\mu], \quad (93)$$

and for  $P \rightarrow V \ell \nu$  the current is

$$\begin{aligned} \langle V(v', \varepsilon)|(V^\mu - A^\mu)|P(v)\rangle &= \sqrt{Mm_V}[ih_V(v \cdot v')\varepsilon^{\mu\nu\alpha\beta}\varepsilon_\nu^*\varepsilon_\alpha^*v'_\mu v_\beta \\ &\quad - h_{A_1}(v \cdot v')\varepsilon^{*\mu}(v \cdot v' + 1) \\ &\quad + h_{A_2}(v \cdot v')v^\mu\varepsilon^* \cdot v + h_{A_3}(v \cdot v')v'^\mu\varepsilon^* \cdot v]. \end{aligned} \quad (94)$$

In the heavy-quark symmetry limit (for example,  $m_b, m_c \rightarrow \infty$  in  $b \rightarrow c \ell^- \bar{\nu}$ ), important simplifications occur:

$$h_+(w) = h_V(w) = h_{A_1}(w) = h_{A_3}(w) = \xi(w), \quad (95)$$

where  $\xi(w)$ , the Isgur-Wise function, is a common form factor for decays into pseudoscalar and vector mesons, since these states are in the same HQET multiplet. In addition,

$$h_-(w) = h_{A_2}(w) = 0. \quad (96)$$

The Isgur-Wise function can also be regarded as the form factor (in the heavy-quark symmetry limit) for the elastic scattering of the meson by a current that gives a kick to the heavy quark, as discussed in Sec. II.C. We emphasize again that although heavy-quark symmetry provides the relations given in Eqs. (95) and (96), it does not give the variation of  $\xi(v \cdot v')$  itself.

Of great practical importance for measuring  $|V_{cb}|$  is the result that, at zero recoil ( $w = v \cdot v' = \gamma_X = 1$ ), the light constituents of the meson are essentially undisturbed by the heavy-quark decay. In the heavy-quark symmetry limit, there is then a complete overlap between the initial and final meson wave functions, and the value of the Isgur-Wise function is known,  $\xi(1) = 1$ . We discuss this result in more detail in Sec. VI.E.4.

The HQET form factors are related to the traditional form factors  $F_1$ ,  $V$ ,  $A_1$ , and  $A_2$  by (Neubert and Rieckert, 1992; Neubert, 1994c)

$$\begin{aligned} RF_1(q^2) &= h_+(w) - \left(\frac{M - m_{P'}}{M + m_{P'}}\right)h_-(w), \\ R^*V(q^2) &= h_V(w), \\ R^{*-1}A_1(q^2) &= \frac{w+1}{2}h_{A_1}(w), \\ R^*A_2(q^2) &= h_{A_3}(w) + \frac{m_V}{M}h_{A_2}(w), \end{aligned} \quad (97)$$

where we have explicitly written  $m_{P'}$  and  $m_V$  instead of  $m$  in order to distinguish between the different masses for the final-state mesons. The constants  $R$  and  $R^*$  are given by

$$R = \frac{2\sqrt{Mm_{P'}}}{M + m_{P'}} \quad \text{and} \quad R^* = \frac{2\sqrt{Mm_V}}{M + m_V}. \quad (98)$$

The heavy-quark symmetry limit has not yet been imposed on Eq. (97); it is generally valid.

We can use these results to show how the traditional form factors  $F_1$ ,  $V$ ,  $A_1$ , and  $A_2$  are themselves related to the Isgur-Wise function in the heavy-quark symmetry limit. For  $P \rightarrow P' \ell \nu$  we have

$$F_1(q^2) = R^{-1}\xi(w), \quad (99)$$

and for  $P \rightarrow V \ell \nu$  we have (also in the heavy-quark symmetry limit)

$$V(q^2) = A_2(q^2) = \frac{A_1(q^2)}{\left[1 - \frac{q^2}{(M + m_V)^2}\right]} = R^{*-1}\xi(w). \quad (100)$$

We should like to be able to describe departures from the heavy-quark symmetry limit, since significant departures are expected, even in  $b \rightarrow c \ell^- \bar{\nu}$  decays. Following Neubert (1994c), we define the form-factor ratios

$$\begin{aligned} R_1(w) &\equiv \frac{h_V(w)}{h_{A_1}(w)} = \left[1 - \frac{q^2}{(M + m_V)^2}\right] \frac{V(q^2)}{A_1(q^2)}, \\ R_2(w) &\equiv \frac{h_{A_3}(w) + (m_V/M)h_{A_2}(w)}{h_{A_1}(w)} \\ &= \left[1 - \frac{q^2}{(M + m_V)^2}\right] \frac{A_2(q^2)}{A_1(q^2)}. \end{aligned} \quad (101)$$

From Eqs. (97) and (100) we see that these ratios are predicted to be unity, independent of  $w$ , in the heavy-quark symmetry limit. Recent measurements from CLEO, discussed in Sec. VI.E, have shown that these ratios are indeed close to unity for  $B \rightarrow D^* \ell^- \bar{\nu}$ .

Many experiments have measured ratios of the traditional form factors

$$r_V = \frac{V(q^2)}{A_1(q^2)} \quad \text{and} \quad r_2 = \frac{A_2(q^2)}{A_1(q^2)}. \quad (102)$$

These quantities are usually assumed to be constant in the fit. However, in the heavy-quark symmetry limit, it is not  $r_V$  and  $r_2$  that should be approximately  $q^2$  independent, but  $R_1$  and  $R_2$ . For charm decays, this consideration is not especially relevant, since the heavy-quark symmetry limit is not expected to hold, even approximately. For  $B$  decays, however, the ratios  $R_1$  and  $R_2$  are preferred. We have seen from Fig. 22 that the relative  $q^2$  dependence of the form factors for  $B \rightarrow D^* \ell^- \bar{\nu}$  assumed in the quark-model calculations of ISGW, KS, and WSB is not generally in accord with the heavy-quark symmetry limit, since the curves shown do not have the same shape. In contrast, the results of the HQET-based calculation (Neubert, 1994c) shown in Fig. 23 do have the same shape.

A major theoretical effort has been undertaken to evaluate corrections to the heavy-quark symmetry limit for various processes. In general, the largest corrections are from terms of order  $1/m_b$ ,  $1/m_c$ , and  $\alpha_s$ , which can be estimated in the framework of HQET. At the zero-recoil point,  $w = 1$ , the two form factors  $h_{A_1}$  and  $h_+$  are protected against  $1/m_Q$  corrections (see Sec. VI.E.4). As  $w$  increases, however, all of the heavy-quark symmetry relations are subject to significant symmetry-breaking corrections. Neubert's (model-dependent) estimate of these corrections for  $B \rightarrow D^* \ell^- \bar{\nu}$  gives (Neubert, 1994c)

$$R_1 \approx 1.3 \quad \text{and} \quad R_2 \approx 0.8. \quad (103)$$

Neubert argues that HQET predicts unambiguously that  $R_1$  for  $B \rightarrow D^* \ell^- \bar{\nu}$  must be considerably larger than unity,

whereas the prediction for  $R_2$  is less certain (Ligeti *et al.*, 1994; Neubert, 1994c). In reality, both  $R_1$  and  $R_2$  are expected to have a mild  $q^2$  (or  $w$ ) dependence,

$$\begin{aligned} R_1(w) &= 1.35 - 0.22(w-1) + 0.09(w-1)^2, \\ R_2(w) &= 0.79 + 0.15(w-1) - 0.04(w-1)^2 \end{aligned} \quad (104)$$

in Neubert's calculation and

$$\begin{aligned} R_1(w) &= 1.15 - 0.07(w-1) + \mathcal{O}(w-1)^2, \\ R_2(w) &= 0.91 + 0.04(w-1) + \mathcal{O}(w-1)^2 \end{aligned} \quad (105)$$

in the calculation by Close and Wambach (1994a, 1994b). Thus the symmetry breaking affects both the equality of the form factors at  $w=1$  and the equality of their slopes. It is important to remember that a typical value of  $w-1$  in  $\bar{B}^0 \rightarrow D^{*+} \ell^- \bar{\nu}$  is about 0.25, so the predicted variation of  $R_1$  and  $R_2$  with  $w$  is rather small.

We should like to describe  $A_1$ ,  $A_2$ , and  $V$  in a way that conveniently parametrizes departures from the heavy-quark symmetry limit. We use Eqs. (97) and (101) to relate all of the  $B \rightarrow D^{*} \ell^- \bar{\nu}$  form factors to  $h_{A_1}(w)$ :

$$\begin{aligned} A_1(q^2) &= \left[ 1 - \frac{q^2}{(M+m_\nu)^2} \right] R^{*-1} h_{A_1}(w), \\ A_2(q^2) &= R_2 R^{*-1} h_{A_1}(w), \\ V(q^2) &= R_1 R^{*-1} h_{A_1}(w). \end{aligned} \quad (106)$$

As written, these equations are exact, since  $R_1$  and  $R_2$  are, in general, functions of  $w$ . In the heavy-quark symmetry limit,  $R_1$  and  $R_2 \rightarrow 1$  and  $h_{A_1}(w) \rightarrow \xi(w)$ , which gives Eq. (100). The estimates of  $R_1$  and  $R_2$  indicate that, to first approximation, it may be reasonable to treat  $R_1$  and  $R_2$  as constants, which, however, are not equal to unity due to symmetry-breaking effects.

Ideally, one would test HQET by measuring the  $q^2$  dependence of each of the form factors separately and then testing whether they are really all governed by a single function. At present, however, the data only allow the measurement of  $R_1$ ,  $R_2$ , and  $h_{A_1}(w)$  under the assumption that all form factors are related as in Eq. (106), with  $R_1$  and  $R_2$  treated as constants. These measurements are discussed in Sec. VI.E.

#### 4. Predictions for the slope of the Isgur-Wise function

Although heavy-quark symmetry relates various form factors to  $\xi(w=v \cdot v')$ , it does not predict the variation of  $\xi$ . Nonperturbative methods, such as lattice QCD or QCD sum rules, are needed to deal with the long-range, soft-gluon strong interactions that the Isgur-Wise function describes. In the key decay mode  $B \rightarrow D^{*} \ell^- \bar{\nu}$ , however, the range of  $v \cdot v' = \gamma_{D^*}$  is fairly small, 1 to 1.5. A Taylor expansion of  $\xi$  about  $w=v \cdot v'=1$  is expected to work well over most of this region:

$$\xi(w) \approx 1 - \rho^2(w-1) + \mathcal{O}[(w-1)^2]. \quad (107)$$

In the region of interest for  $B \rightarrow D^{*} \ell^- \bar{\nu}$ , the Isgur-Wise function is thus characterized primarily by the slope  $\rho^2$ . Several plausible forms for the Isgur-Wise function are discussed in the literature, such as

$$\begin{aligned} \xi(w) &= \frac{2}{w+1} \exp \left[ -(2\rho^2-1) \left( \frac{w-1}{w+1} \right) \right], \\ \xi(w) &= \left( \frac{2}{w+1} \right)^{2\rho^2}, \\ \xi(w) &= \exp[-\rho^2(w-1)], \end{aligned} \quad (108)$$

where  $w=v \cdot v'$ . Experimentally, it is very difficult to distinguish among such forms because the range of  $w$  is so small. There is currently almost no sensitivity to terms beyond the linear term in Eq. (107). More precisely, the quantity that experiments are able to measure well is the average slope over the entire range of  $w$  (or  $q^2$ ).

Although  $\rho^2$  is difficult to calculate, it must be positive and is expected to be roughly in the range 0.5 to 2.0. The primary theoretical tools used to determine the Isgur-Wise function are QCD sum rules, which are based on quark-hadron duality, and lattice QCD, in which a computer calculation is performed using a discrete space-time lattice. Table XVIII gives several predictions for  $\rho^2$ , which is defined as the slope at zero recoil, for  $B \rightarrow D^{(*)} \ell^- \bar{\nu}$ . However, it is not always obvious how to compare  $\rho^2$  predictions from different authors, due to differences in the definitions used. Such differences range from renormalization effects to different functions used in fits to results of lattice calculations. Similarly, the use of different fitting functions by experiments results in a significant variation of the value of  $\rho^2$  quoted. We shall discuss the Isgur-Wise function further in regard to measurements of  $|V_{cb}|$  (Sec. VI.E.4) and the  $B \rightarrow D^{*} \ell^- \bar{\nu}$  form factors (Sec. VI.E.5).

#### 5. Decay distributions for $P \rightarrow P' \ell \nu$

We now consider the decay  $P \rightarrow P' \ell \nu$  where  $P$  and  $P'$  are both pseudoscalar mesons. Important examples are the CKM-favored decays  $D \rightarrow \bar{K} \ell^+ \nu$  and  $B \rightarrow D \ell^- \bar{\nu}$  and the CKM-suppressed decays  $D \rightarrow \pi \ell^+ \nu$  and  $B \rightarrow \pi \ell^- \bar{\nu}$ . As discussed in Sec. VI.A.1, when  $m_\ell \ll M$ , the hadronic current for  $P \rightarrow P' \ell \nu$  can be written in terms of one form factor  $F_1(q^2) = f_+(q^2)$ ,

$$H^\mu(q^2) = f_+(q^2)(p+p')^\mu, \quad (109)$$

where  $f_+$  is a vector form factor,  $p$  and  $p'$  are the four-momenta of the initial and final mesons, respectively, and  $q^2$  is the squared mass of the virtual  $W$ . The differential decay rate is given by

$$\frac{d\Gamma}{dq^2} = \frac{G_F^2 |V_{q'q}|^2 p_{P'}^3}{24\pi^3} |f_+(q^2)|^2, \quad (110)$$

where  $Q$  and  $q'$  are the initial and final-state quarks in the underlying transition  $Q \rightarrow q' \ell \nu$ , and  $p_{P'}$  is the magnitude of the three-momentum of the final-state meson  $P'$  in the rest frame of  $P$  and is a function of  $q^2$  [Eq. (30)]. In fact, the dominant  $q^2$  dependence usually arises not from the falloff of the form factor as  $q^2$  decreases, but from the  $p_{P'}^3$  term, which enhances the rate at low  $q^2$ . The angular distribution of the lepton in the  $W^*$  rest frame is discussed in Sec. II.C.

The most commonly assumed functional forms for the  $q^2$  dependence of the form factor are an exponential form

$f_+(q^2) = f_+(0)e^{\alpha q^2}$  and a pole form  $f_+(q^2) = f_+(0)/(1 - q^2/M_P^2)$ . The pole mass  $M_P$  should not be confused with the mass  $M$  of the decaying particle. (See Sec. VI.A.2 for further discussion of form-factor models.) Over the  $q^2$  range accessible in  $D \rightarrow \bar{K} \ell^+ \nu$  and  $B \rightarrow D \ell^- \bar{\nu}$  decays, the two functional forms given above are both linear to a good approximation. However, the larger  $q^2$  ranges in decays such as  $D \rightarrow \pi \ell^+ \nu$  and  $B \rightarrow \pi \ell^- \bar{\nu}$  result in more sensitivity to the  $q^2$  dependence.

By integrating Eq. (110) over the kinematically allowed  $q^2$  range and assuming a pole form for the  $q^2$  dependence of the form factor with a pole mass of 2.1 GeV/ $c^2$ , we can relate the total decay rate for  $D \rightarrow K e^+ \nu_e$  to the form factor at  $q^2=0$ :

$$\Gamma(D \rightarrow K e^+ \nu_e) = |f_+(0)|^2 |V_{cs}|^2 (15.4 \times 10^{10} \text{ s}^{-1}). \quad (111)$$

In Sec. VI.B.1, we use this result to extract  $f_+(0)$  from the measured decay rate for  $D \rightarrow \bar{K} \ell^+ \nu$ .

When velocities are used as the kinematic variables rather than momenta, as in HQET, two form factors enter into the differential rate:

$$\begin{aligned} \frac{d\Gamma(P \rightarrow P' \ell \nu)}{dw} &= \frac{G_F^2 |V_{cb}|^2}{48\pi^3} (M + m_{P'})^2 m_{P'}^3 (w^2 - 1)^{3/2} \\ &\times \left| h_+(w) - \frac{M - m_{P'}}{M + m_{P'}} h_-(w) \right|^2. \end{aligned} \quad (112)$$

Since  $h_-$  is not protected against  $1/m_Q$  corrections at zero recoil, the decay  $B \rightarrow D \ell^- \bar{\nu}$  is considered less useful for determining  $|V_{cb}|$  than  $B \rightarrow D^* \ell^- \bar{\nu}$  (see Sec. VI.E.4). The  $1/m_Q$  corrections may turn out to be small, however.

## 6. Decay distributions for $P \rightarrow V \ell \nu$

The decay  $P \rightarrow V \ell \nu$ , where  $P$  is a pseudoscalar and  $V$  is a vector meson, is more complicated than the decay to another pseudoscalar. The polarization vector of the meson  $V$  leads to a hadronic current with three form factors (in the limit of zero charged-lepton mass), as we have seen in Eq. (87). The most easily reconstructed semileptonic  $D$  and  $B$  decays in this category are  $D^+ \rightarrow \bar{K}^{*0} \ell^+ \nu$  with  $\bar{K}^{*0} \rightarrow K^- \pi^+$  and  $\bar{B}^0 \rightarrow D^{*+} \ell^- \bar{\nu}$  with  $D^{*+} \rightarrow D^0 \pi^+$ . All of the final-state particles except the neutrino can be reconstructed with fairly high efficiency. The two-body decays of the vector mesons to two pseudoscalars ( $\bar{K}^{*0} \rightarrow K^- \pi^+$  and  $D^{*+} \rightarrow D^0 \pi^+$ ) can be used to measure the polarization of the vector meson.

Four independent kinematic variables completely describe the semileptonic decay  $P \rightarrow V \ell \nu$ , where the vector meson decays to two pseudoscalars,  $V \rightarrow P_1 P_2$ . The four variables most commonly used are  $q^2$  or  $w$  and the three angles shown in Fig. 24. The angle  $\theta_\ell$  is measured in the  $W^*$  (or  $\ell \nu$ ) rest frame, where the lepton and the neutrino are back to back: it is the polar angle between the charged lepton and the direction opposite to that of the vector meson. The angle  $\theta_V$  is measured in the rest frame of the vector meson, where the pseudoscalars  $P_1$  and  $P_2$  are back to back. In this frame,  $\theta_V$  is the polar angle between one of these mesons, say,  $P_1$ , and the direction of the vector meson in the parent meson's rest frame. Although either  $P_1$  or  $P_2$  can be chosen for this definition, one must be careful to use a consistent choice for the angle  $\chi$ , which we define to be the azimuthal angle between the projections of the momenta of the lepton and  $P_1$  in the plane perpendicular to the decay axis.

The differential decay rate for  $P(Q\bar{q}) \rightarrow V(q'\bar{q}') \ell^- \bar{\nu}$ ,  $V \rightarrow P_1 P_2$  can be expressed in terms of these four kinematic variables  $q^2$ ,  $\theta_\ell$ ,  $\theta_V$ , and  $\chi$  (Gilman and Singleton, 1990; Körner and Schuler, 1990):

$$\begin{aligned} &\frac{d\Gamma(P \rightarrow V \ell \nu, V \rightarrow P_1 P_2)}{dq^2 d \cos \theta_V d \cos \theta_\ell d \chi} \\ &= \frac{3}{8(4\pi)^4} G_F^2 |V_{q'q}|^2 \frac{P_V q^2}{M^2} \mathcal{B}(V \rightarrow P_1 P_2) \{ (1 - \eta \cos \theta_\ell)^2 \sin^2 \theta_V |H_+(q^2)|^2 + (1 + \eta \cos \theta_\ell)^2 \sin^2 \theta_V |H_-(q^2)|^2 \\ &\quad + 4 \sin^2 \theta_\ell \cos^2 \theta_V |H_0(q^2)|^2 - 4 \eta \sin \theta_\ell (1 - \eta \cos \theta_\ell) \sin \theta_V \cos \theta_V \cos \chi H_+(q^2) H_0(q^2) \\ &\quad + 4 \eta \sin \theta_\ell (1 + \eta \cos \theta_\ell) \sin \theta_V \cos \theta_V \cos \chi H_-(q^2) H_0(q^2) - 2 \sin^2 \theta_\ell \sin^2 \theta_V \cos 2\chi H_+(q^2) H_-(q^2) \}, \end{aligned} \quad (113)$$

where  $p_V$  is the magnitude of the three-momentum of  $V$  in the rest frame of  $P$  and is a function of  $q^2$  [see Eq. (30)]. The factor  $\eta$  is equal to +1 for  $B$  decays and -1 for  $D$  decays. It is this factor that leads to the different lepton-energy distributions for bottom and charm decays discussed in Sec. II.C. Note that the angle  $\theta_\ell$  is defined with respect to the direction of the virtual  $W$  in the parent rest frame; this accounts for the sign differences between our formula and certain others in the literature (Körner and Schuler, 1988), which use  $\pi - \theta_\ell$ .

Because the parent meson has spin zero, the vector meson

and the  $W^*$  must have the same helicity. The amplitudes for helicities 0, +1, and -1 are proportional to  $H_0(q^2)$ ,  $H_+(q^2)$ , and  $H_-(q^2)$ . The detailed dynamics of the hadronic current are described by the variation of these helicity amplitudes with  $q^2$ , which we have not yet specified. Equation (113) incorporates the  $V-A$  structure of the leptonic current, as well as the assumption that the mass of the charged lepton can be neglected. In general, there is a fourth helicity amplitude corresponding to the timelike helicity component of the virtual  $W$ , but its contribution is negligible when the lepton mass is small. The differential decay-rate

TABLE XVIII. Predictions for the slope  $\rho^2$  of the Isgur-Wise function from QCD sum-rule and lattice QCD calculations, for  $B \rightarrow D^{(*)} \ell^- \bar{\nu}$ .

Calculation	Ref.	$\rho^2$
Bjorken sum rule	Bjorken, 1990	$>0.25$
Blok and Shifman	Blok and Shifman, 1993	$0.7 \pm 0.25$
Voloshin sum rule	Voloshin, 1992	$B \rightarrow D \ell^- \bar{\nu}$ : $<0.75$ $B \rightarrow D^* \ell^- \bar{\nu}$ : $<1.15$
Jin, Huang, and Dai	Jin <i>et al.</i> , 1992	$1.00 - 1.10$
Neubert	Neubert, 1994c	$\approx 0.8$
QCD spectral sum rules	Narison, 1994a	$1.00 \pm 0.02$
Lattice QCD	Bernard <i>et al.</i> , 1993	$1.24 \pm 0.26 \pm 0.33$
Lattice QCD	Booth <i>et al.</i> , 1994	$1.2_{-0.3}^{+0.7}$

formula for finite lepton mass is given, for example, in Körner and Schuler (1990).

It is easy to understand the origin of most of the terms in Eq. (113). For example, in the case where the vector meson and the  $W^*$  have helicity  $+1$ , the decay angular distribution of the charged lepton in the  $W^*$  rest frame is proportional to the Wigner  $d$  function,

$$d_{\lambda_{W^*}, \lambda_{\ell} - \lambda_{\nu}}^1(\theta_{\ell}) = d_{1,-1}^1(\theta_{\ell}) = (1/2)(1 - \cos\theta_{\ell}). \quad (114)$$

Since  $\lambda_{D^*} = +1$  as well, the angular distribution of the  $D$  meson in the  $D^*$  rest frame is given by  $d_{\lambda_{D^*}, \lambda_D - \lambda_{\pi}}^1(\theta_{\nu}) = d_{10}^1(\theta_{\nu}) = -(1/\sqrt{2})\sin\theta_{\nu}$ . These arguments explain the angular dependence of the coefficient of the  $|H_+(q^2)|^2$  term in Eq. (113).

The helicity amplitudes can in turn be related to the two axial-vector form factors,  $A_1(q^2)$  and  $A_2(q^2)$ , and the vector form factor  $V(q^2)$ , which appear in the hadronic current [Eq. (85)]:

$$H_0(q^2) = \frac{1}{2m_V \sqrt{q^2}} \left[ (M^2 - m_V^2 - q^2)(M + m_V)A_1(q^2) - 4 \frac{M^2 p_V^2}{M + m_V} A_2(q^2) \right] \quad (115)$$

and

$$H_{\pm}(q^2) = (M + m_V)A_1(q^2) \mp \frac{2Mp_V}{M + m_V} V(q^2). \quad (116)$$

The form factors  $A_1$ ,  $A_2$ , and  $V$  are dimensionless and relatively real, since  $CP$  is conserved in these decays and there are no final-state strong interactions (Körner and Schuler, 1988). [Possible  $CP$ -violating effects in semileptonic  $B$  decays due to physics beyond the standard model are discussed in Garisto (1995).] We can therefore take them to be real, as assumed in Eq. (113). We note that, while  $A_2$  contributes only to  $H_0$  and  $V$  contributes only to  $H_{\pm}$ ,  $A_1$  contributes to all three helicity amplitudes. At high  $q^2$  (small  $p_V$ ), each of the helicity amplitudes is dominated by  $A_1$ .

We can also relate the helicity amplitudes to the set of form factors defined in HQET. Since this result is applicable mainly to the decay  $B \rightarrow D^* \ell^- \bar{\nu}$ , we write the result with the relevant masses:

$$H_0(w) = (m_B - m_{D^*}) \sqrt{\frac{m_B m_{D^*}}{q^2(w)}} (w+1) h_{A_1}(w) \times \left[ 1 + \left( \frac{w-1}{1-r} \right) [1 - R_2(w)] \right] \quad (117)$$

and

$$H_{\pm}(w) = (m_B - m_{D^*}) \sqrt{\frac{m_B m_{D^*}}{q^2(w)}} (w+1) h_{A_1}(w) \times \frac{\sqrt{1-2wr+r^2}}{1-r} \left[ 1 \mp \sqrt{\frac{w-1}{w+1}} R_1(w) \right], \quad (118)$$

where  $r = m_{D^*}/m_B$ . The terms  $w \pm 1$  are related to  $q^2$  by

$$w \pm 1 = \frac{(m_B \pm m_{D^*})^2 - q^2}{2m_B m_{D^*}}. \quad (119)$$

From inspection of these formulas, it is clear that as  $w \rightarrow 1$ ,  $H_0$  and  $H_{\pm}$  are governed by  $h_{A_1}(w)$ .

In the decay-rate formula [Eq. (113)], we also have the overall kinematic factor  $p_V q^2$ . The momentum can be expressed in terms of  $w$  by

$$p_V = |\mathbf{p}_{D^*}| = m_{D^*} \sqrt{w^2 - 1}. \quad (120)$$

It is interesting to analyze the  $w$  or  $q^2$  dependence of each term contributing to the differential rate. All of the  $w$  dependence resides in the  $H_i H_j$  terms multiplied by the factor  $p_V q^2$ , which form the coefficients of the angular terms in Eq. (113). Figure 25 shows the  $w$  dependence of these coefficients, using as inputs the form factors measured by CLEO for the decay  $\bar{B}^0 \rightarrow D^{*+} \ell^- \bar{\nu}$  (see Sec. VI.E.5). Recall from Eq. (91) that the minimum value,  $w=1$ , corresponds to  $q^2 = q_{\max}^2$ , where the hadronic system has zero recoil velocity in the parent meson's rest frame. There is no phase space for this configuration, which explains why all of the curves in Fig. 25 go to zero at  $w=1$ . However, as  $w \rightarrow 1$ , the rates from the three possible helicities contribute equally, because both the daughter meson and the virtual  $W$  are stationary in the parent rest frame. As we discussed at the end of Sec. II, this forces these particles to be unpolarized.

As  $w$  increases, we see that the  $H_{\pm}^2$  term quickly begins to

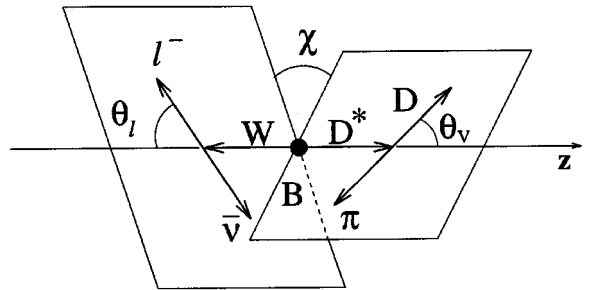


FIG. 24. Definition of the angles  $\theta_V$ ,  $\theta_{\ell}$ , and  $\chi$  in the decay  $B \rightarrow D^* \ell^- \bar{\nu}$ . (These angles are used for any  $P \rightarrow V \ell \nu$  in which the vector meson decays into two pseudoscalars.) The lepton and neutrino are drawn back to back because they are shown in the  $W^*$  rest frame. Similarly, the  $D$  and the  $\pi$  are shown in the  $D^*$  rest frame. In the literature, the angle  $\theta_{\ell}$  is sometimes defined as the direction between the charged lepton and the recoiling vector meson, measured in the  $\ell \nu$  rest frame.

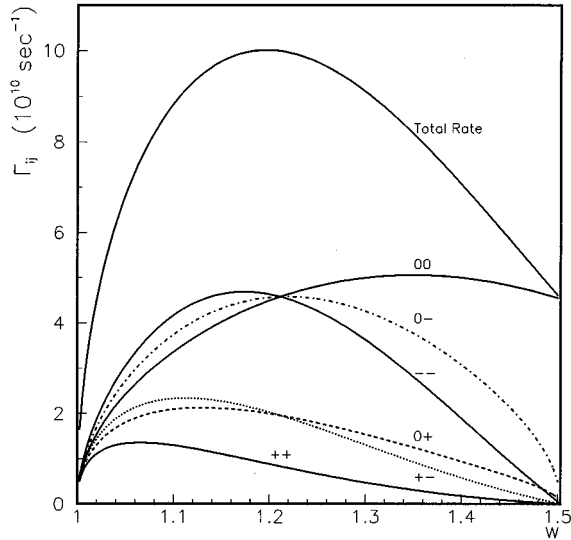


FIG. 25. The predicted  $w$  dependence of different helicity combinations in the decay  $B \rightarrow D^* \ell^- \bar{\nu}$ . The curves show the quantities  $\Gamma_{ij} = (G_F^2 |V_{cb}|^2 p_V q^2 / 96 \pi^3 M^2) H_i(q^2) H_j(q^2)$ ,  $i, j = +, -, 0$ , which appear as coefficients of the angular factors in Eq. (113). We have assumed  $R_1 = 1.3$  and  $R_2 = 0.8$ , with a linear  $w$  dependence (slope =  $\rho^2 = 1.0$ ) for  $h_{A_1}$ . The overall scale is also determined by  $V_{cb} = 0.04$ . The solid lines correspond to the terms that contribute to the total decay rate:  $\Gamma_{ij}$ ,  $i = j$ . The terms  $\Gamma_{ij}$ ,  $i \neq j$ , do not contribute to the total decay rate because the angular functions that they multiply in Eq. (113) integrate to zero. The  $D^*$  helicity can only be zero at maximum recoil ( $w = 1.5$ ); as  $w$  decreases, both helicity  $-1$  and  $+1$  contribute, but helicity  $-1$  dominates due to the  $V-A$  coupling. At minimum  $D^*$  recoil, all three helicities contribute equally, but phase space goes to zero.

dominate over the  $H_+^2$  term. This result is expected from the  $V-A$  nature of the  $W$  couplings, which leads to a higher probability for the vector meson (and the virtual  $W$ ) to have helicity  $\lambda = -1$  than  $\lambda = +1$ . (See Sec. II.C and Fig. 6.) This effect also produces a larger value for the interference term  $H_0 H_-$  than for  $H_0 H_+$  at all values of  $q^2$  except the end points. The CLEO measurements discussed in Sec. VI.E.5 show clear effects in the correlation between  $\chi$  and  $\cos\theta_V$  due to this interference term.

At the other extreme,  $w = w_{\max} \approx 1.5$  or  $q^2 = 0$ , the recoil velocity is maximum. The lepton and neutrino momenta are parallel in the rest frame of  $P$ , and their combined spin projection along their direction of motion is zero. Hence only the  $H_0^2$  combination contributes in this limit. This point is also evident from inspection of Eqs. (115) and Eq. (116), which show that  $p_V q^2 H_0^2$  remains finite as  $q^2 \rightarrow 0$ , whereas both  $p_V q^2 H_+^2$  and  $p_V q^2 H_-^2$  go to zero.

It is also instructive to examine the dependence of Eq. (113) on the form factors themselves via the helicity amplitudes, Eqs. (115) and (116). When the recoil of the hadronic system is small ( $w \approx 1$ ), the terms proportional to  $V(q^2)$  and  $A_2(q^2)$  can be neglected compared with those proportional to  $A_1(q^2)$ , which appear in all the helicity amplitudes. As a consequence, the  $A_1$  form factor dominates the rate at large values of  $q^2$ .

Since the form factor  $A_1(q^2)$  appears in all three helicity

amplitudes [Eqs. (115) and (116)] and typically dominates the rate, it is natural to use the new variables  $r_V \equiv V/A_1$  and  $r_2 \equiv A_2/A_1$  or in HQET,  $R_1$  and  $R_2$  defined in Eq. (101).

It is common to report the values of certain other integrated observables that can be derived from the form factors. These are  $\bar{A}_{\text{FB}}$ , the forward-backward asymmetry of the lepton in the  $W$  rest frame,

$$\begin{aligned} \bar{A}_{\text{FB}} &= \frac{\int_0^1 \frac{d\Gamma}{d \cos\theta_\ell} d \cos\theta_\ell - \int_{-1}^0 \frac{d\Gamma}{d \cos\theta_\ell} d \cos\theta_\ell}{\int_{-1}^1 \frac{d\Gamma}{d \cos\theta_\ell} d \cos\theta_\ell} \\ &= \frac{3}{4} \frac{(\Gamma_- - \Gamma_+)}{(\Gamma_L + \Gamma_T)}, \end{aligned} \quad (121)$$

and  $\bar{A}_{\text{pol}}$ , which is related to the ratio of longitudinal to transverse polarization of the vector meson:

$$\bar{A}_{\text{pol}} = \frac{2 \int p_V q^2 |H_0|^2 dq^2}{\int p_V q^2 (|H_-|^2 + |H_+|^2) dq^2} - 1 = 2 \frac{\Gamma_L}{\Gamma_T} - 1, \quad (122)$$

where

$$\Gamma_i = \frac{G_F^2 |V_{cb}|^2}{96 \pi^3} \int dq^2 p_V \frac{q^2}{m_B^2} |H_i(q^2)|^2, \quad (123)$$

and

$$\Gamma_L = \Gamma_0, \quad \Gamma_T = \Gamma_+ + \Gamma_-. \quad (124)$$

We can easily see which form factors these observables are sensitive to by examining the expressions for the helicity amplitudes, Eqs. (115) and (116). Since the only difference between  $H_+$  and  $H_-$  is the sign of the coefficient of  $V(q^2)$ , it is clear that the difference  $\Gamma_- - \Gamma_+$  is proportional to an integral over  $V(q^2)$ . Thus  $\bar{A}_{\text{FB}}$  provides a measurement of  $r_V$  (or  $R_1$  in the HQET picture). In contrast, the ratio of longitudinal to transverse polarization is almost completely controlled by  $r_2$  (or  $R_2$  in the HQET version). Roughly speaking, then,  $r_V$  (or  $R_1$ ) is determined from the  $\cos\theta_\ell$  distribution and the  $\cos\theta_V$  vs  $\chi$  correlation, whereas  $r_2$  (or  $R_2$ ) is determined from the  $\cos\theta_V$  and  $q^2$  distributions.

## B. Cabibbo-favored semileptonic decays of charm mesons

In this section, we present measurements of the decay rates and form factors for  $D \rightarrow \bar{K} \ell^+ \nu$ ,  $D \rightarrow \bar{K}^* \ell^+ \nu$ , and  $D_s \rightarrow \phi \ell^+ \nu$ . We also discuss experimental searches for semileptonic  $D$  decays to higher mass or nonresonant hadronic states and observations of  $D_s \rightarrow \eta \ell^+ \nu$  and  $D_s \rightarrow \eta' \ell^+ \nu$ . We compare the sum of exclusive semileptonic  $D$  decay rates to the inclusive rate in Sec. VI.D.

### 1. $D \rightarrow \bar{K} \ell^+ \nu$

The most precise experimental studies of  $D \rightarrow \bar{K} \ell^+ \nu$  have been made for the mode  $D^0 \rightarrow K^- \ell^+ \nu$  because the final state contains two easily reconstructed charged particles, both of which are produced at the  $D$  decay point. In fixed-target experiments, for example, the  $K^- \ell^+$  vertex and the reconstructed primary vertex are used to determine the  $D$  flight

TABLE XIX. Measurements of the branching fraction for  $D^0 \rightarrow K^- \ell^+ \nu$ . When not already done by the experimenters, measured branching fractions for the muon mode have been scaled up by 1.03 to account for the reduced phase space relative to the electron mode.

Experiment	No. of events (lepton type)	Normalizing mode	Measured ratio of branching fractions	$B(D^0 \rightarrow K^- \ell^+ \nu)$ (%)
E691 (Anjos <i>et al.</i> , 1989b)	250 ( $e$ )	$D^0 \rightarrow K^- \pi^+$	$0.91 \pm 0.07 \pm 0.11$	$3.65 \pm 0.54$
CLEO (Crawford <i>et al.</i> , 1991)	584 ( $e$ )	$D^0 \rightarrow K^- \pi^+$	$0.90 \pm 0.06 \pm 0.06$	$3.61 \pm 0.37$
CLEO (Crawford <i>et al.</i> , 1991)	231 ( $\mu$ )	$D^0 \rightarrow K^- \pi^+$	$0.81 \pm 0.08 \pm 0.09$	$3.26 \pm 0.50$
E687 (Frabetti <i>et al.</i> , 1993c)	338 ( $\mu$ )	$D^0 \rightarrow K^- \pi^+$	$0.84 \pm 0.13 \pm 0.13$	$3.39 \pm 0.50$
CLEO II (Bean <i>et al.</i> , 1993a)	2700 ( $e, \mu$ )	$D^0 \rightarrow K^- \pi^+$	$0.978 \pm 0.027 \pm 0.044$	$3.92 \pm 0.25$
MARK III (Adler <i>et al.</i> , 1989)	56 ( $e$ )	absolute		$3.4 \pm 0.6$
Average				$3.71 \pm 0.19$

direction, from which the neutrino momentum can be calculated, up to a quadratic ambiguity. In the decay  $D^+ \rightarrow \bar{K}^0 \ell^+ \nu$ , on the other hand, the location of the  $D$  decay usually cannot be determined with adequate precision, since only one-third of neutral kaons decay to charged particles through  $K_S \rightarrow \pi^+ \pi^-$ . Even then, a  $K_S$  will often decay downstream of the high-precision silicon detectors. In  $e^+ e^-$  experiments, such as CLEO, the efficiency for reconstructing a  $K^0$  is significantly lower than that for reconstructing a  $K^-$  because of the limited branching fraction for neutral kaons to decay to charged particles in the detector, and because two charged tracks must be reconstructed.

Because of the relatively large number of reconstructed  $D^0 \rightarrow K^- \ell^+ \nu$  decays, and because the decay rate can be expressed in terms of just one form factor  $f_+(q^2)$ ,  $D^0 \rightarrow K^- \ell^+ \nu$  is the only charm decay for which the  $q^2$  dependence of the form factor has been studied. Since the value of  $V_{cs}$  is known independently, measurements of the decay rate determine the overall normalization of the form factor.

Measurements of the  $D^0 \rightarrow K^- \ell^+ \nu$  branching fraction are shown in Table XIX, along with the number of signal events and the type of lepton used in each study. In most experiments, the branching fraction is measured relative to the topologically similar mode  $D^0 \rightarrow K^- \pi^+$ . The average ratio of branching fractions is

$$\frac{B(D^0 \rightarrow K^- \ell^+ \nu)}{B(D^0 \rightarrow K^- \pi^+)} = 0.933 \pm 0.039.$$

Combined with the 1994 Particle Data Group (PDG) value for  $B(D^0 \rightarrow K^- \pi^+)$  (see Table III), this gives a branching fraction of

$$B(D^0 \rightarrow K^- \ell^+ \nu) = (3.74 \pm 0.20)\%. \quad (125)$$

Table XIX also lists a measurement of the absolute branching fraction for  $D^0 \rightarrow K^- e^+ \nu_e$  by the Mark III Collaboration, based on a tagging technique. With correlated errors due to the branching fraction for the normalizing mode  $D^0 \rightarrow K^- \pi^+$  taken into account, the average of all the measurements in Table XIX is

$$B(D^0 \rightarrow K^- \ell^+ \nu) = (3.71 \pm 0.19)\%. \quad (126)$$

Using the 1994 PDG value of the  $D^0$  lifetime (see Table III), we calculate the corresponding decay rate to be

$$\Gamma(D^0 \rightarrow K^- \ell^+ \nu) = (8.94 \pm 0.47) \times 10^{10} \text{ s}^{-1}. \quad (127)$$

The decay mode  $D^+ \rightarrow \bar{K}^0 \ell^+ \nu$  has been studied by three experiments. The branching-ratio measurements are summarized in Table XX. The E691 and CLEO II measurements have been combined with the 1994 PDG values for  $B(D^+ \rightarrow K^- \pi^+ \pi^+)$  and  $B(D^+ \rightarrow \bar{K}^0 \pi^+)$ , respectively, to extract  $B(D^+ \rightarrow \bar{K}^0 \ell^+ \nu)$ . The average branching fraction, including the absolutely normalized Mark III measurement, is

$$B(D^+ \rightarrow \bar{K}^0 \ell^+ \nu) = (6.6 \pm 0.9)\%.$$

When this is combined with the 1994 PDG value for the  $D^+$  lifetime (see Table III), we obtain a decay rate of

$$\Gamma(D^+ \rightarrow \bar{K}^0 \ell^+ \nu) = (6.2 \pm 0.9) \times 10^{10} \text{ s}^{-1}. \quad (128)$$

Isospin conservation implies that the rates for Cabibbo-favored modes such as  $D^0 \rightarrow K^- \ell^+ \nu$  and  $D^+ \rightarrow \bar{K}^0 \ell^+ \nu$  should be the same. Using Eqs. (127) and (128), we obtain

TABLE XX. Measurements of the branching fraction for  $D^+ \rightarrow \bar{K}^0 \ell^+ \nu$ . When not already done by the experimenters, measured branching fractions for the muon mode have been scaled up by 1.03 to account for the reduced phase space relative to the electron mode.

Experiment	No. of events (lepton type)	Normalizing mode	Measured ratio of branching fractions	$B(D^+ \rightarrow \bar{K}^0 \ell^+ \nu)$ (%)
MARK III (Bai <i>et al.</i> , 1991)	27 ( $e, \mu$ )	absolute		$6.6^{+1.6}_{-1.1} \pm 0.7$
E691 (Anjos <i>et al.</i> , 1991)	250 ( $e$ )	$D^+ \rightarrow K^- \pi^+ \pi^+$	$0.66 \pm 0.09 \pm 0.14$	$6.0 \pm 1.6$
CLEO II (Bean <i>et al.</i> , 1993a)	186 ( $e, \mu$ )	$D^+ \rightarrow \bar{K}^0 \pi^+$	$2.60 \pm 0.35 \pm 0.26$	$7.1 \pm 1.4$
Average				$6.6 \pm 0.9$

TABLE XXI. Measurements of the pole mass  $M_P$  from a fit of the  $q^2$  dependence of the decay rate for  $D^0 \rightarrow K^- \ell^+ \nu$ . The  $q^2$  dependence of the form factor is assumed to be  $f_+(q^2) = f_+(0)/(1 - q^2/M_P^2)$ .

Experiment	No. of events (lepton type)	$M_P$ (GeV)
E691 (Anjos <i>et al.</i> , 1989b)	250 ( $e$ )	$2.1^{+0.4}_{-0.2} \pm 0.2$
CLEO (Crawford <i>et al.</i> , 1991)	815 ( $e, \mu$ )	$2.1^{+0.4+0.3}_{-0.2-0.2}$
MARK III (Bai <i>et al.</i> , 1991)	56 ( $e$ )	$1.8 \pm 0.3 \pm 0.2$
E687 (Frabetti <i>et al.</i> , 1993c)	338 ( $\mu$ )	$2.1^{+0.7+0.7}_{-0.3-0.3}$
CLEO II (Bean <i>et al.</i> , 1993a)	2700 ( $e, \mu$ )	$2.00 \pm 0.12 \pm 0.18$
Average		$2.00 \pm 0.15$

$$\Gamma(D^0 \rightarrow K^- \ell^+ \nu) / \Gamma(D^+ \rightarrow \bar{K}^0 \ell^+ \nu) = 1.4 \pm 0.2,$$

roughly consistent with unity. If we average the rates for the two isospin states, we obtain

$$\Gamma(D \rightarrow \bar{K} \ell^+ \nu) = (8.4 \pm 0.4) \times 10^{10} \text{ s}^{-1}. \quad (129)$$

This rate will be compared to that for  $D \rightarrow \bar{K}^* \ell^+ \nu$  in Sec. VI.B.3.

The sample of  $D^0 \rightarrow K^- \ell^+ \nu$  decay candidates from CLEO (Bean *et al.*, 1993a) is significantly larger than any previous sample, leading to the most sensitive study to date of the  $q^2$  dependence of the form factor  $f_+$ . We shall therefore describe the analysis in more detail here. The decay  $D^{*+} \rightarrow D^0 \pi^+$  is used to obtain a clean sample of  $D^0 \rightarrow K^- \ell^+ \nu$  decays, just as it is often used for  $D^0 \rightarrow K^- \pi^+$ . The only difference is that the  $D^0$  is not fully reconstructed, due to the neutrino in the final state, which broadens the peak in the distribution of mass difference  $\Delta M = m(K \ell \pi) - m(K \ell)$ . The signal-to-background ratio for the selected events is about 3.6. Figure 26 shows the distribution of  $q^2$ , which is measured with a resolution of about  $0.24 \text{ GeV}^2$ . The number of signal events in each  $q^2$  bin is extracted by fitting the  $\Delta M$  distribution. The shape of the  $q^2$  distribution is dominated by the factor of  $p_p^3$  in Eq. (110), which suppresses the decay rate at large  $q^2$ . The form factor itself increases roughly linearly by about a factor of two over the kinematically allowed range of  $q^2$ . The result of a fit to the functional form  $f_+(q^2) = f_+(0)/(1 - q^2/M_P^2)$  is shown in Table XXI, along with the measurements of  $M_P$  from other experiments. The mean pole mass  $M_P$  is somewhat lower than  $M_{D^*} = 2.1 \text{ GeV}$ . As an alternative to the pole form, CLEO also assumed the form  $f_+(q^2) = f_+(0)e^{\alpha q^2}$  and fit for the parameter  $\alpha$ . The measured value of  $\alpha = (0.29 \pm 0.04 \pm 0.06) \text{ GeV}^{-2}$  is about one standard deviation higher than the value used in the ISGW model (Isgur *et al.*, 1989).

The form-factor intercept  $f(0)$  can be extracted by integrating the differential decay rate for a particular assumption for the  $q^2$  dependence of the form factor. Using the average decay rate  $\Gamma(D \rightarrow \bar{K} \ell^+ \nu)$  given in Eq. (129), a pole form for the  $q^2$  dependence with  $M_P = 2.1 \text{ GeV}/c^2$ , and  $|V_{cs}| = 0.97$ , we determine

$$f_+(0) = 0.76 \pm 0.02 \pm 0.02$$

from Eq. (111). The first error is from the uncertainty on the

decay rate and the second error is from the uncertainty in the  $q^2$  dependence (Morrison and Richman, 1994). This result is consistent with theoretical predictions of quark-model, lattice gauge, and QCD sum-rule calculations, which range from 0.6 to 0.9. Theoretical predictions for the  $D \rightarrow \bar{K} \ell^+ \nu$  form factor are summarized and compared with the experimental measurement in Table XXVII below, along with the form factors for  $D \rightarrow \bar{K}^* \ell^+ \nu$ , which are discussed in the next section. In Table XXVIII, the form factors are given at  $q_{\text{max}}^2$  and compared with the theoretical predictions of ISGW (Isgur *et al.*, 1989) and ISGW2 (Scora and Isgur, 1994).

## 2. $D \rightarrow \bar{K}^* \ell^+ \nu$

The largest and cleanest signals for the decay  $D \rightarrow \bar{K}^* \ell^+ \nu$  are extracted from fixed-target experiments in the mode  $D^+ \rightarrow \bar{K}^{*0} \ell^+ \nu$ , where  $\bar{K}^{*0} \rightarrow K^- \pi^+$ . This mode has several advantages over the mode  $D^0 \rightarrow K^{*-} \ell^+ \nu$ , with  $K^{*-} \rightarrow K^- \pi^0$  or  $\bar{K}^0 \pi^-$ . For the  $K^- \pi^+ \ell^+ \nu$  final state, all the particles in the final state (except the neutrino) are long-lived charged particles that can be reconstructed more efficiently than  $\pi^0$ 's or neutral kaons. The noncharm background can be studied with so-called ‘‘wrong-sign’’ candidates, in which the kaon charge is not consistent with the lepton charge (e.g.,  $K^+ \pi^- \ell^+$ ).<sup>6</sup> This definition of a wrong-sign background is not possible with a neutral kaon in the final state.

Six experiments have measured the branching fraction for  $D^+ \rightarrow \bar{K}^{*0} \ell^+ \nu$  relative to that for the topologically similar hadronic mode  $D^+ \rightarrow K^- \pi^+ \pi^+$ . Results are summarized in Table XXII. The average value of the ratio of branching fractions is

$$\frac{B(D^+ \rightarrow \bar{K}^{*0} \ell^+ \nu)}{B(D^+ \rightarrow K^- \pi^+ \pi^+)} = 0.55 \pm 0.04.$$

When combined with the 1994 PDG value for  $B(D^+ \rightarrow K^- \pi^+ \pi^+)$  (see Table III), this gives a semileptonic branching fraction of

<sup>6</sup>This technique requires that the kaon be independently identified with a particle identification system such as Čerenkov detectors. If the kaon is not identified, the wrong-sign combination  $K^+ \pi^+ \ell^-$  can be used, but then the combination of hadrons  $K^+ \pi^+$  is no longer neutral.

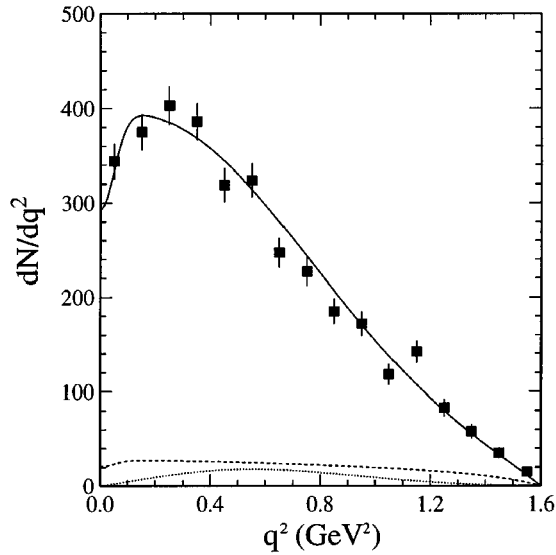


FIG. 26. Distribution of  $q^2$  for  $D^0 \rightarrow K^- \ell^+ \nu$  candidates in the CLEO II data: solid curve, the fit to signal plus background; dashed curve, the combinatorial background; dotted curve, the contribution from  $D^+ \rightarrow \bar{K}^{*0} \ell^+ \nu$  decays. The  $q^2$  dependence is dominated by the  $p_p^3$  factor in the differential decay rate. The form factor itself increases monotonically with  $q^2$  by about a factor of two across the plot.

$$B(D^+ \rightarrow \bar{K}^{*0} \ell^+ \nu) = (5.0 \pm 0.5)\%$$

With the 1994 PDG value for the  $D^+$  lifetime (see Table III), the decay rate is

$$\Gamma(D^+ \rightarrow \bar{K}^{*0} \ell^+ \nu) = (4.7 \pm 0.4) \times 10^{10} \text{ s}^{-1},$$

about 60% of that for  $D \rightarrow \bar{K} \ell^+ \nu$ .

The Mark III Collaboration has measured the absolute branching fractions shown in Tables XXII and XXIII for both  $D^+ \rightarrow \bar{K}^{*0} \ell^+ \nu$  and  $D^0 \rightarrow K^{*-} \ell^+ \nu$ . The experimental uncertainties on the Mark III measurements are quite large compared with more recent measurements, so that they do not affect the averages significantly.

As discussed above, the decay mode  $D^0 \rightarrow K^{*-} \ell^+ \nu$  is more difficult to study experimentally. The CLEO Collabo-

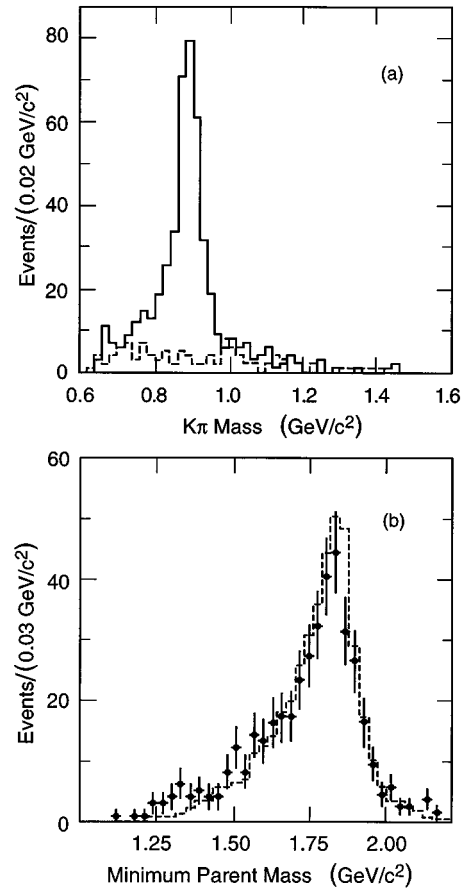


FIG. 27. Distributions for  $D^+ \rightarrow \bar{K}^{*0} \mu^+ \nu_\mu$  candidates from Fermilab E653: (a)  $K^- \pi^+$  mass for candidates that pass the selection criteria, including a cut on the minimum parent mass between 1.60 and 1.97  $\text{GeV}/c^2$ . The solid histogram corresponds to “right-sign” combinations and the dashed histogram to combinations in which the two hadrons have the same charge. (b) Minimum kinematically allowed parent mass for candidates passing the selection criteria, including a cut on  $K^- \pi^+$  mass between 0.83 and 0.95  $\text{GeV}/c^2$ . The points with error bars correspond to data. The dashed histogram represents a Monte Carlo simulation of  $D^+ \rightarrow \bar{K}^{*0} \mu^+ \nu_\mu$ . Redrawn from Kodama *et al.* (1992a).

TABLE XXII. Experimental measurements of the branching fraction for  $D^+ \rightarrow \bar{K}^{*0} \ell^+ \nu$  relative to that for  $D^+ \rightarrow K^- \pi^+ \pi^+$ . When not already done by the experimenters, measured branching fractions for the muon mode have been scaled up by 1.05 to account for the reduced phase space relative to the electron mode.

Experiment	Lepton type	$\frac{B(D^+ \rightarrow \bar{K}^{*0} \ell^+ \nu)}{B(D^+ \rightarrow K^- \pi^+ \pi^+)}$	$B(D^+ \rightarrow \bar{K}^{*0} \ell^+ \nu)$ (%)
E691 (Anjos <i>et al.</i> , 1989a)	$e$	$0.49 \pm 0.04 \pm 0.05$	$4.5 \pm 0.7$
ARGUS (Albrecht <i>et al.</i> , 1991b)	$e$	$0.55 \pm 0.08 \pm 0.10$	$5.0 \pm 1.2$
WA82 (Adamovich <i>et al.</i> , 1991)	$e$	$0.62 \pm 0.15 \pm 0.09$	$5.6 \pm 1.6$
E653 (Kodama <i>et al.</i> , 1992b)	$\mu$	$0.48 \pm 0.07 \pm 0.08$	$4.4 \pm 1.0$
E687 (Frabetti <i>et al.</i> , 1993a)	$\mu$	$0.59 \pm 0.04 \pm 0.06$	$5.4 \pm 0.7$
CLEO II (Bean <i>et al.</i> , 1993a)	$e, \mu$	$0.67 \pm 0.09 \pm 0.07$	$6.1 \pm 1.1$
Mark III (Bai <i>et al.</i> , 1991)	$e$	absolute	$5.8^{+1.9}_{-1.1} \pm 0.6$
Average		$0.55 \pm 0.04$	$5.0 \pm 0.5$

TABLE XXIII. Experimental measurements of the branching fraction for  $D^0 \rightarrow K^{*-} \ell^+ \nu$ .

Experiment	Measured quantity	Measured value	$B(D^0 \rightarrow K^{*-} \ell^+ \nu)$ (%)
CLEO I (Crawford <i>et al.</i> , 1991)	$B(D^0 \rightarrow K^{*-} \ell^+ \nu)$	$0.51 \pm 0.18 \pm 0.06$	$1.9 \pm 0.7$
CLEO II (Bean <i>et al.</i> , 1993a)	$\frac{B(D^0 \rightarrow K^- \ell^+ \nu)}{B(D^0 \rightarrow K^{*-} \ell^+ \nu)}$	$0.38 \pm 0.06 \pm 0.03$	$2.0 \pm 0.4$
	$B(D^0 \rightarrow \bar{K}^0 \pi^+ \pi^-)$		
Mark III (Bai <i>et al.</i> , 1991)	absolute		$4.4^{+1.9}_{-1.0} \pm 0.6$
Average			$2.1 \pm 0.3$

ration has measured the branching fraction for this mode relative to  $D^0 \rightarrow K^- \ell^+ \nu$  with CLEO I and relative to  $D^0 \rightarrow \bar{K}^0 \pi^+ \pi^-$  with CLEO II. Results are shown in Table XXIII, along with the Mark III measurement of the absolute branching fraction. Using the world average value for  $B(D^0 \rightarrow K^- \ell^+ \nu)$  from the previous section (see Table XIX) and the 1994 PDG value for  $B(D^0 \rightarrow \bar{K}^0 \pi^+ \pi^-)$ , we derive the following world average semileptonic branching fraction:

$$B(D^0 \rightarrow K^{*-} \ell^+ \nu) = (2.1 \pm 0.3)\%.$$

The corresponding decay rate from the 1994 PDG value for the  $D^0$  lifetime is

$$\Gamma(D^0 \rightarrow K^{*-} \ell^+ \nu) = (4.9 \pm 0.8) \times 10^{10} \text{ s}^{-1}.$$

Isospin conservation implies that the partial widths for Cabibbo-favored modes, such as  $D^0 \rightarrow K^{*-} \ell^+ \nu$  and  $D^+ \rightarrow \bar{K}^{*0} \ell^+ \nu$ , should be the same. The measured ratio of decay rates is

$$\frac{\Gamma(D^0 \rightarrow K^{*-} \ell^+ \nu)}{\Gamma(D^+ \rightarrow \bar{K}^{*0} \ell^+ \nu)} = 1.0 \pm 0.2,$$

and the world average rate for both isospin states is

$$\Gamma(D \rightarrow \bar{K}^* \ell^+ \nu) = (4.7 \pm 0.4) \times 10^{10} \text{ s}^{-1}. \quad (130)$$

This will be compared with the rate for  $D \rightarrow \bar{K} \ell^+ \nu$  in Sec. VI.B.3.

Ratios of form factors<sup>7</sup>  $r_V = V(0)/A_1(0)$  and  $r_2 = A_2(0)/A_1(0)$  (see Sec. VI.A.6) have been extracted from the observed multidimensional distributions of kinematic variables for the decay  $D^+ \rightarrow \bar{K}^{*0} \ell^+ \nu$  by three Fermilab fixed-target experiments: E691 (Anjos *et al.*, 1990b), E653 (Kodama *et al.*, 1992a), and E687 (Frabetti *et al.*, 1993a). In these experiments, the neutrino momentum is determined up to a quadratic ambiguity from the direction of flight of the  $D$  meson as determined by the measured positions of the  $D$  production and decay points, and the measured momenta of the charged decay products. To extract the form factors in both  $D \rightarrow \bar{K}^* \ell^+ \nu$  and  $B \rightarrow D^* \ell^- \bar{\nu}$  (see Sec. VI.E.5), most experiments now employ an unbinned maximum-likelihood method that uses a Monte Carlo simulation to evaluate the likelihood function.<sup>8</sup> The technique was

<sup>7</sup>In these analyses, each of the three form factors is assumed to have a pole form for the  $q^2$  dependence, with  $M_p = 2.1 \text{ GeV}/c^2$  for the vector form factor and  $M_p = 2.5 \text{ GeV}/c^2$  for the axial form factors.

<sup>8</sup>E687 uses a binned maximum-likelihood fit with three equal bins in  $\cos\theta_V$ , three in  $\cos\theta_\ell$ , and two in  $q^2$ .

first used by the E691 Collaboration (Anjos *et al.*, 1990b; Schmidt *et al.*, 1993). The likelihood of the data sample is calculated, for any given set of theoretical parameters, by computing the density of Monte Carlo events around each data point, where the simulated events are distributed according to the theoretical parameters under consideration. To avoid the need to generate separate Monte Carlo samples for every set of theoretical parameters considered in the fit, a single Monte Carlo sample is reweighted so that the weighted events give the correct density about each data point. As long as the Monte Carlo accurately simulates both the detector and the charm production process, acceptance and smearing effects are automatically incorporated in the fit.

The  $D^+ \rightarrow \bar{K}^{*0} \mu^+ \nu_\mu$  sample from the E653 experiment is shown in Fig. 27. Figure 27(a) shows a clear  $K^{*0}$  signal in the  $K\pi$  mass distribution. Because E653 has no detector for separating kaons from pions, the kaon is identified as the hadron with charge opposite that of the muon. The  $K^{*0}$  is a broad resonance, so it is not practical to use sidebands to estimate the background under the peak. Instead, backgrounds are estimated with “wrong-sign” combinations in which the two hadrons have the same charge, shown as a dashed histogram in Fig. 27(a). The minimum kinematically allowed decay mass, calculated from the invariant mass of the charged decay tracks and the transverse momentum imbalance with respect to the  $D^+$  direction, is shown in Fig. 27(b) for E653 data and for a Monte Carlo simulation of  $D^+ \rightarrow \bar{K}^{*0} \ell^+ \nu$ . A sample of 305 events with  $K^- \pi^+$  mass between 0.83 and 0.95  $\text{GeV}/c^2$  and minimum parent mass between 1.60 and 1.97  $\text{GeV}/c^2$  was used in the E653 analysis of the form factors. Distributions of  $\cos\theta_V$  and  $\cos\theta_\ell$  for E653 data and for the best fit to the data are shown in Fig. 28. Distributions of  $\cos\theta_V$  and  $\cos\theta_\ell$  are shown separately for  $q^2 \leq q_{\text{max}}^2/2$  and for  $q^2 > q_{\text{max}}^2/2$ . As expected from Eqs. (113), (115), and (116), the decay distributions exhibit stronger  $\cos^2\theta_V$  and  $\sin^2\theta_\ell$  components as  $q^2$  decreases and  $H_0$  dominates.

The measured form-factor ratios for all three experiments, along with the number of signal events, are shown in Table XXIV. The experimental average for each ratio is compared with theoretical predictions in Table XXV. As described in Sec. VI.A.6, the ratios of partial widths to different  $K^*$  polarization states can also be extracted from the form-factor ratios. The measured values of  $\Gamma_L/\Gamma_T$  and  $\Gamma_+/ \Gamma_-$  are also shown in Table XXIV. Early predictions of the ratio of longitudinal to transverse  $K^*$  polarization states  $\Gamma_L/\Gamma_T$  were in the range 0.9 to 1.2. In the updated quark model ISGW2 (Scora and Isgur, 1994), the ratio  $\Gamma_L/\Gamma_T$  is predicted to be 0.94, in fair agreement with the measured value of

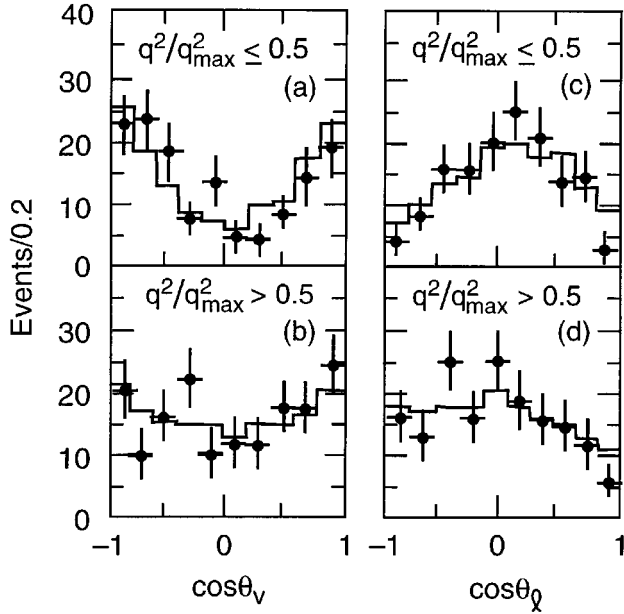


FIG. 28. Projected distributions of the angular variables [(a) and (b)]  $\cos\theta_V$  and [(c) and (d)]  $\cos\theta_Q$  for the E653 raw data (points with error bars) and for Monte Carlo events with the best fit form-factor ratios (histogram) for the decay  $D^+ \rightarrow \bar{K}^{*0} \ell^+ \nu$ . Distributions are shown for [(a) and (c)]  $q^2/q_{\max}^2 \leq 0.5$  and [(b) and (d)]  $q^2/q_{\max}^2 > 0.5$ . Redrawn from Kodama *et al.* (1992a).

$1.23 \pm 0.13$ . The small value of  $\Gamma_+/\Gamma_-$  is due to the  $V-A$  nature of the  $W$  coupling to the quarks. Experimental results are consistent with each other, given the size of the uncertainties on the measurements.

The world average partial decay rate for  $D \rightarrow \bar{K}^* \ell^+ \nu$  given in Eq. (130) can be combined with the form-factor ratios to extract the form factors themselves. The resulting values of  $A_1(0)$ ,  $A_2(0)$ , and  $V(0)$  are given in Table XXVI. In Table XXVII, we compare the average measured values of the form factors with the theoretical predictions from QCD-inspired phenomenological models, lattice calculations, and QCD sum rules. Generally, the measured values of the axial form factors,  $A_1(0)$  (which dominates the decay rate) and  $A_2(0)$ , are low compared with theoretical predictions. The

vector form factors, on the other hand, are in reasonable agreement, for both  $D \rightarrow \bar{K} \ell^+ \nu$  and  $D \rightarrow \bar{K}^* \ell^+ \nu$ .

In Table XXVIII, we extrapolate to  $q_{\max}^2$  the form factors measured at  $q^2=0$ , assuming a pole form for the  $q^2$  dependence with  $M_p=2.1$  GeV/ $c^2$  for the vector form factors and  $M_p=2.5$  GeV/ $c^2$  for the axial form factors. Future measurements of the form factors should be quoted at  $q_{\max}^2$ , as well as at  $q^2=0$ , since the value at  $q_{\max}^2$  is related to a single universal form factor in HQET, up to (large)  $1/m_Q$  corrections. Form factors at  $q^2=0$ , on the other hand, are the product of the value at  $q_{\max}^2$  and a function that depends on the dynamics of the final-state meson recoiling with maximum momentum in the rest frame of the initial meson. In Table XXVIII, we also give the form-factor predictions at  $q_{\max}^2$  of the ISGW (Isgur *et al.*, 1989) quark model and the updated predictions of ISGW2 (Scora and Isgur, 1994). The ISGW2 model incorporates the constraints imposed by HQET, relativistic correction factors, hyperfine distortions of wave functions, and form factors with more realistic high-recoil behavior. The updated predictions are in better agreement with the data. The prediction for  $f_+(q_{\max}^2)$  has shifted upward by about 6% due to four different effects. The prediction for  $A_1(q_{\max}^2)$  has decreased by about 30%, largely due to a relativistic correction. The prediction for  $A_2(q_{\max}^2)$  has moved closer to the measured value, but the agreement is still not very good. The net effect is that the theoretical predictions are now in better agreement with both measurements of the form factors themselves, as shown in Table XXVIII, and measurements of the ratio of decay rates  $\Gamma(D \rightarrow \bar{K}^* \ell^+ \nu)/\Gamma(D \rightarrow \bar{K} \ell^+ \nu)$ , as we discuss in the next section.

The Fermilab E791 Collaboration has a sample of approximately 2000 candidate decays in each of the modes  $D^+ \rightarrow \bar{K}^{*0} e^+ \nu_e$  and  $D^+ \rightarrow \bar{K}^{*0} \mu^+ \nu_\mu$ . This data sample should result in measurements that are significantly more precise than current results.

### 3. Ratio of $\Gamma(D \rightarrow \bar{K}^* \ell^+ \nu)$ to $\Gamma(D \rightarrow \bar{K} \ell^+ \nu)$

Many experiments have directly measured the ratio of decay rates  $\Gamma(D \rightarrow \bar{K}^* \ell^+ \nu)/\Gamma(D \rightarrow \bar{K} \ell^+ \nu)$ . Theoretical models usually predict this ratio more precisely than individual

TABLE XXIV. Parameters extracted from the decay distributions for  $D^+ \rightarrow \bar{K}^{*0} \ell^+ \nu$ : the ratios of form factors  $r_V=V(0)/A_1(0)$  and  $r_2=A_2(0)/A_1(0)$ , the ratio of longitudinal to transverse polarization of the  $K^*$  ( $\Gamma_L/\Gamma_T$ ), and the ratio of positive to negative transverse polarization of the  $K^*$  ( $\Gamma_+/\Gamma_-$ ).

Experiment (No. of events)	$r_V=V(0)/A_1(0)$	$r_2=A_2(0)/A_1(0)$	$\Gamma_L/\Gamma_T$	$\Gamma_+/\Gamma_-$
E691 ( $\sim 200, e$ ) (Anjos <i>et al.</i> , 1990b)	$2.0 \pm 0.6 \pm 0.3$	$0.0 \pm 0.5 \pm 0.2$	$1.8^{+0.6}_{-0.4} \pm 0.3$	$0.15^{+0.07}_{-0.05} \pm 0.03$
E653 ( $\sim 300, \mu$ ) (Kodama <i>et al.</i> , 1992a)	$2.00^{+0.34}_{-0.32} \pm 0.16$	$0.82^{+0.22}_{-0.23} \pm 0.11$	$1.18 \pm 0.18 \pm 0.08$	$0.16 \pm 0.05 \pm 0.02$
E687 ( $\sim 900, \mu$ ) (Frabetti <i>et al.</i> , 1993a)	$1.74 \pm 0.27 \pm 0.28$	$0.78 \pm 0.18 \pm 0.10$	$1.20 \pm 0.13 \pm 0.13$	
Average	$1.89 \pm 0.25$	$0.73 \pm 0.15$	$1.23 \pm 0.13$	$0.16 \pm 0.04$

decay rates. Moreover, systematic errors that contribute to the uncertainty in a measured decay rate sometimes cancel in the ratio. The measurements are summarized in Table XXIX. The average value of  $0.56 \pm 0.05$  is considerably lower than the early quark model (Wirbel *et al.*, 1985; Altomari and Wolfenstein, 1988, Körner and Schuler, 1988; Isgur *et al.*, 1989; Gilman and Singleton, 1990) and lattice gauge (Bernard *et al.*, 1991, 1992, 1993; Lubicz *et al.*, 1992) predictions, which lie in the range 0.9 to 1.2.

From Table XXVII, we see that the measured value of the form factor for  $D \rightarrow \bar{K} \ell^+ \nu$  is quite consistent with theoretical expectations. The inconsistency between experiment and theory was predominantly in the decay  $D \rightarrow \bar{K}^* \ell^+ \nu$ ; the observed rate was lower than theoretical expectations. The measured axial form factors in particular were lower than the theoretically predicted values. As pointed out in Sec. VI.B.2 and illustrated in Table XXVIII, the more recent ISGW2 (Scora and Isgur, 1994) prediction for  $f_+$  is higher and that for  $A_1$  is lower. Therefore the ISGW2 prediction for  $\Gamma(D \rightarrow \bar{K}^* \ell^+ \nu) / \Gamma(D \rightarrow \bar{K} \ell^+ \nu)$  has decreased to 0.54, in good agreement with measurement.

#### 4. $D$ decays to other Cabibbo-favored states

Results of the most sensitive direct searches for nonresonant  $D \rightarrow \bar{K} \pi \ell^+ \nu$  and  $D \rightarrow \bar{K} \pi \pi \ell^+ \nu$  decays, and for  $D \rightarrow \bar{K}^* \pi \ell^+ \nu$  decays are given in Table XXX. There is no evidence for significant decay rates for Cabibbo-favored modes other than  $D \rightarrow \bar{K} \ell^+ \nu$  and  $D \rightarrow \bar{K}^* \ell^+ \nu$ .

#### 5. $D_s \rightarrow \phi \ell^+ \nu$

Two studies of the decay  $D_s \rightarrow \phi \ell^+ \nu$  are of interest: measurement of the branching fraction relative to  $D_s \rightarrow \phi \pi^+$ , which can be used to extract an absolute branching fraction

for  $D_s \rightarrow \phi \pi^+$ , and measurement of the form factors, which can be compared with those for  $D^+ \rightarrow \bar{K}^{*0} \ell^+ \nu$  and with theoretical predictions.

Measurements of  $\Gamma(D_s \rightarrow \phi \ell^+ \nu) / \Gamma(D_s \rightarrow \phi \pi^+)$ , summarized in Table XXXI, yield an average value of  $0.54 \pm 0.05$ . The absolute branching fraction for  $D_s \rightarrow \phi \pi^+$  is related to this measured ratio through the equation

$$B(D_s \rightarrow \phi \pi^+) = B(D_s \rightarrow \phi \ell^+ \nu) \frac{\Gamma(D_s \rightarrow \phi \pi^+)}{\Gamma(D_s \rightarrow \phi \ell^+ \nu)}. \quad (131)$$

We now take advantage of the fact that theory can predict the relative rates for  $D_s \rightarrow \phi \ell^+ \nu$  and  $D^+ \rightarrow \bar{K}^{*0} \ell^+ \nu$  with reasonable accuracy. The measured  $D_s$  and  $D^+$  lifetimes can be used to relate the decay rates to branching fractions. Therefore we have the relation

$$B(D_s \rightarrow \phi \ell^+ \nu) = F \cdot B(D^+ \rightarrow \bar{K}^{*0} \ell^+ \nu) \frac{\tau_{D_s}}{\tau_{D^+}}, \quad (132)$$

where  $F$  is the theoretical prediction for  $\Gamma(D_s \rightarrow \phi \ell^+ \nu) / \Gamma(D^+ \rightarrow \bar{K}^{*0} \ell^+ \nu)$ . A value of  $F = 0.9 \pm 0.1$  is consistent with the predictions of a number of theorists (Wirbel *et al.*, 1985; Bauer and Wirbel, 1989; Isgur *et al.*, 1989; Scora, 1991, 1993). Using the value of  $B(D^+ \rightarrow \bar{K}^{*0} \ell^+ \nu) = (5.0 \pm 0.5)\%$  from the previous section and the ratio of lifetimes  $\tau_{D_s} / \tau_{D^+} = 0.44 \pm 0.02$  (Particle Data Group, 1994), we predict  $B(D_s \rightarrow \phi \pi^+) = (3.7 \pm 0.5 \pm 0.4)\%$ , where the last uncertainty reflects the range of theoretical predictions for  $F$ . This is consistent with the upper limit of 4.1% that Mark III obtained from a double-tagging technique (Adler *et al.*, 1990). It is also consistent with a BES measurement (Bai *et al.*, 1995b) of  $B(D_s \rightarrow \phi \pi^+) = (3.9_{-1.9}^{+5.1+1.8})\%$  based on  $41 \pm 7$  single-

TABLE XXV. Theoretical predictions for ratios of form factors at  $q^2=0$  for  $D \rightarrow \bar{K}^* \ell^+ \nu$  compared with experimental measurements.

Reference	$r_V = V(0)/A_1(0)$	$r_2 = A_2(0)/A_1(0)$
Experimental average	$1.89 \pm 0.25$	$0.73 \pm 0.15$
Quark models		
ISGW (Isgur <i>et al.</i> , 1989)	1.4	1.0
WSB (Wirbel <i>et al.</i> , 1985)	1.4	1.3
KS (Körner and Schuler, 1988)	1.0	1.0
AW/GS (Altomari and Wolfenstein, 1988; Gilman and Singleton, 1990)	2.0	0.8
Lattice gauge		
BKS (Bernard <i>et al.</i> , 1991, 1992, 1993)	$1.99 \pm 0.22 \pm 0.33$	$0.7 \pm 0.16 \pm 0.17$
LMMS (Lubicz <i>et al.</i> , 1992)	$1.6 \pm 0.2$	$0.4 \pm 0.4$
LANL (Bhattacharya and Gupta, 1994a, 1994b)	$1.75 \pm 0.09$	$0.87 \pm 0.21$
ELC (Abada <i>et al.</i> , 1994)	$1.3 \pm 0.2$	$0.6 \pm 0.3$
APE (Allton <i>et al.</i> , 1995)	$1.6 \pm 0.3$	$0.7 \pm 0.4$
UKQCD (Nieves <i>et al.</i> , 1994; Bowler <i>et al.</i> , 1994)	$1.4_{-0.2}^{+0.5}$	$0.9 \pm 0.2$
Sum rules		
BBD (Ball <i>et al.</i> , 1991)	$2.2 \pm 0.2$	$1.2 \pm 0.2$

TABLE XXVI. Magnitudes of individual form factors  $A_1(0)$ ,  $A_2(0)$ , and  $V(0)$  in the decay  $D^+ \rightarrow \bar{K}^{*0} \ell^+ \nu$  for a decay rate of  $\Gamma(D \rightarrow \bar{K}^* \ell^+ \nu) = (4.7 \pm 0.4) \times 10^{10} \text{ s}^{-1}$ .

Experiment	$A_1(0)$	$A_2(0)$	$V(0)$
E691 ( Anjos <i>et al.</i> , 1990b)	$0.50 \pm 0.07$	$0.0 \pm 0.2$	$1.0 \pm 0.3$
E653 (Kodama <i>et al.</i> , 1992b)	$0.58 \pm 0.07$	$0.47 \pm 0.14$	$1.2 \pm 0.3$
E687 ( Culbertson, 1993)	$0.59 \pm 0.05$	$0.46 \pm 0.11$	$1.0 \pm 0.3$
Average	$0.56 \pm 0.04$	$0.39 \pm 0.08$	$1.1 \pm 0.2$

tagged  $D_s \rightarrow \phi \pi^+$  decays and two events in which both  $D_s$  mesons are reconstructed in the mode  $D_s \rightarrow \phi \pi^+$ , or other hadronic modes for which the branching fractions relative to  $D_s \rightarrow \phi \pi^+$  have been measured.

It is important to measure the form factors in  $D_s \rightarrow \phi \ell^+ \nu$  because the theoretical models that predict the ratio  $\Gamma(D_s \rightarrow \phi \ell^+ \nu) / \Gamma(D \rightarrow \bar{K}^* \ell^+ \nu)$  [ $F$  in Eq. (132)] also predict similar form factors for  $D \rightarrow \bar{K}^* \ell^+ \nu$  and  $D_s \rightarrow \phi \ell^+ \nu$ . If the measured form factors are not consistent, there is further theoretical uncertainty on extracting the absolute  $D_s$  branching fractions from Eq. (132).

Two fixed-target experiments (E687 and E653) and CLEO have now measured the form factors in the decay  $D_s \rightarrow \phi \ell^+ \nu$ , albeit with large uncertainties. The statistical errors are large because of limited  $D_s$  production in both fixed-target and  $e^+e^-$  machines. Also, the background level is also considerably higher than that for  $D^+ \rightarrow \bar{K}^{*0} \ell^+ \nu$ . Unlike the decay mode  $D^+ \rightarrow \bar{K}^{*0} \ell^+ \nu$  with  $\bar{K}^{*0} \rightarrow K^- \pi^+$ , there is no analogous “wrong-sign” mode for  $D_s \rightarrow \phi \ell^+ \nu$  that can be used to measure the noncharm background because the  $\phi$  is reconstructed in a final state with two oppo-

sitely charged but identical particles. E653 monitors their background with  $K^+ K^+ \ell^-$  candidates. E687 and CLEO use sidebands to the  $\phi$  peak; since the  $\phi$  resonance is much narrower than the  $K^*$  resonance, sidebands to the  $K^+ K^-$  mass peak can be used to monitor the background level and to incorporate the background in the fit.

Measurements of form factor ratios in  $D_s \rightarrow \phi \ell^+ \nu$  by E653, E687, and CLEO are shown in Table XXXII. The experimental average of each ratio is consistent with the value measured for the decay mode  $D^+ \rightarrow \bar{K}^{*0} \ell^+ \nu$  (see Table XXIV), although the value of  $r_2$  for  $D_s \rightarrow \phi \ell^+ \nu$  is about two standard deviations high.

6.  $D_s \rightarrow \eta \ell^+ \nu$  and  $D_s \rightarrow \eta' \ell^+ \nu$

In  $D_s$  decays, the Cabibbo-favored semileptonic modes with a pseudoscalar in the final state are  $D_s \rightarrow \eta \ell^+ \nu$  and  $D_s \rightarrow \eta' \ell^+ \nu$ . Both experiment E653 (Kodama *et al.*, 1993a) and CLEO II (Battle *et al.*, 1994) have evidence for these decays. The measured quantities are summarized in Table XXXIII.

TABLE XXVII. Theoretical predictions for form factors at  $q^2=0$  for  $D \rightarrow \bar{K} \ell^+ \nu$  ( $f_+$ ) and for  $D \rightarrow \bar{K}^* \ell^+ \nu$  ( $A_1, A_2, V$ ) compared with experimental measurements.

	$f_+(0)$	$A_1(0)$	$A_2(0)$	$V(0)$
Experimental average	$0.76 \pm 0.03$	$0.56 \pm 0.04$	$0.39 \pm 0.08$	$1.1 \pm 0.2$
Quark models				
ISGW ( Isgur <i>et al.</i> , 1989)	0.8	0.8	0.8	1.1
WSB (Wirbel <i>et al.</i> , 1985)	0.76	0.88	1.2	1.3
KS (Körner and Schuler, 1988)	0.7	0.82	0.8	0.8
AW/GS (Altomari and Wolfenstein, 1988; Gilman and Singleton, 1990)				
	0.7	0.8	0.6	1.5
Lattice gauge				
BKS (Bernard <i>et al.</i> , 1991, 1992, 1993)				
	$0.9 \pm 0.1 \pm 0.2$	$0.8 \pm 0.1 \pm 0.2$	$0.6 \pm 0.1 \pm 0.2$	$1.4 \pm 0.5 \pm 0.5$
LMMS (Lubicz <i>et al.</i> , 1992)	$0.63 \pm 0.08$	$0.53 \pm 0.03$	$0.2 \pm 0.2$	$0.9 \pm 0.1$
LANL (Bhattacharya and Gupta, 1994a)				
	$0.71 \pm 0.05$	$0.75 \pm 0.05$	$0.64 \pm 0.19$	$1.33 \pm 0.10$
Wuppertal (Gusken <i>et al.</i> , 1995)	$0.84 \pm 0.16$	$0.64 \pm 0.08$	$0.61 \pm 0.41$	$1.17 \pm 0.38$
ELC (Abada <i>et al.</i> , 1994)	$0.60 \pm 0.15 \pm 0.07$	$0.64 \pm 0.16$	$0.41 \pm 0.28 \pm 0.04$	$0.86 \pm 0.24$
APE (Allton <i>et al.</i> , 1995)	$0.78 \pm 0.08$	$0.67 \pm 0.11$	$0.49 \pm 0.34$	$1.08 \pm 0.22$
UKQCD (Nieves <i>et al.</i> , 1994)	$0.67 \pm 0.08$	$0.70^{+0.07}_{-0.10}$	$0.66^{+0.10}_{-0.15}$	$1.01^{+0.30}_{-0.13}$
Sum rules				
BBD (Ball <i>et al.</i> , 1991)	0.60	0.5	0.6	1.1

TABLE XXVIII. Theoretical predictions of ISGW and ISGW2 for form factors at  $q^2=q_{\max}^2$  for  $D \rightarrow \bar{K} \ell^+ \nu$  ( $f_+$ ) and for  $D \rightarrow \bar{K}^* \ell^+ \nu$  ( $A_1, A_2, V$ ) compared with experimental measurements. Form factors measured at  $q^2=0$  are extrapolated to  $q_{\max}^2$  assuming a pole form for the  $q^2$  dependence with  $M_p=2.1$  GeV/ $c^2$  for the vector form factors and  $M_p=2.5$  GeV/ $c^2$  for the axial form factors.

Reference	$f_+(q_{\max}^2)$	$A_1(q_{\max}^2)$	$A_2(q_{\max}^2)$	$V(q_{\max}^2)$
Experimental average	$1.31 \pm 0.04$	$0.66 \pm 0.05$	$0.46 \pm 0.09$	$1.4 \pm 0.3$
ISGW (Isgur <i>et al.</i> , 1989)	1.16	1.0	1.0	1.3
ISGW2 (Scora and Isgur, 1994)	1.23	0.70	0.94	1.52

E653 does not reconstruct the neutral particles in the  $\eta$  or  $\eta'$  decays, but observes an enhancement in the  $\pi^+ \pi^-$  mass distribution just below the  $\eta$  mass. E653 also sets an upper limit (Kodama *et al.*, 1993b) on  $B(D_s \rightarrow \eta' \mu^+ \nu_\mu) / B(D_s \rightarrow \phi \mu^+ \nu_\mu)$  by simply searching for secondary vertices with four charged hadrons (from  $\eta' \rightarrow \pi^+ \pi^- \eta, \eta \rightarrow \pi^+ \pi^- \gamma, \pi^+ \pi^- \pi^0$ ) with invariant mass less than 1 GeV/ $c^2$ , and an identified muon.

CLEO reconstructs the decay modes  $\eta \rightarrow \gamma \gamma$  and  $\eta' \rightarrow \eta \pi^+ \pi^-$ . For the mode  $D_s \rightarrow \eta \ell^+ \nu$ , the decay chain  $D_s^* \rightarrow D_s \gamma, D_s \rightarrow \eta \ell^+ \nu$  is used to reduce the background. To increase efficiency in the  $D_s \rightarrow \eta' \ell^+ \nu$  analysis, the  $D_s^*$  tag is not used.

From Table XXXIII, we see that the Cabibbo-favored semileptonic decay rate of the  $D_s$  to a pseudoscalar particle is larger than the rate to a vector particle, in agreement with experimental observations in the  $D$  system [ $B(D \rightarrow \bar{K} \ell^+ \nu) / B(D \rightarrow \bar{K}^* \ell^+ \nu) = 1.78 \pm 0.16$ ]. The ratio of the decay rate to pseudoscalar mesons relative to vector mesons is about 1.5 standard deviations higher for the  $D_s$  than the  $D$ . The measured  $D_s$  decay rates for nonleptonic final states involving an  $\eta$  or  $\eta'$  are also observed to be

unexpectedly large (Alexander *et al.*, 1992a, 1992b). Kamal, Xu, and Czarnecki (1993) used the factorization hypothesis to predict  $B(D_s \rightarrow (\eta \text{ or } \eta') \ell^+ \nu) / B(D_s \rightarrow \phi \ell^+ \nu) \approx 4$ , based on the related hadronic rates for  $D_s \rightarrow \eta \rho^+$  and  $D_s \rightarrow \eta' \rho^+$  relative to  $D_s \rightarrow \phi \pi^+$  measured by CLEO (Alexander *et al.*, 1992a, 1992b).

### C. Cabibbo-suppressed semileptonic decays of charm mesons

The ratio of Cabibbo-suppressed to Cabibbo-favored semileptonic decays of the  $D$  meson to a pseudoscalar meson in the final state can be used to determine the product of the ratio of Cabibbo-Kobayashi-Maskawa matrix elements  $|V_{cd}/V_{cs}|$  and the ratio of form factors  $f_+^\pi(0)/f_+^K(0)$ . In particular,

$$\begin{aligned} \frac{B(D^0 \rightarrow \pi^- e^+ \nu_e)}{B(D^0 \rightarrow K^- e^+ \nu_e)} &= 2 \frac{B(D^+ \rightarrow \pi^0 e^+ \nu_e)}{B(D^+ \rightarrow \bar{K}^0 e^+ \nu_e)} \\ &= 1.97 \left| \frac{V_{cd}}{V_{cs}} \right|^2 \left( \frac{f_+^\pi(0)}{f_+^K(0)} \right)^2, \end{aligned} \quad (133)$$

TABLE XXIX. Experimental measurements of the ratio of Cabibbo-favored  $D$  decay rates to states with a vector or a pseudoscalar meson in the final state.

Experiment	Measured ratio	Measured value
Mark III (Bai <i>et al.</i> , 1991)	$\frac{\Gamma(D \rightarrow \bar{K}^* \ell^+ \nu)}{\Gamma(D \rightarrow \bar{K} \ell^+ \nu)}$	$1.00 \pm 0.25$
E691 (Anjos <i>et al.</i> , 1989b, 1990b, 1991)	$\frac{\Gamma(D^+ \rightarrow \bar{K}^* 0 e^+ \nu_e)}{\Gamma(D^0 \rightarrow K^- e^+ \nu_e)}$	$0.48 \pm 0.10$
E653 (Kodama <i>et al.</i> , 1992b)	$\frac{\Gamma(D^+ \rightarrow \bar{K}^* 0 \mu^+ \nu_\mu)}{\Gamma(D^0 \rightarrow K^- \mu^+ \nu_\mu)}$	$0.43 \pm 0.09 \pm 0.09$
E687 (Frabetti <i>et al.</i> , 1993c)	$\frac{\Gamma(D^+ \rightarrow \bar{K}^* 0 \mu^+ \nu_\mu)}{\Gamma(D^0 \rightarrow K^- \mu^+ \nu_\mu)}$	$0.61 \pm 0.10 \pm 0.13$
CLEO (Crawford <i>et al.</i> , 1991)	$\frac{\Gamma(D^0 \rightarrow K^* - e^+ \nu_e)}{\Gamma(D^0 \rightarrow K^- e^+ \nu_e)}$	$0.51 \pm 0.18 \pm 0.06$
CLEO II (Bean <i>et al.</i> , 1993a)	$\frac{\Gamma(D^0 \rightarrow K^* - e^+ \nu_e)}{\Gamma(D^0 \rightarrow K^- e^+ \nu_e)}$	$0.60 \pm 0.09 \pm 0.07$
CLEO II (Bean <i>et al.</i> , 1993a)	$\frac{\Gamma(D^+ \rightarrow \bar{K}^* 0 e^+ \nu_e)}{\Gamma(D^+ \rightarrow \bar{K}^0 e^+ \nu_e)}$	$0.65 \pm 0.09 \pm 0.10$
Average	$\frac{\Gamma(D \rightarrow \bar{K}^* \ell^+ \nu)}{\Gamma(D \rightarrow \bar{K} \ell^+ \nu)}$	$0.56 \pm 0.05$

TABLE XXX. Results of direct searches for nonresonant (NR) hadronic states and higher-multiplicity resonances in semileptonic  $D$  decays. All quoted limits correspond to 90% confidence level.

Experiment	Decay mode	Branching fraction (%)	Decay rate ( $10^{10} \text{ s}^{-1}$ )
E691 (Anjos <i>et al.</i> , 1989a)	$D^+ \rightarrow (K^- \pi^+)_{NR} e^+ \nu_e$	<0.7	<0.7
E687 (Frabetti <i>et al.</i> , 1993a)	$D^+ \rightarrow (K^- \pi^+)_{NR} \mu^+ \nu_\mu$	<0.4	<0.4
E691 (Anjos <i>et al.</i> , 1992)	$D^+ \rightarrow \bar{K}^* \pi e^+ \nu_e$ , all charges	<1.2	<1.1
E687 (Frabetti <i>et al.</i> , 1993a)	$D^+ \rightarrow \bar{K}^{*0} \pi^0 \mu^+ \nu_\mu$	<0.2	<0.2
E691 (Anjos <i>et al.</i> , 1992)	$D^+ \rightarrow (K \pi)_{NR} \pi e \nu_e$ , all charges	<0.9	<0.9
E653 (Kodama <i>et al.</i> , 1993b)	$D^0 \rightarrow K^- \pi^+ \pi^- \mu^+ \nu_\mu$	<0.13	<0.3
E653 (Kodama <i>et al.</i> , 1993b)	$D^0 \rightarrow (K^* \pi)^- \mu^+ \nu_\mu$	<0.15	<0.4

TABLE XXXI. Measurements of the decay rate for  $D_s \rightarrow \phi \ell^+ \nu$  relative to that for  $D_s \rightarrow \phi \pi^+$ . When not already done by the experimenters, measured branching fractions for the muon mode have been scaled up by 1.05 to account for the reduced phase space relative to the electron mode.

Experiment	No. of events (lepton type)	$\Gamma(D_s \rightarrow \phi \ell^+ \nu) / \Gamma(D_s \rightarrow \phi \pi^+)$
E691 (Anjos <i>et al.</i> , 1990a)	no signal ( $e$ )	<0.45
CLEO (Alexander <i>et al.</i> , 1990)	$54 \pm 11$ ( $e, \mu$ )	$0.49 \pm 0.10_{-0.14}^{+0.10}$
ARGUS (Albrecht <i>et al.</i> , 1991b)	$104 \pm 26$ ( $e$ )	$0.57 \pm 0.15 \pm 0.15$
E687 (Frabetti <i>et al.</i> , 1993b)	$97 \pm 28$ ( $\mu$ )	$0.61 \pm 0.18 \pm 0.07$
CLEO II (Butler <i>et al.</i> , 1994)	$367 \pm 27$ ( $e, \mu$ )	$0.54 \pm 0.05 \pm 0.04$
Average		$0.54 \pm 0.05$

TABLE XXXII. Measurements of the form factors for the decay  $D_s \rightarrow \phi \ell^+ \nu$ .

Experiment	No. of events (lepton type)	Variables used in analysis	$r_V = V(0)/A_1(0)$	$r_2 = A_2(0)/A_1(0)$	$\Gamma_L / \Gamma_T$
E653 (Kodama <i>et al.</i> , 1993a)	19 ( $\mu$ )	$\cos \theta_\ell, \cos \theta_V, q^2$	$2.3_{-0.9}^{+1.1} \pm 0.4$	$2.1_{-0.5}^{+0.6} \pm 0.2$	$0.54 \pm 0.21 \pm 0.10$
E687 (Frabetti <i>et al.</i> , 1994)	90 ( $\mu$ )	$\cos \theta_\ell, \cos \theta_V, q^2, \chi$	$1.8 \pm 0.9 \pm 0.2$	$1.1 \pm 0.8 \pm 0.1$	$1.0 \pm 0.5 \pm 0.1$
CLEO II (Avery <i>et al.</i> , 1994b)	308 ( $e$ )	$\cos \theta_\ell,  \cos \theta_V , q^2$	$0.9 \pm 0.6 \pm 0.3$	$1.4 \pm 0.5 \pm 0.3$	$1.0 \pm 0.3 \pm 0.2$
Average			$1.4 \pm 0.5$	$1.6 \pm 0.4$	$1.0 \pm 0.3$

TABLE XXXIII. Measurements of the branching fraction for  $D_s \rightarrow \eta \ell^+ \nu$  and  $D_s \rightarrow \eta' \ell^+ \nu$  relative to that for  $D_s \rightarrow \phi \ell^+ \nu$ .

Experiment	$\frac{B(D_s \rightarrow \eta \ell^+ \nu)}{B(D_s \rightarrow \phi \ell^+ \nu)}$	$\frac{B(D_s \rightarrow \eta' \ell^+ \nu)}{B(D_s \rightarrow \phi \ell^+ \nu)}$	$\frac{B(D_s \rightarrow (\eta \text{ or } \eta') \ell^+ \nu)}{B(D_s \rightarrow \phi \ell^+ \nu)}$
E653 (Kodama <i>et al.</i> , 1993a, 1993b)		$< 1.6$	$3.9 \pm 1.6$
CLEO II (prelim.) (Battle <i>et al.</i> , 1994)	$1.74 \pm 0.34 \pm 0.24$	$0.71_{-0.18}^{+0.19+0.08}$	$2.46 \pm 0.39 \pm 0.26$
Average			$2.6 \pm 0.5$

where the factor of 2 difference between the two ratios arises from the  $1/\sqrt{2}$  coupling of  $d\bar{d}$  to the  $\pi^0$ .

CLEO uses the decay  $D^{*+} \rightarrow D^+ \pi^0$  to tag 58 Cabibbo-suppressed  $D^+ \rightarrow \pi^0 \ell^+ \nu$  decays (Alam *et al.*, 1993). The branching ratio relative to the Cabibbo-favored decay  $D^+ \rightarrow \bar{K}^0 \ell^+ \nu$  was measured to be  $B(D^+ \rightarrow \pi^0 \ell^+ \nu)/B(D^+ \rightarrow \bar{K}^0 \ell^+ \nu) = 0.085 \pm 0.027 \pm 0.014$ , leading to

$$\left| \frac{V_{cd}}{V_{cs}} \right|^2 \left( \frac{f_+^\pi(0)}{f_+^K(0)} \right)^2 = 0.085 \pm 0.027 \pm 0.014.$$

More recently, CLEO has used a similar technique for the mode  $D^0 \rightarrow \pi^- \ell^+ \nu$  (Butler *et al.*, 1995). From a signal of  $87 \pm 33$   $D^0 \rightarrow \pi^- \ell^+ \nu$  decays, they extract  $B(D^0 \rightarrow \pi^- \ell^+ \nu)/B(D^0 \rightarrow K^- \ell^+ \nu) = 0.103 \pm 0.039 \pm 0.013$ , leading to

$$\left| \frac{V_{cd}}{V_{cs}} \right|^2 \left( \frac{f_+^\pi(0)}{f_+^K(0)} \right)^2 = 0.052 \pm 0.020 \pm 0.007.$$

These results can be compared with the Mark III measurement (Adler *et al.*, 1989) of  $0.057_{-0.017}^{+0.038} \pm 0.005$  for the same quantity, based on 7  $D^0 \rightarrow \pi^- e^+ \nu_e$  and 56  $D^0 \rightarrow K^- e^+ \nu_e$  events. Using  $|V_{cd}/V_{cs}|^2 = 0.051 \pm 0.002$  from the unitarity of the CKM matrix, we can use the average of the Mark III and CLEO measurements to extract the ratio of form factors

$$f_+^\pi(0)/f_+^K(0) = 1.2 \pm 0.3.$$

This result is consistent with theoretical predictions, which range from 0.7 to 1.4 (Lepage and Brodsky, 1980; Bauer *et al.*, 1987; Dominguez, 1988; Aliev *et al.*, 1989; Crisafulli *et al.*, 1989; Isgur *et al.*, 1989; Lubicz *et al.*, 1992; Narison, 1994b).

The E653 Collaboration has observed a signal of  $4.0_{-2.3}^{+2.8}$  events in the mode  $D^+ \rightarrow \rho^0 \mu^+ \nu_\mu$  (Kodama *et al.*, 1993c). The measured decay rate relative to the corresponding Cabibbo-favored mode is

$$\frac{B(D^+ \rightarrow \rho^0 \mu^+ \nu_\mu)}{B(D^+ \rightarrow \bar{K}^{*0} \mu^+ \nu_\mu)} = 0.044_{-0.025}^{+0.031} \pm 0.014.$$

The central value for this measurement is about half the 90%-confidence-level limit previously reported by the Mark III Collaboration (Bai *et al.*, 1991). A model by Scora and Isgur (1994) predicts that the measured ratio should equal  $0.42 |V_{cd}/V_{cs}|^2 = 0.022$ , consistent with the value given above.

#### D. Summary of exclusive charm decays

In Table XXXIV, exclusive semileptonic decay rates for  $D$

mesons are summarized and compared with the inclusive decay rate. For the Cabibbo-suppressed modes, we have assumed the rate predicted in the ISGW2 model (Scora and Isgur, 1994). This rate is about 20% lower than the rate predicted by Wirbel *et al.* (1985), which is sometimes cited in the literature. The exclusive rates account for  $(84 \pm 5)\%$  of the inclusive rate. The inclusive rate exceeds the sum of the exclusive rates by  $(2.7 \pm 0.9) \times 10^{10} \text{ s}^{-1}$ . Recall from Table XXX that the upper limits for decay rates to other nonresonant and higher-mass modes are  $\leq 10^{10} \text{ s}^{-1}$  each. Therefore the semileptonic decays of  $D$  mesons may be saturated by the Cabibbo-favored and Cabibbo-suppressed decays to a single vector or pseudoscalar meson, although a discrepancy of three standard deviations remains between the inclusive rate and the sum of the exclusive rates.

Historically, theoretical predictions for the rate of decay to a vector meson relative to a pseudoscalar have been higher than the measured value (Sec. VI.B.3). Measurements of form factors indicated that this discrepancy was mainly due to smaller measured axial form factors ( $A_1$  and  $A_2$ ) than were predicted by theory (Table XXVII). More recent theoretical predictions are in better agreement with the experimental results (see Table XXVIII).

Semileptonic  $D_s$  decays appear to follow the pattern of  $D$  decays, both in terms of form-factor ratios and in the relative decay rates to pseudoscalar and vector mesons.

#### E. Exclusive $b \rightarrow c$ semileptonic decays of $B$ mesons and $|V_{cb}|$

##### 1. Overview and experimental techniques

The decays  $B \rightarrow X_c \ell^- \bar{\nu}$ , where  $X_c$  is a hadronic system with charm, account for 98% to 99% of the total  $B$ -meson

TABLE XXXIV. Summary of measured semileptonic decay rates for  $D$  mesons. The rate for Cabibbo-suppressed modes is based on predictions of the ISGW2 model (Scora and Isgur, 1994). No theoretical uncertainty has been included for the Cabibbo-suppressed rate.

Decay mode	Decay rate ( $10^{10} \text{ s}^{-1}$ )
$D \rightarrow \bar{K} \ell^+ \nu$	$8.4 \pm 0.4$
$D \rightarrow \bar{K}^* \ell^+ \nu$	$4.7 \pm 0.4$
$D \rightarrow (\pi, \eta, \eta', \rho, \omega) \ell^+ \nu$	0.7
Total exclusive rate	$13.8 \pm 0.6$
Inclusive rate	$16.5 \pm 0.7$

TABLE XXXV.  $B$  semileptonic decays to final states with charm. Measurements at the  $Y(4S)$  assume that  $f_{+-} = f_{00} = 0.5$ , where  $f_{+-} = B(Y(4S) \rightarrow B^+ B^-)$  and  $f_{00} = B(Y(4S) \rightarrow B^0 \bar{B}^0)$ . Measurements with an asterisk (\*) have been updated to reflect more recent values of  $D$  and  $D^*$  branching fractions. Those with a dagger (†) used early  $D^*$  branching fractions, but, due to the complexity of the analysis procedure, are difficult to correct. We also list averages for  $\bar{B}^0 \rightarrow D^{*+} \ell^- \bar{\nu}$  and  $B^- \rightarrow D^{*0} \ell^- \bar{\nu}$  branching fractions, whereas for  $\bar{B}^0 \rightarrow D^+ \ell^- \bar{\nu}$  we recommend using the ARGUS measurement only, since the CLEO I measurement is not corrected. In quoting the ALEPH and OPAL results, we have assumed  $B(b \rightarrow \bar{B}^0) = B(b \rightarrow B^-) = 0.4$  (with no uncertainty) at the  $Z$ . The charge of the  $B$  meson is not determined in the decays to  $P$ -wave mesons from LEP, since  $X$  may be a charged particle, but most  $D_1^0$  and  $D_2^{*0}$  states are probably produced in charged  $B$  decays and most charged  $D_1^+$  and  $D_2^{*+}$  states in neutral  $B$  decays. In the text, various assumptions are made to derive results on decays to these states that are easier to interpret than those in the table. The ARGUS measurement of  $B \rightarrow D^{**} \ell^- \bar{\nu}$  assumes a set of  $D^{**}$  states distributed according to the ISGW model.

Mode	Experiment	Reference	Branching fraction (%)
$\bar{B}^0 \rightarrow D^+ \ell^- \bar{\nu}$	ARGUS*	Albrecht <i>et al.</i> , 1989b	$2.0 \pm 0.7 \pm 0.6$
$\bar{B}^0 \rightarrow D^+ \ell^- \bar{\nu}$	CLEO I†	Fulton <i>et al.</i> , 1991	$1.8 \pm 0.6 \pm 0.3$
$B^- \rightarrow D^0 \ell^- \bar{\nu}$	CLEO I†	Fulton <i>et al.</i> , 1991	$1.6 \pm 0.6 \pm 0.3$
$\bar{B}^0 \rightarrow D^{*+} \ell^- \bar{\nu}$	ARGUS*	Albrecht <i>et al.</i> , 1993c	$4.7 \pm 0.5 \pm 0.5$
$\bar{B}^0 \rightarrow D^{*+} \ell^- \bar{\nu}$	ARGUS (part. rec.)	Albrecht <i>et al.</i> , 1994a	$4.5 \pm 0.3 \pm 0.4$
$\bar{B}^0 \rightarrow D^{*+} \ell^- \bar{\nu}$	CLEO I*	Bortoletto <i>et al.</i> , 1989	$4.0 \pm 0.4 \pm 0.6$
$\bar{B}^0 \rightarrow D^{*+} \ell^- \bar{\nu}$	ALEPH (prelim.)	ALEPH Collaboration, 1994	$5.36 \pm 0.50 \pm 0.76$
$\bar{B}^0 \rightarrow D^{*+} \ell^- \bar{\nu}$	CLEO II	Barish <i>et al.</i> , 1995	$4.49 \pm 0.32 \pm 0.39$
$\bar{B}^0 \rightarrow D^{*+} \ell^- \bar{\nu}$	Average		$4.53 \pm 0.32$
$B^- \rightarrow D^{*0} \ell^- \bar{\nu}$	ARGUS*	Albrecht <i>et al.</i> , 1992a	$6.6 \pm 1.6 \pm 1.5$
$B^- \rightarrow D^{*0} \ell^- \bar{\nu}$	CLEO I†	Fulton <i>et al.</i> , 1991	$4.1 \pm 0.8_{-0.9}^{+0.8}$
$B^- \rightarrow D^{*0} \ell^- \bar{\nu}$	CLEO II	Barish <i>et al.</i> , 1995	$5.13 \pm 0.54 \pm 0.64$
$B^- \rightarrow D^{*0} \ell^- \bar{\nu}$	Average		$5.34 \pm 0.80$
$B \rightarrow D^{*+} \pi^- \ell^- \bar{\nu} X$	ALEPH	Buskalic <i>et al.</i> , 1995b	$0.93 \pm 0.25 \pm 0.18$
$B \rightarrow D_1^0(2420) \ell^- \bar{\nu} X$ $\times D_1^0(2420) \rightarrow D^{*+} \pi^-$	ALEPH	Buskalic <i>et al.</i> , 1995b	$0.51 \pm 0.15 \pm 0.09$
$B \rightarrow D_2^{*0}(2460) \ell^- \bar{\nu} X$ $\times D_2^{*0}(2460) \rightarrow D^{*+} \pi^-$	ALEPH	Buskalic <i>et al.</i> , 1995b	$< 0.20$ @ 95% C.L.
$B \rightarrow D_2^{*0}(2460) \ell^- \bar{\nu} X$ $\times D_2^{*0}(2460) \rightarrow D^+ \pi^-$	OPAL (prelim.)	Akers <i>et al.</i> , 1995	$0.40 \pm 0.18 \pm 0.08$
$B \rightarrow D_2^{*+}(2460) \ell^- \bar{\nu} X$ $\times D_2^{*+}(2460) \rightarrow D^0 \pi^+$	OPAL (prelim.)	Akers <i>et al.</i> , 1995	$1.1 \pm 0.3_{-0.3}^{+0.2}$
$B^0 \rightarrow D^{**+} \ell^- \bar{\nu}$	ARGUS	Albrecht <i>et al.</i> , 1993c	$2.5 \pm 0.5 \pm 0.5$

semileptonic rate (see Sec. V.E). An overall picture of exclusive  $B \rightarrow X_c \ell^- \bar{\nu}$  decays can be obtained from Table XXXV, which lists the branching fractions measured thus far.

Several features stand out from an inspection of Table XXXV. Together, the decays  $B \rightarrow D \ell^- \bar{\nu}$  and  $B \rightarrow D^* \ell^- \bar{\nu}$  account for only 60% to 70% of the inclusive semileptonic rate. This result contrasts with the situation in  $D$  decays, where  $D \rightarrow \bar{K} \ell^+ \nu$  and  $D \rightarrow \bar{K}^* \ell^+ \nu$  nearly saturate the Cabibbo-favored rate. Furthermore, theoretical calculations had predicted that  $B \rightarrow D \ell^- \bar{\nu}$  and  $B \rightarrow D^* \ell^- \bar{\nu}$  would account for most of the semileptonic rate (Voloshin and Shifman, 1988; Isgur *et al.*, 1989; Colangelo *et al.*, 1992). The decay  $B \rightarrow D^* \ell^- \bar{\nu}$  has the largest branching fraction of any semileptonic mode (in fact, of any exclusive  $B$  decay), and it is the only semileptonic mode whose branching fraction has been precisely measured. Due to a fortunate convergence of experimental and theoretical advantages,  $B \rightarrow D^* \ell^- \bar{\nu}$  offers what may well be the best method for determining  $|V_{cb}|$ , as

well as an excellent environment for testing the predictions of HQET through form-factor measurements. Although the branching fraction for  $B \rightarrow D \ell^- \bar{\nu}$  is also relatively large, its value is not well known. However, all of the published mea-

TABLE XXXVI. Partial widths for  $B \rightarrow D \ell^- \bar{\nu}$  and  $B \rightarrow D^* \ell^- \bar{\nu}$  decays. The uncertainties include the errors on the individual charged and neutral  $B$ -meson lifetimes, as listed in Table III. The rate for  $B^- \rightarrow D^0 \ell^- \bar{\nu}$  is marked with a dagger (†) because the associated branching-fraction measurement could not be adequately corrected for changes in  $D$  and  $D^*$  branching-fraction results.

Mode	$\Gamma / (10^{10} \text{ s}^{-1})$
$\bar{B}^0 \rightarrow D^+ \ell^- \bar{\nu}$	$1.3 \pm 0.6$
$B^- \rightarrow D^0 \ell^- \bar{\nu}$	$1.0 \pm 0.4^\dagger$
$\bar{B}^0 \rightarrow D^{*+} \ell^- \bar{\nu}$	$3.0 \pm 0.3$
$B^- \rightarrow D^{*0} \ell^- \bar{\nu}$	$3.5 \pm 0.6$

TABLE XXXVII. Predictions for exclusive  $\bar{B}^0 \rightarrow X_{c\bar{d}} \ell^- \bar{\nu}$  decays from the ISGW2 model. The quantum numbers of the final-state charm meson are expressed in the heavy-quark symmetry notation  $n^{j_\ell}/L_J$ , where  $n$  is the radial quantum number,  $j_\ell$  is the total angular momentum of the light degrees of freedom,  $L$  is their orbital angular momentum, and  $J$  is the total spin of the meson. The masses in parenthesis are expectations for unobserved particles.

$n^{j_\ell}/L_J(X_{c\bar{d}})$	$M(X_{c\bar{d}})$ GeV/ $c^2$	$\frac{\Gamma(\bar{B}^0 \rightarrow X_{c\bar{d}} \ell^- \bar{\nu})}{( V_{cb} ^2 10^{13} \text{ s}^{-1})}$
$1^{1/2}S_0$	1.87	1.42
$1^{1/2}S_1$	2.01	2.81
$1^{3/2}P_1$	2.42	0.20
$1^{3/2}P_2$	2.46	0.10
$1^{1/2}P_0$	(2.40)	0.03
$1^{1/2}P_1$	(2.49)	0.04
$2^{1/2}S_0$	(2.58)	0.00
$2^{1/2}S_1$	(2.64)	0.06
Total		4.66

measurements of  $B \rightarrow D \ell^- \bar{\nu}$  are old, and improvements should be forthcoming. The vector-to-pseudoscalar ratio,  $\Gamma(B \rightarrow D^* \ell^- \bar{\nu})/\Gamma(B \rightarrow D \ell^- \bar{\nu}) \approx 2.3$ , is very different<sup>9</sup> from the analogous ratio in charm semileptonic decays:  $\Gamma(D \rightarrow \bar{K}^* \ell^+ \nu)/\Gamma(D \rightarrow \bar{K} \ell^+ \nu) \approx 0.6$ . The ratio for  $B$  semileptonic decays is in accord with most theoretical predictions, unlike that for charm decays. For example, Neubert (1994c) predicts a ratio of 2.79 for  $\rho_{A_1}^2 = 0.8$  and 3.0 for  $\rho_{A_1}^2 = 1.1$ , while the ISGW2 model (Scora and Isgur, 1994) predicts a ratio of 2.6. Table XXXVI lists the partial widths for  $B \rightarrow D l^- \bar{\nu}$  and  $B \rightarrow D^* l^- \bar{\nu}$ . Finally, we note that the decays to orbitally excited charm mesons, including the  $D_1(2420)$  and  $D_2^*(2460)$ , represent a significant and poorly understood part of the semileptonic rate. Rapid progress is being made in this area by the LEP experiments. A mode that is not listed, but which may be significant (Cheng *et al.*, 1993), is  $B \rightarrow D \pi \ell^- \bar{\nu}$ , where the hadronic part of the final state is nonresonant. For reference, we include in Table XXXVII the predictions of ISGW2 for exclusive  $B \rightarrow X_{c\bar{d}} \ell^- \bar{\nu}$  decays.

Reconstruction of exclusive semileptonic decays is more difficult than that of hadronic decays because the neutrino cannot be directly observed. Furthermore, an identified lepton and a reconstructed  $D^*$  meson do not in themselves constitute evidence for the decay  $B \rightarrow D^* \ell^- \bar{\nu}$ , since such combinations could arise from several other sources. The actual decay could be  $B \rightarrow D^{**} \ell^- \bar{\nu}$ , followed by  $D^{**} \rightarrow D^* \pi$ , or it could be  $B \rightarrow D^* \pi \ell^- \bar{\nu}$ , in which the  $D^* \pi$  system is nonresonant. Similarly, both  $B \rightarrow D^* \ell^- \bar{\nu}$  and  $B \rightarrow D^{**} \ell^- \bar{\nu}$  produce  $D \ell^-$  combinations that can mimic a  $B \rightarrow D \ell^- \bar{\nu}$  signal.

<sup>9</sup>One might guess from simple spin counting that this ratio, in the limit of identical masses for the vector and pseudoscalar mesons, might be equal to three. This argument is not correct because the three helicity states for the vector meson have very different probabilities, which are determined by the detailed physics of the underlying weak couplings as well as the form factors.

At the  $Y(4S)$ , there is the additional difficulty that each event contains two  $B$  mesons, each decaying nearly at rest in the lab frame. A  $D^{*+} \ell^-$  pair, for example, can originate from  $\bar{B}^0 \rightarrow D^{*+} \ell^- \bar{\nu}$ , but the same correlation of charges can also arise if the  $D^*$  and the lepton are produced in the decay chains of different  $B$ 's: either the lepton from the other  $B$  is secondary, or it is primary and  $B^0 \bar{B}^0$  mixing has occurred.

Fortunately, there are a number of powerful techniques for establishing semileptonic signals. At the  $Y(4S)$ , the energy of the  $B$  meson is known:  $E_B = E_{\text{beam}}$ . Using this constraint and the four-vectors for the candidate lepton and daughter hadron, one can determine whether the measured four-vectors are consistent with a missing neutrino. In a  $B \rightarrow D^* \ell^- \bar{\nu}$  decay, for example, one can calculate the mass of the particles recoiling against the  $D^* \ell^-$  system under the assumption that the observed  $D^*$  and lepton are produced from a single  $B$  meson:

$$p_{\text{miss}}^2 = (p_B - p_{D^* \ell^-})^2 = m_B^2 + m_{D^* \ell^-}^2 - 2E_B E_{D^* \ell^-} + 2|\mathbf{p}_B||\mathbf{p}_{D^* \ell^-}| \cos \theta_{B, D^* \ell^-}, \quad (134)$$

where  $p_{D^* \ell^-} = p_{D^*} + p_{\ell^-}$ . If the hypothesis is correct (that is, if the only other particle produced in the semileptonic decay is a neutrino), then  $p_{\text{miss}}^2 = p_{\nu}^2 = 0$ . If additional daughter particles are produced, such as pions, then  $p_{\text{miss}}^2$  increases. However, there is not enough information to calculate  $p_{\text{miss}}^2$  exactly, because the direction of the  $B$ -momentum vector is unknown. As a consequence, the angle  $\theta_{B, D^* \ell^-}$  between the  $B$ - and the  $(D^* + \ell^-)$ -momentum directions is also unknown. Fortunately, the magnitude of the  $B$  momentum at the  $Y(4S)$  is fairly small,  $|\mathbf{p}_B| = 330 \text{ MeV}/c$ , so that one can ignore the last term in Eq. (134) to good approximation. The quantity

$$M_{\text{miss}}^2 \equiv m_B^2 + m_{D^* \ell^-}^2 - 2E_B E_{D^* \ell^-} \quad (135)$$

still peaks near zero when the neutrino is the only missing particle, although there is significant smearing (of typical size  $\Delta M_{\text{miss}}^2 \approx 0.5 \text{ GeV}^2/c^4$ ) due to our approximation. An alternative way to use Eq. (134), requiring no approximations, is to set  $p_{\text{miss}}^2 = 0$  and solve for  $\cos \theta_{B, D^* \ell^-}$ . If the hypothesis is correct (that is, if the only other particle in the  $B$  decay is a neutrino), then  $\cos \theta_{B, D^* \ell^-}$  must lie in the range  $-1$  to  $+1$ . If there are additional particles produced in the  $B$  decay, however, then the value of  $\cos \theta_{B, D^* \ell^-}$  calculated in this way often takes on nonphysical values, and such candidates can be rejected.

Recently, a new approach has been used by CLEO in the measurement of  $B \rightarrow \pi \ell^- \bar{\nu}$ . Here it was possible to use the missing-momentum vector in the event to estimate the neutrino four-momentum, and then to reconstruct a  $B$  mass peak as in a hadronic analysis. This approach appears to be very promising and will be applied to exclusive  $B \rightarrow X_{c\bar{d}} \ell^- \bar{\nu}$  decays as well. In addition to these techniques, several other kinematic properties can be used to identify semileptonic decays at the  $Y(4S)$ , which we discuss further in the sections on specific modes.

Experiments using  $Z \rightarrow b\bar{b}$  cannot impose a strict beam-energy constraint, because the  $b$  hadron does not necessarily

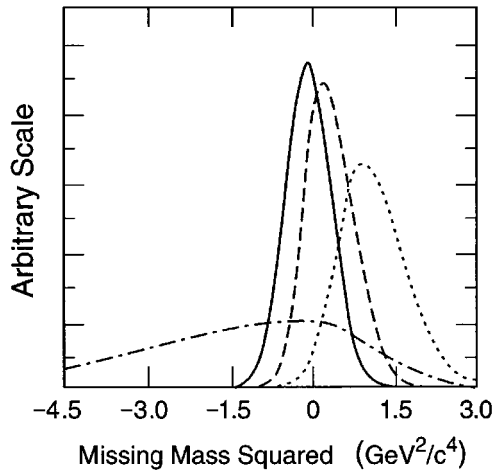


FIG. 29. Distributions of the missing mass squared recoiling against the  $D\ell^-$  system, generated with the CLEO Monte Carlo. These shapes are used in extracting the rate for  $B \rightarrow D\ell^- \bar{\nu}$ : solid line,  $B \rightarrow D\ell^- \bar{\nu}$ ; dashed line,  $B \rightarrow D^*\ell^- \bar{\nu}$ ; dotted line,  $B \rightarrow D^{**}\ell^- \bar{\nu}$ ; dot-dashed line,  $B \rightarrow D(D^*)X$ ,  $\bar{B} \rightarrow Y\ell^- \bar{\nu}$ . All curves are normalized to the same area. In the measurement of the rate for  $B \rightarrow D^*\ell^- \bar{\nu}$ , one computes the missing mass squared recoiling against the  $D^*\ell^-$  system.

receive the full beam energy in the fragmentation process. However, there are other very effective ways to reduce background. The  $b$  hadron travels a relatively large distance before decaying, so that precise vertex-detector information is a powerful tool for associating  $b$ -decay tracks. In addition, the jet structure of the event separates the tracks from the two  $b$  hadrons into different regions of the solid angle, so that the problem of overlapping decay products from the  $b$  hadrons is much reduced.

## 2. Branching fraction for $B \rightarrow D\ell^- \bar{\nu}$

Although the decay  $B \rightarrow D\ell^- \bar{\nu}$  has a substantial branching fraction, measurements to date have suffered from large statistical errors, as well as difficulty with background from  $B \rightarrow D^*\ell^- \bar{\nu}$ , where  $D^* \rightarrow D\pi$  or  $D^* \rightarrow D\gamma$ . Although  $D^0$ 's are easier to reconstruct than  $D^+$ 's, there is more background for  $B^- \rightarrow D^0\ell^- \bar{\nu}$  than  $\bar{B}^0 \rightarrow D^+\ell^- \bar{\nu}$  because all  $D^{*0}$  decays and about two-thirds of  $D^{*+}$  decays produce  $D^0$ 's. The lepton-energy spectrum from  $B \rightarrow D\ell^- \bar{\nu}$  is softer than that for  $B \rightarrow D^*\ell^- \bar{\nu}$  (see Sec. II.C) and does not provide a particularly useful tool for isolating a  $B \rightarrow D\ell^- \bar{\nu}$  signal. At the  $Y(4S)$ , the two best variables for this purpose are the momentum of the  $D$  meson, which is substantially harder for  $D$ 's from  $B \rightarrow D\ell^- \bar{\nu}$  than for those from  $B \rightarrow D^*\ell^- \bar{\nu}$ , and the missing mass of the system recoiling against the  $D\ell^-$  system, defined analogously to Eq. (135). (The  $D$  momentum is typically hard because the  $P$ -wave effect in  $P \rightarrow P'\ell\nu$  decays favors low  $q^2$  configurations, as discussed in Sec. II.C.) The usual procedure is to make a cut on  $p_D$  at some minimum value (e.g.,  $p > 1.5$  GeV/ $c$ ) and then to fit the  $M_{\text{miss}}^2$  distribution to contributions from  $B \rightarrow D\ell^- \bar{\nu}$  and  $B \rightarrow D^*\ell^- \bar{\nu}$ . Figure 29 shows the shapes that would be observed in the missing mass squared recoiling against the ob-

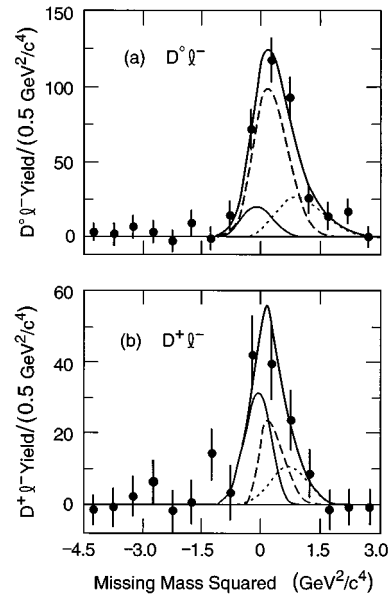


FIG. 30. Missing-mass-squared distributions for the CLEO I  $B \rightarrow D\ell^- \bar{\nu}$  analysis. The points with error bars are data after subtraction of the contribution from events containing fake leptons and events in which the  $D$  and the lepton are real but are from different  $B$  mesons: (a) distribution for  $D^0\ell^-$  combinations; (b) distribution for  $D^+\ell^-$  combinations. The total fit is broken down into the contributions displayed in Fig. 29. Note that the contribution from the  $B \rightarrow D\ell^- \bar{\nu}$  signal (lower solid line in each plot) is small compared with the backgrounds in the  $D^0\ell^-$  channel and comparable to the backgrounds in the  $D^+\ell^-$  channel. Redrawn from Fulton *et al.* (1991).

served  $D\ell^-$  system for various decay hypotheses. Figures 30 and 31 show data from CLEO I and ARGUS.

Measurements of  $B \rightarrow D\ell^- \bar{\nu}$  from ARGUS (Albrecht *et al.*, 1989b) and CLEO (Fulton *et al.*, 1991) are listed in Table XXXV. The published values are in general somewhat different from those in the table, because there have been significant changes in measured  $D$  and  $D^*$  branching fractions since the original publications. (The  $D^*$  branching fractions are needed for background calculations.) Stone (1993) has used more recent  $D^*$  and  $D$  branching fractions (Adler *et al.*, 1988a; Butler *et al.*, 1992; Akerib *et al.*, 1993) to correct these measurements when the original publication contains sufficient information. Morrison and Richman (1994) have used a similar procedure, together with the  $D$  and  $D^*$  branching fractions given in Table III. The  $B \rightarrow D\ell^- \bar{\nu}$  values given in Table XXXV are obtained from Morrison and Richman. Unfortunately, it is not possible to correct all of the early measurements, since inadequate information is given in the papers, and in other cases some judgment is required. It should be possible to measure  $B \rightarrow D\ell^- \bar{\nu}$  much better now that the background process  $B \rightarrow D^*\ell^- \bar{\nu}$  has been measured with good precision.

## 3. Branching fractions for $B \rightarrow D^*\ell^- \bar{\nu}$ and $B \rightarrow D^{**}\ell^- \bar{\nu}$

The branching fraction for  $B \rightarrow D^*\ell^- \bar{\nu}$  has been measured using both full and partial reconstruction of the  $D^*$ . In

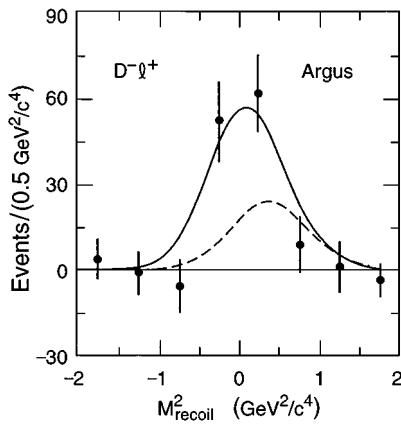


FIG. 31. The missing-mass-squared distribution in the ARGUS  $\bar{B}^0 \rightarrow D^+ \ell^- \bar{\nu}$  analysis. The solid curve is the total fit, and the dashed curve shows the contribution from  $\bar{B}^0 \rightarrow D^{*+} \ell^- \bar{\nu}$ . The contribution from  $B \rightarrow D^{**} \ell^- \bar{\nu}$  decays was found to be negligible. Redrawn from Albrecht *et al.* (1989b).

the first approach, which has been used by ALEPH (ALEPH Collaboration, 1994), ARGUS (Albrecht *et al.*, 1992a, 1993c), and CLEO (Bortoletto *et al.*, 1989; Fulton *et al.*, 1991; Barish *et al.*, 1995a), all of the decay products of the  $D^*$  are identified. This method has the advantage that the difference  $\delta M$  between the invariant masses reconstructed for the  $D^*$  and  $D$  candidates [for example,  $M(D^{*+}) - M(D^0) = M(K^- \pi^+ \pi^+) - M(K^- \pi^+)$ ] provides a powerful tool for rejecting background. This method is superior to simply reconstructing a  $D^*$  mass peak, because the tracking-related errors in the two masses are highly correlated, and there are substantial cancellations of the errors in the difference. The resolution on  $\delta M$  is consequently very good (better than  $1 \text{ MeV}/c^2$  in CLEO). A difficulty for  $B \rightarrow D^* \ell^- \bar{\nu}$  measurements in the  $\Upsilon(4S)$  experiments is that the “soft pion”  $\pi_s^+$  from the  $D^{*+} \rightarrow D^0 \pi_s^+$  decay has very low momentum: all of the spectrum is below  $225 \text{ MeV}/c$ . In the high magnetic field (1.5 T) of CLEO, 100  $\text{MeV}/c$  pions are restricted to the inner half of the tracking system, and great care must be taken to determine the detection efficiency of the soft pions as a function of momentum. ARGUS has a substantially lower field (0.8 T), so the  $D^{*+}$  reconstruction problem is less severe. At LEP, reconstruction of this pion does not pose a problem because there is a large boost between the  $B$  rest frame and the lab frame.

We first describe the ARGUS measurement (Albrecht *et al.*, 1993c) of  $\bar{B}^0 \rightarrow D^{*+} \ell^- \bar{\nu}$ , which uses the channels  $D^0 \rightarrow K^- \pi^+$  and  $D^0 \rightarrow K^- \pi^+ \pi^- \pi^+$ . As we have discussed, signal events produce a narrow peak in the  $\delta M$  distribution and a peak near zero (indicating a neutrino) in the distribution of the missing mass recoiling against the  $D^{*+} \ell^-$  system. [ARGUS uses the definition  $M_{\text{rec}}^2 = (E_{\text{beam}} - E_{D^{*+}} - E_{\ell})^2 - (\mathbf{p}_{D^{*+}} + \mathbf{p}_{\ell})^2$ , which differs only slightly from the definition of  $M_{\text{miss}}^2$  given in Eq. (135).] Figure 32 shows the distributions of  $M_{\text{rec}}^2$  for the two channels studied. In addition to the dominant contribution from  $\bar{B}^0 \rightarrow D^{*+} \ell^- \bar{\nu}$ , the fits include a term for  $B \rightarrow D^{**} \ell^- \bar{\nu}$ . This term, whose shape is taken from a Monte Carlo simu-

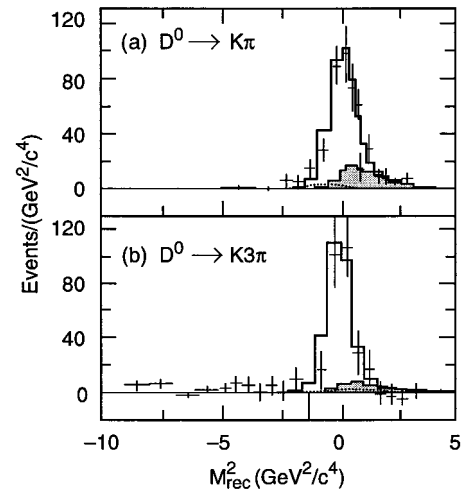


FIG. 32. The ARGUS missing-mass distribution for  $D^* \ell$  events in which the  $D^*$  is fully reconstructed in the decay  $D^{*+} \rightarrow D^0 \pi^+$  where (a)  $D^0 \rightarrow K^- \pi^+$  or (b)  $D^0 \rightarrow K^- \pi^+ \pi^- \pi^+$ . Most of the events are attributed to the decay  $\bar{B}^0 \rightarrow D^{*+} \ell^- \bar{\nu}$ . The data are the points with error bars, and the unshaded histogram is the contribution from  $\bar{B}^0 \rightarrow D^{*+} \ell^- \bar{\nu}$  determined from the fit. The shaded regions at the upper end of the spectra show the estimated contribution from  $B \rightarrow D^{**} \ell^- \bar{\nu}$ , and the dotted curves represent the small contribution from continuum background. Redrawn from Albrecht *et al.* (1993c).

lation based on the ISGW model, is used to fit the broad shoulder in the upper end of the distribution. The  $\bar{B}^0 \rightarrow D^{*+} \ell^- \bar{\nu}$  signal contains  $235 \pm 24 \pm 11$  events, leading to the ARGUS published value of  $B(\bar{B}^0 \rightarrow D^{*+} \ell^- \bar{\nu}) = (5.2 \pm 0.5 \pm 0.6)\%$ . However, this number assumed  $B(D^0 \rightarrow K^- \pi^+) = 3.65\%$ , which is significantly below the 1994 PDG value. The corrected branching fraction given in Table XXXV uses 1994 PDG information.

There are many  $D^{**}$  states that can contribute to the shoulder of the missing-mass distribution, but they cannot be distinguished by this measurement. Thus  $D^{**}$  is used generically to represent either orbitally or radially excited  $D$  mesons or nonresonant  $D^* X$  systems. To measure their combined contribution, ARGUS uses a Monte Carlo simulation based on the ISGW model, which provides the relative detection efficiencies for the different states, as well as the shapes that they would produce in the  $M_{\text{rec}}^2$  distribution. The  $D^{**}$  states included in the fit are  $D(1^1 P_1)$ ,  $D(1^3 P_1)$ ,  $D(1^3 P_2)$ ,  $D(2^1 S_0)$ , and  $D(2^3 S_1)$ . [The  $D(1^3 P_0)$  cannot decay into  $D^{*+} \pi^-$ .] Based on their combined signal of  $63 \pm 15 \pm 6$  events in both  $D^0$  channels, ARGUS obtains the model-dependent result

$$B(\bar{B}^0 \rightarrow D^{**+} \ell^- \bar{\nu}) = (2.7 \pm 0.5 \pm 0.5)\%, \quad (136)$$

which we have corrected in Table XXXV to reflect more recent measurements of  $D^0 \rightarrow K^- \pi^+$ . The model dependence is not included in the systematic error.

In the CLEO II analysis (Barish *et al.*, 1995a), both  $\bar{B}^0 \rightarrow D^{*+} \ell^- \bar{\nu}$  and  $B^- \rightarrow D^{*0} \ell^- \bar{\nu}$  are measured using  $D^{*+} \rightarrow D^0 \pi^+$  and  $D^{*0} \rightarrow D^0 \pi^0$ , with  $D^0 \rightarrow K^- \pi^+$  in each case. The  $\pi^0$  reconstruction uses the CsI calorimeter, which provides excellent photon detection down to low energies.

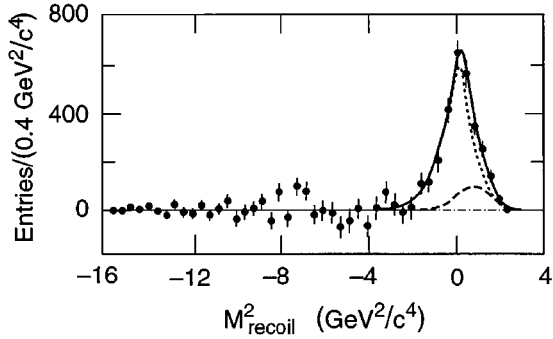


FIG. 33. The ARGUS missing-recoil-mass distribution for  $D^*$  events in which the  $D^*$  is identified only by the presence of the slow pion from the decay  $D^* \rightarrow D\pi$ . Background from wrong-sign  $\pi\ell$  combinations has been subtracted. The dotted curve shows the  $B \rightarrow D^* \ell^- \bar{\nu}$  contribution, and the dashed curve shows the contribution from  $B \rightarrow D^{**} \ell^- \bar{\nu}$  decays. Redrawn from Albrecht *et al.* (1994a).

The analysis technique is roughly similar to that used by ARGUS, but the separate  $B \rightarrow D^* \ell^- \bar{\nu}$  and  $B \rightarrow D^* X \ell^- \bar{\nu}$  contributions are determined not only from the missing-mass distribution, but also from the fact that  $B \rightarrow D^* \ell^- \bar{\nu}$  has a harder lepton-momentum spectrum than  $B \rightarrow D^* X \ell^- \bar{\nu}$ . The total yield of signal events in the two semileptonic decays is about 700, and the dominant systematic errors are due to uncertainties in the detection efficiencies for the soft  $\pi^+$ 's and  $\pi^0$ 's. This analysis yields the most precisely measured branching fractions for  $B \rightarrow D^* \ell^- \bar{\nu}$  using full reconstruction:

$$\begin{aligned} B(\bar{B}^0 \rightarrow D^{*+} \ell^- \bar{\nu}) &= (4.49 \pm 0.32 \pm 0.39)\%, \\ B(B^- \rightarrow D^{*0} \ell^- \bar{\nu}) &= (5.13 \pm 0.54 \pm 0.64)\%. \end{aligned} \quad (137)$$

The evidence for a  $B \rightarrow D^* X \ell^- \bar{\nu}$  or  $B \rightarrow D^{**} \ell^- \bar{\nu}$  signal is weak:

$$\begin{aligned} B(\bar{B} \rightarrow D^{*+} X \ell^- \bar{\nu}) &= (0.6 \pm 0.3 \pm 0.1)\%, \\ B(\bar{B} \rightarrow D^{*0} X \ell^- \bar{\nu}) &= (0.6 \pm 0.6 \pm 0.1)\%, \end{aligned} \quad (138)$$

where  $X$  represents at least one pion, so CLEO quotes a 95% C.L. upper limit

$$\sum_i B(\bar{B} \rightarrow D_i^{**} \ell^- \bar{\nu}) < 2.8\%. \quad (139)$$

As in the ARGUS analysis, a number of model-dependent assumptions are made in obtaining the  $B \rightarrow D^{**} \ell^- \bar{\nu}$  results.

Recently, ALEPH (ALEPH Collaboration, 1994) has presented preliminary results from a measurement of  $\bar{B}^0 \rightarrow D^{*+} \ell^- \bar{\nu}$  using a sample of 1.6 million hadronic  $Z$  decays. Using  $D^0 \rightarrow K^- \pi^+$ ,  $D^0 \rightarrow K^- \pi^+ \pi^- \pi^+$ , and  $D^0 \rightarrow K_s^0 \pi^+ \pi^-$ , this analysis obtained  $176 \pm 14$  candidate  $D^{*+} \ell^- \bar{\nu}$  events, which include an estimated background of  $35 \pm 6$  events. The dominant systematic errors are due to tracking efficiency uncertainties (10%) and the unknown value of  $B(b \rightarrow B^0)$  (8.2% uncertainty). The ALEPH result,  $B(\bar{B}^0 \rightarrow D^{*+} \ell^- \bar{\nu}) = (5.36 \pm 0.50 \pm 0.76)\%$ , is consistent with those of ARGUS and CLEO.

ARGUS (Albrecht *et al.*, 1994a) has used a second method to measure  $\bar{B}^0 \rightarrow D^{*+} \ell^- \bar{\nu}$  based on a partial recon-

struction of the  $D^{*+}$  decay. The  $D^{*+}$  is identified using only the soft pion, giving this technique a large statistical advantage over full reconstruction. Due to the very small energy release in  $D^{*+} \rightarrow D^0 \pi^+$  (about 6 MeV), the soft-pion direction in the lab frame provides a good estimate of the  $D^{*+}$  direction. Furthermore, the velocities of the soft pion and the  $D^{*+}$  are nearly the same, so the soft-pion velocity can be used to determine the  $D^{*+}$  energy. This information is sufficient to construct the same missing-recoil-mass squared that is used in the full reconstruction method. Although there are many random low-momentum pions, they do not produce a peak in the missing-mass distribution when considered together with the lepton. However, they do constitute a very large background that varies substantially under the peak. Careful evaluation of this background is crucial, and in the ARGUS analysis it is determined from  $D^*$ -lepton pairs with the wrong charge correlation. Figure 33 shows the background-subtracted distribution of missing mass squared for the ARGUS analysis. From a fit to this distribution, ARGUS obtains a yield of about 2700  $\bar{B}^0 \rightarrow D^{*+} \ell^- \bar{\nu}$  events, leading to

$$B(\bar{B}^0 \rightarrow D^{*+} \ell^- \bar{\nu}) = (4.5 \pm 0.3 \pm 0.4)\%, \quad (140)$$

consistent with the results from the full reconstruction methods discussed above.

The evidence for  $B \rightarrow D^{**} \ell^- \bar{\nu}$  obtained from the  $M_{\text{miss}}^2$  distributions is not compelling. Recently, both ALEPH and OPAL have performed more direct searches for  $B \rightarrow D^{**} \ell^- \bar{\nu}$  decays. In these analyses, vertex detector information is extremely helpful in associating tracks from the decay, especially when the hadronic part of the final state involves a complicated decay sequence or is nonresonant.

These searches are directed towards final states containing an excited charm meson that decays into  $D^* \pi$  or  $D \pi$ . The spectroscopy of orbitally excited charm mesons has been addressed with HQET (see, for example, Isgur and Wise, 1991b), and we comment briefly on some of the results here. Since the spin of the heavy quark decouples from the dynamics in the heavy-quark limit, the angular momentum of the light constituents,  $j_\ell$ , is a conserved quantum number. Thus the states can be labeled not only by their total spin  $J$ , but also by  $j_\ell$ . The decoupling of the heavy-quark spin is expected to lead to approximately degenerate doublet states. The quantum numbers  $j_\ell = 1/2$  should be associated with a doublet containing a meson of total spin  $J=0$  and another of total spin  $J=1$ , whereas the quantum numbers  $j_\ell = 3/2$  are associated with a doublet containing mesons of total spin  $J=1$  and  $J=2$ . Table XXXVIII lists the relevant states and some of their properties. In particular, two narrow, orbitally excited states are observed, the  $D_1(2420)$  and the  $D_2^*(2460)$ , and they have the properties expected for the  $j_\ell = 3/2$  doublet. In the HQET picture, they are narrow because their decays involve  $j_\ell = 3/2 \rightarrow 1/2$  transitions and conserve parity, restricting them to a  $D$  wave, whereas the  $j_\ell = 1/2$  states can decay in an  $S$  wave and hence are broad.

ALEPH has searched (Buskulic *et al.*, 1995b) for  $B$  semileptonic decays to final states containing a  $D^{*+}$  and at least one additional pion. To reduce background from fragmentation pions, the additional pion is required to have a significant impact parameter with respect to the primary event ver-

TABLE XXXVIII. Orbitally excited charm mesons and some of their properties. The quantum number  $j_\ell$  is the angular momentum of the light constituents of the meson, including the spin of the light quark. The allowed strong decays in the heavy-quark symmetry limit are also listed.

	$J^P$	$j_\ell$	Mass (MeV)	Width (MeV)	Decays
	$1^+$	$1/2$	$\sim 2490$ (unobserved)	broad	$D^*\pi$
	$0^+$	$1/2$	$\sim 2400$ (unobserved)	broad	$D\pi$
$D_1$	$1^+$	$3/2$	$2421 \pm 2$	$20 \pm 4$	$D^*\pi$
$D_2^*$	$2^+$	$3/2$	$2458 \pm 3$	$23 \pm 6$	$D\pi, D^*\pi$

tex. Vertex detector information is also used to reconstruct the  $D^0$  decay and to associate the additional pion with a  $D^{*+}\ell^-$  vertex. ALEPH observes roughly 24 events with  $D_1^0 \rightarrow D^{*+}\pi^-$ , leading to the result

$$B(b \rightarrow B) \times B(B \rightarrow D_1^0(2420)X\ell^- \bar{\nu}) \times B(D_1^0(2420) \rightarrow D^{*+}\pi^-) = (2.04 \pm 0.58 \pm 0.34) \times 10^{-3}. \quad (141)$$

Figure 34 shows the signal obtained from one of the two event selection procedures used by ALEPH. Since the system  $X$  is inclusive, the charge of the  $B$  is not strictly determined. However, it is probable that most of the  $D_1^0$  mesons are produced in charged  $B$  decays, with no additional particles in  $X$ . In this case, one should use  $B(b \rightarrow B) = B(b \rightarrow B^-) \approx 0.4$ . Furthermore, if the  $D_1^0(2420)$  decays only to  $D^*\pi$ , then isospin symmetry implies that  $D^{*0}\pi^+$  accounts for 2/3 of the rate. These assumptions give

$$B(B^- \rightarrow D_1^0(2420)\ell^- \bar{\nu}) = (0.77 \pm 0.22 \pm 0.13)\%. \quad (142)$$

No signal events are observed with the  $D_2^{*0}$ , leading to the upper limit quoted in Table XXXV. If we assume that the  $D_2^{*0}$  decays only to  $D^*\pi$  and  $D\pi$  and use the measured ratio (Particle Data Group, 1994; Avery *et al.*, 1994c),

$$\frac{B(D_2^{*0} \rightarrow D^+\pi^-)}{B(D_2^{*0} \rightarrow D^{*+}\pi^-)} = 2.3 \pm 0.6, \quad (143)$$

then isospin symmetry leads to

$$B(B^- \rightarrow D_2^0(2460)\ell^- \bar{\nu}) < 1.0\%, \quad 95\% \text{ C.L.} \quad (144)$$

We have not included the uncertainty in  $B(b \rightarrow B)$  or in the ratio given in Eq. (143), and we have assumed that the case where  $X$  represents no additional particles dominates the rate.

A separate topological search by ALEPH yields the result

$$B(b \rightarrow B) \times B(B \rightarrow D^{*+}\pi^- X\ell^- \bar{\nu}) = (3.7 \pm 1.0 \pm 0.7) \times 10^{-3}, \quad (145)$$

where both resonant and nonresonant contributions are included. Using  $B(b \rightarrow B^-) = 0.4$  and the isospin constraint  $B(D_1^0 \rightarrow D^{*+}\pi^-) < 2/3$ , we can conclude that  $B(B \rightarrow D^*\pi\ell^- \bar{\nu}X) > (1.4 \pm 0.5)\%$ , accounting for a significant part ( $\approx 34\%$ ) of the unidentified semileptonic decays of  $B$  mesons.

OPAL has also used vertex detector information to obtain results on semileptonic decays to charm mesons. By measuring the inclusive production for  $b \rightarrow D^+\ell^- X$  and  $b \rightarrow D^0\ell^- X$  and comparing with CLEO results, OPAL extracts the quantity

$$f(b \rightarrow \bar{B}^0) + f(b \rightarrow B^-) = 0.81 \pm 0.07 \pm 0.09 \quad (146)$$

at the  $Z$ , in good agreement with our assumed value of 0.8.

OPAL also observes signals (Fig. 35) for production of the tensor meson  $D_2^*$  in both charged and neutral states. The  $D_2^*$  can decay strongly into  $D\pi$ , whereas the  $D_1^0$  cannot, by  $J^P$  conservation. Furthermore, we have seen that the  $D_2^{*+}$  branching fraction to  $D\pi$  is about twice that to  $D^*\pi$ . The reconstructed mass difference,  $\Delta_m = M(D\pi) - M(D)$ , is expected to peak around  $590 \text{ MeV}/c^2$ , and OPAL observes peaks near this mass for final states with the  $D_2^{*+}$  (18 events) and the  $D_2^{*0}$  (7 events). The measured branching fractions are given in Table XXXV, and we can make the same assumptions as were applied to the ALEPH measurements to obtain

$$B(B^- \rightarrow D_2^{*0}(2460)\ell^- \bar{\nu}) = (0.86 \pm 0.39 \pm 0.17)\%, \quad (147)$$

which is within the limit set by ALEPH, and

$$B(B^0 \rightarrow D_2^{*+}(2460)\ell^- \bar{\nu}) = (2.4 \pm 0.7^{+0.4}_{-0.6})\%. \quad (148)$$

We emphasize that we have made a number of assumptions in deriving these results from the original measurements.

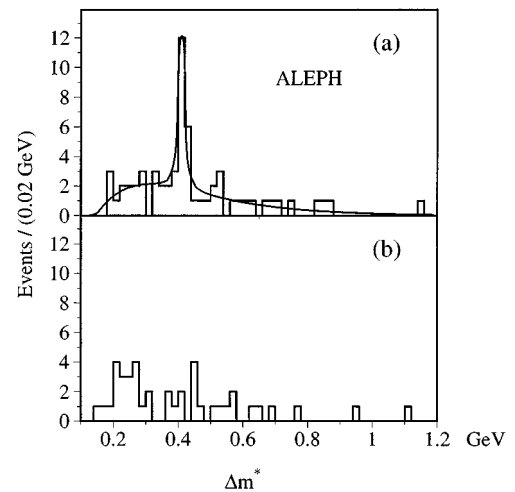


FIG. 34. ALEPH search for  $B \rightarrow D_1^0 X \ell^- \bar{\nu}$ , where  $D_1^0 \rightarrow D^{*+}\pi^-$ ,  $D^{*+} \rightarrow D^0\pi^+$ , and  $D^0 \rightarrow K^+\pi^+$  or  $D^0 \rightarrow K^+\pi^+\pi^-\pi^-$ . The histogram shows the difference,  $\Delta m^* = M(D^{*+}\pi^-) - M(D^{*+})$ , where the reconstructed  $D^{*+}$  mass is used. Right-sign charge combinations are shown in (a), whereas wrong-sign combinations are shown in (b). The peak at  $\Delta m^* \approx 0.4 \text{ GeV}/c^2$  is attributed to  $B \rightarrow D_1^0 X \ell^- \bar{\nu}$ ; no signal for the decay  $B \rightarrow D_2^{*0} X \ell^- \bar{\nu}$  is evident. The data shown are those for one of two event selection procedures whose results are averaged to obtain the final branching fraction.

TABLE XXXIX. Theoretical predictions for exclusive  $B \rightarrow X_c \ell^- \bar{\nu}$  decays and values of  $|V_{cb}|$  using these predictions together with measurements of exclusive partial widths. The table lists the values of the factor  $\gamma_c$ , where  $\Gamma = \gamma_c |V_{cb}|^2$  and the values of  $|V_{cb}|$  extracted using measurements of  $B \rightarrow D \ell^- \bar{\nu}$  and  $B \rightarrow D^* \ell^- \bar{\nu}$ . For  $B \rightarrow D \ell^- \bar{\nu}$  we use only the ARGUS measurement of  $\bar{B}^0 \rightarrow D^+ \ell^- \bar{\nu}$ , for the reasons discussed in Table XXXV. For  $B \rightarrow D^* \ell^- \bar{\nu}$ , we use the average of the  $B^-$  and  $B^0$  partial widths,  $\Gamma(B \rightarrow D^* \ell^- \bar{\nu}) = (3.1 \pm 0.3) \times 10^{10} \text{ s}^{-1}$ .

Model	$\gamma_c(D)/(10^{12} \text{ s}^{-1})$	$ V_{cb} (D)$	$\gamma_c(D^*)/(10^{12} \text{ s}^{-1})$	$ V_{cb} (D^*)$
ISGW	11.1	$0.034 \pm 0.008$	24.6	$0.036 \pm 0.002$
ISGW2	11.9	$0.033 \pm 0.008$	24.8	$0.035 \pm 0.002$
KS	8.3	$0.040 \pm 0.009$	25.8	$0.035 \pm 0.002$
WSB	8.1	$0.040 \pm 0.009$	21.9	$0.038 \pm 0.002$

Both the  $D_1^0$  and the  $D_2^{*0}$  can decay into  $D^* \pi$ , and OPAL observes broad peaks in  $\Delta_m = M(D^* \pi) - M(D^*)$  near  $440 \text{ MeV}/c^2$  that can have contributions from both states. The separate contributions are not resolved, but OPAL uses the measured signals in the  $D_2 \rightarrow D \pi$  modes to estimate the contribution of the  $2^+$  to the peak at  $440 \text{ MeV}/c^2$ . This technique yields branching fractions for semileptonic decay to the  $D_1(2420)$ :

$$B(B \rightarrow D_1^0 \ell^- \bar{\nu}) = (2.0 \pm 0.5 \pm 0.5)\%,$$

$$B(B \rightarrow D_1^+ \ell^- \bar{\nu}) = (2.0 \pm 0.7 \pm 0.5)\%, \tag{149}$$

where we have assumed  $B(b \rightarrow B) = 0.4$  to convert the published branching fractions for  $b$ -hadron decay to those for  $B$ -meson decay. We have also assumed that any additional particles  $X$  are present only in a small fraction of these decays.

These analyses, though still in their infancy, demonstrate the power of vertexing for studying decays to multibody and nonresonant final states.

#### 4. The determination of $|V_{cb}|$ with exclusive decays

The magnitude of the CKM element  $V_{cb}$  can be determined in three ways, using: (1) the inclusive semileptonic rate; (2) the total rates for exclusive  $b \rightarrow c \ell^- \bar{\nu}$  processes such as  $B \rightarrow D \ell^- \bar{\nu}$  or  $B \rightarrow D^* \ell^- \bar{\nu}$ ; or (3) the partial rate for  $B \rightarrow D^* \ell^- \bar{\nu}$  in the region of phase space where the  $D^*$  has very low momentum in the  $B$  rest frame. We have already described the inclusive method in Sec. V.D.4. This method has the advantage that the inclusive semileptonic branching fraction is now measured with high precision. However, there is not yet a consensus on the size of the theoretical uncertainty, which is currently larger than that from the measurement of the branching fraction itself.

Historically, decay rates for exclusive  $B \rightarrow X_c \ell^- \bar{\nu}$  processes were considered even harder to predict, because the details of the formation of the specific final-state hadronic system are involved. With the development of HQET, this situation has changed. While the total rate for an exclusive decay remains difficult to predict, the decay rate for the zero-recoil configuration—in which the final-state charm hadron is at rest—can now be predicted rather precisely. The reason for the difference between the reliability of these two approaches is simple. To predict the decay rate for a semileptonic decay, one must integrate the form factors over all values of  $q^2$ . In the language of HQET, one would need to know the Isgur-Wise function, as well as the corrections to the heavy-quark symmetry limit, over the full kinematic range. In contrast, when the region of phase space is restricted to large values of  $q^2$  (or values of  $w$  near 1), the light constituents of the initial meson are relatively undisturbed, and the rate is less sensitive to the full details of the wave functions. We shall see that the absolute normalization of the Isgur-Wise function can be predicted with good precision for the zero-recoil configuration.

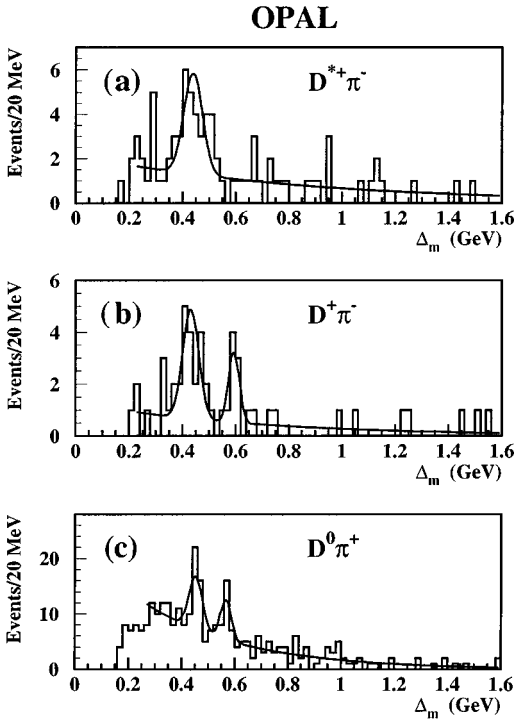


FIG. 35. OPAL search for  $B \rightarrow D_1 X \ell^- \bar{\nu}$  and  $B \rightarrow D_2^* X \ell^- \bar{\nu}$ . The mass difference plots are (a)  $\Delta_m = (D^{*+} \pi^-) - M(D^{*+})$ , (b)  $\Delta_m = M(D^+ \pi^-) - M(D^+)$ , and (c)  $\Delta_m = M(D^0 \pi^+) - M(D^0)$ . The  $D_2^*$  can decay directly to  $D \pi$ , and the peaks in (b) and (c) at  $\Delta_m \approx 590 \text{ MeV}/c^2$  are attributed to  $D_2^{*0}$  and  $D_2^{*+}$  decays, respectively. The lower peaks, at masses from  $410 \text{ MeV}/c^2$  to  $450 \text{ MeV}/c^2$  in all three plots, are attributed to a mixture of  $D_1$  and  $D_2^*$  decays.

Before turning to measurements of  $|V_{cb}|$  using the high- $q^2$  region in  $B \rightarrow D^* \ell^- \bar{\nu}$  decays, we briefly discuss measurements using semileptonic branching fractions. Table XXXIX lists the model predictions for the parameter  $\gamma_c$  needed to extract  $|V_{cb}|$  from the measured decay rates for  $B \rightarrow D \ell^- \bar{\nu}$  and  $B \rightarrow D^* \ell^- \bar{\nu}$ . The table also lists the values of  $|V_{cb}|$  obtained using the branching fractions from Table XXXV, together with the 1994 PDG  $B$  lifetime values. Although these results give us a reasonable idea of  $|V_{cb}|$ , it is very difficult to assign an uncertainty to the assumptions built into the models. We therefore do not include theory-related errors on the values of  $|V_{cb}|$  quoted in this table.

We now consider determinations of  $|V_{cb}|$  using the high- $q^2$  region of the decay  $B \rightarrow D^* \ell^- \bar{\nu}$ , an approach that was emphasized initially by Neubert (1991), but which has since been studied by many others as well. In the heavy-quark symmetry limit, all three of the  $B \rightarrow D^* \ell^- \bar{\nu}$  form factors are related to the Isgur-Wise function  $\xi(w)$  [see Eq. (100)]. In this limit, one also obtains the extremely important result that the value of  $\xi(w)$  at the zero-recoil point,  $w=1$ , is known:  $\xi(1)=1$ . This result follows from the fact that, if both the bottom and charm quark masses are taken to be very heavy, the light constituents of the hadron are essentially undisturbed by the  $b \rightarrow c$  transition at  $w=1$ , and there is complete overlap between the initial and final hadronic state. However, we shall see that the corrections to the heavy-quark symmetry limit at  $w=1$  are not so small that they can be neglected. The corrections have now been calculated by several theorists, and there is some confidence that the results are reliable to within the stated uncertainties.

Prior to the development of HQET, the decay  $B \rightarrow D \ell^- \bar{\nu}$  might have appeared simpler than  $B \rightarrow D^* \ell^- \bar{\nu}$  from a theoretical perspective, because it is governed by only one form factor. However, corrections to the prediction  $\xi(1)=1$  for  $B \rightarrow D^* \ell^- \bar{\nu}$  are constrained by Luke's theorem (Luke, 1990), which protects the form factors  $h_+$  and  $h_{A_1}$  from  $1/m_Q$  corrections at zero recoil. The form factors  $h_-$ ,  $h_V$ ,  $h_{A_2}$ , and  $h_{A_3}$ , however, do have  $1/m_Q$  corrections at this point. In  $B \rightarrow D^* \ell^- \bar{\nu}$ , only  $h_{A_1}$  affects the rate at  $w=1$ , since the other form factors are multiplied by various powers of  $w-1$  [see Eqs. (117) and (118)]. Thus the heavy-quark symmetry prediction for the  $B \rightarrow D^* \ell^- \bar{\nu}$  rate escapes  $1/m_Q$  corrections at  $w=1$ , and the leading corrections arise at order  $1/m_Q^2$ . In contrast, both  $h_+$  and  $h_-$  affect the  $B \rightarrow D \ell^- \bar{\nu}$  rate at zero recoil, so the heavy-quark symmetry prediction for this mode does have  $1/m_Q$  corrections. Furthermore,  $B \rightarrow D^* \ell^- \bar{\nu}$  is much easier to study experimentally than  $B \rightarrow D \ell^- \bar{\nu}$  because the rate is larger and the backgrounds are smaller.

The differential decay rate for  $B \rightarrow D^* \ell^- \bar{\nu}$  with respect to  $w$  is given by

$$\frac{1}{\tau_B} \frac{dB(\bar{B}^0 \rightarrow D^* \ell^- \bar{\nu})}{dw} = \frac{G_F^2}{48\pi^3} m_{D^*}^3 (m_B - m_{D^*})^2 \sqrt{w^2 - 1} (w+1)^2 \times \left[ 1 + \frac{4w}{w+1} \frac{1-2wr+r^2}{(1-r)^2} \right] |V_{cb}|^2 \mathcal{F}(w)^2, \quad (150)$$

where  $r = m_{D^*}/m_B$  and  $w$  is given by Eq. (91). In the analysis of Neubert (1994b), the function  $\mathcal{F}(w)$  is written as the

product of a perturbative QCD correction factor  $\eta_A = 0.985 \pm 0.015$  and a function of the form factors called  $\hat{\xi}(w)$ :

$$\mathcal{F}(w) = \eta_A \hat{\xi}(w). \quad (151)$$

In the heavy-quark symmetry limit,  $\hat{\xi}(w)$  becomes the Isgur-Wise function  $\xi(w)$ . Both  $\hat{\xi}(w)$  and  $\xi(w)$  are often written as an expansion in  $w$ ; for example,

$$\hat{\xi}(w) = \hat{\xi}(1) \{ 1 - \hat{\rho}^2 (w-1) + \mathcal{O}[(w-1)^2] \}. \quad (152)$$

The result in Eq. (150) can be obtained by integrating the differential decay-rate formula, Eq. (117), over all variables except  $q^2$ , substituting the helicity amplitudes given in Eq. (118), and performing a change of variable from  $q^2$  to  $w$ . Following this procedure, one would discover that the resulting expression for  $d\Gamma/dw$  depends explicitly on  $R_1$ ,  $R_2$ , and  $h_{A_1}$ . The function  $\hat{\xi}(w)$  in Eq. (150) is defined such that it contains all of this dependence. It is related to  $h_{A_1}(w)$  by a somewhat complicated expression involving  $R_1$  and  $R_2$ , through the helicity amplitudes  $H_i$ :

$$\hat{\xi}^2(w) = \frac{\sum_i |\tilde{H}_i(w)|^2}{\left[ 1 + \frac{4w}{w+1} \frac{1-2wr+r^2}{(1-r)^2} \right]} \eta_A^{-2} |h_{A_1}(w)|^2, \quad (153)$$

where

$$\tilde{H}_i(w) = \frac{H_i(w)}{(m_B - m_{D^*}) \sqrt{m_B m_{D^*} / q^2(w)} (w+1) h_{A_1}(w)}. \quad (154)$$

In the heavy-quark symmetry limit  $R_1 = R_2 = 1$ , and these complications disappear, yielding  $\hat{\xi}(w) = h_{A_1}(w)$ .

Thus, if we wish to consider the corrections to the heavy-quark symmetry limit,  $\hat{\xi}(w)$  should be regarded as a quantity that depends on all three form factors,  $h_{A_1}$ ,  $h_{A_2}$ , and  $h_V$ , since the  $H_i(w)$  depend on  $R_1(w)$  and  $R_2(w)$ . CLEO has in fact measured both the slope  $\hat{\rho}^2$  of  $\hat{\xi}(w)$  [using Eq. (150)] and the slope  $\rho_{A_1}^2$  of  $h_{A_1}$  [using the full differential decay distribution Eq. (113) with Eqs. (116) and (115)], so it is useful to relate these quantities (Neubert, 1994b):

$$\Delta \rho^2 = \hat{\rho}^2 - \rho_{A_1}^2 = -\frac{1}{6} (R_1^2 - 1) - \frac{1}{3} \frac{m_B}{m_B - m_{D^*}} (1 - R_2). \quad (155)$$

The form factor  $h_{A_1}$  can be related to the Isgur-Wise function  $\xi(w)$ , but this relation involves subtleties of renormalization dependence. Neubert gives the relation between the slopes

$$\rho_{A_1}^2 = \rho^2 + (0.21 \pm 0.02) + \mathcal{O}(1/m_Q), \quad (156)$$

where  $\rho^2$  is the slope of  $\xi(w)$ . The differences in definitions among different authors for various versions of the Isgur-Wise function can sometimes be difficult to follow, but with the present precision of the measurements, it is already becoming important to keep track of them.

The calculation of  $\mathcal{F}(1)$  has been the subject of many investigations. While the perturbative QCD effects do not present serious problems, calculation of the  $1/m_Q^2$  corrections for  $B \rightarrow D^* \ell^- \bar{\nu}$  is far from trivial and involves some model

TABLE XL. Calculations of the quantity  $\mathcal{F}(1)$ , which is used to extract  $|V_{cb}|$  from measurements of  $B \rightarrow D^* \ell^- \bar{\nu}$  at the zero-recoil point. The value from Neubert (1994b) supersedes that from Neubert (1994c).

Reference	$\mathcal{F}(1)$
Mannel, 1994	$0.96 \pm 0.03$
Neubert, 1994c	$0.97 \pm 0.04$
Neubert, 1994b	$0.93 \pm 0.03$
Shifman <i>et al.</i> , 1995	$0.89 \pm 0.03$

dependence. Table XL lists theoretical predictions for  $\mathcal{F}(1)$ , which we shall use to extract  $|V_{cb}|$  from the  $B \rightarrow D^* \ell^- \bar{\nu}$  measurements. It is evident that there is a significant spread among the estimates of  $\mathcal{F}(1)$ , and that taking  $\mathcal{F}(1) = 1$  would not be an adequate approximation. The calculation of the  $1/m_Q^2$  corrections is an active area of research, and their reliability should continue to improve.

These predictions can be used to determine  $|V_{cb}|$  by measuring the rate at zero recoil. Strictly speaking, however, phase space goes to zero for this configuration. (In Fig. 3, the area of the region within the Dalitz-plot boundary becomes smaller as  $q^2$  increases.) Thus the best one can do is to measure the rate in a small region of phase space below  $q_{\max}^2$  ( $w = 1$ ). Unfortunately, current data samples are not large enough to restrict the measurement to such a small region. Instead, one measures the rate as a function of  $q^2$  (or  $w$ ) and then extrapolates to  $q_{\max}^2$ . This technique uses the full statistical power of the data sample, but it introduces some model dependence, because the exact shape of the curve used to perform the extrapolation of  $d\Gamma/dw$  is not known. The range of  $w$  is small, however, so a linear extrapolation is expected to be good. To assess the dependence of the results on the assumed shapes, other simple functions are usually tried as well.

We now consider measurements of  $d\Gamma(B \rightarrow D^* \ell^- \bar{\nu})/dw$  from ARGUS, CLEO, and ALEPH. These measurements are sensitive to the detection efficiency for the soft pion  $\pi_s$  from

the decay  $D^* \rightarrow D \pi_s$ . Recall that  $w$  is just  $\gamma_{D^*} = E_{D^*}/m_{D^*}$  in the  $B$  rest frame. The soft pion is produced nearly at rest in the  $D^*$  frame, so  $p_{\pi_s}$  in the  $B$  frame increases with  $w$ . In particular, the  $\pi_s$  momentum is lowest at  $w = 1$ , precisely where one wants the best measurement. To measure  $d\Gamma/dw$ , it is therefore crucial to have accurate knowledge of the soft-pion detection efficiency as a function of its momentum. As discussed in Sec. VI.E.3., the momenta of the soft pions in the  $B$  rest frame are nearly all below 225 MeV/ $c$ . In CLEO II, the charged-particle detection efficiency falls rapidly below 100 MeV/ $c$ . Apart from the geometric acceptance, the efficiency for detecting a 100 MeV/ $c$  charged pion is about 70% and falls to zero around 50 MeV/ $c$ . Fortunately, it is possible to measure this efficiency as a function of momentum using data by studying  $D^*$  decays in continuum events. It is also important to take into account the effects of smearing caused by the small  $B$  motion.

The situation is more favorable for the LEP experiments, where the  $B$  momentum is very high. As a result, the soft-pion detection efficiency is quite uniform in  $w$ . However, the LEP  $B$ -meson data samples are smaller, and there is uncertainty on the fraction of  $b$  quarks that hadronize into  $B$  mesons, introducing an uncertainty in the overall normalization.

Figure 36 shows the distribution of  $\mathcal{F}(w)|V_{cb}|$  from ARGUS (Albrecht *et al.*, 1993c), which performed the first measurement using this technique. Because the  $w$ -dependent coefficients in Eq. (150) have been factored out, one can read off the value of  $\mathcal{F}(1)|V_{cb}|$  from the intercept of the extrapolation. (ARGUS used  $\tau_B = 1.32$  ps, but in our summary of  $|V_{cb}|$  values we have adjusted the result to reflect more recent values of the  $B$ -meson lifetime.) It is clear from the large statistical error in the lowest bin that  $|V_{cb}|\mathcal{F}(1)$  could not be precisely determined from that bin alone. The results for various fitting functions are listed in Table XLI. There is a substantial spread in the values of both  $|V_{cb}|$  and  $\hat{\rho}^2$  obtained using different assumptions for the function  $\mathcal{F}(w)$  in the extrapolation.

Figure 37 shows the raw  $w$  distributions for the CLEO II analysis (Barish *et al.*, 1995a), which uses both  $\bar{B}^0 \rightarrow D^{*+} \ell^- \bar{\nu}$  and  $B^- \rightarrow D^{*0} \ell^- \bar{\nu}$  and has a much larger data sample. The  $B^- \rightarrow D^{*0} \ell^- \bar{\nu}$  produces a soft  $\pi^0$  rather than a soft charged pion; although the resulting photon spectrum is also soft, the CLEO II CsI calorimeter has good detection efficiency for photons with energies down to about 30 MeV, where fake photons from hadronic splittings become a problem. The  $B^- \rightarrow D^{*0} \ell^- \bar{\nu}$  channel, however, does have more background than  $\bar{B}^0 \rightarrow D^{*+} \ell^- \bar{\nu}$ , as seen from the dashed background curves in these plots. Figure 38 shows the distributions of  $\mathcal{F}(w)|V_{cb}|$ , in which the data from the two channels have been combined, backgrounds subtracted, and efficiency corrections included. The statistical errors, including that on the lowest bin, are much smaller than those in the ARGUS measurement. The data are consistent with a linear fit; a quadratic fit does not significantly change the central value of  $|V_{cb}|$ , although the uncertainty becomes somewhat larger. The CLEO II result from the linear fit yields

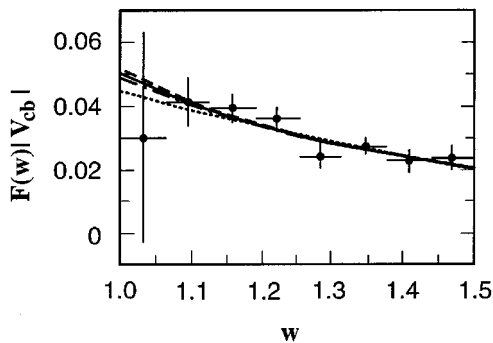


FIG. 36. The measurement of  $|V_{cb}|$  from the ARGUS distribution of  $d\Gamma(B \rightarrow D^* \ell^- \bar{\nu})/dw$ , which has been transformed to correspond to  $|V_{cb}|\mathcal{F}(w)$ . At low values of  $w$  the amount of phase space is reduced, and the statistical error becomes large. The value of  $|V_{cb}|$  is therefore obtained by extrapolating the distribution to  $w = 1$  using various assumptions for the form of  $\mathcal{F}(w)$ . The dotted line in the figure corresponds to a linear form for  $\mathcal{F}(w)$ . Redrawn from Albrecht *et al.* (1993c).

TABLE XLI. Measurements of  $\mathcal{F}(1)|V_{cb}|$  and  $\hat{\rho}^2$  using the decay  $B \rightarrow D^* \ell^- \bar{\nu}$ . By taking  $\mathcal{F}(1)$  from theoretical calculations based on HQET, one can convert these values into  $|V_{cb}|$ . The values listed in this table have been corrected to the  $B$  lifetimes given in Table III. Because the shape of the fitting function is not known, one must estimate an additional systematic error based on the differences among fit results obtained using different shapes.

Expt.	$\mathcal{F}(w)$ fit function	$\hat{\rho}^2$	$\mathcal{F}(1) V_{cb} $
ALEPH	$\mathcal{F}(1)[1 - \hat{\rho}^2(w-1)]$	$0.46 \pm 0.34$	$0.0396 \pm 0.0044 \pm 0.0037$
ARGUS	$\mathcal{F}(1)[1 - \hat{\rho}^2(w-1)]$	$1.17 \pm 0.23$	$0.040 \pm 0.005 \pm 0.003$
CLEO II	$\mathcal{F}(1)[1 - \hat{\rho}^2(w-1)]$	$0.84 \pm 0.15$	$0.0360 \pm 0.0019 \pm 0.0020$
Average	$\mathcal{F}(1)[1 - \hat{\rho}^2(w-1)]$	$0.88 \pm 0.12$	$0.0371 \pm 0.0025$
ARGUS	$\mathcal{F}(1)\exp[-\hat{\rho}^2(w-1)]$	$1.88 \pm 0.38 \pm 0.16$	$0.045 \pm 0.008 \pm 0.002$
ARGUS	$\mathcal{F}(1)[2/(w+1)]^2 \hat{\rho}^2$	$2.10 \pm 0.38 \pm 0.18$	$0.046 \pm 0.008 \pm 0.003$
CLEO II	$\mathcal{F}(1)[1 - \hat{\rho}^2(w-1) - b(w-1)^2]$	$\hat{\rho}^2 = 0.92 \pm 0.75$ $b = 0.15 \pm 1.53$	$0.0363 \pm 0.033 \pm 0.031$

$$\mathcal{F}(1)|V_{cb}| = 0.0351 \pm 0.0019(\text{stat}) \pm 0.0018(\text{sys}) \pm 0.0008(\text{lifetime}), \quad (157)$$

assuming  $\tau_{B^0} = 1.53 \pm 0.09$  ps and  $\tau_{B^+} = 1.68 \pm 0.12$  ps. Correcting this result to the Particle Data Group values of the  $B$  lifetimes used throughout this paper (see Table III) yields

$$\mathcal{F}(1)|V_{cb}| = 0.0360 \pm 0.0019(\text{stat}) \pm 0.0018(\text{sys}) \pm 0.0009(\text{lifetime}). \quad (158)$$

The ALEPH analysis (ALEPH Collaboration, 1994) yields the preliminary result

$$\mathcal{F}(1)|V_{cb}| = 0.0392 \pm 0.0044(\text{stat}) \pm 0.0035(\text{sys}), \quad (159)$$

which assumes  $\tau_{B^0} = 1.53 \pm 0.09$  ps. Here, the dominant contributions to the systematic error are from the uncertainty in the absolute efficiency, the efficiency shape, and the uncertainty on  $B(b \rightarrow \bar{B}^0)$ .

As this paper was going to press, the ALEPH Collaboration (1995) presented an updated measurement of the branching fraction for  $\bar{B}^0 \rightarrow D^{*+} \ell^- \bar{\nu}$  and an associated value of  $|V_{cb}|$ . The new values are slightly lower than those given here.

Table XLI lists the resulting values of  $\mathcal{F}(1)|V_{cb}|$ , as well as the values of  $\hat{\rho}^2$ . In the case of CLEO and ALEPH, fits to both linear and quadratic forms for  $\mathcal{F}(w)$  were performed. In CLEO, the results with the quadratic fit are slightly dif-

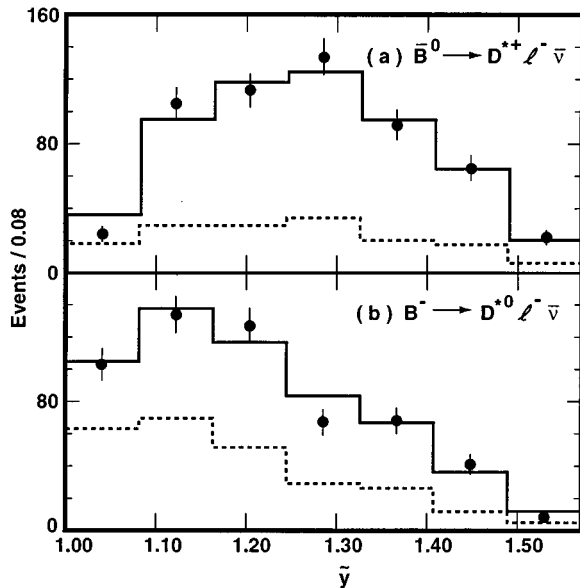


FIG. 37. The CLEO II distribution of  $d\Gamma(B \rightarrow D^* \ell^- \bar{\nu})/d\bar{y}$  for the  $|V_{cb}|$  measurement. (The variable  $\bar{y}$  is the same as  $w$ , except that it is smeared due to the  $B$  motion.) Two channels are used, (a)  $\bar{B}^0 \rightarrow D^{*+} \ell^- \bar{\nu}$  and (b)  $B^- \rightarrow D^{*0} \ell^- \bar{\nu}$ . The points with errors are the data, the dashed histogram represents the total background, and the solid histogram represents the result of a fit using the linear form  $\mathcal{F}(w) = 1 - \hat{\rho}^2(w-1)$ . Before they are used to compute  $|V_{cb}|$  these plots are corrected for efficiency, and the effects of smearing due to the  $B$  motion are taken into account.

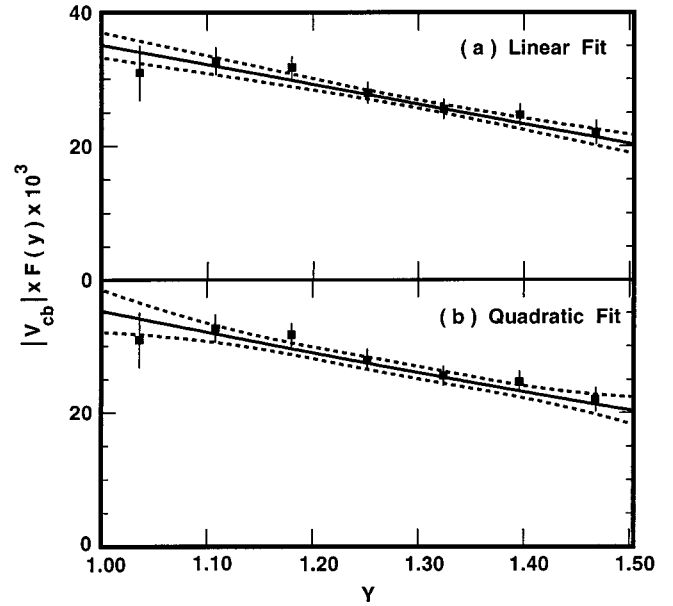


FIG. 38. The CLEO II distribution of  $|V_{cb}| \mathcal{F}(w)/10^{-3}$ , including both the  $\bar{B}^0 \rightarrow D^{*+} \ell^- \bar{\nu}$  and  $B^- \rightarrow D^{*0} \ell^- \bar{\nu}$  samples (the variable  $y$  is the same as  $w$ ): (a) the fit to a linear form for  $\mathcal{F}(w)$ ; (b) the fit assuming a quadratic form. The dotted lines show contours for  $\pm 1\sigma$  (statistical) variations in the fit parameters. The data are well described by a linear function.

TABLE XLII. Determination of  $|V_{cb}|$  using measurements of  $\mathcal{F}(1)$  from the rate at zero recoil for  $\bar{B}^0 \rightarrow D^{*+} \ell^- \bar{\nu}$  and predictions based on HQET. The first column shows the results obtained by averaging the ALEPH, ARGUS, and CLEO II values of  $\mathcal{F}(1)|V_{cb}|$  obtained from a linear fit to the data, whereas the second column is from the CLEO II fit using a quadratic fit. This fit tends to shift  $\mathcal{F}(1)|V_{cb}|$  down by about 0.001 (2.5%), which can be regarded as an estimate of the theoretical uncertainty associated with the unknown shape of  $\mathcal{F}(w)$ . The errors given in the table are the measurement error for a given fitting function and the theoretical error on  $\mathcal{F}(1)$ . Our final uncertainty on  $|V_{cb}|$ , given in Eq. (160), includes an additional contribution due to the uncertainty in the shape  $\mathcal{F}(w)$ .

$\mathcal{F}(1)$	$ V_{cb} $ using linear fit (ALEPH, ARGUS, CLEO II avg.)	$ V_{cb} $ using quadratic fit CLEO II
$0.93 \pm 0.03$ (Neubert, 1994b)	$0.040 \pm 0.003 \pm 0.001$	$0.039 \pm 0.005 \pm 0.001$
$0.96 \pm 0.03$ (Mannel, 1994)	$0.039 \pm 0.003 \pm 0.001$	$0.038 \pm 0.005 \pm 0.001$
$0.89 \pm 0.03$ (Shifman <i>et al.</i> , 1995)	$0.042 \pm 0.003 \pm 0.001$	$0.041 \pm 0.005 \pm 0.001$

ferent; for ALEPH the quadratic term is found to be zero, resulting in no shift in the central values of  $|V_{cb}| \mathcal{F}(1)$  and  $\hat{\rho}^2$ . We shall compare the values of  $\hat{\rho}^2$  with those predicted by theory in the next section, where we discuss direct measurements of the form factors.

Table XLII lists the values of  $|V_{cb}|$  obtained from the  $B \rightarrow D^{*+} \ell^- \bar{\nu}$  measurements of  $|V_{cb}| \mathcal{F}(1)$  and theoretical predictions for  $\mathcal{F}(1)$ . These results agree well with the values of  $|V_{cb}|$  obtained from the inclusive semileptonic branching fraction (Table XI) and our final inclusive value given in Eq. (78). The errors are comparable, although evaluation of the precise theoretical uncertainty in each case is difficult. We conclude that the best value of  $|V_{cb}|$  from the exclusive measurements of  $B \rightarrow D^{*+} \ell^- \bar{\nu}$  is

$$|V_{cb}| = 0.040 \pm 0.003(\text{expt}) \pm 0.001(\text{shape}) \pm 0.001(\mathcal{F}(1)). \tag{160}$$

To obtain this value, we averaged the values of  $|V_{cb}|$  obtained with the different values of  $\mathcal{F}(1)$ . The shape error is obtained from the difference between the CLEO results when linear and quadratic forms for  $\hat{\xi}(w)$  are used in the extrapolation to  $w=1$ . The error labeled  $\mathcal{F}(1)$  is simply the 3% uncertainty given by each of the theoretical groups listed in Table XLII. The experimental uncertainty on  $|V_{cb}|$  from the exclusive method should continue to improve, while improvements on the inclusive measurement will come more slowly, since systematic errors are now dominant.

### 5. Measurement of the $B \rightarrow D^{*+} \ell^- \bar{\nu}$ form factors

Given that the measurement of  $|V_{cb}|$  described in the previous section relies on HQET to predict the rate at zero recoil, the question naturally arises, to what extent can we test HQET, rather than simply assume its predictions are correct? The goal of understanding the dynamics of semileptonic bottom decays goes well beyond testing HQET, however. Although heavy-quark symmetry relates the form factors to each other, it does not predict their common  $q^2$  dependence. We should therefore like to test not only heavy-quark symmetry predictions and their corrections, but also predictions for the overall  $q^2$  variation of the form factors, which are obtained from nonperturbative methods such as lattice QCD or QCD sum rules.

Ideally, experiments would provide measurements of each form factor at every value of  $q^2$ . With present-size data samples, however, it is extremely difficult to measure the

rather mild  $q^2$  dependence of each of the three  $B \rightarrow D^{*+} \ell^- \bar{\nu}$  form factors independently. As a consequence, all of the measurements incorporate constraints (based on theoretical input) to reduce the number of degrees of freedom. It is important to be aware of these constraints when assessing the implications of the measurements.

In the decay  $B \rightarrow D^{*+} \ell^- \bar{\nu}$ , the  $q^2$  range is small, and theoretical predictions indicate that the variation of the form factors should be well approximated by linear functions. This conclusion is consistent with measurements of  $\mathcal{F}(w)$  (see Fig. 38), which is well described by a linear function of modest slope. Thus, with sufficiently large data samples, one would allow five parameters to vary in the fit: two form-factor ratios  $R_1(w=1)$  and  $R_2(w=1)$  and three form-factor slopes. (With even larger samples one might try to determine the size of the quadratic coefficients.)

For comparison, we review the constraints imposed in measurements of form factors for charm semileptonic decays. For  $D \rightarrow \bar{K}^{*0} \ell^+ \nu$ , the constraints take the form of an assumed  $q^2$  dependence for each form factor: pole forms are most often used, with pole masses taken from theory. Because these shapes are assumed, the only quantities measured are the values of the form factors at a particular value of  $q^2$ , taken mainly for historical reasons to be  $q^2=0$ . The overall scale of the form factors is determined from the decay rate, since  $|V_{cs}|$  is independently known from CKM unitarity or charm production in neutrino-nucleon scattering. The shapes of the kinematic distributions are therefore used to determine two parameters, the ratios,  $A_2(0)/A_1(0)$  and  $V(0)/A_1(0)$ . The decay  $D \rightarrow \bar{K}^{*0} \ell^+ \nu$ , where there is only one form factor, is the only  $D$  decay mode in which the pole mass has been determined from a fit.

At present, the size of even the CLEO II data sample permits statistically meaningful information to be extracted for at most three parameters. These are selected to be  $R_1(w=1)$ ,  $R_2(w=1)$ , and a single slope parameter  $\rho_{A_1}^2$ , whose variation with  $w$  is assumed to be given by the linear form  $h_{A_1}(w) = [1 - \rho_{A_1}^2(w-1)]$ . From Eq. (106),  $A_1$ ,  $A_2$ , and  $V$  are then given by the forms

$$A_1(q^2) = \left[ 1 - \frac{q^2}{(M+m_\nu)^2} \right] R^{*-1} [1 - \rho_{A_1}^2(w-1)],$$

$$A_2(q^2) = R_2(1) R^{*-1} [1 - \rho_{A_1}^2(w-1)],$$

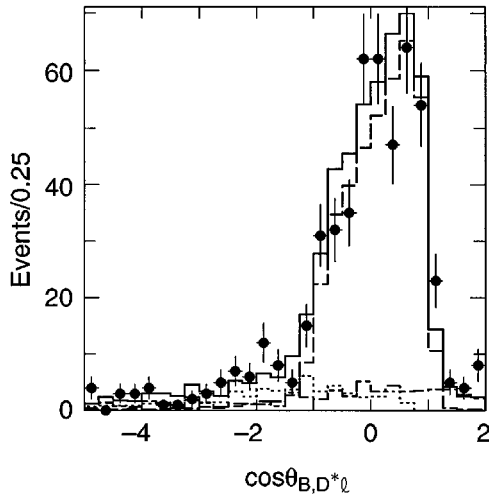


FIG. 39. The distribution of  $\cos\theta_{B,D^*l}$ , defined in Eq. (134), from the CLEO II form-factor analysis of  $\bar{B}^0 \rightarrow D^{*+} l^- \bar{\nu}$ . The data are represented by points with error bars and are from the electron channel with  $D^0 \rightarrow K^- \pi^+$ . (The form-factor analysis also uses events with muons and the  $D^0 \rightarrow K^- \pi^+ \pi^0$  channel.) The broad peak in the physical region  $|\cos\theta_{B,D^*l}| \leq 1.0$  is due to the signal. The dashed line is a prediction for the signal shape based on the ISGW Monte Carlo (although this shape does not depend significantly on the model); the dot-dashed line represents the combinatorial background under the  $D^{*+}$  signal; the dotted line is the estimated  $B \rightarrow D^{*+} l^- \bar{\nu}$  background (also simulated with the ISGW Monte Carlo); and the solid histogram is the sum of the absolutely normalized backgrounds plus the Monte Carlo signal shape, normalized to give the correct total number of events.

$$V(q^2) = R_1(1)R^{*-1} [1 - \rho_{A_1}^2(w-1)], \quad (161)$$

where  $R^* = 2\sqrt{Mm_\nu/(M+m_\nu)}$ . These relations neglect the symmetry-breaking corrections to the predictions for the slopes, but allow for such corrections to  $R_1(1) = R_2(1) = 1$ . A justification for this procedure is that, for the typical value of  $w-1 = 0.25$ , the leading corrections to the slopes are expected to be smaller than the leading corrections to  $R_1(1)$  and  $R_2(1)$  [see Eq. (104)]. With more data, these assumptions could be removed.

Both ARGUS (Albrecht, 1993c) and CLEO (Bortoletto *et al.*, 1989; Sanghera *et al.*, 1993; Avery *et al.*, 1994a) have used measurements of kinematic distributions to obtain information on the form factors for  $B \rightarrow D^* l^- \bar{\nu}$ . The first complete analysis using all of the kinematic variables, including their correlations, has been performed (Avery, 1994a) with the CLEO II detector. We consider this analysis in some detail. After background subtraction, there are 656 signal events in the channel  $\bar{B}^0 \rightarrow D^{*+} l^- \bar{\nu}$ ,  $D^{*+} \rightarrow D^0 \pi^+$ , where  $D^0 \rightarrow K^- \pi^+$  or  $D^0 \rightarrow K^- \pi^+ \pi^0$ . The backgrounds, which total 127 events, arise mainly from combinatorial background under the  $D^{*+}$  peak and  $B \rightarrow D^{*+} l^- \bar{\nu}$  decays. Figure 39 shows the signal in the electron channel for  $\bar{B}^0 \rightarrow D^{*+} l^- \bar{\nu}$  in the  $D^0 \rightarrow K^- \pi^+$  mode.

To extract the parameters in Eq. (161), CLEO fits the joint distribution in  $q^2$ ,  $\cos\theta_l$ ,  $\cos\theta_\nu$ , and  $\chi$ , which were defined in Fig. 24. It is important to incorporate the effects of detector acceptance and smearing, so a Monte Carlo technique is used to evaluate the likelihood function in the fit. Figures

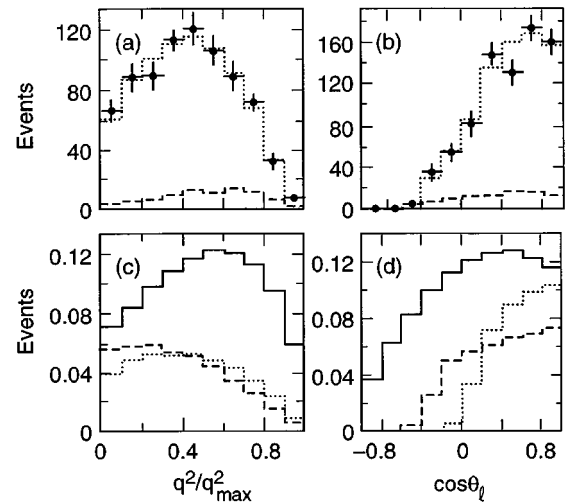


FIG. 40. Distributions of  $q^2$  and  $\cos\theta_l$  from the CLEO II form-factor analysis of  $\bar{B}^0 \rightarrow D^{*+} l^- \bar{\nu}$ . In plots (a) and (b), the points with error bars are the data, the dotted histograms show the maximum-likelihood form-factor fit, and the dashed histograms show the estimated background contribution. These distributions are affected by large acceptance corrections. Although these corrections are taken into account by the fitter, they make it difficult to interpret the observed distributions directly. Plots (c) and (d) show the acceptance for electron events (dashed histogram) and muon events (dotted histogram), as well as the theoretical distributions corresponding to the measured values of the form factors (solid histogram). The efficiency at high values of  $q^2$  is lower than that at low values because the  $D^{*+}$  is nearly at rest at high  $q^2$ , producing a very soft pion  $\pi_s^+$  from the decay  $D^{*+} \rightarrow D^0 \pi_s^+$ . The efficiency for detecting a lepton with a negative value of  $\cos\theta_l$  is much smaller than that for detecting a lepton with a positive value because those with negative values have lower momentum in the lab frame. The overall scale of the plots in (c) and (d) is arbitrary.

40(a) and 40(b) show the observed distributions of  $q^2$  and  $\cos\theta_l$ , together with the fit result and background level. Although the fits describe the data well, the distributions are strongly affected by acceptance and are difficult to interpret directly. Figures 40(c) and 40(d) show the shape of the acceptance curves for these two variables. The main effects are due to the fall in detection efficiency for very low-momentum pions and for leptons whose momenta are below the cuts ( $p_e > 1.0$  GeV/c,  $p_\mu > 1.4$  GeV/c). These plots also show the shapes for  $q^2$  and  $\cos\theta_l$  as they would appear for a perfect detector, assuming the values of  $R_1$ ,  $R_2$ , and  $\rho_{A_1}^2$  that were obtained from the fit.

A large amount of information is extracted from the correlations among the variables. Figures 41(a) and 41(b) show the distributions of  $\cos\theta_\nu$  for the lower and upper half of the  $q^2$  range. The difference in the  $\cos\theta_\nu$  distributions for these ranges can be easily understood from the differential decay distribution, Eq. (113). At  $q^2 = 0$ , the lepton and neutrino are nearly parallel, and their opposite helicities require that the  $D^*$  must have helicity zero. The helicity-zero component is therefore prominent at low  $q^2$  (see also Fig. 25). It yields a distribution of  $\cos\theta_\nu$  proportional to  $\cos^2\theta_\nu$ , which produces the peaking at large values of  $|\cos\theta_\nu|$ . The region near  $\cos\theta_\nu = +1$  is somewhat depleted relative to that at  $\cos\theta_\nu = -1$ . This depletion is due to the fact that

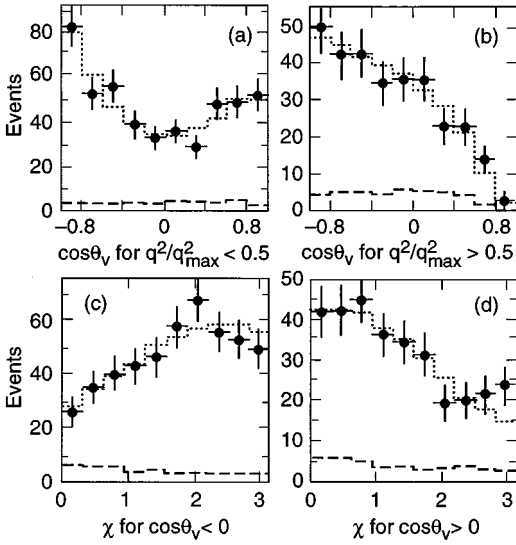


FIG. 41. Distributions of  $\cos\theta_V$  and  $\chi$  from the CLEO II form-factor analysis of  $\bar{B}^0 \rightarrow D^{*+} \ell^- \bar{\nu}$ . The points with error bars are data, the dotted histograms are the result of the form-factor fit, and the dashed histograms represent the background contribution. Plots (a) and (b) show the distributions of  $\cos\theta_V$  in two  $q^2$  regions:  $q^2/q_{\max}^2 < 0.5$  and  $q^2/q_{\max}^2 > 0.5$ . The lower region contains a much stronger helicity-zero component, which produces a  $\cos^2\theta_V$  behavior. Plots (c) and (d) show the  $\chi$  angle for two regions of  $\cos\theta_V$ :  $\cos\theta_V < 0$  and  $\cos\theta_V > 0$ . The opposite-sign slopes in these two regions results from a quantum interference term proportional to  $(H_- - H_+)H_0$ . These two plots would be interchanged if the  $W$  couplings were of the form  $(V \mp A)(V \pm A)$ .

$\cos\theta_V = +1$  corresponds to forward-going  $D^0$ 's in the  $D^{*+}$  rest frame, or backward-going pions, which therefore have lower momentum and lower detection efficiency in the lab frame. In the upper  $q^2$  region, the helicity  $+1$  and  $-1$  components of the  $D^*$  become more important, and at  $q_{\max}^2$ , all three components are present with equal probability, resulting in a uniform  $\cos\theta_V$  distribution. In the upper half of the  $q^2$  range, the  $\cos\theta_V$  distribution shows a convolution of these effects with the acceptance.

Figures 41(c) and 41(d) show the azimuthal angle  $\chi$  for the lower and upper half of the  $\cos\theta_V$  range. The striking

difference between these two plots is the result of the interference term in Eq. (113) proportional to  $[H_+(q^2) - H_-(q^2)]H_0(q^2)$ . The difference  $H_+ - H_-$  is large and negative as a consequence of the  $V-A$  coupling at the  $b \rightarrow c$  vertex, as discussed in Sec. VI.A. The observed effect would actually be the same if the couplings at the two  $W$  vertices were  $(V+A)(V+A)$  instead of  $(V-A)(V-A)$ , but the two plots would be interchanged if the couplings were  $(V \pm A)(V \mp A)$ . These mixed couplings are clearly inconsistent with the data. [For discussions of the chirality of  $b$  quark couplings, see Gronau and Wakaizumi (1992) and Gronau (1994)].

The preliminary values of  $R_1$ ,  $R_2$ , and  $\rho_{A_1}^2$  are given in Table XLIII. Although the errors on  $R_1$  and  $R_2$  are fairly large, the values are consistent with HQET-based results, which predict  $R_1 > R_2$  [see Eq. (103)]. The measurement of  $\rho_{A_1}^2$  is fairly precise, even though  $R_1$  and  $R_2$  are simultaneously determined from the fit. For the measured values of  $R_1$  and  $R_2$ , Eq. (155) predicts a downward shift from  $\rho_{A_1}^2$  to  $\hat{\rho}^2$  of about 0.3, consistent with CLEO measurements.

Information related to the form factors has also been extracted in earlier CLEO measurements and by ARGUS. The measured quantities are the lepton forward-backward asymmetry  $\bar{A}_{FB}$ , defined in Eq. (121), and the  $D^*$  polarization parameter  $\bar{A}_{pol}$  (often called  $\alpha$ ), defined in Eq. (122). In the ARGUS analysis (Albrecht *et al.*, 1993c), the kinematic distributions are fitted directly to models in which the only free parameters are form-factor ratios. The values of  $\bar{A}_{FB}$  and  $\bar{A}_{pol}$  are then derived from each model using the fitted values for the form factors. Thus the dependence of  $\bar{A}_{FB}$  and  $\alpha$  on the lepton-momentum cut is removed model by model. ARGUS finds that their values of  $\bar{A}_{FB}$  and  $\bar{A}_{pol}$  are insensitive to the model used. (They do not quote the form-factor ratios obtained from the fits.) Table XLIV lists all of the measurements of  $\bar{A}_{FB}$  and  $\bar{A}_{pol}$ , including those that are derived from the CLEO II form-factor measurement described above.

As this paper was going to press, CLEO presented (Gronberg, 1995) an updated set of form-factor measurements that differ slightly from those given here.

TABLE XLIII. CLEO II preliminary results on the form-factor parameters  $R_1$ ,  $R_2$  and the slope  $\rho_{A_1}^2$  for  $\bar{B}^0 \rightarrow D^{*+} \ell^- \bar{\nu}$ . The first error is statistical and the second is systematic. In calculating the errors on quantities derived from the form factors, it is important to take into account the correlations between the errors. The correlation coefficients are  $C(R_1 R_2) = -0.83$ ,  $C(R_1 \rho^2) = -0.63$ , and  $C(R_2 \rho^2) = -0.82$ . Although we have reported the predictions of the ISGW, KS, and WSB models for comparison, the relative  $q^2$  dependence of  $A_1$  to that of the other form factors in these models is not consistent with HQET, and it is not what is assumed in the fit (see Sec. VI.A.3). Thus, although the comparison below focuses on the values of the form factors at a particular point, the shapes are also somewhat different among the models.

	CLEO II Measurement	Neubert (1994b) (HQET)	Close and Wambach (1994a, 1994b) (HQET)	ISGW	KS	WSB
$R_1(1)$	$1.30 \pm 0.36 \pm 0.16$	1.35	1.15	1.27	1.00	1.09
$R_2(1)$	$0.64 \pm 0.26 \pm 0.12$	0.79	0.91	1.14	1.00	1.06
$\rho_{A_1}^2$	$1.01 \pm 0.15 \pm 0.09$					

TABLE XLIV. Comparison of  $\bar{A}_{\text{FB}}$  and  $\bar{A}_{\text{pol}}$  from different experiments. The earlier CLEO measurements quote the observed asymmetry and polarization for the lepton momentum cut given in the table. The ARGUS results were obtained using models to extrapolate over the full lepton-momentum range and can therefore be directly compared to this measurement and the theoretical prediction based on HQET. The CLEO II results are preliminary.

	$\bar{A}_{\text{FB}}$	$\bar{A}_{\text{pol}}$
ARGUS (Albrecht <i>et al.</i> , 1993c)	$0.20 \pm 0.08 \pm 0.06$	$1.1 \pm 0.4 \pm 0.2$
CLEO (Sanghera <i>et al.</i> , 1993; Bortoletto <i>et al.</i> , 1989)	$0.14 \pm 0.06 \pm 0.03$ $p_{\ell} > 1 \text{ GeV}/c$	$0.65 \pm 0.66 \pm 0.25$ $p_{\ell} > 1.4 \text{ GeV}/c$
CLEO II (Avery <i>et al.</i> , 1994a)	$0.209 \pm 0.034 \pm 0.015$	$1.48 \pm 0.32 \pm 0.14$
HQET (Neubert, 1994c) ( $\rho^2 = 1.0$ )	0.22	1.37

### F. Exclusive $b \rightarrow u$ semileptonic decays of bottom mesons and $|V_{ub}|$

The measurement of exclusive  $B \rightarrow X_u \ell^- \bar{\nu}$  decays is one of the major goals of  $B$  physics. With improvements in lattice QCD and other theoretical methods, the uncertainties in predicting the rate for exclusive  $B \rightarrow X_u \ell^- \bar{\nu}$  modes may become smaller than those for the inclusive end-point spectrum, and hence provide a more precise value of  $|V_{ub}|$ .

For  $B \rightarrow X_u \ell^- \bar{\nu}$  decays, unlike  $B \rightarrow X_c \ell^- \bar{\nu}$ , model predictions indicate that the rate should be distributed over many exclusive channels, with no dominant modes. The hadronic system  $X_u$  can range over much of the light-quark hadron spectrum, including radially excited and  $p$ -wave mesons. However, this picture is somewhat modified for the lepton-spectrum end-point region, where the backgrounds from  $B \rightarrow X_c \ell^- \bar{\nu}$  are suppressed and experimental sensitivity is best. In this region, theoretical models indicate that a small number of exclusive decays are dominant:  $B^- \rightarrow \rho^0 \ell^- \bar{\nu}$ ,  $\bar{B}^0 \rightarrow \rho^+ \ell^- \bar{\nu}$ ,  $B^- \rightarrow \omega \ell^- \bar{\nu}$ , and, to a lesser extent,  $\bar{B}^0 \rightarrow \pi^+ \ell^- \bar{\nu}$  and  $B^- \rightarrow \pi^0 \ell^- \bar{\nu}$ . A key prediction underlying this conclusion is that the lepton spectra for the decays to final states with vector mesons are expected to peak at very high energy. For example, in the ISGW, KS, and WSB models, the fraction of the leptons from these decays with  $E > 2.0 \text{ GeV}/c$  is 0.72, 0.68, and 0.52, respectively. Although  $B \rightarrow \pi \ell^- \bar{\nu}$  also contributes to the end-point region, it is expected to have both a smaller overall rate and a softer lepton momentum spectrum. (The basic reasons for this result are discussed in Sec. II.C, and examples of predicted spectra are given in Fig. 7.) At present, there are large un-

certainties in the theoretical predictions for all  $B \rightarrow X_u \ell^- \bar{\nu}$  modes, as well as uncertainty in the size of the contribution from nonresonant  $B \rightarrow \pi \pi \ell^- \bar{\nu}$  decays (see Sec. V.E). Table XLV gives some of the theoretical predictions for exclusive rates in terms of  $\gamma_u$ , where the decay rate is  $\Gamma = \gamma_u |V_{ub}|^2$ .

The application of HQET to  $b \rightarrow u \ell^- \bar{\nu}$  is much more limited than it is for  $b \rightarrow c \ell^- \bar{\nu}$  decays, since the  $u$  quark is not heavy compared to  $\Lambda_{\text{QCD}}$ . Nevertheless, HQET does provide useful insights. In particular, there is a strong interest in relating the form factors for  $B \rightarrow \pi \ell^- \bar{\nu}$  to those for  $D \rightarrow \pi \ell^+ \nu$  and the form factors for  $B \rightarrow \rho \ell^- \bar{\nu}$  to those for  $D \rightarrow \rho \ell^+ \nu$  or  $D \rightarrow \bar{K}^* \ell^+ \nu$ . The technical issues are discussed by several authors, and we refer the reader to the references for details (Dib and Vera, 1993; Burdman *et al.*, 1994). The lattice QCD Collaboration APE (Allton *et al.*, 1995) has used HQET-based scaling laws to extrapolate their form-factor results for  $D$  semileptonic decays to obtain predictions for  $B \rightarrow \rho \ell^- \bar{\nu}$  and  $B \rightarrow \pi \ell^- \bar{\nu}$ . Their prediction for  $B \rightarrow \pi \ell^- \bar{\nu}$ , given in Table XLV, is similar to most of the quark-model predictions.

The rates for  $B^- \rightarrow \rho^0 \ell^- \bar{\nu}$  and  $\bar{B}^0 \rightarrow \rho^+ \ell^- \bar{\nu}$  are connected by isospin symmetry, since the  $B^-$  and  $\bar{B}^0$  have the same space and spin-wave functions in this limit, as do the  $\rho^0$  and  $\rho^+$ . Although the rate for  $B^- \rightarrow \omega \ell^- \bar{\nu}$  cannot be related to these by a flavor symmetry, it is expected in the quark model to be approximately equal to that for  $B^- \rightarrow \rho^0 \ell^- \bar{\nu}$ . Thus

$$\Gamma(\bar{B}^0 \rightarrow \rho^+ \ell^- \bar{\nu}) = 2\Gamma(B^- \rightarrow \rho^0 \ell^- \bar{\nu}) \approx 2\Gamma(B^- \rightarrow \omega \ell^- \bar{\nu}). \quad (162)$$

TABLE XLV. Theoretical predictions for  $\bar{B}^0 \rightarrow \rho^+ \ell^- \bar{\nu}$  and  $\bar{B}^0 \rightarrow \pi^+ \ell^- \bar{\nu}$ . (The rates for  $B^- \rightarrow \rho^0 \ell^- \bar{\nu}$  and  $B^- \rightarrow \omega \ell^- \bar{\nu}$  are half as large.) The factor  $\gamma_u$  is used to predict the partial decay rate using  $\Gamma = \gamma_u |V_{ub}|^2$ . The branching fractions  $B(\rho^+)$  and  $B(\pi^+)$  are calculated using  $B = \gamma_u |V_{ub}|^2 \tau_B$  with  $|V_{ub}| = |V_{cb}| (|V_{ub}|/|V_{cb}|) = 0.04 \times 0.08 = 0.0032$  and  $\tau_B = 1.54 \text{ ps}$ .

Model	$\gamma_u(\rho^+)/10^{12} \text{ s}^{-1}$	$\gamma_u(\pi^+)/10^{12} \text{ s}^{-1}$	$B(\rho^+)/10^{-4}$	$B(\pi^+)/10^{-4}$
ISGW	8.3	2.1	1.3	0.33
ISGW2	14.2	9.6	2.2	1.5
KS	32.9	7.25	5.2	1.1
WSB	18.7	6.32	3.0	1.0
Lattice (APE)		$8 \pm 4$		$1.3 \pm 0.6$

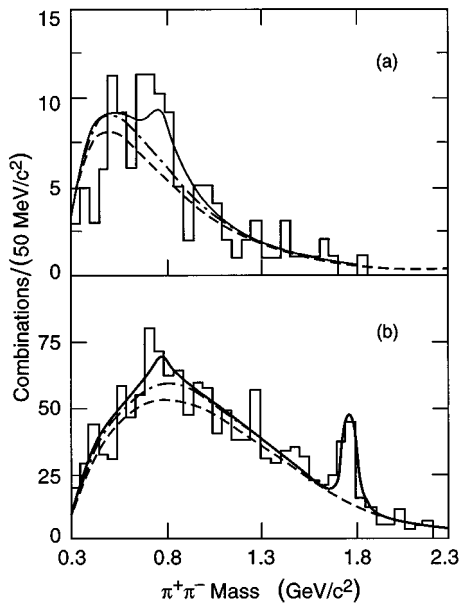


FIG. 42. The CLEO II  $\pi^+\pi^-$  mass spectra from searches for  $B^- \rightarrow \rho^0 \ell^- \bar{\nu}$ . The upper spectrum is for leptons in the range  $E_\gamma > 2.3$  GeV, in which the background is dominated by continuum events, while the lower spectrum is for the range  $2.0 < E_\gamma < 2.3$  GeV, in which the background is predominantly due to  $B \rightarrow X_c \ell^- \bar{\nu}$  decays. In each plot, the dashed curve is the estimated background, except for the contribution of combinatoric background that would arise in  $B^- \rightarrow \rho^0 \ell^- \bar{\nu}$  events themselves (dot-dashed line). The solid curve is the total, including a  $B^- \rightarrow \rho^0 \ell^- \bar{\nu}$  contribution that is not statistically significant. In the lower plot, the peak just below 1.8  $\text{GeV}/c^2$  is due to  $D^0 \rightarrow K^- \pi^+$  decays in which the charged kaon was misidentified as a pion.

Experimentally, the  $B^- \rightarrow \omega \ell^- \bar{\nu}$  channel has the advantage of the narrow  $\omega$  mass peak, but it has a lower reconstruction efficiency than the  $B^- \rightarrow \rho^0 \ell^- \bar{\nu}$  decay due to the larger number of final-state particles. Isospin symmetry also predicts that the rate for  $B^- \rightarrow \pi^0 \ell^- \bar{\nu}$  is half that for  $\bar{B}^0 \rightarrow \pi^+ \ell^- \bar{\nu}$ .

Both CLEO and ARGUS have searched for exclusive  $B \rightarrow X_u \ell^- \bar{\nu}$  decays. Although ARGUS (Albrecht *et al.*, 1991a) observed a small number of candidate events consistent with particular  $B \rightarrow X_u \ell^- \bar{\nu}$  modes, there have been no established signals until recently. Using a sample of

$2.2 \times 10^6 B\bar{B}$  pairs, CLEO has presented (Gibbons, 1995) the first measurement of  $B \rightarrow \pi \ell^- \bar{\nu}$ . The most sensitive limits on  $B \rightarrow \rho \ell^- \bar{\nu}$  and  $B^- \rightarrow \omega \ell^- \bar{\nu}$  have also been obtained by CLEO; these results are inconsistent with a preliminary (unpublished) branching fraction for  $B^- \rightarrow \rho^0 \ell^- \bar{\nu}$  from ARGUS (Paulini, 1991). We first describe the  $B \rightarrow \rho \ell^- \bar{\nu}$  and  $B^- \rightarrow \omega \ell^- \bar{\nu}$  analyses and then turn to the new results on  $B \rightarrow \pi \ell^- \bar{\nu}$ .

The basic procedure in the CLEO  $B \rightarrow \rho(\omega) \ell^- \bar{\nu}$  analysis (Bean *et al.*, 1993b) is to select events whose kinematic features are consistent with a  $B \rightarrow \pi \pi \ell^- \bar{\nu}$  or  $B^- \rightarrow \pi^+ \pi^- \pi^0 \ell^- \bar{\nu}$  decay, and then to search for  $\rho^0$ ,  $\rho^\pm$ , or  $\omega$  signals in the multipion mass spectra. The  $\omega$  channel is particularly powerful, because the CLEO II CsI calorimeter provides a  $\pi^0$  mass resolution of about 5  $\text{MeV}/c^2$ , and the  $\omega$  mass peak is only slightly broadened with respect to its natural width of 8  $\text{MeV}/c^2$ . To reduce combinatoric background, extensive use is made of the constraints arising from the presence of two  $B$  mesons, each nearly at rest. Although the minimum lepton-energy cut is high (2.0 GeV), we have seen above that model predictions indicate that this cut is at least 50% efficient for the signal. In fact, most of the sensitivity in the analysis is due to the region above 2.3 GeV. In this higher region, the  $B \rightarrow X_c \ell^- \bar{\nu}$  background is small, and the dominant background is due to continuum processes. A major advantage of applying such a stringent lepton-energy cut is that one does not need Monte Carlo to determine the absolute scale of the dominant background, since the continuum contribution is measured directly by running at a center-of-mass energy about 60 MeV below the  $Y(4S)$ . A disadvantage is that the model-to-model variation in the predicted efficiency of the lepton-energy cut is significant, resulting in model dependence in the limits on the branching fractions and on  $|V_{ub}|$ .

Figure 42 shows the  $\pi^+\pi^-$  mass spectra for the CLEO II analysis. The upper plot shows events with leptons in the range  $E_\gamma > 2.3$  GeV, where the background is dominated by the continuum, and the lower plot shows events with  $2.0 < E_\gamma < 2.3$  GeV, where the background is predominantly from  $B \rightarrow X_c \ell^- \bar{\nu}$ . These mass spectra are fit to extract the contributions from  $\rho^0$  production, but in neither case is the signal statistically significant. The limits from this channel and from similar searches in the  $\bar{B}^0 \rightarrow \rho^+ \ell^- \bar{\nu}$  and  $B^- \rightarrow \omega \ell^- \bar{\nu}$  channels are listed in Table XLVI. The limits

TABLE XLVI. Branching fractions for exclusive  $B$  semileptonic decays to final states without charm. The limits on  $b \rightarrow u$  semileptonic decays from CLEO are based on efficiencies calculated using the ISGW model; other models give different lepton-energy and  $q^2$  distributions and hence somewhat different efficiencies. The results from the  $B^- \rightarrow \omega \ell^- \bar{\nu}$ ,  $B^- \rightarrow \rho^0 \ell^- \bar{\nu}$ , and  $\bar{B}^0 \rightarrow \rho^+ \ell^- \bar{\nu}$  searches can be combined statistically, since the branching fractions for these modes are related. We express this result as  $B(\bar{B}^0 \rightarrow \rho_{avg}^+ \ell^- \bar{\nu})$ .

Mode	Experiment	Ref.	Branching fraction
$B^- \rightarrow \omega \ell^- \bar{\nu}$	CLEO II	Bean <i>et al.</i> , 1993b	$< 2.1 \times 10^{-4}$ (90% C.L.)
$B^- \rightarrow \rho^0 \ell^- \bar{\nu}$	CLEO II	Bean <i>et al.</i> , 1993b	$< 2.1 \times 10^{-4}$ (90% C.L.)
$\bar{B}^0 \rightarrow \rho^+ \ell^- \bar{\nu}$	CLEO II	Bean <i>et al.</i> , 1993b	$< 4.1 \times 10^{-4}$ (90% C.L.)
$\bar{B}^0 \rightarrow \rho_{avg}^+ \ell^- \bar{\nu}$	CLEO II	Bean <i>et al.</i> , 1993b	$< 3.2 \times 10^{-4}$ (90% C.L.)
$\bar{B}^0 \rightarrow \pi^+ \ell^- \bar{\nu}$	CLEO II (prelim.)	Gibbons, 1995	$(1.19 \pm 0.41 \pm 0.28) \times 10^{-4}$

TABLE XLVII. Limits on  $|V_{ub}/V_{cb}|$  using measurements of  $B^- \rightarrow \rho^0 \ell^- \bar{\nu}$ ,  $\bar{B}^0 \rightarrow \rho^+ \ell^- \bar{\nu}$ , and  $B^- \rightarrow \omega \ell^- \bar{\nu}$ . The results from these modes have been combined statistically, which we signify by  $B(B^- \rightarrow \rho_{\text{avg}}^0 \ell^- \bar{\nu})$ . The results on  $|V_{ub}|$  have been corrected to  $\tau_B = 1.54$  ps. Model dependence in the branching fractions results from different shapes of kinematic distributions, which leads to different detection efficiencies. Model dependence in  $|V_{ub}/V_{cb}|$  is also sensitive to differences in the predicted rates, corresponding to different values of  $\gamma_u$ .

Model	$B(B^- \rightarrow \rho_{\text{avg}}^0 \ell^- \bar{\nu})/10^{-4}$ (90% C.L.)	$ V_{ub}/V_{cb} $ (90% C.L.)
ISGW	< 1.6	< 0.13
WSB	< 2.7	< 0.10
KS	< 2.3	< 0.08

assume efficiencies obtained from the ISGW model.

Since the branching fractions for these modes are related, the results from all three can be combined to obtain a statistically more sensitive limit. The limit obtained by averaging the three channels is expressed in terms of a branching fraction for  $B \rightarrow \rho_{\text{avg}}^0 \ell^- \bar{\nu}$ , where the subscript avg indicates that information from the  $\rho$  and  $\omega$  channels has been averaged. Table XLVII lists the model-dependent upper limits for the  $B^- \rightarrow \rho_{\text{avg}}^0 \ell^- \bar{\nu}$  branching fraction and for  $|V_{ub}/V_{cb}|$ . The limits for  $|V_{ub}/V_{cb}|$  range from  $|V_{ub}/V_{cb}| < 0.08$  (90% C.L.) for the KS model to  $|V_{ub}/V_{cb}| < 0.13$  for the ISGW model. These values are consistent with the CLEO II inclusive measurement (using the ISGW model) given in Table XIV. The similarity between the limits on  $|V_{ub}|$  from the exclusive searches and the measurement of  $|V_{ub}|$  from the inclusive analysis suggests that these exclusive modes may be observed in the not too distant future.

The new CLEO analysis of  $B \rightarrow \pi \ell^- \bar{\nu}$  is unusual in that it relies on the hermeticity of the detector to determine the

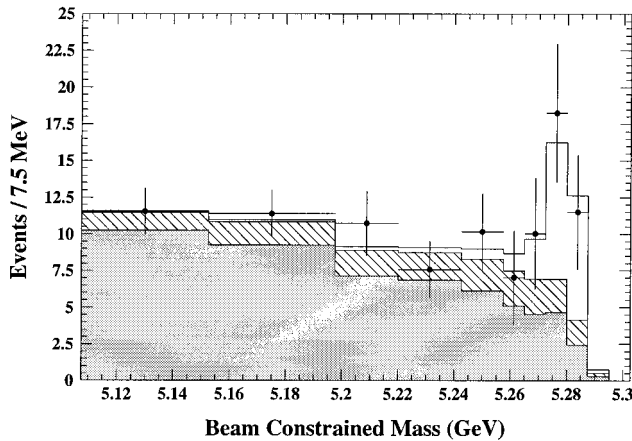


FIG. 43. The reconstructed mass spectrum from the CLEO II search for  $\bar{B}^0 \rightarrow \pi^+ \ell^- \bar{\nu}$  and  $B^- \rightarrow \pi^0 \ell^- \bar{\nu}$ . The neutrino four-momentum used to calculate  $m_B$  is estimated from the missing momentum in the event, a technique that requires careful removal of events in which there are additional unobserved particles, such as  $K_L$ 's or other neutrinos. The points with errors represent the data after subtraction of continuum background and events with fake leptons. The solid histogram shows the total fit, which includes contributions from the signal (dashed histogram, shown on top of backgrounds),  $B \rightarrow X_c \ell^- \bar{\nu}$  (shaded region), and other  $B \rightarrow X_u \ell^- \bar{\nu}$  decays (hatched region).

neutrino four-momentum; once this quantity is obtained, a  $B$  mass peak is reconstructed much as in a hadronic decay analysis. It might appear surprising that such a technique would work, since the presence of undetected particles in addition to the neutrino would distort the measurement of missing energy and momentum. Events with undetected  $K_L$ 's, for example, usually have a large missing energy, since CLEO does not have a hadronic calorimeter. However, the neutrino momentum can be determined with good resolution in a carefully selected sample of events, as we discuss below.

The missing energy and momenta of the event are defined by

$$E_{\text{miss}} = 2E_{\text{beam}} - \sum_i E_i, \quad \mathbf{p}_{\text{miss}} = - \sum_i \mathbf{p}_i, \quad (163)$$

where the index  $i$  runs over all detected charged tracks and CsI calorimeter clusters satisfying cuts designed to suppress fakes. In particular, hadronic interactions in the calorimeter often result in energy deposits that are separated somewhat from the trajectory of the track; as many of these split-off clusters are removed as possible before computing  $E_{\text{miss}}$  and  $\mathbf{p}_{\text{miss}}$ . The presence of more than one neutrino would also complicate the neutrino momentum measurement, so only events with a single lepton are used. Events are also removed if the charges of all observed tracks do not sum to zero, since there must then be at least one unobserved particle whose energy and momentum are not being accounted for. Finally, events with large missing mass are removed by requiring that  $M_{\text{miss}}^2/2E_{\text{miss}} < 300$  MeV, where  $M_{\text{miss}}^2 = E_{\text{miss}}^2 - |\mathbf{p}_{\text{miss}}|^2$ . This cut removes many of the events that contain a  $K_L$ . The cut is made on the ratio  $M_{\text{miss}}^2/2E_{\text{miss}}$ , since the resolution on  $M_{\text{miss}}^2$  scales linearly with  $E_{\text{miss}}$ . With these cuts applied, Monte Carlo studies show that the missing momentum in signal events can be measured with a resolution of roughly  $\sigma \approx 110$  MeV. Although the missing energy is used in the  $M_{\text{miss}}^2$  cut, the neutrino four-momentum used in the  $B$  reconstruction is calculated only from the missing momentum:

$$p_\nu = (|\mathbf{p}_{\text{miss}}|, \mathbf{p}_{\text{miss}}). \quad (164)$$

The resolution on  $\mathbf{p}_{\text{miss}}$  is substantially better than that on  $E_{\text{miss}}$  since no particle ID information is required and because the contributions of spurious photon clusters tend to cancel in  $\mathbf{p}_{\text{miss}}$  but add in  $E_{\text{miss}}$ .

Using this neutrino four-vector, one proceeds as in a hadronic analysis, defining  $\Delta E$ , the difference between the beam

energy and that of the candidate  $B$  meson, and  $M_B$ , the beam-energy-constrained  $B$  mass:

$$\Delta E = E_{\text{beam}} - (E_\nu + E_\ell + E_\pi),$$

$$M_B = [E_{\text{beam}}^2 - (|\mathbf{p}_\nu + \mathbf{p}_\ell + \mathbf{p}_\pi|^2)]^{1/2}. \quad (165)$$

Signal events are expected to have small values of  $\Delta E$  and values of  $M_B$  that peak at the  $B$  mass. To suppress continuum background, event-shape cuts similar to those used in the CLEO  $B \rightarrow \rho \ell^- \bar{\nu}$  analysis are applied. The lepton energy is required to satisfy  $E_\ell > 1.5$  GeV, which helps to suppress  $B \rightarrow X_c \ell^- \bar{\nu}$  background. This cut is lower than that used in the  $B \rightarrow \rho \ell^- \bar{\nu}$  analysis because the  $B \rightarrow \pi \ell^- \bar{\nu}$  lepton-energy spectrum is softer.

Figure 43 shows the reconstructed  $B$  mass spectrum for  $B^- \rightarrow \pi^0 \ell^- \bar{\nu}$  and  $\bar{B}^0 \rightarrow \pi^+ \ell^- \bar{\nu}$  candidates with  $-0.25 < \Delta E < 0.15$  GeV. The background from continuum and fake leptons has been subtracted. A small signal at the  $B$  mass is evident. The number of signal events is obtained from a fit that takes into account background contributions from  $B \rightarrow X_c \ell^- \bar{\nu}$  decays and  $B \rightarrow X_u \ell^- \bar{\nu}$  processes other than  $B \rightarrow \pi \ell^- \bar{\nu}$ . In fact, the reconstructed  $B$  mass distributions for the five modes  $\bar{B}^0 \rightarrow \pi^+ \ell^- \bar{\nu}$ ,  $B^- \rightarrow \pi^0 \ell^- \bar{\nu}$ ,  $B^- \rightarrow \rho^0 \ell^- \bar{\nu}$ ,  $\bar{B}^0 \rightarrow \rho^+ \ell^- \bar{\nu}$ , and  $B^- \rightarrow \omega \ell^- \bar{\nu}$  are fit simultaneously, thereby constraining the background from the vector modes into  $B \rightarrow \pi \ell^- \bar{\nu}$  with the data. Isospin constraints are imposed on the two  $B \rightarrow \pi \ell^- \bar{\nu}$  modes and on the two  $B \rightarrow \rho \ell^- \bar{\nu}$  modes. In each mode, the shape of the  $B \rightarrow X_c \ell^- \bar{\nu}$  background is determined from Monte Carlo, and the level of this background floats independently. The background from other  $B \rightarrow X_u \ell^- \bar{\nu}$  processes is determined from Monte Carlo with the rate fixed by the observed rate in the end-point region of the inclusive lepton spectrum.

The total yield for  $B^- \rightarrow \pi^0 \ell^- \bar{\nu}$  and  $\bar{B}^0 \rightarrow \pi^+ \ell^- \bar{\nu}$  is

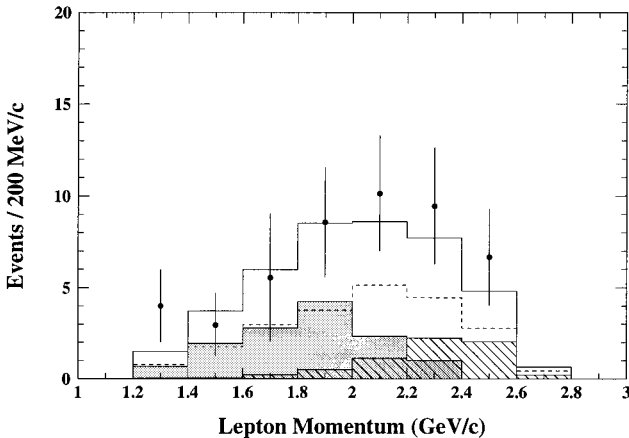


FIG. 44. The reconstructed lepton-energy spectrum from the CLEO II search for  $\bar{B}^0 \rightarrow \pi^+ \ell^- \bar{\nu}$  and  $B^- \rightarrow \pi^0 \ell^- \bar{\nu}$ . The points with errors represent the data after subtraction of continuum background and events with fake leptons. The solid histogram shows the total fit, which includes contributions from the signal (dashed histogram),  $B \rightarrow X_c \ell^- \bar{\nu}$  (shaded histogram), and other  $B \rightarrow X_u \ell^- \bar{\nu}$  decays (hatched histogram). The shape of the spectrum for  $B \rightarrow \pi \ell^- \bar{\nu}$  events is obtained from a Monte Carlo based on the ISGW model. The spectrum associated with the signal events is significantly harder than that of the  $B \rightarrow X_c \ell^- \bar{\nu}$  background.

$20.7 \pm 7.0$  events, where the ISGW model was used to obtain the signal shapes used in the fit. (The yield for the WSB model is very similar, since the shape of the  $B$  mass peak is essentially the same for the two models.) The corresponding preliminary branching fraction is

$$B(\bar{B}^0 \rightarrow \pi^+ \ell^- \bar{\nu}) = (1.19 \pm 0.41 \pm 0.21 \pm 0.19) \times 10^{-4} \quad (\text{ISGW}),$$

$$B(\bar{B}^0 \rightarrow \pi^+ \ell^- \bar{\nu}) = (1.70 \pm 0.51 \pm 0.31 \pm 0.27) \times 10^{-4} \quad (\text{WSB}), \quad (166)$$

where the theoretical models used to calculate the signal shapes and detection efficiencies are indicated. The errors given are statistical, systematic on the yield from the fit, and systematic on the detection efficiency, respectively. The fit also leads to limits on  $B \rightarrow \rho \ell^- \bar{\nu}$  and  $B^- \rightarrow \omega \ell^- \bar{\nu}$  that are virtually identical to those from the CLEO search described earlier in this section. The ratio of the branching fractions for  $B \rightarrow \rho \ell^- \bar{\nu}$  to  $B \rightarrow \pi \ell^- \bar{\nu}$  can be constrained:

$$B(\bar{B}^0 \rightarrow \rho^+ \ell^- \bar{\nu}) / B(\bar{B}^0 \rightarrow \pi^+ \ell^- \bar{\nu}) < 3.4 \quad (90\% \text{ C.L.}) \quad (167)$$

This limit is obtained when either the ISGW or the WSB model is used.

Evidence supporting the conclusion that the signal is indeed due to  $B \rightarrow \pi \ell^- \bar{\nu}$  decays can be obtained from kinematic distributions. Figure 44 shows the lepton spectrum ob-

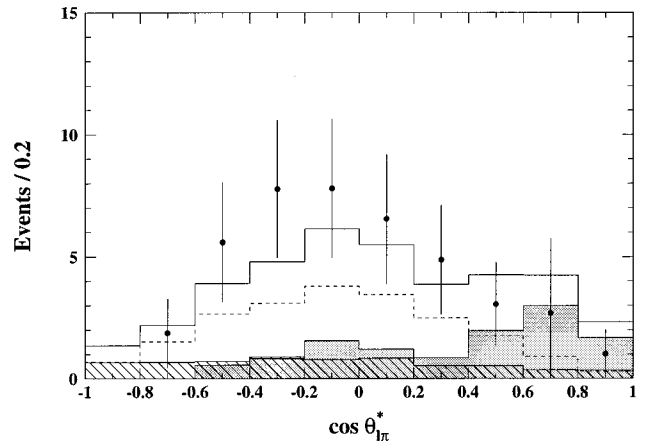


FIG. 45. The reconstructed distribution for the polar angle of the lepton in the  $W^*$  rest frame from the CLEO II search for  $\bar{B}^0 \rightarrow \pi^+ \ell^- \bar{\nu}$  and  $B^- \rightarrow \pi^0 \ell^- \bar{\nu}$  candidates. The points with errors represent the data after subtraction of continuum background and events with fake leptons. The solid histogram shows the total fit, which includes contributions from the signal (dashed histogram),  $B \rightarrow X_c \ell^- \bar{\nu}$  (shaded histogram), and other  $B \rightarrow X_u \ell^- \bar{\nu}$  decays (hatched histogram). For signal events, this distribution should be  $dN/d\cos\theta_\ell \propto \sin^2\theta_\ell$ , independent of model, and the data are consistent with this prediction. (The angle plotted in this figure is equal to  $\pi$  minus the angle  $\theta_\ell$  shown in Fig. 5; the expected signal distribution is unaffected by this difference.)

tained from the fit. The spectrum is significantly harder than that of the  $B \rightarrow X_c \ell^- \bar{\nu}$  background, and it is consistent with model predictions for  $B \rightarrow \pi \ell^- \bar{\nu}$  decay. One can also examine the angle of the lepton in the  $W^*$  rest frame. As discussed in Sec. II.C, the distribution of this angle is  $dN/d\cos\theta_\ell \propto \sin^2\theta_\ell$ , independent of models. The observed distribution, shown in Fig. 45, is quite consistent with this prediction. The statistical significance for the signal, including information from this angular distribution, is about  $3.8\sigma$ . The measured branching fraction is somewhat higher than that expected from the original ISGW model (assuming  $|V_{ub}| = 0.003$ ), but it is very similar to the value expected in the ISGW2 model, as well as to those in the WSB and KS models (see Table XLV).

As this paper was going to press, CLEO presented (Ammar *et al.*, 1995) evidence for the decay  $B \rightarrow \rho \ell^- \bar{\nu}$ , with a branching fraction consistent with the CLEO upper limits given here.

### G. Semileptonic decays of charm and bottom baryons

Of the observed charm and bottom baryons, the  $\Lambda_c$ ,  $\Xi_c$ ,  $\Omega_c$ , and  $\Lambda_b$  decay through the weak interaction. The light quarks in these ground-state spin- $\frac{1}{2}$  baryons are in a spin-zero state in the  $\Lambda_Q$  and  $\Xi_Q$  baryons and in a spin-one state in the  $\Omega_Q$  baryons. This leads to a simpler theoretical description and greater predictive power for models of semileptonic  $\Lambda_Q$  and  $\Xi_Q$  decays than for semileptonic decays of mesons or other baryons. The decay  $\Lambda_b \rightarrow \Lambda_c \ell^- \bar{\nu}$  has been analyzed in the HQET framework to order  $1/m_Q$ , including next-to-leading-order QCD corrections (Neubert, 1994c). The motivation for studying semileptonic baryon decays is twofold. First the decay  $\Lambda_b \rightarrow \Lambda_c \ell^- \bar{\nu}$  could be used to reliably extract  $V_{cb}$  at the zero-recoil point (the kinematic point at which the associated form factors are normalized in HQET) if sufficiently large samples could be isolated. Secondly, the joint angular decay distributions for  $\Lambda_c \rightarrow \Lambda \ell^+ \nu$  and  $\Lambda_b \rightarrow \Lambda_c \ell^- \bar{\nu}$  could be used to study the hadronic matrix elements, just as has already been done in the decays  $D \rightarrow \bar{K}^* \ell^+ \nu$  and  $B \rightarrow D^* \ell^- \bar{\nu}$ .

In semileptonic decays of  $\Lambda_b$  and  $\Lambda_c$  baryons to final states containing another  $\Lambda$ -type baryon, charge correlations between the lepton and the daughter baryon can be used to identify signal and background. For example, in  $\Lambda_c$  decays, the final states  $\Lambda \ell^+ X$  and  $\bar{\Lambda} \ell^- X$  can occur, but the final states  $\Lambda \ell^- X$  and  $\bar{\Lambda} \ell^+ X$  cannot. ‘‘Wrong-sign’’ candidates are used as a measure of the background contribution to the ‘‘right-sign’’ signal. Samples of hundreds of semileptonic charm-baryon decays have been identified and used to measure branching fractions and decay asymmetries. The analysis of their joint decay distributions is just beginning. Studies of semileptonic bottom-baryon decays are even less mature and are limited to branching fraction and lifetime measurements.

#### 1. Decay distributions for $\Lambda_c \rightarrow \Lambda \ell^+ \nu$

Since measurements of the decay distributions of semileptonic  $\Lambda_c$  decays have already been published, while no such experimental studies for  $\Lambda_b$  decay exist yet, we give the decay distributions for  $\Lambda_c \rightarrow \Lambda \ell^+ \nu$  and note how those for  $\Lambda_b \rightarrow \Lambda_c \ell^- \bar{\nu}$  differ. For a recent review of the experimental and theoretical status of baryons containing one heavy quark, including semileptonic decays, we refer the reader to Körner, Kramer, and Pirjol (1994).

The decay of unpolarized  $\Lambda_c$ 's to  $\Lambda \ell^+ \nu$ , with the daughter baryon  $\Lambda$  subsequently decaying to  $p \pi^-$ , can be described by four independent kinematic variables. The four variables that are usually used are analogous to those used in the analysis of  $D^+ \rightarrow \bar{K}^{*0} \ell^+ \nu$ , described in Sec. VI.A.6. They are  $q^2$ , the square of the  $\ell^+ \nu$  invariant mass;  $\theta_W$ , the angle between the charged lepton and the direction of the  $\Lambda$  measured in the  $\ell^+ \nu$  rest frame;<sup>10</sup>  $\theta_\Lambda$ , the angle between the proton and the direction opposite that of the  $W^-$  measured in the rest frame of the  $\Lambda$ ; and  $\chi$ , the azimuthal angle between the projections of the charged lepton and the proton momenta in the plane perpendicular to the  $W$  and  $\Lambda$  direction in the rest frame of the  $\Lambda_c$ . The differential decay rate for  $\Lambda_c \rightarrow \Lambda \ell^+ \nu$  with  $\Lambda \rightarrow p \pi^-$  can be expressed in terms of these four kinematic variables (Körner and Krämer, 1992):

$$\begin{aligned} \frac{d\Gamma}{dq^2 d\cos\theta_\Lambda d\cos\theta_W d\chi} = & \frac{B(\Lambda \rightarrow p \pi)}{2(2\pi)^4} G_F^2 |V_{cs}|^2 \frac{p_\Lambda q^2}{24M^2} \left\{ \frac{3}{8} (1 - \cos\theta_W)^2 (1 + \alpha_\Lambda \cos\theta_\Lambda) |H_{\frac{1}{2}1}(q^2)|^2 \right. \\ & + \frac{3}{8} (1 + \cos\theta_W)^2 (1 - \alpha_\Lambda \cos\theta_\Lambda) |H_{-\frac{1}{2}-1}(q^2)|^2 \\ & + \frac{3}{4} \sin^2\theta_W [(1 + \alpha_\Lambda \cos\theta_\Lambda) |H_{\frac{1}{2}0}(q^2)|^2 + (1 - \alpha_\Lambda \cos\theta_\Lambda) |H_{-\frac{1}{2}0}(q^2)|^2] \\ & + \frac{3}{2\sqrt{2}} \sin\theta_W (1 - \cos\theta_W) \alpha_\Lambda \sin\theta_\Lambda \cos\chi H_{-\frac{1}{2}0} H_{\frac{1}{2}1} \\ & \left. + \frac{3}{2\sqrt{2}} \sin\theta_W (1 + \cos\theta_W) \alpha_\Lambda \sin\theta_\Lambda \cos\chi H_{\frac{1}{2}0} H_{-\frac{1}{2}-1} \right\}, \end{aligned} \quad (168)$$

<sup>10</sup>Note that  $\theta_W$  is  $180^\circ$  minus  $\theta_\ell$  defined in Sec. VI.A.5 for  $D^+ \rightarrow \bar{K}^{*0} \ell^+ \nu$  decay.

TABLE XLVIII. Experimental measurements of the product  $\sigma(e^+e^- \rightarrow \Lambda_c X)B(\Lambda_c \rightarrow \Lambda \ell^+ X)$  at  $e^+e^-$  center-of-mass energies near 10.4 GeV.

	ARGUS (Albrecht <i>et al.</i> , 1991c)	CLEO II (Bergfeld <i>et al.</i> , 1994)
$\sigma(e^+e^- \rightarrow \Lambda_c X)B(\Lambda_c \rightarrow \Lambda e^+ X)$ (pb)	$4.20 \pm 1.28 \pm 0.71$	$4.87 \pm 0.28 \pm 0.69$
$\sigma(e^+e^- \rightarrow \Lambda_c X)B(\Lambda_c \rightarrow \Lambda \mu^+ X)$ (pb)	$3.91 \pm 2.02 \pm 0.90$	$4.43 \pm 0.51 \pm 0.64$
Average (pb)	$4.15 \pm 1.03 \pm 1.18$	$4.77 \pm 0.25 \pm 0.66$

where  $p_\Lambda$  is the magnitude of the  $\Lambda$  three-momentum in the rest frame of the  $\Lambda_c$  and hence is a function of  $q^2$ .  $\alpha_\Lambda$  is the asymmetry parameter for the parity-violating nonleptonic decay  $\Lambda \rightarrow p \pi^-$ . The measured value is  $\alpha_\Lambda = 0.642 \pm 0.013$  (Particle Data Group, 1994). For  $\Lambda_b \rightarrow \Lambda_c \ell^- \bar{\nu}$ , the above equation holds with  $\cos\theta_W$  replaced with  $-\cos\theta_W$  and  $\sin\theta_W$  replaced with  $-\sin\theta_W$ .

The subscripts on the helicity amplitudes  $H_{\lambda_\Lambda \lambda_W}$  correspond to the helicities of the  $\Lambda$  ( $\lambda_\Lambda$ ) and  $W$  ( $\lambda_W$ ). Each helicity amplitude contains an axial and a vector piece,  $H_{\lambda_\Lambda \lambda_W} = H_{\lambda_\Lambda \lambda_W}^V + H_{\lambda_\Lambda \lambda_W}^A$ . We have assumed that the helicity amplitudes are real, as we did in Sec. VI.A.6 for  $P \rightarrow V \ell \nu$ . The helicity amplitudes contain the dependence on the invariant form factors that parametrize the hadronic current. In the limit of zero lepton mass, there are four form factors,  $F_1^V, F_2^V, F_1^A,$  and  $F_2^A$  (Körner and Krämer, 1992). The helicity amplitudes are related to the form factors through the equations

$$\begin{aligned} \sqrt{q^2} H_{\frac{1}{2}0}^V &= \sqrt{Q_-} [(M + M_\Lambda) F_1^V - q^2 F_2^V], \\ H_{\frac{1}{2}1}^V &= \sqrt{2Q_-} [-F_1^V + (M + M_\Lambda) F_2^V], \\ \sqrt{q^2} H_{\frac{1}{2}0}^A &= \sqrt{Q_+} [(M - M_\Lambda) F_1^A + q^2 F_2^A], \\ H_{\frac{1}{2}1}^A &= \sqrt{2Q_+} [-F_1^A - (M - M_\Lambda) F_2^A], \end{aligned} \quad (169)$$

where  $Q_\pm = (M \pm M_\Lambda)^2 - q^2$ . The remaining helicity amplitudes can be obtained through the parity relations  $H_{-\lambda_\Lambda -\lambda_W}^{V(A)} = +(-)H_{\lambda_\Lambda \lambda_W}^{V(A)}$ .

In the heavy-quark symmetry limit, when the quark involved in the decay is heavy in both the initial and final baryon (for example,  $\Lambda_b \rightarrow \Lambda_c \ell^- \bar{\nu}$ ), all four form factors are related to a single form factor (Georgi *et al.*, 1990; Georgi, 1991; Isgur and Wise, 1991a; Mannel *et al.*, 1991a):

$$F_1^V(q^2) = -F_1^A(q^2), \quad F_2^V(q^2) = F_2^A(q^2) = 0. \quad (170)$$

When the quark in the initial state is heavy and that in the final state is light (for example,  $\Lambda_c \rightarrow \Lambda \ell^+ \nu$ ), the four form factors  $F_1^V, F_2^V, F_1^A,$  and  $F_2^A$  can be expressed in terms of two independent form factors  $f_1$  and  $f_2$  (Hussain *et al.*, 1991; Mannel *et al.*, 1991a, 1991b; Falk and Neubert, 1993b; Mannel and Roberts, 1993),

$$F_1^V(q^2) = -F_1^A(q^2) = f_1(q^2) + \frac{M_\Lambda}{M} f_2(q^2),$$

$$F_2^V(q^2) = -F_2^A(q^2) = \frac{1}{M} f_2(q^2). \quad (171)$$

In general, the magnitude of  $f_2$  is expected to be less than that of  $f_1$ . CLEO has recently measured the ratio  $R = f_2/f_1$  for the decay  $\Lambda_c \rightarrow \Lambda \ell^+ \nu$ . (See next section.)

If we integrate Eq. (168) over the azimuthal angle  $\chi$  and the polar angle  $\theta_W$ , we obtain

$$\frac{d\Gamma}{dq^2 d \cos\theta_\Lambda} \propto 1 + \alpha_{\Lambda_c} \alpha_\Lambda \cos\theta_\Lambda, \quad (172)$$

where the asymmetry parameter  $\alpha_{\Lambda_c}$  is defined by

$$\alpha_{\Lambda_c} = \frac{|H_{\frac{1}{2}1}|^2 - |H_{-\frac{1}{2}-1}|^2 + |H_{\frac{1}{2}0}|^2 - |H_{-\frac{1}{2}0}|^2}{|H_{\frac{1}{2}1}|^2 + |H_{-\frac{1}{2}-1}|^2 + |H_{\frac{1}{2}0}|^2 + |H_{-\frac{1}{2}0}|^2}. \quad (173)$$

The parameter  $\alpha_{\Lambda_c}$  gives the longitudinal polarization of the daughter baryon  $\Lambda$  that is being analyzed by its subsequent decay to  $p \pi^-$ . Both ARGUS and CLEO have measured  $\alpha_{\Lambda_c}$ .

## 2. Charm-baryon decays

The earliest studies of semileptonic  $\Lambda_c$  decays were published by Mark II at SPEAR (Vella *et al.*, 1982) and PEP (Klein *et al.*, 1989). However, these results were of very limited statistical significance. More recently, the decay  $\Lambda_c \rightarrow \Lambda \ell^+ \nu$  has been studied most extensively by the ARGUS (Albrecht *et al.*, 1991c) and CLEO (Bergfeld *et al.*, 1994; Crawford *et al.*, 1995) Collaborations. The ARGUS sample consists of about 100 signal events over a background of about 140. CLEO published branching fractions and decay asymmetries based on a signal of about 430 events over a background of 190 events and, more recently, has presented results on the form factor ratio  $R$  and has updated the asymmetry parameter with a sample about twice as large.

Both ARGUS and CLEO measure the product  $\sigma(e^+e^- \rightarrow \Lambda_c X)B(\Lambda_c \rightarrow \Lambda \ell^+ X)$  at an  $e^+e^-$  center-of-mass energy near the  $Y(4S)$ . The experimental results are shown in Table XLVIII for electrons and muons separately. The branching fraction itself is extracted by normalizing to the  $\Lambda_c \rightarrow p K^- \pi^+$  rate, as follows. ARGUS and CLEO have each measured  $\sigma(e^+e^- \rightarrow \Lambda_c X)B(\Lambda_c \rightarrow p K^- \pi^+)$ . The weighted average is

TABLE XLIX. Experimental measurements of semileptonic  $\Xi_c$  and  $\Omega_c$  baryon decays.

Experiment	Measurement
ARGUS (Albrecht <i>et al.</i> , 1993a)	$\sigma(e^+e^- \rightarrow \Xi_c^0 X)B(\Xi_c^0 \rightarrow \Xi^- \ell^+ X) = (0.74 \pm 0.24 \pm 0.09)$ pb
CLEO II (Alexander <i>et al.</i> , 1994b)	$\sigma(e^+e^- \rightarrow \Xi_c^0 X)B(\Xi_c^0 \rightarrow \Xi^- e^+ \nu_e) = (0.63 \pm 0.12 \pm 0.10)$ pb
CLEO II (Alexander <i>et al.</i> , 1994b)	$\sigma(e^+e^- \rightarrow \Xi_c^+ X)B(\Xi_c^+ \rightarrow \Xi^0 e^+ \nu_e) = (1.55 \pm 0.33 \pm 0.25)$ pb
CLEO II (Alexander <i>et al.</i> , 1994b)	$B(\Xi_c^0 \rightarrow \Xi^- e^+ \nu_e)/B(\Xi_c^0 \rightarrow \Xi^- \pi^+) = 3.1 \pm 1.0^{+0.3}_{-0.4}$
CLEO II (Alexander <i>et al.</i> , 1994b)	$B(\Xi_c^+ \rightarrow \Xi^0 e^+ \nu_e)/B(\Xi_c^+ \rightarrow \Xi^- \pi^+ \pi^+) = 2.3 \pm 0.6^{+0.3}_{-0.5}$
ARGUS (Albrecht <i>et al.</i> , 1993e)	$B(\Omega_c \rightarrow \Omega^- \ell^+ X)/B(\Omega_c \rightarrow \Omega^- \pi^- \pi^+ \pi^+) = 0.87 \pm 0.53$

$$\sigma(e^+e^- \rightarrow \Lambda_c X)B(\Lambda_c \rightarrow pK^- \pi^+) = (11.3 \pm 0.8 \pm 1.0) \text{ pb}. \quad (174)$$

ARGUS and CLEO have also been able to measure the branching fraction  $B(\Lambda_c \rightarrow pK^- \pi^+)$  under the assumption that all baryons produced in  $B$  decay come from  $\Lambda_c$  decay. The weighted average of the two measurements is

$$B(\Lambda_c \rightarrow pK^- \pi^+) = (4.3 \pm 1.1)\%. \quad (175)$$

Therefore the  $\Lambda_c$  semileptonic branching fraction for  $\Lambda_c \rightarrow \Lambda \ell^+ X$  can be extracted for each experiment:  $B(\Lambda_c \rightarrow \Lambda \ell^+ X) = (1.6 \pm 0.6)\%$  for ARGUS and  $B(\Lambda_c \rightarrow \Lambda \ell^+ X) = (1.8 \pm 0.5)\%$  for CLEO. The average of the two measurements is

$$B(\Lambda_c \rightarrow \Lambda \ell^+ X) = (1.7 \pm 0.4)\%. \quad (176)$$

This branching fraction can be combined with the measured  $\Lambda_c$  lifetime of  $(2.00 \pm 0.11) \times 10^{-13}$  s (Particle Data Group, 1994) to extract a decay rate of

$$\Gamma(\Lambda_c \rightarrow \Lambda \ell^+ X) = (8.5 \pm 2.1) \times 10^{10} \text{ s}^{-1}. \quad (177)$$

This is considerably lower than the inclusive semileptonic  $D$  decay rate  $\Gamma(D \rightarrow X \ell^+ \nu) = (17.1 \pm 0.7) \times 10^{10} \text{ s}^{-1}$  (see Sec. VI.D). In the simple spectator quark model, we would expect the inclusive semileptonic rates to be the same. We could conclude that this is evidence for sizable semileptonic  $\Lambda_c$  decays to final states not containing a  $\Lambda$ . However, theoretical expectations are that semileptonic  $\Lambda_c$  decays will be dominated by  $\Lambda_c \rightarrow \Lambda \ell^+ \nu$ . Therefore, at this time, there appears to be a discrepancy between the measurements and theoretical expectations for the inclusive semileptonic  $\Lambda_c$  decay rate. However, the experimental uncertainties on the branching fractions for  $\Lambda_c \rightarrow pK^- \pi^+$  and  $\Lambda_c \rightarrow \Lambda \ell^+ X$  are still large.

CLEO has chosen to interpret their measurements of  $\Lambda_c \rightarrow \Lambda \ell^+ X$  and  $\Lambda_c \rightarrow pK^- \pi^+$  as a limit on the branching fraction for  $\Lambda_c \rightarrow pK^- \pi^+$ . They assume that the  $\Lambda_c$  inclusive semileptonic decay rate is the same as that for  $D$  mesons, and they use only their measurements of  $\sigma(e^+e^- \rightarrow \Lambda_c X)B(\Lambda_c \rightarrow pK^- \pi^+)$  and  $\sigma(e^+e^- \rightarrow \Lambda_c X)B(\Lambda_c \rightarrow \Lambda \ell^+ \nu)$  for  $p_{\Lambda_c} > 0.5p_{\text{max}}$ . CLEO concludes that

$$B(\Lambda_c \rightarrow pK^- \pi^+) = f(6.67 \pm 0.35 \pm 1.35)\%, \quad (178)$$

where  $f = B(\Lambda_c \rightarrow \Lambda \ell^+ X)/B(\Lambda_c \rightarrow \ell^+ X)$ . Since  $f$  must be less than one, the result is an upper limit on  $B(\Lambda_c \rightarrow pK^- \pi^+)$  that is consistent with the average of the CLEO and ARGUS measurements [Eq. (175)].

CLEO searches its  $\Lambda_c \rightarrow \Lambda \ell^+ X$  candidates for final states

other than  $\Lambda \ell^+ \nu$ . They find that fewer than 15% of the candidates have decay products in addition to  $\Lambda \ell^+ \nu$ , at the 90% confidence level.

Both ARGUS and CLEO use two-body hadronic decays of the daughter baryon as a polarization analyzer to extract a decay asymmetry parameter for  $\Lambda_c \rightarrow \Lambda \ell^+ \nu$ . As described in the previous section, the differential decay rate is given by

$$\frac{d\Gamma}{dq^2 d \cos\theta_\Lambda} \propto 1 + \alpha_{\Lambda_c} \alpha_\Lambda \cos\theta_\Lambda, \quad (179)$$

where  $\theta_\Lambda$  is the angle between the proton and the direction opposite that of the  $W$ , measured in the  $\Lambda$  rest frame. The  $\Lambda$  asymmetry parameter  $\alpha_\Lambda = 0.642 \pm 0.013$  (Particle Data Group, 1994) is well measured for  $\Lambda \rightarrow p\pi$ , and  $\alpha_{\Lambda_c}$  is the  $q^2$ -dependent parity-violating parameter to be extracted from the observed decay distributions in  $\Lambda_c \rightarrow \Lambda \ell^+ \nu$ . In the ARGUS analysis, the  $\Lambda_c$  direction is assumed to be the same as the  $\Lambda \ell^+$  direction, which is a good approximation when the mass of the  $\Lambda \ell^+$  system is relatively large. In the CLEO analysis, the neutrino momentum is extracted by approximating the  $\Lambda_c$  direction by the thrust axis of the event. Each experiment observes a large negative polarization of the  $\Lambda$ , as expected:  $\alpha_\Lambda = -0.91 \pm 0.49$  for ARGUS (Albrecht *et al.*, 1994b) for  $\Lambda \ell^+$  mass in the range 1.85 to 2.20 GeV/ $c^2$ , and  $\alpha_{\Lambda_c} = -0.82^{+0.09+0.06}_{-0.06-0.03}$  for CLEO (Crawford *et al.*, 1995). These results are in good agreement with the asymmetry parameter measured in  $\Lambda_c \rightarrow \Lambda \pi^+$  decays and with HQET, which predicts that  $\alpha_{\Lambda_c} = -1$  as  $q^2$  approaches zero.

CLEO has presented results from a three-dimensional unbinned maximum-likelihood fit to the kinematic variables  $q^2$ ,  $\cos\theta_W$ , and  $\cos\theta_\Lambda$ , for about 1000 events with a signal-to-background ratio of about 2:1 (Crawford *et al.*, 1995). A dipole form is assumed for the  $q^2$  dependence of the form factor with a pole mass of 2.11 GeV/ $c^2$ . They extract the ratio of form factors  $R = f_2/f_1$  discussed in Sec. VI.G.1. The result is  $R = -0.25 \pm 0.14 \pm 0.08$ , in agreement with the expectation that the magnitude of  $f_2$  is less than that of  $f_1$ .

ARGUS has presented evidence for semileptonic decays of  $\Xi_c^0$  and  $\Omega_c$ . The results are summarized in Table XLIX. Since the production rate for these baryons is not known, they report the product of the production cross section and the inclusive semileptonic branching fraction. More recently, CLEO has also observed semileptonic  $\Xi_c^0$  decays and has reported the first evidence of semileptonic  $\Xi_c^+$  decays. Their results are also shown in Table XLIX. In addition to the product of the production cross section and branching fraction, they have measured the ratio of the semileptonic

TABLE L. Experimental measurements of inclusive  $\Lambda_b$  semileptonic decay rates, from LEP experiments.

Experiment	No. of signal events	Measurement
OPAL (Acton <i>et al.</i> , 1992)	$55 \pm 9_{-3.1}^{+0.3}$	$f(b \rightarrow \Lambda_b)B(\Lambda_b \rightarrow \Lambda \ell^- X) = (0.29 \pm 0.05 \pm 0.11)\%$
ALEPH (Buskulic <i>et al.</i> , 1992b)	$122 \pm 18_{-23}^{+22}$	$f(b \rightarrow \Lambda_b)B(\Lambda_b \rightarrow \Lambda \ell^- X) = (0.35 \pm 0.05 \pm 0.09)\%$
DELPHI (Abreu <i>et al.</i> , 1993)	$30 \pm 10$	$f(b \rightarrow \Lambda_b)B(\Lambda_b \rightarrow \Lambda \ell^- X) = (0.41 \pm 0.13 \pm 0.09)\%$
ALEPH (Buskulic <i>et al.</i> , 1992a)	$21 \pm 5$	$f(b \rightarrow \Lambda_b)B(\Lambda_b \rightarrow \Lambda_c \ell^- X) = (3.0 \pm 0.7 \pm 0.9)\%$

branching fraction to that for a hadronic mode. By assuming that the  $\Xi_c^+$  and  $\Xi_c^-$  are produced at equal rates in  $e^+e^-$  annihilation at 10 GeV and that the semileptonic decay rates to  $\Xi e^+ \nu_e$  are the same, CLEO deduces the ratio of lifetimes to be  $\tau(\Xi_c^+)/\tau(\Xi_c^0) = 2.46 \pm 0.70_{-0.23}^{+0.33}$ . This is in good agreement with the ratios of directly measured lifetimes:  $4.06 \pm 1.26$  by E687 (Frabetti *et al.*, 1993d) and  $2.44 \pm 1.68$  by NA32 (Barlag *et al.*, 1989). The observed ratio is also in agreement with the predicted hierarchy of lifetimes for charmed baryons (Guberina *et al.*, 1986; Voloshin and Shifman, 1986).

While experimental results on semileptonic charm-baryon decays currently have limited statistical significance, much larger data samples are expected in the future, allowing tests of the various baryon semileptonic decay models.

### 3. Bottom-baryon decays

At present, semileptonic decays of bottom baryons are studied mainly by the LEP experiments to extract lifetimes. Since the fraction of  $b$  quarks from  $Z$  decays that fragment as a  $\Lambda_b$  [ $f(b \rightarrow \Lambda_b)$ ] is not known, measurements of decay rates are expressed as the product of a particular semileptonic  $\Lambda_b$  branching fraction and  $f(b \rightarrow \Lambda_b)$ . The LEP measurements are summarized in Table L. OPAL (Acton *et al.*, 1992), ALEPH (Buskulic *et al.*, 1992b), and DELPHI (Abreu *et al.*, 1993b) have net signals for  $\Lambda_b \rightarrow \Lambda \ell^- X$  in the range of 30 to 150 events with a signal-to-background ratio of about 1.5 to 2. They have each measured the  $\Lambda_b$  lifetime with these events or a subset of them. In the mode  $\Lambda_b \rightarrow \Lambda_c \ell^- X$ , ALEPH (Buskulic *et al.*, 1992a) has used about an order of magnitude fewer events to measure the product branching fraction (shown in Table L) and the  $\Lambda_b$  lifetime.

## VII. CONCLUSIONS

The considerable progress in understanding charm and bottom physics is due both to major experiments at  $e^+e^-$  and fixed-target experiments and to the continued strong efforts of the theoretical community. Here we summarize the most important results and their implications. We look back on many of the key questions that have been answered and the new questions that have been raised, and we attempt to indicate which directions should be most strongly pursued in the future. We shall start with the CKM matrix, assessing the implications of measurements of  $|V_{cb}|$  and  $|V_{ub}|$ . We then turn to results on charm and bottom decays and their interpretation.

### A. CKM measurements

An enormous experimental and theoretical effort has been directed towards better measurements of  $|V_{cb}|$  and  $|V_{ub}|$ , which are summarized in Table LI. Broadly speaking, measurements of  $|V_{cb}|$  are in a process of gradual refinement, while measurements of  $|V_{ub}|$  are still in their infancy, dominated by large theoretical uncertainties.

There is good agreement between the values of  $|V_{cb}|$  obtained from measurements of the inclusive  $B$  semileptonic branching fraction (Sec. V.D.4) and the rate for  $B \rightarrow D^* \ell^- \bar{\nu}$  at zero recoil (Sec. VI.E.4). We take as our final value  $|V_{cb}| = 0.040 \pm 0.003$  from the  $B \rightarrow D^* \ell^- \bar{\nu}$  measurement (adding the errors in quadrature), regarding the inclusive measurement as a check. A point that merits continued investigation is the sensitivity of this value of  $|V_{cb}|$  to different assumptions for the shape of the extrapolation function  $\xi(w)$ . The uncertainty associated with the extrapolation appears to be relatively small ( $\pm 0.001$  in  $|V_{cb}|$ ), but this

TABLE LI. Summary of results on the CKM matrix elements determined from  $B$  semileptonic decays. When two errors are given, the first is experimental and the second is theoretical. The measurement of  $|V_{cb}|$  using  $B \rightarrow D^* \ell^- \bar{\nu}$  at zero recoil has an error associated with the unknown shape used in the  $q^2$  extrapolation and a theory-related normalization error, as discussed in Sec. VI.E.4. The limit on  $|V_{ub}|/|V_{cb}|$  corresponds to the CLEO II result using the ISGW model, which gives the highest value of the models considered. Note that the 35% error in  $|V_{ub}|/|V_{cb}|$  corresponds to a 70% error in the rate.

Quantity	Method for determination	Value	Total rel. error
$ V_{cb} $	Inclusive $B \rightarrow X_c \ell^- \bar{\nu}$	$0.041 \pm 0.001 \pm 0.003$	8%
$ V_{cb} $	$B \rightarrow D^* \ell^- \bar{\nu}$	$0.040 \pm 0.003 \pm 0.001 \pm 0.001$	8%
$ V_{cb} $	Recommended value	$0.040 \pm 0.003$	8%
$ V_{ub} / V_{cb} $	Inclusive end point	$0.076 \pm 0.008 \pm 0.025$	35%
$ V_{ub} / V_{cb} $	Exclusive $B \rightarrow \rho \ell^- \bar{\nu}$ and $B^- \rightarrow \omega \ell^- \bar{\nu}$	$< 0.13$	

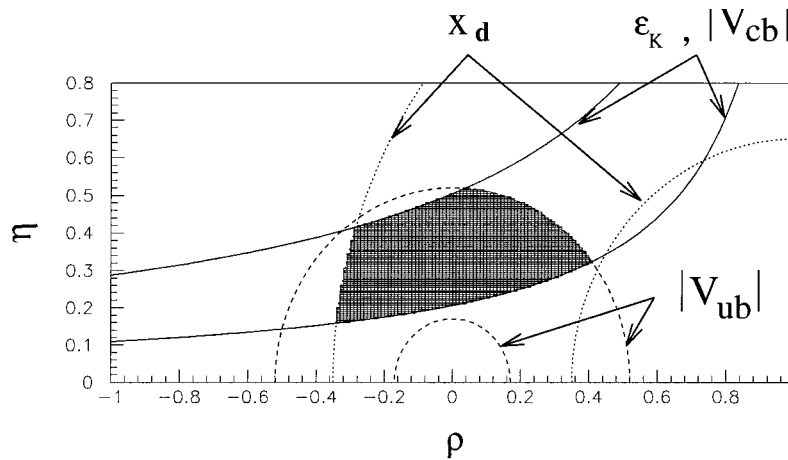


FIG. 46. The constraints in the  $(\rho, \eta)$  plane arising from measurements of  $|V_{ub}|$ ,  $B^0\bar{B}^0$  mixing ( $x_d$ ), and  $CP$  violation in kaon decays ( $\epsilon$ ). To extract the constraint on  $(\rho, \eta)$  from  $\epsilon$ , one also needs  $|V_{cb}|$ , which enters to the fourth power. The dark region indicates the values of  $\rho$  and  $\eta$  that are consistent with all of the current constraints, assuming  $\pm 1.5\sigma$  bands.

result should be checked with larger data samples as they become available. These two methods for extracting  $|V_{cb}|$  have not always agreed so well; part of the improvement can be traced to the newer values for the theoretical quantity  $\mathcal{F}(1)$ , which are lower than some earlier predictions.

We do not use measurements of  $|V_{cb}|$  from overall exclusive rates (Table XXXIX) because the associated theoretical error is much more difficult to evaluate, and because there is a large experimental correlation between the measurement errors for the overall rate for  $B \rightarrow D^* \ell^- \bar{\nu}$  and the rate at zero recoil. It is interesting, however, that the values of  $|V_{cb}|$  obtained from total rates are systematically lower than those obtained with the other methods. This result could be related to the fact that predictions of overall rates depend on form-factor slopes as well as their normalization at  $q_{\max}^2$ , and the slopes are much more difficult to predict. Underestimation of the magnitudes of the slopes would lead to predicted rates that are too large for a given  $|V_{cb}|$ , or, equivalently, to values of  $|V_{cb}|$  that are too small for a given rate. The discrepancy between the values of  $|V_{cb}|$  obtained from total semileptonic rates and from the  $B \rightarrow D^* \ell^- \bar{\nu}$  rate at zero recoil merits further investigation.

For  $|V_{ub}|$ , we take as the central value the CLEO II inclusive end-point measurement using the ACCMM model (Sec. V.E), and we define the theoretical error as the difference between the results for the ACCMM and ISGW models. This error must be regarded as only a rough guide to the uncertainty. The larger value of  $|V_{ub}|$  from ISGW is certainly expected, since the authors of that model intended to provide a lower limit for the rate in the end-point region. Better theoretical calculations for  $B \rightarrow X_u \ell^- \bar{\nu}$  inclusive decays are clearly desirable, as are results for exclusive  $B \rightarrow X_u \ell^- \bar{\nu}$  channels. The CLEO II observation of  $B \rightarrow \pi \ell^- \bar{\nu}$  is a milestone for these studies. It is encouraging that the observed rate for  $B \rightarrow \pi \ell^- \bar{\nu}$  (Sec. VI.F) is consistent with that expected from the inclusive end-point value for  $|V_{ub}|$  and most theoretical predictions for the  $B \rightarrow \pi \ell^- \bar{\nu}$  rate. It is also interesting that lattice QCD and HQET are being combined to predict this rate, an approach that is likely to be refined in the future.

The allowed region in the  $(\rho, \eta)$  plane is shown in Fig. 46. As discussed in Sec. II.B, this region is determined by three constraints:

(i) The allowed range of  $|V_{ub}/V_{cb}|$  defines an annulus between the extreme values of  $\sqrt{\rho^2 + \eta^2} = |V_{ub}^*|/|V_{cd}V_{cb}| = 0.34 \pm 0.12$ . The uncertainty in  $|V_{ub}|$  is much larger than that on  $|V_{cb}|$ , so the error on the radius in the  $(\rho, \eta)$  plane is dominated by the error on  $|V_{ub}|$ .

(ii) The measurement of the  $CP$ -violation parameter  $|\epsilon| = |\eta_{+-}| = 2.269 \pm 0.023 \times 10^{-3}$  (PDG 1994) in kaon decays determines the hyperbolic curves that extend from the lower left to the upper right. (Here we have used  $|\epsilon'| \ll |\epsilon|$ .) We shall see below that this constraint is very sensitive to  $|V_{cb}|$  and its uncertainty, so that it is more appropriate to say that the curves are determined by both  $|\epsilon|$  and  $|V_{cb}|$ .

(iii) The parameter  $\Delta m_{B^0} = (0.51 \pm 0.06) \times 10^{12} \text{ h s}^{-1}$ , which measures the  $B^0\bar{B}^0$  oscillation frequency, allows one to determine  $|V_{td}| = A\lambda^3[(1-\rho)^2 + \eta^2]^{1/2}$ , giving an annulus centered at  $(\rho, \eta) = (1, 0)$ . This constraint suffers from large theoretical uncertainties in predicting the mixing rate in terms of fundamental constants.

The constraint from  $|V_{ub}|$  is straightforward, but the other two involve a number of inputs. We now review the data on each of these constraints.

Using our value for  $|V_{cb}|$  and the PDG 1994 value for  $\lambda = |V_{us}| = 0.2205 \pm 0.0018$ , we calculate  $A = |V_{cb}|/\lambda^2 = 0.82 \pm 0.06$ . This constant enters into the extraction of the  $(\rho, \eta)$  constraints from both  $|\epsilon|$  and the  $B\bar{B}$  mixing parameter  $x_d$ .

Equations (21) and (22) show that  $\epsilon$  depends on the parameters  $A$ ,  $\mathcal{B}_K$ ,  $m_c$ ,  $m_t$ ,  $\eta_{cc}$ ,  $\eta_{ct}$ , and  $\eta_{tt}$ . We take  $\mathcal{B}_K = 0.75 \pm 0.10$ , doubling the quoted error on the value  $0.75 \pm 0.05$  obtained from a lattice QCD calculation in the quenched approximation (Gupta, 1995). Although the authors of this calculation believe that the error due to this approximation is small, they have not yet included a corresponding uncertainty in their result. It appears that the lattice is very well suited to calculating  $\mathcal{B}_K$ , and many theorists are

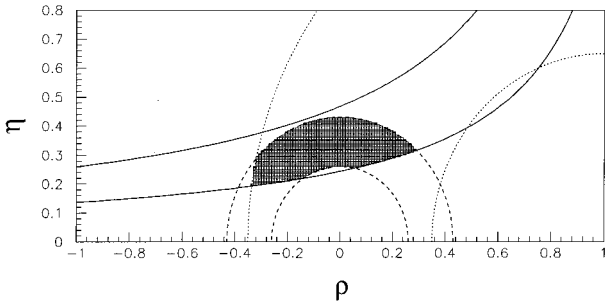


FIG. 47. A possible future scenario for the constraints in the  $(\rho, \eta)$  plane after improvements in measurements of semileptonic  $B$  decays. The uncertainty on  $|V_{cb}|$  has been reduced from 8% to 4.5%, and the uncertainty on  $|V_{ub}|$  is reduced from 35% to 17%, as discussed in the text.

optimistic that the errors will continue to improve. For the  $c$ -quark mass, we use  $m_c = 1.4 \pm 0.2 \text{ GeV}/c^2$ ; box diagrams with  $c$  quarks are important mainly for values of  $\rho$  near 1, where the  $t$ -quark contribution is suppressed. For the  $t$ -quark mass, we obtain an average  $m_t = (180 \pm 12) \text{ GeV}/c^2$  from the CDF (Abe *et al.*, 1995) value of  $m_t = (176 \pm 8 \pm 10) \text{ GeV}/c^2$  and the D0 value (Abachi *et al.*, 1995) of  $m_t = (199^{+19}_{-21} \pm 22) \text{ GeV}/c^2$ . (We have ignored possible correlations in their errors.) Following the prescription of Buras *et al.* (1994), we correct this average downward by  $(7 \pm 1) \text{ GeV}/c^2$  to obtain a running top-quark mass of  $m_t = (173 \pm 12) \text{ GeV}/c^2$  suitable for substitution into the relevant formulas. We also take the values of the QCD correction factors  $\eta_{cc} = 1.1$ ,  $\eta_{ct} = 0.36$ , and  $\eta_{tt} = 0.57$  from Buras *et al.* Further discussion of these parameters at next-to-leading order is given by Herrlich and Nierste (1994, 1995).

Because  $\mathcal{B}_K$  is reasonably well known, the uncertainty in  $|V_{cb}|$  is important in determining the constraint from  $|\epsilon|$ . The reason is simple: the box diagram with two internal  $t$ -quark lines is dominant unless  $\rho$  is near 1, and the corresponding term in the  $\epsilon$  calculation is proportional to  $\mathcal{B}_K A^4$ . The error on  $|V_{cb}|$  is thus magnified by a factor of four relative to that on  $\mathcal{B}_K$ . At  $\rho = 0$ , for example, the uncertainty on  $\eta$  from this diagram due to  $|V_{cb}|$  is about 29%, while that from  $\mathcal{B}_K$  is only 13%. Better measurements of  $|V_{cb}|$  will therefore lead directly to a tightening of the  $\epsilon$  constraint.

The constraint from  $B\bar{B}$  mixing, in contrast, depends on the poorly known quantity  $f_B \sqrt{B_B}$ , which we take to be  $(200 \pm 40) \text{ MeV}$ . It may be quite some time before  $f_B \sqrt{B_B}$  is known precisely, so better  $x_d$  measurements will not lead immediately to a better  $(\rho, \eta)$  constraint. Even with the high-luminosity  $B$  factories, it will be a long time before  $f_B$  is determined from  $B \rightarrow \tau^- \bar{\nu}_\tau$ .

What can we expect in the future? In the next few years we should be able to determine  $|V_{ub}|$  from exclusive decays such as  $B \rightarrow \pi \ell^- \bar{\nu}$ ,  $B \rightarrow \rho \ell^- \bar{\nu}$ , and  $B^- \rightarrow \omega \ell^- \bar{\nu}$ . Progress in lattice calculations suggests that eventually there may be reliable predictions for the decay rate for these modes in the high- $q^2$  region, such as HQET allows one to predict the rate for  $B \rightarrow D^* \ell^- \bar{\nu}$  at high  $q^2$ . Additional information will come from form-factor measurements of semileptonic  $D$  decays, which can be related to those for exclusive

$B \rightarrow X_u \ell^- \bar{\nu}$  decays over part of the  $q^2$  range. Measurements of  $B \rightarrow X_s \gamma$  may provide information on the  $b$ -quark motion within the  $B$  meson; these results should help to reduce the uncertainty on  $|V_{ub}|$  as determined from the inclusive lepton-energy spectrum above the  $B \rightarrow X_c \ell^- \bar{\nu}$  end point. The measurement of  $|V_{cb}|$  from the rate for  $B \rightarrow D^* \ell^- \bar{\nu}$  at zero recoil will improve as data samples increase in the future, and it should be possible for the experimental precision to reach the current level of theoretical uncertainty on the constant  $\mathcal{F}(1)$  (6% in the rate, 3% in  $|V_{cb}|$ ), which is used to extract  $|V_{cb}|$  from the  $B \rightarrow D^* \ell^- \bar{\nu}$  rate at zero recoil. We also note the importance of precise measurements of  $D^*$  and  $D$  branching fractions that enter into the  $B \rightarrow D^* \ell^- \bar{\nu}$  measurement. Fortunately,  $B(D^{*+} \rightarrow D^0 \pi^+)$  has already been measured to about 2%, and  $D^0 \rightarrow K^- \pi^+$  to 3.5%.

In our final  $(\rho, \eta)$  plot, we assume for purposes of illustration that a total precision of 4.5% is achieved on  $|V_{cb}|$  (compared with the current precision of about 8%). We also assume that the theoretical error on  $|V_{ub}|$  will be reduced to roughly the size of the current experimental error, which will halve the overall uncertainty on  $|V_{ub}|$ . Figure 47 shows what the constraints in the  $(\rho, \eta)$  plane would look like if the errors improved in this manner, with the central values unchanged. (We have not included any improvement in the uncertainty on  $\mathcal{B}_K$  or  $m_t$ .) Eventually, these results will be compared with measurements of  $CP$  violation in  $B$  decays, which will determine the interior angles of the unitarity triangle. Such measurements will provide crucial information towards determining whether the observed  $CP$ -violating processes can be explained in terms of the phenomenology of the CKM matrix, or whether physics outside the standard-model framework is required.

## B. Summary of leptonic and semileptonic charm decays

Whereas studies of semileptonic bottom decays are largely motivated by the desire to measure the CKM matrix elements  $V_{cb}$  and  $V_{ub}$ , the matrix elements relevant for semileptonic charm decay,  $V_{cs}$  and  $V_{cd}$ , are determined quite precisely from the unitarity constraint on the CKM matrix. Therefore the important impact of semileptonic charm studies is on dynamics, not CKM matrix elements. The measurements are used to test predictions of quantities such as decay rates and form factors. Many of the models and theories used for these predictions are necessary ingredients in extracting CKM matrix elements from bottom decays. Both experimental and theoretical work on semileptonic charm decays will play a role in the ultimate precision with which we determine the elements of the quark mixing matrix.

We began our review of experimental results with a discussion of leptonic charm and bottom decays. Here only one parameter, called the decay constant, is required to describe the nonperturbative physics. The decay constants are also used to describe other processes, such as  $D^0 \bar{D}^0$  and  $B^0 \bar{B}^0$  mixing, and hence are quite important. Unfortunately, leptonic decays have small branching fractions and are experimentally difficult to reconstruct. Although four experiments have shown evidence for the decay  $D_s \rightarrow \mu^+ \nu_\mu$  in the last two years (see Table VI), the statistical and systematic errors are still very large. Most experiments normalize the leptonic

rate to that of another decay mode of the  $D_s$ . As the statistical precision improves, quantitative interpretation of the measured decay constant will be limited by the uncertainty on the absolute  $D_s$  branching fractions. BES has made a self-normalizing measurement of the  $D_s$  decay constant. However, the statistical uncertainty is very large. CLEO and ALEPH have set upper limits on the rate for  $B^- \rightarrow \tau^- \bar{\nu}_\tau$  that are at least an order of magnitude above the expected value. It is important to continue to improve the measurements of both the  $D$  and  $B$ -meson decay constants as larger data samples are accumulated. Since the  $B$  decay constant is more difficult to measure, we would benefit from more theoretical work relating the  $B$  decay constant to the more easily measured  $D$  and  $D_s$  decay constants.

The inclusive branching fraction for  $D^0 \rightarrow X \ell^+ \nu$  has now been measured by CLEO with just 5% uncertainty. Therefore we can perform a significant comparison of the inclusive semileptonic rate and the sum of the exclusive semileptonic rates for the  $D$  meson. (See Table XXXIV.) The exclusive decays  $D \rightarrow \bar{K} \ell^+ \nu$  and  $D \rightarrow \bar{K}^* \ell^+ \nu$ , plus their Cabibbo-suppressed counterparts, account for  $(84 \pm 5)\%$  of the inclusive rate. No evidence for higher mass resonances or non-resonant final states has been observed. In contrast,  $B \rightarrow D \ell^- \bar{\nu}$  and  $B \rightarrow D^* \ell^- \bar{\nu}$  represent only 60% to 70% of semileptonic bottom decays, and  $B \rightarrow D^{**} \ell^- \bar{\nu}$  and  $B \rightarrow D^* X \ell^- \bar{\nu}$  account for part of the rest.

The ratio  $\Gamma(D \rightarrow \bar{K}^* \ell^+ \nu) / \Gamma(D \rightarrow \bar{K} \ell^+ \nu)$  has now been well measured, confirming the initial—and somewhat surprising—experimental result that the rate to a vector meson in the final state is only a little over half the rate to a pseudoscalar. (See Table XXIX.) Initially, these results were not in good agreement with theoretical predictions. Since the measured form factor for  $D \rightarrow \bar{K} \ell^+ \nu$  was in good agreement with theory, the inconsistency was traced to the lower-than-expected rate for  $D \rightarrow \bar{K}^* \ell^+ \nu$ . However, by taking into account effects originally ignored, such as relativistic corrections, theorists have managed to accommodate the observed ratio of rates in quark-model calculations. (See Sec. VI.B.2.) Lattice gauge calculations are also in reasonable agreement with the measured ratio.

The  $q^2$  dependence of the  $D \rightarrow \bar{K} \ell^+ \nu$  decay rate has now been measured by many experiments, most precisely by CLEO. Because only one significant form factor is needed to describe this decay, information on the  $q^2$  dependence of the form factor can be extracted. This is the only  $D$  decay mode in which the parameter that characterizes the slope of the form factor has been measured, rather than assumed. The measurements are in reasonable agreement with the model of nearest-pole dominance. (See Table XXI.)

Significant progress has been made in reducing the statistical errors on the three form factors in  $D \rightarrow \bar{K}^* \ell^+ \nu$ . (See Table XXIV.) Close to a thousand events have already been used in a single study. Fermilab experiment E791 anticipates publishing results based on at least twice this many events in each of the two lepton modes. Although initial quark-model predictions showed some discrepancies with the data, more recent predictions are in good agreement. (See Table XXVIII.) A great deal of progress has been made on lattice gauge calculations. The agreement with experiment is good for the vector form factors for  $D \rightarrow \bar{K} \ell^+ \nu$  and

$D \rightarrow \bar{K}^* \ell^+ \nu$ , while the lattice predictions for the axial form factors are somewhat higher than the measured values.

The methods developed to extract form factors in  $D \rightarrow \bar{K}^* \ell^+ \nu$  decays have now been extended to the decays  $D_s^+ \rightarrow \phi \ell^+ \nu$  and  $\Lambda_c \rightarrow \Lambda \ell^+ \nu$ . Although the experimental results are statistically limited, the semileptonic decays  $D_s^+ \rightarrow \phi \ell^+ \nu$  and  $D_s \rightarrow (\eta \text{ or } \eta') \ell^+ \nu$  appear to follow the pattern of  $D$  decays, both in terms of form-factor ratios and in terms of the relative decay rates to vector and pseudoscalar mesons. The study of form factors in the baryon decay  $\Lambda_c \rightarrow \Lambda \ell^+ \nu$  is in its infancy, but should be pursued, because theoretical predictions are often simpler for  $\Lambda$ -type baryons than for mesons. The measurement of the ratio of semileptonic decays of  $\Xi_c^0$  and  $\Xi_c^+$  has led to an estimate of the lifetime ratio, competitive and consistent with the direct measurement of lifetimes.

Although we have barely seen evidence for  $D \rightarrow \rho \ell^+ \nu$  and have not seen any evidence for  $D \rightarrow \omega \ell^+ \nu$ , these are very important modes for understanding the dynamics of transitions from heavy to light quarks. This information will be helpful in extracting  $V_{ub}$  from exclusive  $B$  decays in the future.

The prospects for advances in the precision of charm measurements are very good. CLEO II has recorded millions of  $e^+e^- \rightarrow c\bar{c}$  interactions. The experiment has installed a silicon vertex detector, which will allow the use of charm lifetime information to reduce the background in modes such as  $D \rightarrow \bar{K}^* \ell^+ \nu$  and to improve form-factor analyses. Larger data samples in the future will have a significant impact on measurements such as form factors in  $D_s^+ \rightarrow \phi \ell^+ \nu$  and  $\Lambda_c \rightarrow \Lambda \ell^+ \nu$ , and studies of modes that have barely been observed such as  $D_s^+ \rightarrow \mu^+ \nu_\mu$ ,  $D_s \rightarrow \eta \ell^+ \nu$ ,  $D \rightarrow \pi \ell^+ \nu$ , and  $D \rightarrow \rho \ell^+ \nu$ .

Fermilab hadroproduction experiment E791 has a very large data sample in hand. Results are expected soon on form factors and decay rates for suppressed modes. Fermilab photoproduction experiment E687 will run again in the next fixed-target run as E831. They expect to increase their data sample by a factor of at least 10. On a longer time scale,  $B$  factories will also produce very large samples of charmed particles. Discussions continue on a possible dedicated  $\tau$ /charm factory. Therefore the future looks bright for studies of leptonic and semileptonic charm decays: many measurements are currently limited by the size of existing data samples, but the prospects for significantly larger samples are good.

### C. $B$ semileptonic branching fractions

Apart from the average  $B$  lifetime, the inclusive  $B$  semileptonic branching fraction  $\mathcal{B}_{\text{SL}}$  is the best measured quantity in  $B$  physics. The fact that the value of  $\mathcal{B}_{\text{SL}}$  lies at the extreme lower end of theoretical expectations has generated much discussion. It is not clear how seriously to take this situation. One view is that it merely indicates the difficulties in calculating the hadronic rate, which is sensitive to QCD corrections and quark masses. Alternatively, it could indicate the presence of a new, unexpected contribution to the hadronic rate. Measurements of the semileptonic branching frac-

tion are now on solid ground: the uncertainties are fairly small, and the results are confirmed by different experiments and methods. The traditional technique of using the single-lepton spectrum at the  $Y(4S)$  has reached the point where the relative experimental error is only  $\approx 3\%$  on the latest CLEO II measurement. Averaging over all  $Y(4S)$  experiments gives  $\mathcal{B}_{\text{SL}} = (10.51 \pm 0.21)\%$  in the ACCMM model. However, the model dependence of these results is higher, giving a 4% to 5% relative uncertainty (see Table VII). To circumvent this problem, a new technique using dilepton events has been used in place of models to separate the primary from the secondary lepton spectrum. The model dependence is substantially reduced, since models are only needed to extrapolate from the lowest accepted lepton momentum ( $0.6 \text{ GeV}/c$ ) down to zero, which is only 6% of the spectrum. The recent CLEO II dilepton analysis gives

$$\mathcal{B}_{\text{SL}} = (10.49 \pm 0.17 \pm 0.43)\%, \quad (180)$$

with a relative systematic error of 4%. The LEP measurements of  $\mathcal{B}_{\text{SL}}$  tend to be systematically slightly higher than those obtained at the  $Y(4S)$  (a point that merits further investigation), but are consistent within errors. Better measurements of the charm content of hadronic  $B$  decays, although difficult, will be important in determining the source of the discrepancy between experiment and theory. The semileptonic branching fraction provides an excellent reality check of our understanding of the inclusive hadronic rate, and better calculations and measurements should be vigorously pursued.

Substantial progress has been made in predicting the  $B$ -meson semileptonic decay rate using heavy-quark expansions, and the inclusive approach may provide a measurement of  $|V_{cb}|$  with precision comparable to that from  $B \rightarrow D^* \ell^- \bar{\nu}$  at zero recoil. The size of the uncertainty on the inclusive calculation is currently a matter of controversy, but it is clear that having two competing methods is very useful.

Turning to exclusive semileptonic decays, we have seen that  $B \rightarrow D^* \ell^- \bar{\nu}$  is the most important  $B \rightarrow X_c \ell^- \bar{\nu}$  process for determining  $|V_{cb}|$ , both because it is experimentally very clean and because it has desirable features from a theoretical point of view. The absence of leading-order ( $1/m_Q$ ) corrections to the rate at zero recoil means that  $|V_{cb}|$  can be determined with rather small theoretical errors. In addition, this mode provides a way to test many HQET predictions through form-factor measurements, a program that is now well underway.

A conspicuous difference between  $B$  and  $D$  exclusive decays is the vector-to-pseudoscalar ratio, which in  $B$  decays is given by  $\Gamma(B \rightarrow D^* \ell^- \bar{\nu}) / \Gamma(B \rightarrow D \ell^- \bar{\nu})$ . This ratio is poorly measured at present (since the branching fraction for  $B \rightarrow D \ell^- \bar{\nu}$  is not yet well known), but it certainly differs greatly from the analogous quantity in  $D$  or  $D_s$  decays, where the ratio is significantly less than unity. If  $\rho^2$  is close to the measured value of 1, theoretical predictions for the vector-to-pseudoscalar ratio in  $B$  decays are completely consistent with the measured value. Better measurements of  $B \rightarrow D \ell^- \bar{\nu}$  are very desirable and should be forthcoming in the relatively near future. It would also be useful to compare the  $q^2$  dependence of the form factor for this mode with that of the form factors in  $B \rightarrow D^* \ell^- \bar{\nu}$ .

Whereas the inclusive semileptonic rate is nearly accounted for by known exclusive modes in  $D$  decays, this is not the case in  $B$  semileptonic decays. (The known  $B \rightarrow X_c \ell^- \bar{\nu}$  modes were summarized in Table XXXV.) Together,  $B \rightarrow D \ell^- \bar{\nu}$  and  $B \rightarrow D^* \ell^- \bar{\nu}$  account for 60% to 70% of the inclusive semileptonic rate. It is clear from ALEPH and OPAL measurements that  $B \rightarrow D_1 X \ell^- \bar{\nu}$ ,  $B \rightarrow D_2^* X \ell^- \bar{\nu}$ , and other  $B \rightarrow D^* X \ell^- \bar{\nu}$  decays account for a significant part of the rest. In these studies, the LEP experiments have exploited the long  $B$  lifetime and used high-precision silicon detectors to associate tracks to decay vertices. If we sum the branching fractions for  $\bar{B}^0 \rightarrow D^+ \ell^- \bar{\nu}$ ,  $\bar{B}^0 \rightarrow D^{*+} \ell^- \bar{\nu}$ , and  $B \rightarrow D^{*+} \pi^- \ell^- \bar{\nu} X$  (multiplying the last by 1.5 as an estimate of the total rate including  $D^{*0}$ ), we obtain  $(7.9 \pm 1.1)\%$ , or  $(76 \pm 11)\%$  of the semileptonic branching fraction. With an additional contribution from  $B \rightarrow D_2^* X \ell^- \bar{\nu}$  (as yet poorly known), we are beginning to see a large part of the semileptonic rate, but the uncertainties are still quite large.

We now turn to  $B \rightarrow X_u \ell^- \bar{\nu}$  decays. The challenge of understanding these processes is formidable, as we have discussed in Sec. VI.F. While  $B \rightarrow \rho \ell^- \bar{\nu}$ ,  $B^- \rightarrow \omega \ell^- \bar{\nu}$ , and  $B \rightarrow \pi \ell^- \bar{\nu}$  may well be a large fraction of the rate in the end-point region of the lepton-energy spectrum, over the entire spectrum there are no dominant modes, so an already small rate is divided among a large number of exclusive modes. There is considerable uncertainty associated with the measurement of  $|V_{ub}|$  from the end-point region of the inclusive lepton spectrum, since such a small part of phase space is involved. The difference between the values of  $|V_{ub}/V_{cb}|$  extracted using two different models (ACCMM and ISGW) is 33%, corresponding to a 66% difference in the rate! (This difference may represent a somewhat pessimistic view of the theoretical uncertainty, since the ISGW model was constructed to give a lower limit for the rate in the end-point region.) We have also seen that calculations based on HQET can only predict the rate in the end-point region if that region is defined to be quite large (Sec. V.B). A measurement of the inclusive  $q^2$  spectrum in the region of high lepton momenta may help to clarify these issues. This measurement is difficult in an inclusive study, since one must calculate  $q^2$  using only the lepton momentum and the missing energy of the event, which is used to estimate the momentum of the neutrino. Even so, the technique looks promising, at least at a crude level.

The CLEO II measurement of  $B \rightarrow \pi \ell^- \bar{\nu}$  represents a milestone in the search for exclusive  $B \rightarrow X_u \ell^- \bar{\nu}$  modes, and observations of other such decays should not be too far in the future. Mapping out these modes and studying their kinematic distributions is one of the most important long-term goals in the ongoing program to understand semileptonic  $B$  decays. Eventually, measurement of the rate for  $B \rightarrow \pi \ell^- \bar{\nu}$ ,  $B \rightarrow \rho \ell^- \bar{\nu}$ , or  $B^- \rightarrow \omega \ell^- \bar{\nu}$  at high  $q^2$  should provide a reasonably good determination of  $|V_{ub}|$  by comparison with the rate predicted from lattice QCD calculations. Measurements of kinematic distributions will provide tests of the predictions for  $B \rightarrow X_u \ell^- \bar{\nu}$  decays, just as they currently are for  $B \rightarrow X_c \ell^- \bar{\nu}$  modes.

## D. Form factors for $B$ semileptonic decays

Confidence in our understanding of the dynamics of semileptonic decays will come from comparisons of form-factor measurements with predictions. With the recent CLEO II measurement of the form factors for  $B \rightarrow D^* \ell^- \bar{\nu}$ , a step has been taken in this direction. This measurement is the first to fit all observable quantities (three angles and  $q^2$ ) and to incorporate their correlations. The analysis differs from  $D \rightarrow \bar{K}^* \ell^+ \nu$  form-factor studies in two significant ways, even though the quantum numbers involved are identical. First, in the  $D \rightarrow \bar{K}^* \ell^+ \nu$  measurements, the  $q^2$  dependence of the form factors is completely fixed by the assumption of pole forms with given masses. Thus three parameters (pole masses) are fixed, while the remaining two parameters (form-factor ratios at  $q^2=0$ ) are determined by the fit. In the  $B \rightarrow D^* \ell^- \bar{\nu}$  analysis, three parameters are determined from the fit: two form-factor ratios and a form-factor slope, which is closely related to the slope of the Isgur-Wise function. The pole form for the  $q^2$  dependence is not used. Since the  $q^2$  range is quite limited, a simple linear form is assumed, which is consistent with expectations. It is significant that the analysis determines the form-factor ratios without fixing this slope; similarly, it determines the slope without fixing the ratios. As for  $D \rightarrow \bar{K}^* \ell^+ \nu$ , one would really like to allow all five parameters to vary, but the three form factors have been tied to each other using results from heavy-quark symmetry. Thus the analysis does not go as far as one would like, either in precision or in allowing all parameters to vary. Nevertheless, the observed agreement between HQET predictions and experiment on the two form-factor ratios is certainly not required by the constraints imposed on the measurement. In fact, most models are in approximate agreement in predicting these form factors, indicating that  $B \rightarrow D^* \ell^- \bar{\nu}$  is on relatively solid ground theoretically. This mode will undoubtedly be studied extensively in the future, as much larger data samples are obtained.

Tremendous progress has been made in understanding semileptonic  $B$  decays and in using them to measure the magnitudes of the CKM elements  $V_{cb}$  and  $V_{ub}$ . Much work remains to be done: we need higher-precision measurements of  $B \rightarrow X_c \ell^- \bar{\nu}$  modes, and we have just begun to explore  $B \rightarrow X_u \ell^- \bar{\nu}$  decays. With the large  $B$  data samples expected at several laboratories around the world, these studies will be an important part of the high-energy physics program over the next five to ten years.

## ACKNOWLEDGMENTS

It is a pleasure to thank the many people who helped us to write this review. Guy Blaylock, Thomas Browder, Persis Drell, Lawrence Gibbons, Jeffrey Gronberg, David Lange, Rollin Morrison, Harry Nelson, Ritchie Patterson, Chris Quigg, Douglas Roberts, Anders Ryd, Sheldon Stone, and Michael Witherell provided valuable criticism and ideas; their help vastly improved this paper. Anders Ryd, a UCSB graduate student, had a major influence not only in helping to produce figures and in improving the text, but also in developing ideas and methods for studying semileptonic  $B$  decays. Our colleagues in CLEO and E791 provided valuable ideas

and made many contributions to the work presented in this review. We also wish to thank our theoretical colleagues, in particular, Mathias Neubert, who provided Figures 22 and 23; Daryl Scora, who provided Figures 7 and 8; and Nathan Isgur, Aneesh Manohar, Martin Savage, K. Uraltsev, A. Vainshtein, and Mark Wise for many valuable discussions and comments. The text was substantially improved through the efforts of Kate Metropolis and Pat Metropolis, and Debbie Ceder helped enormously with the manuscript. Nora Rogers provided assistance with the references, and Ray Cowan advised us on TEX.

## REFERENCES

- Abachi, S., *et al.*, 1988, Phys. Lett. B **205**, 411.  
 Abachi, S., *et al.*, 1995, Phys. Rev. Lett. **74**, 2632.  
 Abada, A., *et al.*, 1992, Nucl. Phys. B **376**, 172.  
 Abada, A., *et al.*, 1994, Nucl. Phys. B **416**, 675.  
 Abe, F., *et al.*, 1993, Phys. Rev. Lett. **71**, 500.  
 Abe, F., *et al.*, 1995, Phys. Rev. Lett. **74**, 2626.  
 Abreu, P., *et al.*, 1993, Phys. Lett. B **311**, 379.  
 Acosta, D., *et al.*, 1994, Phys. Rev. D **49**, 5690.  
 Acton, P.D., *et al.*, 1992, Phys. Lett. B **281**, 394.  
 Adamovich, M., *et al.*, 1991, Phys. Lett. B **208**, 142.  
 Adeva, B., *et al.*, 1994, Phys. Lett. B **332**, 201.  
 Adler, J., *et al.*, 1988a, Phys. Rev. Lett. **60**, 89.  
 Adler, J., *et al.*, 1988b, Phys. Rev. Lett. **60**, 1375.  
 Adler, J., *et al.*, 1989, Phys. Rev. Lett. **62**, 1821.  
 Adler, J., *et al.*, 1990, Phys. Rev. Lett. **64**, 169.  
 Akerib, D.S., *et al.*, 1993, Phys. Rev. Lett. **71**, 3070.  
 Akers, R., *et al.*, 1993, Z. Phys. C **60**, 199.  
 Akers, R., *et al.*, 1995, "A Study of Charm Meson Production in Semileptonic B Decays," CERN Preprint No. CERN-PPE/95-02.  
 Alam, M.S., *et al.*, 1993, Phys. Rev. Lett. **71**, 1311.  
 Alam, M.S., *et al.*, 1994, Cornell University Preprint No. CLNS-94-1314.  
 Albrecht, H., *et al.*, 1987, Phys. Lett. B **192**, 245.  
 Albrecht, H., *et al.*, 1989a, Nucl. Instrum. Methods A **275**, 1.  
 Albrecht, H., *et al.*, 1989b, Phys. Lett. B **229**, 175.  
 Albrecht, H., *et al.*, 1990a, Phys. Lett. B **234**, 409.  
 Albrecht, H., *et al.*, 1990b, Phys. Lett. B **249**, 359.  
 Albrecht, H., *et al.*, 1991a, Phys. Lett. B **255**, 297.  
 Albrecht, H., *et al.*, 1991b, Phys. Lett. B **255**, 634.  
 Albrecht, H., *et al.*, 1991c, Phys. Lett. B **269**, 234.  
 Albrecht, H., *et al.*, 1992a, Phys. Lett. B **275**, 195.  
 Albrecht, H., *et al.*, 1992b, Z. Phys. C **54**, 1.  
 Albrecht, H., *et al.*, 1993a, Phys. Lett. B **303**, 368.  
 Albrecht, H., *et al.*, 1993b, Phys. Lett. B **318**, 397.  
 Albrecht, H., *et al.*, 1993c, Z. Phys. C **57**, 533.  
 Albrecht, H., *et al.*, 1993d, Z. Phys. C **60**, 11.  
 Albrecht, H., *et al.*, 1993e, "Evidence for  $\Omega_c$  Semileptonic Decays," contribution to the 16th International Symposium on Lepton and Photon Interactions at High Energies, Cornell University, Ithaca, New York, 1993, unpublished.  
 Albrecht, H., *et al.*, 1994a, Phys. Lett. B **324**, 249.  
 Albrecht, H., *et al.*, 1994b, Phys. Lett. B **326**, 320.  
 ALEPH Collaboration, 1994, contribution to the 27th International Conference on High Energy Physics, Glasgow, Scotland, 1994, unpublished.  
 ALEPH Collaboration, 1995, CERN Report No. CERN-PPE/95-094, submitted to Phys. Lett. B.  
 Alexander, J., *et al.*, 1990, Phys. Rev. Lett. **65**, 1531.

- Alexander, J., *et al.*, 1992a, Phys. Rev. Lett. **68**, 1275.
- Alexander, J., *et al.*, 1992b, Phys. Rev. Lett. **68**, 1279.
- Alexander, J.P., *et al.*, 1994a, Cornell University Report No. CLEO-CONF-94-5.
- Alexander, J., *et al.*, 1994b, Cornell University Report No. CLNS 94/1288.
- Alexandrou, C., S. Guesken, F. Jegerlehner, K. Schilling, and R. Sommer, 1994, Z. Phys. C **62**, 659.
- Ali, A., 1994, in *B Decays, Revised 2nd Edition*, edited by S. Stone (World Scientific, Singapore), p. 1.
- Ali, A., and C. Greub, 1993, Z. Phys. C **60**, 433.
- Aliev, T.M., and V.L. Eletskii, 1983, Yad. Fiz. **38**, 1537 [Sov. J. Nucl. Phys. **38**, 936 (1983)].
- Aliev, T.M., A.A. Ovchinnikov, and V.A. Slobodenyuk, 1989, Trieste Report No. IC/89/382.
- Allton, C.R., *et al.*, 1994a, Phys. Lett. B **326**, 295.
- Allton, C.R., *et al.*, 1994b, in *Lattice 93: Proceedings of the International Symposium on Lattice Field Theory*, edited by T. Draper, S. Gottlieb, A. Soni, and D. Toussaint, Nucl. Phys. B (Proc. Suppl.) **34**, p. 456.
- Allton, C.R., *et al.*, 1995, Phys. Lett. B **345**, 513.
- Altarelli, G., and L. Maiani, 1974, Phys. Lett. B **52**, 351.
- Altarelli, G., *et al.*, 1981a, Phys. Lett. B **99**, 141.
- Altarelli, G., *et al.*, 1981b, Nucl. Phys. B **187**, 461.
- Altarelli, G., N. Cabibbo, G. Corbò, L. Maiani, and G. Martinelli, 1982, Nucl. Phys. B **208**, 365.
- Altarelli, G., and S. Petrarca, 1991, Phys. Lett. B **261**, 303.
- Altomari, T., and L. Wolfenstein, 1988, Phys. Rev. D **37**, 681.
- Ammar, R., *et al.*, 1993, Phys. Rev. Lett. **71**, 674.
- Ammar, R., *et al.*, 1995, Cornell University Report No. CLEO-CONF-95-9.
- Anderson, G., S. Raby, S. Dimopoulos, L.J. Hall, and G.D. Starkman, 1994, Phys. Rev. D **49**, 3660.
- Anjos, J.C., *et al.*, 1989a, Phys. Rev. Lett. **62**, 722.
- Anjos, J.C., *et al.*, 1989b, Phys. Rev. Lett. **62**, 1587.
- Anjos, J.C., *et al.*, 1990a, Phys. Rev. Lett. **64**, 2885.
- Anjos, J.C., *et al.*, 1990b, Phys. Rev. Lett. **65**, 2630.
- Anjos, J.C., *et al.*, 1991, Phys. Rev. Lett. **67**, 1507.
- Anjos, J.C., *et al.*, 1992, Phys. Rev. D **45**, R2177.
- Aoki, S., *et al.*, 1993, Prog. Theor. Phys. **89**, 131.
- Appel, J.A., 1992, Annu. Rev. Nucl. Part. Sci. **42**, 367.
- Artuso, M., 1993, in *Proceedings of the Workshop on B Physics at Hadron Accelerators*, Snowmass, Colorado, 1993, edited by C. Shekhar Mishra and P. McBride, Report No. SSCL-SR-1225 and Fermilab-Conf-93/267, p. 97.
- Athanas, M., *et al.*, 1994, Phys. Rev. Lett. **73**, 393.
- Atwood, D., and W. Marciano, 1990, Phys. Rev. D **41**, 1736.
- Aubert, J.J., *et al.*, 1974, Phys. Rev. Lett. **33**, 1404.
- Aubert, J.J., *et al.*, 1983, Nucl. Phys. B **213**, 31.
- Augustin, J.-E., *et al.*, 1974, Phys. Rev. Lett. **33**, 1406.
- Avery, P., *et al.*, 1994a, Cornell University Report No. CLEO CONF 94-7.
- Avery, P., *et al.*, 1994b, Phys. Lett. B **337**, 405.
- Avery, P., *et al.*, 1994c, Phys. Lett. B **331**, 236.
- BaBar Collaboration, 1994, "Letter of Intent for the Study of CP Violation and Heavy Flavor Physics at PEP-II," SLAC Report No. SLAC-443.
- Bacino, W., *et al.*, 1979, Phys. Rev. Lett. **43**, 1073.
- Bacino, W., *et al.*, 1980, Phys. Rev. Lett. **45**, 329.
- Bagan, E., P. Ball, V.M. Braun, and H.G. Dosch, 1992, Phys. Lett. B **278**, 457.
- Bagan, E., P. Ball, V.M. Braun, and P. Gosdzinsky, 1994, Nucl. Phys. B **432**, 3.
- Bagan, E., P. Ball, V.M. Braun, and P. Gosdzinsky, 1995, Phys. Lett. B **342**, 362.
- Bai, Z., *et al.*, 1991, Phys. Rev. Lett. **66**, 1011.
- Bai, J.Z., *et al.*, 1995a, Phys. Rev. Lett. **74**, 4599.
- Bai, J.Z., *et al.*, 1995b, Phys. Rev. D **52**, 3781.
- Baillie, G., 1994, Phys. Lett. B **324**, 446.
- Ball, P., V.M. Braun, and H.G. Dosch, 1991, Phys. Rev. D **44**, 3567.
- Ball, P., M. Beneke, and V.M. Braun, 1995, CERN-TH/95-65, UM-TH-95-07, hep-ph/9503492.
- Baltrusaitis, R.M., *et al.*, 1985, Phys. Rev. Lett. **54**, 1976.
- Bareiss, A., and E.A. Paschos, 1989, Nucl. Phys. B **327**, 353.
- Barish, B., *et al.*, 1995a, Phys. Rev. D **51**, 1014.
- Barish, B., *et al.*, 1995b, Cornell University Preprint No. CLNS-95-1362, CLEO 95-17.
- Barlag, S., *et al.*, 1989, Phys. Lett. B **233**, 522.
- Barlag, S., *et al.*, 1990, Phys. Lett. B **236**, 495.
- Bartelt, J., *et al.*, 1993a, Phys. Rev. Lett. **71**, 4111.
- Bartelt, J., *et al.*, 1993b, Cornell University Report No. CLEO-CONF-93-19.
- Battle, M., *et al.*, 1994, Cornell University Report No. CLEO-CONF-94-18.
- Bauer, M., B. Stech, and M. Wirbel, 1987, Z. Phys. C **34**, 103.
- Bauer, M., and M. Wirbel, 1989, Z. Phys. C **42**, 671.
- Baxter, R.M., *et al.*, 1994, Phys. Rev. D **49**, 1594.
- Bean, A., *et al.*, 1993a, Phys. Lett. B **317**, 647.
- Bean, A., *et al.*, 1993b, Phys. Rev. Lett. **70**, 2681.
- Belle Collaboration, 1994, "Letter of Intent for a Study of CP Violation in B Meson Decays," KEK Report 94-2.
- Bergfeld, T., *et al.*, 1994, Phys. Lett. B **323**, 219.
- Bernard, C.W., Z.X. El-Khadra, and A. Soni, 1991, Phys. Rev. D **43**, 2140.
- Bernard, C.W., Z.X. El-Khadra, and A. Soni, 1992, Phys. Rev. D **45**, 869.
- Bernard, C.W., Z.X. El-Khadra, and A. Soni, 1993, Phys. Rev. D **47**, 998.
- Bernard, C., Y. Shen, and A. Soni, 1993, Phys. Lett. B **317**, 164.
- Bernard, C., J.N. Labrenz, and A. Soni, 1994, Phys. Rev. D **49**, 2536.
- Bhattacharya, T., and R. Gupta, 1994a, Los Alamos Report No. LA-UR-95-72.
- Bhattacharya, T., and R. Gupta, 1994b, Los Alamos Report No. LA-UR-94-3079, and in *The Albuquerque Meeting: Proceedings of the 8th Meeting, Division of Particles and Fields of the American Physical Society*, the University of New Mexico, 1994, edited by Sally Seidel (World Scientific, Singapore), p. 605.
- Bhattacharya, T., and R. Gupta, 1994c, private communication to J. Shigemitsu.
- Bigi, I.I., B. Blok, M. Shifman, and A. Vainshtein, 1994, Phys. Lett. B **323**, 408.
- Bigi, I.I., M. Shifman, N.G. Uraltsev, and A.I. Vainshtein, 1993, Phys. Rev. Lett. **71**, 496.
- Bigi, I.I., M. Shifman, N.G. Uraltsev, and A. Vainshtein, 1994, Int. J. Mod. Phys. A **9**, 2467.
- Bigi, I.I., and N.G. Uraltsev, 1992, Phys. Lett. B **280**, 271.
- Bigi, I.I., N.G. Uraltsev, and A.I. Vainshtein, 1992, Phys. Lett. B **293**, 430.
- Bitar, K.M., *et al.*, 1994, in *Proceedings of the International Symposium on Lattice Field Theory*, edited by T. Draper, S. Gottlieb, A. Soni and D. Toussaint, Nucl. Phys. B (Proc. Suppl.) **34**, p. 379.
- Bjorken, J.D., 1990, in *Results and Perspectives in Physics, Proceedings of the 4th Rencontres de Physique de la Vallée d'Aoste*, La Thuile, Italy, 1990, edited by M. Greco (Editions Frontières, Gif-sur-Yvette, France), p. 583; also in *Proceedings of the Eighth*

- teenth SLAC Summer Institute on Particle Physics, Gauge Bosons and Heavy Quarks*, 1990, edited by J.F. Hawthorne, SLAC Report-378, p. 167; SLAC Report No. SLAC-PUB-5278.
- Blok, B., and M. Shifman, 1993, *Phys. Rev. D* **47**, 2949.
- Booth, S.P., *et al.* (UKQCD), 1994, *Phys. Rev. Lett.* **72**, 462.
- Bortoletto, D., 1992, in *Physics in Collision 12: 12th International Conference on Physics in Collision*, Boulder, Colorado, 1992, edited by J. Cumalat (Editions Frontières, Gif-sur-Yvette, France), p. 467.
- Bortoletto, D., *et al.*, 1989, *Phys. Rev. Lett.* **63**, 1667.
- Bortoletto, D., and S. Stone, 1990, *Phys. Rev. Lett.* **65**, 2951.
- Bowler, K.C., *et al.*, 1994, University of Edinburgh Report No. EDINBURGH-94-546.
- Britton, D.I., *et al.*, 1994, *Phys. Rev. D* **49**, 28.
- Broadhurst, D.J., and A.G. Grozin, 1992, *Phys. Lett. B* **274**, 421.
- Buras, A.J., M.E. Lautenbacher, and G. Ostermaier, 1994, *Phys. Rev. D* **50**, 3433.
- Buras, A.J., W. Slominski, and J. Steger, 1984, *Nucl. Phys. B* **238**, 529.
- Buras, A.J., and P.H. Weisz, 1990, *Nucl. Phys. B* **333**, 66.
- Burdman, G., and J.F. Donoghue, 1992, *Phys. Rev. Lett.* **68**, 2887.
- Burdman, G., Z. Ligeti, M. Neubert, and Y. Nir, 1994, *Phys. Rev. D* **49**, 2331.
- Buskulic, D., *et al.*, 1992a, *Phys. Lett. B* **294**, 145.
- Buskulic, D., *et al.*, 1992b, *Phys. Lett. B* **297**, 449.
- Buskulic, D., *et al.*, 1993, *Phys. Lett. B* **298**, 479.
- Buskulic, D., *et al.*, 1994a, *Z. Phys. C* **62**, 179.
- Buskulic, D., *et al.*, 1994b, *Nucl. Instrum. Methods A* **346**, 461.
- Buskulic, D., *et al.*, 1995a, *Phys. Lett. B* **343**, 444.
- Buskulic, D., *et al.*, 1995b, *Phys. Lett. B* **345**, 103.
- Butler, F., *et al.*, 1992, *Phys. Rev. Lett.* **69**, 2041.
- Butler, F., *et al.*, 1994, *Phys. Lett. B* **324**, 255.
- Butler, F., *et al.*, 1995, Cornell University Preprint No. CLNS 95/1324.
- Cabibbo, N., 1963, *Phys. Rev. Lett.* **10**, 531.
- Cabibbo, N., and L. Maiani, 1978, *Phys. Lett. B* **79**, 109.
- Capstick, S., and S. Godfrey, 1990, *Phys. Rev. D* **41**, 2856.
- CDF Collaboration, 1994, CDF Experiment, Fermilab, CDF-DOC-ADVISORY-PUBLIC/2436.
- Cea, P., 1988, *Phys. Lett. B* **206**, 691.
- CERN Reports, 1992, CERN-LHCC/92-3 and CERN-LHCC/92-4.
- CERN Reports, 1993, CERN-LHCC/93-50 and CERN-LHCC/93-54.
- Chau, L.L., and W.Y. Keung, 1984, *Phys. Rev. Lett.* **53**, 1802.
- Chay, J., H. Georgi, and B. Grinstein, 1990, *Phys. Lett. B* **247**, 399.
- Cheng, H.-Y., *et al.*, 1993, Cornell University Preprint No. CLNS 93/1204.
- CLEO Collaboration, 1994, "CLEO III Detector Proposal," Cornell University Preprint No. CLNS 94/1277.
- Close, F.E., and A. Wambach, 1994a, *Nucl. Phys. B* **412**, 169.
- Close, F.E., and A. Wambach, 1994b, Rutherford Laboratory Preprint No. RAL-94-041.
- Colangelo, P., G. Nardulli, and N. Paver, 1992, *Phys. Lett. B* **293**, 207.
- Colangelo, P., G. Nardulli, and M. Pietroni, 1991, *Phys. Rev. D* **43**, 3002.
- Cortes, J.L., X.Y. Pham, and A. Tounsi, 1982, *Phys. Rev. D* **25**, 188.
- Crawford, G., *et al.*, 1991, *Phys. Rev. D* **44**, 3394.
- Crawford, G., *et al.*, 1995, Cornell University Preprint No. CLNS-94-1306.
- Crisafulli, M., *et al.*, 1989, *Phys. Lett. B* **223**, 90.
- Csaki, C., and L. Randall, 1994, *Phys. Lett. B* **324**, 451.
- Culbertson, R.L., 1993, Ph.D. thesis, University of Illinois, p. 87.
- Czapek, G., *et al.*, 1993, *Phys. Rev. Lett.* **70**, 17.
- Czarnecki, A., and M. Jezabek, 1994, *Nucl. Phys. B* **427**, 3.
- DELPHI Collaboration, 1995, CERN Preprint PPE/95-08.
- Dib, C.O., and F. Vera, 1993, *Phys. Rev. D* **47**, 3938.
- Dimopoulos, S., L.J. Hall, and S. Raby, 1992, *Phys. Rev. Lett.* **68**, 1984.
- Dominguez, C.A., 1988, *Phys. Lett. B* **207**, 499.
- Dominguez, C.A., 1992, University of Cape Town Report No. UCT-TP 180/92.
- Dominguez, C., and N. Paver, 1987, *Phys. Lett. B* **197**, 423; **199**, 596(E).
- Dominguez, C., and N. Paver, 1992, *Phys. Lett. B* **276**, 179.
- Duncan, A., E. Eichten, J. Flynn, B. Hill, G. Hockney, and H. Thacker, 1994, Fermilab Report No. FERMILAB-PUB-94/164-T.
- E653 Collaboration, 1993, contribution to the 16th International Symposium on Lepton and Photon Interactions at High Energies, Cornell University, Ithaca, New York, 1993, unpublished.
- Eichten, E., and B. Hill, 1990a, *Phys. Lett. B* **234**, 511.
- Eichten, E., and B. Hill, 1990b, *Phys. Lett. B* **243**, 427.
- Falk, A.F., H. Georgi, B. Grinstein, and M.B. Wise, 1990, *Nucl. Phys. B* **343**, 1.
- Falk, A.F., E. Jenkins, A.V. Manohar, and M.V. Wise, 1994, *Phys. Rev. D* **49**, 4553.
- Falk, A.F., Z. Ligeti, M. Neubert, and Y. Nir, 1994, *Phys. Lett. B* **326**, 145.
- Falk, A.F., and M. Neubert, 1993a, *Phys. Rev. D* **47**, 2965.
- Falk, A.F., and M. Neubert, 1993b, *Phys. Rev. D* **47**, 2982.
- Falk, A.F., M.B. Wise, and I. Dunietz, 1994, Caltech Preprint No. CALT-68-1933.
- Fox, G., and S. Wolfram, 1978, *Phys. Rev. Lett.* **41**, 1581.
- Frabetti, P.L., *et al.*, 1993a, *Phys. Lett. B* **307**, 262.
- Frabetti, P.L., *et al.*, 1993b, *Phys. Lett. B* **313**, 253.
- Frabetti, P.L., *et al.*, 1993c, *Phys. Lett. B* **315**, 203.
- Frabetti, P.L., *et al.*, 1993d, *Phys. Rev. Lett.* **70**, 1381; **70**, 2058.
- Frabetti, P.L., *et al.*, 1994, *Phys. Lett. B* **328**, 187.
- Fulton, R., *et al.*, 1990, *Phys. Rev. Lett.* **64**, 16.
- Fulton, R., *et al.*, 1991, *Phys. Rev. D* **43**, 651.
- Gaillard, M.K., and B.W. Lee, 1974, *Phys. Rev. Lett.* **33**, 108.
- Garisto, R., 1995, *Phys. Rev. D* **51**, 1107.
- Gasser, J., and H. Leutwyler, 1982, *Phys. Rep.* **87**, 77.
- Georgi, H., 1990, *Phys. Lett. B* **240**, 447.
- Georgi, H., 1991, *Nucl. Phys. B* **348**, 293.
- Georgi, H., B. Grinstein, and M.B. Wise, 1990, *Phys. Lett. B* **252**, 456.
- Gibbons, L., 1995, University of Rochester Report No. UR-1427. To appear in Proceedings of the 30th Rencontres de Moriond: Electroweak Interactions and Unified Theories, Meribel les Allues, France, 1995 (Editions Frontières, Gif-sur-Yvette), in press.
- Gilman, F.J., and R.L. Singleton, Jr., 1990, *Phys. Rev. D* **41**, 93.
- Gilman, F.J., and M.B. Wise, 1983, *Phys. Rev. D* **27**, 1128.
- Grinstein, B., 1990, *Nucl. Phys. B* **339**, 253.
- Grinstein, B., 1992, *Annu. Rev. Nucl. Part. Phys.* **42**, 101.
- Gronau, M., 1994, in *B Decays, Revised 2nd Edition*, edited by S. Stone (World Scientific, Singapore), p. 644.
- Gronau, M., and S. Wakaizumi, 1992, *Phys. Lett. B* **280**, 79.
- Gronberg, J., *et al.*, 1994, Cornell University Report No. CLEO-CONF-94-6.
- Gronberg, J., *et al.*, 1995, Cornell University Report No. CLEO-CONF-95-27.
- Gross, D.J., and F. Wilczek, 1973, *Phys. Rev. Lett.* **30**, 1343.
- Grossman, Y., and Z. Ligeti, 1994, *Phys. Lett. B* **332**, 373.
- Grzadkowski, B., and W.-S. Hou, 1992, *Phys. Lett. B* **283**, 427.
- Guberina, B., R. Ruckl, and J. Trampetic, 1986, *Z. Phys. C* **33**, 297.

- Gupta, R., 1995, Talk presented at the Eleventh Aspen Winter Conference on Elementary Particle Physics: Heavy Quarks, Heavy Leptons, and Massive Neutrinos, Aspen, Colorado, 1995, unpublished.
- Gusken, S., K. Schilling, and G. Siegert, 1995, HLRZ, Jülich Report No. HLRZ-94-74. Available on Bulletin Board hep-lat@ftp.scri.fsu.edu-9501013.
- Hagiwara, K., A.D. Martin, and J.F. Wade, 1989, Nucl. Phys. B **327**, 569.
- Hashimoto, S., 1994, Phys. Rev. D **50**, 4639.
- Heiliger, P., and L.M. Sehgal, 1989, Phys. Lett. B **229**, 409.
- Henderson, S., *et al.*, 1992, Phys. Rev. D **45**, 2212.
- Herb, S.W., *et al.*, 1977, Phys. Rev. Lett. **39**, 252.
- Herrlich, S., and U. Nierste, 1994, Nucl. Phys. B **419**, 292.
- Herrlich, S., and U. Nierste, 1995, Technische Universität München Preprint TUM-T31-81/95.
- Hussain, F., J.G. Körner, M. Krämer, and G. Thompson, 1991, Z. Phys. C **51**, 321.
- Inami, T., and C.S. Lim, 1981, Prog. Theor. Phys. **65**, 297; **65**, 1772(E).
- Isgur, N., and M.B. Wise, 1989, Phys. Lett. B **232**, 113.
- Isgur, N., and M.B. Wise, 1990a, Phys. Lett. B **237**, 527.
- Isgur, N., and M.B. Wise, 1990b, Phys. Rev. D **41**, 151.
- Isgur, N., and M.B. Wise, 1991a, Nucl. Phys. B **348**, 276.
- Isgur, N., and M.B. Wise, 1991b, Phys. Rev. Lett. **66**, 1130.
- Isgur, N., D. Scora, B. Grinstein, and M.B. Wise, 1989, Phys. Rev. D **39**, 799.
- Jarlskog, C., 1989, in *CP Violation*, edited by C. Jarlskog (World Scientific, Singapore), p. 3.
- Jezabek, M., and J.H. Kuhn, 1989, Nucl. Phys. B **320**, 20.
- Jin, H.Y., C.S. Huang, and Y.B. Dai, 1992, Z. Phys. C **56**, 707.
- Kagan, A.L., 1994, SLAC Preprint No. SLAC-PUB-6626.
- Kamal, A.N., Q.P. Xu, and A. Czarnecki, 1993, University of Alberta Report No. Alberta Thy-3-93.
- Klein, S., *et al.*, 1989, Phys. Rev. Lett. **62**, 2444.
- Kobayashi, M., and T. Maskawa, 1973, Prog. Theor. Phys. **49**, 652.
- Kodama, K., *et al.*, 1992a, Phys. Lett. B **274**, 246.
- Kodama, K., *et al.*, 1992b, Phys. Lett. B **286**, 187.
- Kodama, K., *et al.*, 1993a, Phys. Lett. B **309**, 483.
- Kodama, K., *et al.*, 1993b, Phys. Lett. B **313**, 260.
- Kodama, K., *et al.*, 1993c, Phys. Lett. B **316**, 455.
- Kodama, K., *et al.*, 1994, Phys. Lett. B **336**, 605.
- Korchemsky, G., and G. Sterman, 1994, Phys. Lett. B **340**, 96.
- Körner, J.G., and M. Krämer, 1992, Phys. Lett. B **275**, 495.
- Körner, J.G., M. Krämer, and D. Pirjol, 1994, Prog. Part. Nucl. Phys. **33**, 787.
- Körner, J.G., K. Schilcher, M. Wirbel, and Y.L. Wu, 1990, Z. Phys. C **48**, 663.
- Körner, J.G., and G.A. Schuler, 1988, Z. Phys. C **38**, 511; **41**, 690(E).
- Körner, J.G., and G.A. Schuler, 1989, Phys. Lett. B **226**, 185.
- Körner, J.G., and G.A. Schuler, 1990, Z. Phys. C **46**, 93.
- Kramer, G., and W.F. Palmer, 1990, Phys. Rev. D **42**, 85.
- Krasemann, H., 1980, Phys. Lett. B **96**, 397.
- Kubota, Y., *et al.*, 1992, Nucl. Instrum. Methods A **320**, 66.
- Kubota, Y., *et al.*, 1995, Cornell University Preprint No. CLNS-95-1363, CLEO 95-18.
- Lepage, G.P., and S.J. Brodsky, 1980, Phys. Rev. D **22**, 2157.
- Ligeti, Z., Y. Nir, and M. Neubert, 1994, Phys. Rev. D **49**, 1302.
- Lohse, T., *et al.* (HERA-B Collaboration), 1994, "Letter of Intent, HERA-B: An Experiment to Study CP Violation in the B System Using an Internal Target at the HERA Proton Ring," DESY Report No. DESY-PRC-94/02.
- Lubicz, V., G. Martinelli, M.S. McCarthy, and C.T. Sachrajda, 1992, Phys. Lett. B **274**, 415.
- Luke, M.E., 1990, Phys. Lett. B **252**, 447.
- Luke, M., and M.J. Savage, 1994, Phys. Lett. B **321**, 88.
- Mannel, T., 1993, in *Proceedings of the 5th International Symposium on Heavy Flavour Physics*, Montreal, Canada, 1993, edited by D.I. Britton, D.B. MacFarlane, and P.M. Patel (Editions Frontières, Gif-sur-Yvette, France), p. 21.
- Mannel, T., 1994, Phys. Rev. D **50**, 428.
- Mannel, T., and W. Roberts, 1993, Phys. Rev. D **47**, 4963.
- Mannel, T., W. Roberts, and Z. Ryzak, 1991a, Nucl. Phys. B **355**, 38.
- Mannel, T., W. Roberts, and Z. Ryzak, 1991b, Phys. Lett. B **255**, 593.
- Manohar, A.V., and M.B. Wise, 1994, Phys. Rev. D **49**, 1310.
- Morrison, R.J., and J.D. Richman, 1994, in Review of Particle Properties, Part I, p. 1565 and Part II, p. 1602, Phys. Rev. D **50**, 1173.
- Muheim, F., 1994, Cornell University Report No. CLEO-Talk94-11. Also in *The Albuquerque Meeting: Proceedings of the 8th Meeting, Division of Particles and Fields of the American Physical Society*, the University of New Mexico, 1994, edited by Sally Seidel (World Scientific, Singapore), p. 851.
- Nachtmann, O., 1990, *Elementary Particle Physics* (Springer-Verlag, Berlin), pp. 361–368 and pp. 506–508.
- Narison, S., 1987, Phys. Lett. B **198**, 104.
- Narison, S., 1994a, Phys. Lett. B **325**, 197.
- Narison, S., 1994b, Phys. Lett. B **337**, 163.
- Nelson, H.N., 1992, in *Proceedings of the Twentieth SLAC Summer Institute on Particle Physics, The Third Family and the Physics of Flavor*, 1992, edited by L. Vassilian, SLAC-Report-412, p. 47.
- Neubert, M., 1991, Phys. Lett. B **264**, 455.
- Neubert, M., 1992, Phys. Rev. D **45**, 2451.
- Neubert, M., 1994a, Phys. Rev. D **49**, 3392.
- Neubert, M., 1994b, Phys. Lett. B **338**, 84.
- Neubert, M., 1994c, Phys. Rep. **245**, 259.
- Neubert, M., 1994d, Phys. Rev. D **49**, 4623.
- Neubert, M., and V. Rieckert, 1992, Nucl. Phys. B **382**, 97.
- Nieves, M., *et al.*, 1994, Southampton University Report No. SHEP-94-95-09. Available on Bulletin Board hep-lat@ftp.scri.fsu.edu-9412013.
- Nir, Y., 1992, in *Proceedings of the Twentieth SLAC Summer Institute on Particle Physics, The Third Family and the Physics of Flavor*, 1992, edited by L. Vassilian, SLAC-Report-412, p. 81.
- Nussinov, S., and W. Wetzel, 1987, Phys. Rev. D **36**, 130.
- Pais, A., 1986, *Inward Bound* (Oxford University, Oxford), pp. 142–161 and pp. 309–323.
- Particle Data Group, Review of Particle Properties, 1994, Phys. Rev. D **50**, 1173.
- Paulini, M., 1991, in *Proceedings of the Joint International Lepton-Photon Symposium & Europhysics Conference on High Energy Physics*, Geneva, Switzerland, 1991, edited by S. Hegarty, K. Potter, and E. Quercigh (World Scientific, Singapore), p. 592.
- Perl, M.L., *et al.*, 1975, Phys. Rev. Lett. **35**, 1489.
- Poling, R., 1993, in *Proceedings of the 5th International Symposium on Heavy Flavour Physics*, Montreal, Canada, 1993, edited by D.I. Britton, D.B. MacFarlane, and P.M. Patel (Editions Frontières, Gif-sur-Yvette, France), p. 213.
- Politzer, H.D., 1973, Phys. Rev. Lett. **30**, 1346.
- Ramirez, C., J.F. Donoghue, and G. Burdman, 1990, Phys. Rev. D **41**, 1496.
- Reinders, L.J., 1988, Phys. Rev. D **38**, 947.

- Renton, P., 1990, *Electroweak Interactions* (Cambridge University, New York).
- Rolandi, L., 1993, in *Proceedings of the XXVI International Conference on High Energy Physics*, Dallas, 1992, AIP Conf. Proc. No. 272, edited by J. R. Sanford (AIP, New York), Vol. I, p. 56.
- Rosner, J.L., 1990, Phys. Rev. D **42**, 3732.
- Rosner, J.L., 1992, in *B Decays*, edited by S. Stone (World Scientific, Singapore), p. 312.
- Sanghera, S., *et al.*, 1993, Phys. Rev. D **47**, 791.
- Schilcher, K., and Y.L. Wu, 1992, Z. Phys. C **54**, 163.
- Schindler, R.H., *et al.*, 1981, Phys. Rev. D **24**, 78.
- Schmidt, D.M., R.J. Morrison, and M.S. Witherell, 1993, Nucl. Instrum. Methods A **328**, 547.
- Scora, D., 1991, Nucl. Phys. A **527**, 743c.
- Scora, D., 1993, Ph.D. thesis, University of Toronto.
- Scora, D., and N. Isgur, 1994, CEBAF Preprint No. CEBAF-TH-94-14.
- Shifman, M.A., 1987, Usp. Fiz. Nauk. **151**, 193 [Sov. Phys. Usp. **30**, 91 (1987)].
- Shifman, M., N.G. Uraltsev, and A. Vainshtein, 1995, Phys. Rev. D **51**, 2217.
- Shigemitsu, J., 1994, in *Proceedings of the 27th International Conference on High Energy Physics*, Glasgow, Scotland, July 20–27, 1994 (IOP, Philadelphia, in press).
- Shuryak, E.V., 1980, Nucl. Phys. B **93**, 134.
- Sinha, S.N., 1986, Phys. Lett. B **178**, 110.
- Spalding, J., 1993, in *Proceedings of the Workshop on B Physics at Hadron Accelerators, Snowmass, Colorado, June 21–July 2, 1993*, edited by C. Shekhar Mishra and P. McBride, Report No. SSCL-SR-1225 and Fermilab-Conf-93/267, p. 45.
- Stone, S., 1993, in *B Decays*, Revised 2nd Edition, edited by S. Stone (World Scientific, Singapore), p. 283.
- Suzuki, M., 1985, Phys. Lett. B **162**, 392.
- Tajima, H., 1994, in *The Albuquerque Meeting: Proceedings of the 8th Meeting, Division of Particles and Fields of the American Physical Society*, the University of New Mexico, 1994, edited by Sally Seidel (World Scientific, Singapore), p. 599.
- Vella, E., *et al.*, 1982, Phys. Rev. Lett. **48**, 1515.
- Venus, W., 1993, in *Proceedings of the 16th International Symposium on Lepton and Photon Interactions*, AIP Conf. Proc. No. 302, edited by P. Drell and D. Rubin (AIP, New York), p. 274.
- Voloshin, M.B., 1992, Phys. Rev. D **46**, 3062.
- Voloshin, M.B., 1994, “Topics in Heavy Quark Physics,” Lectures presented at the 1994 ITEP Winter School, 1994, University of Minnesota Preprint No. TIP-MINN-94/18-T and UMN-TH-1257-94.
- Voloshin, M.B., and M.A. Shifman, 1986, Sov. Phys. JETP **64**, 698.
- Voloshin, M.B., and M.A. Shifman, 1987, Yad. Fiz. **45**, 463 [Sov. J. Nucl. Phys. **45**, 292 (1987)].
- Voloshin, M.B., and M.A. Shifman, 1988, Yad. Fiz. **47**, 801 [Sov. J. Nucl. Phys. **47**, 511 (1988)].
- Wachs, K., *et al.*, 1989, Z. Phys. C **42**, 33.
- Winstein, B., and L. Wolfenstein, 1993, Rev. Mod. Phys. **65**, 1113.
- Wirbel, M., B. Stech, and M. Bauer, 1985, Z. Phys. C **29**, 637.
- Wise, M., 1993, in *Proceedings of the 5th International Symposium on Heavy Flavour Physics*, Montreal, Canada, 1993, edited by D.I. Britton, D.B. MacFarlane, and P.M. Patel (Editions Frontières, Gif-sur-Yvette, France), p. 5.
- Wise, M., 1994, in *Proceedings of the 16th International Symposium on Lepton and Photon Interactions*, AIP Conf. Proc. No. 302, edited by P. Drell and D. Rubin (AIP, New York), p. 253.
- Wolfenstein, L., 1983, Phys. Rev. Lett. **51**, 1945.
- Yanagisawa, C., *et al.*, 1991, Phys. Rev. Lett. **66**, 2436.
- Yaouanc, A.Le, 1994, Nucl. Instrum. Methods A **351**, 15.